Interaction of pulsed electric fields with membrane models for controlled release of drugs

Maura Casciola

INTERACTION OF PULSED ELECTRIC FIELDS WITH MEMBRANE MODELS FOR CONTROLLED RELEASE OF DRUGS

INTERACTION DES CHAMPS ÉLECTRIQUES PULSÉS AVEC DES MODÈLES DE MEMBRANES POUR LE RELARGAGE CONTROLÉ DE MÉDICAMENTS

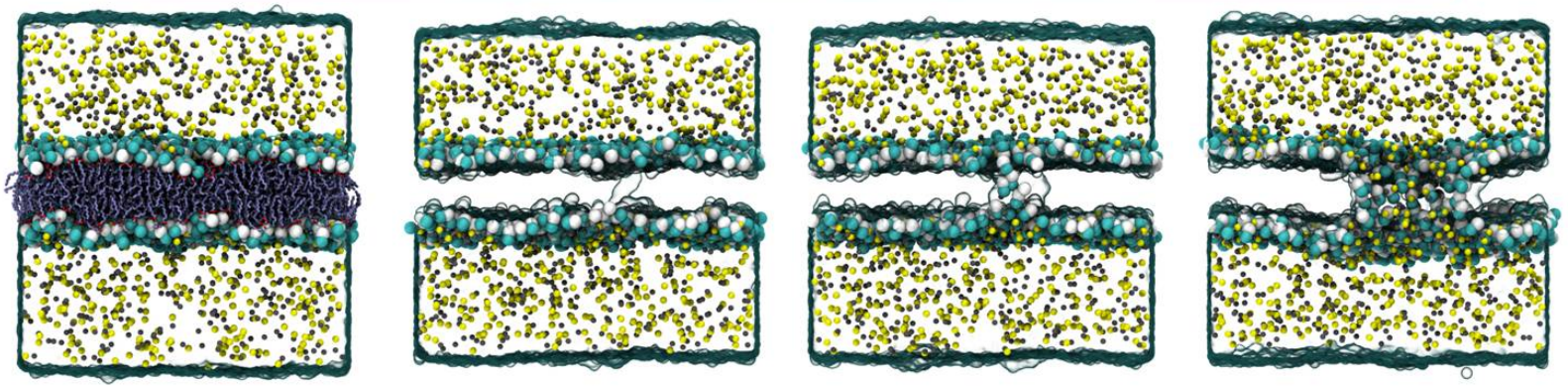

Maura CASCIOLA

Publicly held on March 24^{th} 2016
at La Sapienza University of Rome, Rome, Italy

Joint PhD Thesis

Between La Sapienza University of Rome, Faculty of Engineering, PhD school of Information and Communications Technologies
and l'Université de Lorraine, Collegium Sciences et Technologies, École doctorale SESAMES Lorraine

Submitted to obtain the titles of
PhD in **Electronic Engineering** at La Sapienza
and of PhD in **Chemistry** at l'Université de Lorraine

Interaction of pulsed electric fields with membrane models for controlled release of drugs

Interaction des champs électriques pulsés avec des modèles de membranes pour le relargage controlé de médicaments

Maura CASCIOLA

Publicly held on March 24th 2016
at La Sapienza University of Rome, Rome, Italy

Rapporteurs:	**Prof. C. Ramseyer**	Universitè de Franche-Comté, Besançon, France
	Prof. P. Ruggerone	University of Cagliari, Cagliari, Italy
Examiners:	**Prof. L. Tarricone**	University of Salento, Lecce, Italy
	Prof. P. Lamberti	University of Salerno, Salerno, Italy
Directors:	**Dr. M. Tarek**	Universitè de Lorraine, Nancy, France
	Dr. F. Apollonio	La Sapienza University of Rome, Rome, Italy

Note that the main text of this thesis is in English. The introduction and conclusion are presented in both languages (French and English) and each chapter starts with a short summary of the content in French.

Note also that the symbols X for physical quantities will be given as X/unit.

ACKNOWLEDGMENTS

I would like to express my deepest gratitude to my advisers Francesca, Micaela and Mounir, for their support and guidance over the past years. Each of them, in his own way, with his own time, not only transferred knowledge and expertise to me, but also taught me how to behave or not to become the kind of researcher that I want to be.

To my dear friend Tom, who was the first person that showed me how interesting and fun this work can be, and who advised me and believed in me since the very first moment. I want to thank him for being always at my side.

I am extremely grateful to Caterina, Julian, Paolo and Zach who assisted me in overcoming the challenges I have encountered along the way, and who helped me take the first steps into this world.

I also want to thank my colleagues and friends Agnese, Elena, Elly, Ilke, Marina and Zimmerí who have continuously helped me navigate through this experience, without them this journey would not have been so bright.

Throughout my life, I have been incredibly lucky to be surrounded by people that loved me and supported me. To mention just a few of them, Angela, Anna, Chiara, Elisa, Fernanda, Francesca, Serena, Valentina I want to thank you for being my daily fantastic life.

To all the colleagues at the Équipe Théorie Simulations et Modélisation Laboratory and at the D.I.E.T department, all of you have made these three years in the labs a great time.

Last, but certainly not least, I thank my crazy, smart and extravagant family. ALL of you have inspired me to be a better person, through your experience I have learned that passion, interest and curiosity are the keys to open the doors of fulfillment and happiness. In particular, I thank my parents Mauro and Vittoria, and my brother Valerio for being the pillars of my life.

Finally, I dedicate this work to my safe harbor, my past, my present and my future, my love Oreste.

Contents

List of Figures

List of Tables

Chapter 1

Introduction / Introduction

L'Électroporation (EP) est une technique qui permet de corrompre l'intégrité des membranes cellulaires plasmiques et celles d'organites internes, conséquence de l'application d'un champ électrique externe d'énergie (intensité et durée) suffisante.

Il est montré par de nombreuses études expérimentales et *in silico* que ce phénomène se traduit par la perméabilisation des structures membranaires par formation de pores qui permettent le transport de molécules peu- ou non perméantes comme par exemple, des ions, des petits solutés présents dans la solution extracellulaire et dans le cytoplasme ou du matériel génétique [1-2]. Les applications de l'EP se retrouvent dans les domaines de la biologie, de la biotechnologie et la médecine. On notera par exemple la vectorisation de médicaments et de gènes, le traitement des tumeurs, etc., qu'on retrouve déjà dans des traitements pré-cliniques et cliniques [3-9] (Chapitre **2**).

Il y a une grande variété d'impulsions utilisées en EP [10]. Elles sont classés en deux familles en fonction de leur durée et intensité. Les deux principales applications sont nommés d'après ces catégories. Dans l'EP standard, la longueur des impulsions est de l'ordre de la micro- a milli-seconde et l'amplitude de l'ordre de quelques kV/cm (μs-ms PEF); Elles affectent principalement la membrane cellulaire plasmique des cellules [11]. Les impulsions d'intensité beaucoup plus élevée (MV/m) et de très courtes durée (ordre de la nanoseconde) sont nommés nsPEFs; ces impulsions sont trop courtes pour charger la membrane, mais agissent directement sur elle et sont capables de perméabiliser les organites internes ainsi que la membrane cellulaire plasmique [12]. De telles impulsions présentent l'avantage d'éviter les effets thermiques indésirables. Cette dernière famille de pulses a suscité un grand intérêt dans la communauté scientifique mais ils sont chronologiquement plus récente (années 2000) en raison de la technologie sophistiquée nécessaire pour leur mise en place [13].

L'EP a été développée au début des années 1980 [14] et est largement utilisée dans les laboratoires, mais les mécanismes exactes qui ont lieu au niveau moléculaire ne sont pas encore bien compris. L'effet initial de ces deux familles d'impulsions est l'augmentation

du voltage transmembranaire (de la cellule et / ou des organelles). Quand ce dernier dépasse un certain seuil, le champ électrique local intense qu'il induit au niveau de la membrane, diminue la barrière énergétique à la pénétration d'espèces polaires comme l'eau, et favorise la formation de pores [15-17]. Néanmoins on sait peu sur les caractéristiques des pores formés (par exemple la taille, la morphologie, la conductance, sélectivité, le transport de molécules, ...).

La raison pour laquelle, après toutes ces années, notre connaissance de ce processus est encore limitée, réside dans les caractéristiques des processus dynamiques engendrées notamment la taille "nanométrique" des électropores et les échelles de temps "sub-microsecondes" nécessaires pour leur création. Il est donc très difficile d'observer par des techniques expérimentales l'effet de ses impulsions. Notre compréhension fragmentaire de ce phénomène limite le développement de nouvelles technologies et engendre des difficultés à contrôler le processus dans les applications cliniques. La caractérisation des électropores, est d'une importance considérable dans la détermination de la perméabilité et la sélectivité des membranes de différentes espèces ioniques et moléculaires, et par conséquent l'efficacité potentielle d'une application donnée.

Expérimentalement, la perméabilisation d'une membrane peut être mise en évidence indirectement en mesurant le transport de molécules normalement non perméantes à travers la membrane cellulaire ou en mesurant les changements dans les propriétés électriques de la membrane [18 à 24], ce, avec des limitations non négligeables dans la précision et la fiabilité des résultats. Ce n'est que très récemment qu'une visualisation des pores dans les bicouches déposées à l'interface de gouttelettes a été rendue possible en utilisant microscopie de fluorescence à réflexion interne totale (TIRF) [25]. Cependant, la résolution de cette technique (quelques microns) ne permet pas une visualisation directe des pores et donc ne permet pas une mesure directe de peur taille.

Les simulations de dynamique moléculaire (DM) (Chapitre **3**), en permettent la description microscopique avec une résolution atomique, de la structure d'une membranes et son interaction avec la solution environnante, fournissent un appui substantiel aux résultats expérimentaux. Par conséquent, de telles simulations de modèles de membranes soumises à des champs électriques ont été largement réalisées dans les dix dernières années [16,17,26-40] pour faire la lumière sur le processus d'EP.

Deux protocoles de simulations de DM ont été proposés à ce jour pour imiter l'effet soit des nsPEFs ou les μs-msPEFs sur bicouches lipidiques planes. étant donné que pour la première catégorie d'impulsions, le champ électrique augmente la tension transmembranaire par la polarisation directe de l'eau interfaciale, leur effet est modélisé en imposant une force sur chaque particule (atome) chargée proportionnel au champ électrique appliqué perpendiculairement à la membrane [16,17]. L'effet des μs-msPEFs est lui reproduit en imposant un déséquilibre de charge nette à travers la bicouche [32] pour modéliser l'accumulation de charges (ions) des deux côtés de la membrane qu'induit l'application d'une impulsion électrique plus longue. Un nombre considérable de travaux, illustrée plus

en détail dans le Chapitre 2, ont été consacrés à décrire certains des aspects de la PE à l'aide de ces deux approches néanmoins de nombreuses questions restent inexplorées:

- Comment la composition d'une bicouche lipidique influence le seuil d'EP ?
- Quelle est la morphologie des pores formés par nsPEFs ou μs-msPEFs, leur dimension et leur conductance ?
- Quel sont les mécanismes et l'échelle de temps de translocation de petites molécules aux travers des électropores. Ces derniers varient ils selon le d'impulsion (nsPEFs vs μs-msPEFs)?

Dans le cadre de ce travail, en utilisant des simulations de DM et en comparant nos résultats à d'autres résultats de notre groupe, nous avons abordé certaines de ces questions extrêmement pertinentes.

Les résultats de nos simulations sont présentés au Chapitre **4** et sont divisés en quatre sections. Dans la Section **4.1**, dans le cadre de l'étude du comportement des membranes complexes, nous présentons les résultats concernant la modulation des caractéristiques de bicouches lipidiques contenant 30% de cholestérol. En particulier, nous décrivons les propriété structurelles et électriques des interfaces lipides/eau. Dans la Section **4.2** nous quantifions les seuils d'EP de bicouches lipidiques contenant des concentrations croissantes de cholestérol (0, 20, 30 à 50 mole%) lorsqu'elles sont soumises à des impulsions nsPEFs et μs-msPEFs. Dans la Section suivante, **4.3**, nous développons une procédure, modélisant l'application des μs-msPEFs, qui permet de stabiliser les électropores sous différentes tensions transmembranaires suffisamment longtemps pour déterminer leur dimension, leur conductance et leur sélectivité aux ions. Dans la dernière Section, **4.4**, nous utilisons cette même méthode pour étudier le transport de petites molécules chargées (Tat_{11} et brins d'ARN), et comparons nos résultats à des études similaires menées dans les conditions des nsPEFs [33,40] afin de caractériser la vectorisation moléculaire par PEFs.

Bien que les nsPEFs présentent l'avantage d'affecter les membranes cellulaires et les organites internes et de réduire les effets thermiques [12], leur exploitation pour la vectorisation de médicament est encore en cours de développement. Cette technique assez récente, présente plusieurs challenges que de nombreux laboratoires de recherches essayent de relever. Parmi ceux ci: la capacité à générer et imposer de manière fiable des impulsions ultra-courtes intenses à un échantillon biologique n'est pas triviale. La technologie nécessite de suivre des protocoles et critères spécifiques, plus strictes que pour le cas des μs-msPEFs. De ce fait, encore dans de nombreux cas, cette technologie n'est pas disponible dans le commerce (pour plus de détails voir le Chapitre **2**).

En effet, une attention particulière doit être prêtée dans la conception des applicateurs de microchambre pour réaliser des dispositifs à large bande passante[13], capables de transmettre sans atténuation ni de distorsion des impulsions ultra courtes (quelques ns) avec des temps de montée et de décharge d'une fraction de nanosecondes, ce qui représente

un large spectre de composantes spectrales, allant du MHz jusqu'à GHz [10]. En outre, la durée de l'impulsion est une condition nécessaire mais pas suffisante pour obtenir la réponse souhaitée: l'impulsion doit être également suffisamment intense (MV/m) pour induire des effets subcellulaires. Par conséquent, deux conditions préalables principales doivent être remplies pour bien concevoir une microchambre pour les nsPEFs:

- Une bonne efficacité pour atteindre l'intensité nécessaire pour l'EP de composantes intracellulaires
- Le signal pulsé doit se propager sans atténuation du plateau et de la distorsion des temps de montée et de décharge.

Dans ce contexte, une partie importante des travaux en cours a été consacrée à la conception (utilisant les méthodes d'éléments finis) d'un dispositif d'exposition, basé sur des systèmes de propagation de micro-ondes, capable de délivrer des impulsions jusqu'à 1 ns avec temps de montée et de décharge de 0,5 et un rendement supérieur à 0,9.

Dans le Chapitre **5**, nous présentons les résultats relatifs à ces travaux. Ils sont divisées en quatre sections. Au paragraphe **5.1.1**, nous décrivons les fonctionnalités que notre dispositif devrait avoir pour améliorer l'état d'art actuel de la technique [41-46]. Le paragraphe suivant, **5.1.2**, est consacré à la description de la procédure en termes de modèles analytiques [47] que nous avons utilisé pour le dimensionnement de notre structure de guidage. Au paragraphe **5.1.3**, nous caractérisons l'efficacité et le comportement fréquentiel de notre microchambre dans deux configurations différentes: pour les expériences sur mono et multi- cellulaires. Enfin, à la section **5.1.4**, nous discutons de nos résultats mettant en évidence les principaux avantages proposés. On montre comment les performances globales de ce dispositif sont une amélioration par rapport à des structures similaires disponibles dans la littérature [41-46].

Ce travail fait partie d'un grand projet "Joint ITI-Sapienza LABon life-NanoScience", et aborde le Work Package 2 "Nouvelles stratégies pour l'imagerie et le traitement des tumeurs cérébrales ciblant les voies de signalisation des cellules souches cancéreuses". Pour étudier les aspects reliés à l'Electroporation, nous avons exploité à la fois une méthodologie théorique basée sur des simulations de dynamique moléculaire (MD), et une approche technologique / expérimentale.

Ce projet interdisciplinaire et le travail présenté dans cette Thèse, ont été effectués dans le cadre d'une cotutelle entre l'Université de Rome La Sapienza et de l'Université de Lorraine à Nancy, France. En ce qui concernent le groupe de recherche italien à DIET (Encadrement par le Pr. Francesca Apollonio), le domaine d'expertise est l'interaction des champs électromagnétiques avec des structures macromoléculaires ainsi que l'expérience dans la conception de systèmes de micro-ondes pour l'exposition *in vitro* et des expériences *in vivo*. Dans le groupe français, le Dr. Tarek Mounir (D.R. CNRS) est l'un des principaux experts des simulations de dynamique moléculaire de membranes lipidiques. et à

l'élaboration de protocoles adéquats pour simuler l'application de champs électriques.

Je tiens à souligner qu'une grande partie du présent travail est le résultat de simulations de DM menés sur les ressources informatiques HPC du CINES (http://www.cines.fr/?lang=fr), Centre Informatique National de l'Enseignement Supérieur, grâce à des projets retenus par GENCI (grand équipement national de calcul intensif):

Grants obtained for computational resources:

- Project number hpe0053, Cholesterol Rich Lipid Membranes Electroporation: A Molecular Dynamic Study, for 5000 cpu hours on SGI (Jade).
- Project number lct2523, Electroporation of membranes using nanosecond high intensity electric pulses, for 300000 cpu hours on SGI (Jade).
- Project number lct2523, Electroporation of biological bilayers driven by constant charge imbalance: transport of ions and small molecules through pores, a MD study (dossier number DARI c2014075136) for 553000 cpu hours on Bull machine (OCCIGEN).

Publications relatives à ce travail:

- **M. Casciola**, M. Liberti, A. Denzi, C. Merla, A. Paffi and F. Apollonio, Versatile Microchamber for nsPEFs experiments: single and multi cell exposures, Medical & Biological Engineering & Computing, submitted (Nov. 2015).
- **M. Casciola**, M. Tarek, A molecular insight into the electro-transfer of small molecules through electropores driven by μsPEFs, BBA Biomembranes, submitted (Jan. 2016).
- **M. Casciola**, M. A. Kasimova, L. Rems, S. Zullino, F. Apollonio, M. Tarek, Properties of lipid electropores I: Molecular Dynamics simulations of stabilized pores by constant charge imbalance, Bioelectrochemistry, in press (Oct. 2015).
- L. Rems, M. Tarek, **M. Casciola**, D. Miklavčič, Properties of lipid electropores II: Comparison of continuum-level modeling of pore conductance to molecular dynamics simulations, Bioelectrochemistry, submitted (Oct. 2015).
- P. Marracino, **M. Casciola**, M. Liberti, F. Apollonio, Evaluation of Protein Electrostatic Potential from Molecular Dynamics Simulations in the Presence of Exogenous Electric Fields: The Case Study of Myoglobin, in: W. Rocchia, M. Spagnuolo (Eds.), Comput. Electrost. Biol. Appl., Springer International Publishing, 2015: pp. 255-270, doi:10.1007/978-3-319-12211-3-13..
- **M. Casciola**, D. Bonhenry, M. Liberti, F. Apollonio, M. Tarek, A molecular dynamic study of cholesterol rich lipid membranes: comparison of electroporation protocols, Bioelectrochemistry 100 (2014) 11-17, doi:10.1016/j.bioelechem.2014.03.009.

Presentations dans des Conferences:

- Poster at Electroporation World Conference 2015, Molecular Dynamics evaluation of structural and electrical properties of hydrated bilayers exposed to nsPEF, **M. Casciola**, M. Marracino, M. Liberti, F. Apollonio.

- Poster at Electroporation World Conference 2015, Coupled microstrip lines for nsPEFs applications on living cells, **M. Casciola**, A. Denzi, A. Paffi, M. Liberti, F. Apollonio.

- Poster at Electroporation World Conference 2015, Molecular insights into the electrotransfer through lipid cell membranes driven by microsecond electric pulses, **M. Casciola**, F. Apollonio, M. Tarek.

- Platform at BioEM Conference 2015, Dielectric permittivity of hydrated bilayers from molecular dynamics simulations, **M. Casciola**, M. Marracino, M. Liberti, F. Apollonio.

- Poster at BioEM Conference 2015, Coupled microstrip lines for the exposure of living cells to nanosecond pulsed electric fields, **M. Casciola**, A. Denzi, A. Paffi, M. Liberti, F. Apollonio.

- Poster at BioEM Conference 2015, Mapping the electrostatics of bio-systems subject to exogenous electric fields: a full-atomistic approach, **M. Casciola**, M. Marracino, M. Liberti, F. Apollonio.

- Platform at EBTT 2014, On the characteristics of pores created by high voltages, recent MD investigations, **M. Casciola**, S. Zullino, M. Kasimova, M. Tarek.

- Poster at IJB, Institut Jean Barriol 2014, Molecular Insights into Electroporation and Electrotransfer through Model Cell Membranes, **M. Casciola**, M. Kasimova, L. Delemotte, A. Polak, D. Miklavcic, F. Apollonio, M. Breton, L. Mir, A. Shaytan, K. Shaitan, M. Tarek.

- Poster at GRC, Bioelectrochemistry Gordon Research Conference 2014, Response of the water at the membrane interfaces to nanosecond electric pulses, a MD study, **M. Casciola**, P. Marracino, M. Liberti, F. Apollonio.

- Platform at Bioelectrics Symposium 2013, A MD study of Cholesterol Rich Lipid Membranes Electroporation, **M. Casciola**, P. Marracino, D. Bonhenry, M. Liberti, F. Apollonio, M. Tarek.

- Poster at CEBA Meeting 2013 - Computational Electrostatics for Biological Applications, A Molecular Dynamic (MD) insight to electrostatic of biological (lipid) bilayers. A tool for understanding electroporation mechanisms, **M. Casciola**, P. Marracino, D. Bonhenry, M. Liberti, F. Apollonio, M. Tarek.

- Platform at BioEM Conference 2013, MD simulations of transient water pores produced by transmembrane ionic Charge Imbalance in cholesterol containing bilayers, **M. Casciola**, D. Bonhenry, M. Liberti, F. Apollonio, M. Tarek.

- Platform at EBTT 2012, Ion Transport in POPC Field-Stabilized Nanoscale Electropores: Molecular Dynamics Simulations, **M. Casciola**, M. C. Ho, Z. A. Levine, P. T. Vernier.

Introduction / Introduction

Electroporation (EP) is a technique to corrupt the integrity of plasma cell membranes and/or internal organelles, consequence of the application of an external pulsed electric field of sufficient energy content, tuned by its strength and duration.

It is proven by extensive indirect experimental and *in silico* evidences that this phenomenon results in the permeabilization of membrane structures by aqueous pores, allowing the transport of poorly- or non-permeant molecules, e.g. salts, ions, genetic material, and any other small solutes present in the extracellular solution and in the cytoplasm [1-2]. The applications of EP span from biology and biotechnology to medicine, e.g. drug and gene delivery into cells, tumor therapy, etc., resulting also in pre-clinical and clinical treatments [3-9] (Chapter **2**).

There is a great variety of pulses used in EP [10], yet they are categorized in two families based on their length and intensity. The two main collective applications are named after these categories. In standard EP, the length of the pulses is in the μs-ms scale and the amplitude in the order of kV/cm, termed μs-msPEF; their effect takes place mainly at the plasma cell membrane of cells [11]. Pulses of much higher magnitude (MV/m) over very short time scale (nanosecond) are named nsPEFs; such pulses are too short to charge the membrane, but act directly on it and are able to permeabilize internal organelles as well as the plasma cell membrane [12], presenting the advantage of avoiding undesired thermal effects. The latter family has gained great interest in the scientific community for such capabilities, however they are chronologically more recent (2000's) because of the sophisticated technology they require [13].

EP was developed in the early 1980's [14] and it is nowadays widely used in laboratory, however the exact mechanism taking place at the molecular level is still not well understood: generally, it is supported the hypothesis that the macroscopic effect of these two families of pulses is the local increase in the transmembrane (i.e. of the cell and/or organelles) voltage that, when it overcomes a certain threshold, produces an intense local electric field at the membrane level, decreasing the energetic barrier to the penetration of polar species and prompting pore formation [15-17]. Nevertheless little is known about the characteristics of the pores formed (e.g. size, morphology, conductance, selectivity, transport of molecules).

The reason why after all these years there is still lack in the knowledge of this process resides in the nanometer size of the electropores and in the fast temporal scales of their process dynamic, thus it is very difficult to visualize the pores in physical experiments. Our limited comprehension of this phenomenon restricts the development of new technologies and causes difficulties in controlling the process in clinical applications. The characterization of electropores, indeed, is of tremendous importance in determining the permeability and selectivity of the membranes to different ionic and molecular species and consequently the potential efficacy of a given EP application.

Experimentally, the permeabilization has been monitored indirectly by tracking the transport of normally impermeant materials across the cell membrane or by measuring changes in the electrical properties of the membrane [18-24], with not negligible limitations in the accuracy and reliability of the results. Only very recently, time resolved visualization of pores in droplet interface bilayers was made possible using total internal reflection fluorescence microscopy [25]. Nevertheless, currently such fluorescence imaging does not allow a straight visualization of the pore needed for a thorough measurement of the pore size and of the transport process of small molecules.

Molecular dynamics (MD) simulations (Chapter **3**) allow the microscopic description of the membrane structure with atomic resolution and its interaction with the surrounding solution, providing a substantial support to experimental findings. Therefore, MD simulations of membrane models subject to electric fields have been extensively carried out in the past ten years [16,17,26-40] to shed light on the EP process.

Two MD protocols have been proposed so far to mimic the effect of either nsPEFs or μs-msPEFs on planar bilayers. Since for the first category of pulses the electric field increases the transmembrane voltage by direct polarization of the interfacial water and lipid headgroups, their effect is modeled by imposing a force on each charge in the system proportional to the electric field applied perpendicularly to the membrane [16,17], whereas, the effect of μs-msPEFs should be reproduced by imposing a net charge imbalance across the bilayer [32] modeling the accumulation of electrical charges at both sides of the cell membrane that follows the application of a longer pulse. A considerable amount of work, illustrated in more detail in Chapter **2**, has been devoted to describe some of the aspects of EP using these two approaches, nevertheless many outstanding questions remain unexplored:

- When using the two MD protocols, how do complex bilayer modulate the response of the membrane and affect the EP threshold?
- What is the pore morphology, the dimension and the conductance of pores formed under nsPEFs or μs-msPEFs?
- What is the mechanism and the time scale of translocation of small molecules through these electropores and how the characteristic of the pulse influences the transport?

As part of the present work, using MD simulations and comparing our results to previous findings, we addressed some of these extremely relevant questions.

The MD results of our study are presented in Chapter **4** and are divided in four Sections. In Section **4.1**, we describe structural and electric effects at the lipid headgroups/water interface of pure lipid bilayer and when 30 mol % of cholesterol is added (physiological concentration). In Section **4.2** we quantify the EP threshold of libid bilayes with increasing concentration of cholesterol (0, 20, 30, 50 mol %) when nsPEFs and μs-msPEFs are modeled. In the successive Section, **4.3**, we developed a procedure, mimicking μs-msPEFs, to stabilize electropores under different transmembrane voltages for long enough to determine the pore dimension, its conductance and selectivity to ion species. In the last Section, **4.4**, we employed the latter method to investigate the transport of small charged molecules, used in drug delivery, comparing our findings with similar studies conducted under nsPEFs conditions [33,40] with the attempt to rationalize the molecular up take.

Despite nsPEFs have the advantage to affect both cell membranes and internal organelles and to further reduce thermal effects [12], the possibility to exploit nsPEFs for drug delivery is an ongoing research. The reason why many laboratories all over the world are still working on it dwells in the quite recent utilization of this technique; the ability to reliably generate and deliver these ultra-short intense pulses to the biological load is not trivial, hence the technology required must follow specific restrains (for more details see Chapter **2**).

Indeed, particular attention must be payed in the design of microchamber applicators to realize broadband devices [13], able to transmit without attenuation and distortion ultra short (few ns) pulsed signals with rise and fall time of fractions of ns, which exhibit large spectral components, i.e. spanning from MHz up to GHz [10]. Additionally, the pulse must also be intense enough (MV/m) to induce cellular and subcellular effects.

Therefore, two main prerequisites must be met to properly design a microchamber for nsPEFs:

- A good efficiency to reach the intensity needed for EP of intracellular components
- The pulsed signal must propagate without attenuation of the plateau and distortion of the rise and fall time

In this scenario an important part of the current work has been devoted to the design (with Finite Element Method) of an exposure device, based on microwave propagating systems, which is able to deliver pulses down to 1 ns with rise and fall time of 0.5 ns and efficiency above 0.9.

In Chapter **5** we present the related results divided in four Sections. In Subsection **5.1.1**, we target the features our device should have to improve the current state of the art. The following subsection, **5.1.2**, is dedicated to the description of the synthesis procedure based

on available analytical closed-form expressions [47] we used for the dimensioning of our guiding structure, to the illustration of the numerical model for its optimization and to summarize the measurements of different cell buffers carried out to solve a reliable and realistic model of the cell suspension. In Subsection **5.1.3**, we characterize the efficiency and the frequency behavior of our microchamber in two different configurations: for single- and multi-cell experiments. Finally, in **5.1.4** we discuss our findings highlighting the main advantages proposed. The overall performances of this device are an improvement compared to similar structures available in literature [41-46].

The core of this work is part of a major project "Joint IIT-Sapienza LAB on Life-NanoScience", and addresses the WP2 of the research line "Novel strategies for the imaging and treatment of brain tumors through targeting cancer stem cell-specific signaling pathways". To properly investigate the aforesaid described aspects of EP, both a theoretical methodology based on molecular dynamics (MD) simulations, and a technological/experimental approach were exploited.

At the basis of this interdisciplinary project there is a joint research doctorate between La Sapienza University of Rome (Italy) and the University of Lorraine (France). For what concerns the Italian research group at D.I.E.T., Dr. Francesca Apollonio has an assessed experience in the study of the interaction of electromagnetic fields with macromolecular structures, as well as in designing microwave systems for the exposure *in vitro* and *in vivo* experiments. In the French group, Dr. Mounir Tarek (D.R. CNRS) is one of the main expert large-scale state-of-the-art molecular dynamics simulations of lipid membranes. Dr. Tarek's seminal and extensive work is focused on probing the structure and dynamics of membranes and bio-molecules and in devising protocols to apply electric field to membranes.

We would like to highlight that part of the present work is the result of massive MD simulations computed on High Performing Computers (HPC) at CINES (http://www.cines.fr/?lang=fr).

Grants obtained for computational resources:

- Project number hpe0053, Cholesterol Rich Lipid Membranes Electroporation: A Molecular Dynamic Study, for 5000 cpu hours on SGI (Jade).
- Project number lct2523, Electroporation of membranes using nanosecond high intensity electric pulses, for 300000 cpu hours on SGI (Jade).
- Project number lct2523, Electroporation of biological bilayers driven by constant charge imbalance: transport of ions and small molecules through pores, a MD study (dossier number DARI c2014075136) for 553000 cpu hours on Bull machine (OCCIGEN).

Finally, we report the publications related to the present work.

In Peer-reviewed Journal Articles are:

- **M. Casciola**, M. Liberti, A. Denzi, C. Merla, A. Paffi and F. Apollonio, Versatile Microchamber for nsPEFs experiments: single and multi cell exposures, Medical & Biological Engineering & Computing, submitted (Nov. 2015).

- **M. Casciola**, M. Tarek, A molecular insight into the electro-transfer of small molecules through electropores driven by μsPEFs, BBA Biomembranes, submitted (Jan. 2016).

- **M. Casciola**, M. A. Kasimova, L. Rems, S. Zullino, F. Apollonio, M. Tarek, Properties of lipid electropores I: Molecular Dynamics simulations of stabilized pores by constant charge imbalance, Bioelectrochemistry, in press (Oct. 2015).

- L. Rems, M. Tarek, **M. Casciola**, D. Miklavčič, Properties of lipid electropores II: Comparison of continuum-level modeling of pore conductance to molecular dynamics simulations, Bioelectrochemistry, submitted (Oct. 2015).

- P. Marracino, **M. Casciola**, M. Liberti, F. Apollonio, Evaluation of Protein Electrostatic Potential from Molecular Dynamics Simulations in the Presence of Exogenous Electric Fields: The Case Study of Myoglobin, in: W. Rocchia, M. Spagnuolo (Eds.), Comput. Electrost. Biol. Appl., Springer International Publishing, 2015: pp. 255-270, doi:10.1007/978-3-319-12211-3-13..

- **M. Casciola**, D. Bonhenry, M. Liberti, F. Apollonio, M. Tarek, A molecular dynamic study of cholesterol rich lipid membranes: comparison of electroporation protocols, Bioelectrochemistry 100 (2014) 11-17, doi:10.1016/j.bioelechem.2014.03.009.

In International Scientific Conferences are:

- Poster at Electroporation World Conference 2015, Molecular Dynamics evaluation of structural and electrical properties of hydrated bilayers exposed to nsPEF, **M. Casciola**, M. Marracino, M. Liberti, F. Apollonio.

- Poster at Electroporation World Conference 2015, Coupled microstrip lines for nsPEFs applications on living cells, **M. Casciola**, A. Denzi, A. Paffi, M. Liberti, F. Apollonio.

- Poster at Electroporation World Conference 2015, Molecular insights into the electrotransfer through lipid cell membranes driven by microsecond electric pulses, **M. Casciola**, F. Apollonio, M. Tarek.

- Platform at BioEM Conference 2015, Dielectric permittivity of hydrated bilayers from molecular dynamics simulations, **M. Casciola**, M. Marracino, M. Liberti, F. Apollonio.

- Poster at BioEM Conference 2015, Coupled microstrip lines for the exposure of living cells to nanosecond pulsed electric fields, **M. Casciola**, A. Denzi, A. Paffi, M. Liberti, F. Apollonio.

- Poster at BioEM Conference 2015, Mapping the electrostatics of bio-systems subject to exogenous electric fields: a full-atomistic approach, **M. Casciola**, M. Marracino,

M. Liberti, F. Apollonio.

- Platform at EBTT 2014, On the characteristics of pores created by high voltages, recent MD investigations, **M. Casciola**, S. Zullino, M. Kasimova, M. Tarek.

- Poster at IJB, Institut Jean Barriol 2014, Molecular Insights into Electroporation and Electrotransfer through Model Cell Membranes, **M. Casciola**, M. Kasimova, L. Delemotte, A. Polak, D. Miklavcic, F. Apollonio, M. Breton, L. Mir, A. Shaytan, K. Shaitan, M. Tarek.

- Poster at GRC, Bioelectrochemistry Gordon Research Conference 2014, Response of the water at the membrane interfaces to nanosecond electric pulses, a MD study, **M. Casciola**, P. Marracino, M. Liberti, F. Apollonio.

- Platform at Bioelectrics Symposium 2013, A MD study of Cholesterol Rich Lipid Membranes Electroporation, **M. Casciola**, P. Marracino, D. Bonhenry, M. Liberti, F. Apollonio, M. Tarek.

- Poster at CEBA Meeting 2013 - Computational Electrostatics for Biological Applications, A Molecular Dynamic (MD) insight to electrostatic of biological (lipid) bilayers. A tool for understanding electroporation mechanisms, **M. Casciola**, P. Marracino, D. Bonhenry, M. Liberti, F. Apollonio, M. Tarek.

- Platform at BioEM Conference 2013, MD simulations of transient water pores produced by transmembrane ionic Charge Imbalance in cholesterol containing bilayers, **M. Casciola**, D. Bonhenry, M. Liberti, F. Apollonio, M. Tarek.

- Platform at EBTT 2012, Ion Transport in POPC Field-Stabilized Nanoscale Electropores: Molecular Dynamics Simulations, **M. Casciola**, M. C. Ho, Z. A. Levine, P. T. Vernier.

References

[1] E. Neumann, A.E. Sowers, C.A. Jordan, Electroporation and Electrofusion in Cell Biology, Springer Science & Business Media, 1989.

[2] J.A. Nickoloff, Animal Cell Electroporation and Electrofusion Protocols, Humana Press,NJ, 1995.

[3] M. Breton, L.M. Mir, Microsecond and nanosecond electric pulses in cancer treatments, Bioelectromagnetics. 33 (2012) 106-123.

[4] D. Miklavčič, B. Mali, B. Kos, R. Heller, G. Sersa, Electrochemotherapy: from the drawing board into medical practice, Biomed. Eng. OnLine. 13 (2014) 29.

[5] M. Sällberg, L. Frelin, G. Ahlen, M. Sällberg-Chen, Electroporation for therapeutic DNA vaccination in patients, Med. Microbiol. Immunol. (Berl.). 204 (2014) 131-135.

[6] G. Sersa, J. Teissie, M. Cemazar, E. Signori, U. Kamensek, G. Marshall, et al., Electrochemotherapy of tumors as in situ vaccination boosted by immunogene electrotransfer, Cancer Immunol. Immunother. CII. 64 (2015) 1315-1327.

[7] L.C. Heller, R. Heller, In Vivo Electroporation for Gene Therapy, Hum. Gene Ther. 17 (2006) 890-897.

[8] S. Chabot, J. Teissié, M. Golzio, Targeted electro-delivery of oligonucleotides for RNA interference: siRNA and antimiR, Adv. Drug Deliv. Rev. 81 (2015) 161-168.

[9] C. Jiang, R.V. Davalos, J.C. Bischof, A Review of Basic to Clinical Studies of Irreversible Electroporation Therapy, IEEE Trans. Biomed. Eng. 62 (2015) 4-20.

[10] C. Merla, A. Denzi, A. Paffi, M. Casciola, G. D'Inzeo, F. Apollonio, et al., Novel Passive Element Circuits for Microdosimetry of Nanosecond Pulsed Electric Fields, IEEE Trans. Biomed. Eng. 59 (2012) 2302-2311.

[11] I.G. Abidor, V.B. Arakelyan, L.V. Chernomordik, Y.A. Chizmadzhev, V.F. Pastushenko, M.P. Tarasevich, Electric breakdown of bilayer lipid membranes: I. The main experimental facts and their qualitative discussion, J. Electroanal. Chem. Interfacial Electrochem. 104 (1979) 37-52.

[12] L. Chopinet, M.P. Rols, Nanosecond electric pulses: a mini-review of the present state of the art, Bioelectrochemistry Amst. Neth. 103 (2015) 2-6.

[13] A. Silve, J. Villemejane, V. Joubert, A. Ivorra, L.M. Mir, Nanosecond pulsed electric field delivery to biological samples: Difficulties and potential solutions, Adv. Electroporation Tech. Biol. Med. Boca Raton FL CRC Press Taylor Francis Group. (2011).

[14] E. Neumann, M. Schaefer-Ridder, Y. Wang, P.H. Hofschneider, Gene transfer into

mouse lyoma cells by electroporation in high electric fields., EMBO J. 1 (1982) 841-845.

[15] T. Kotnik, G. Pucihar, D. Miklavčič, Induced Transmembrane Voltage and Its Correlation with Electroporation-Mediated Molecular Transport, J. Membr. Biol. 236 (2010) 3-13.

[16] D.P. Tieleman, The molecular basis of electroporation, BMC Biochem. 5 (2004) 10.

[17] M. Tarek, Membrane Electroporation: A Molecular Dynamics Simulation, Biophys. J. 88 (2005) 4045-4053.

[18] S. Kalinowski, G. Ibron, K. Bryl, Z. Figaszewski, Chronopotentiometric studies of electroporation of bilayer lipid membranes, Biochim. Biophys. Acta BBA - Biomembr. 1369 (1998) 204-212.

[19] S. Koronkiewicz, S. Kalinowski, Influence of cholesterol on electroporation of bilayer lipid membranes: chronopotentiometric studies, Biochim. Biophys. Acta BBA - Biomembr. 1661 (2004) 196-203.

[20] M. Kotulska, Natural Fluctuations of an Electropore Show Fractional Lévy Stable Motion, Biophys. J. 92 (2007) 2412-2421.

[21] H. Krassen, U. Pliquett, E. Neumann, Nonlinear current-voltage relationship of the plasma membrane of single CHO cells, Bioelectrochemistry. 70 (2007) 71-77.

[22] O.M. Nesin, O.N. Pakhomova, S. Xiao, A.G. Pakhomov, Manipulation of cell volume and membrane pore comparison following single cell permeabilization with 60- and 600-ns electric pulses, Biochim. Biophys. Acta. 1808 (2011) 792-801.

[23] A. Silve, I. Leray, L.M. Mir, Demonstration of cell membrane permeabilization to medium-sized molecules caused by a single 10 ns electric pulse, Bioelectrochemistry. 87 (2012) 260-264.

[24] A.G. Pakhomov, E. Gianulis, P.T. Vernier, I. Semenov, S. Xiao, O.N. Pakhomova, Multiple nanosecond electric pulses increase the number but not the size of long-lived nanopores in the cell membrane, Biochim. Biophys. Acta. 1848 (2015) 958-966.

[25] M. Szabo, M.I. Wallace, Imaging potassium-flux through individual electropores in droplet interface bilayers, Biochim. Biophys. Acta. (2015).

[26] P.T. Vernier, M.J. Ziegler, Y. Sun, M.A. Gundersen, D.P. Tieleman, Nanopore-facilitated, voltage-driven phosphatidylserine translocation in lipid bilayers-in cells and in silico, Phys. Biol. 3 (2006) 233.

[27] M.J. Ziegler, P.T. Vernier, Interface Water Dynamics and Porating Electric Fields for Phospholipid Bilayers, J. Phys. Chem. B. 112 (2008) 13588-13596.

[28] R.A. Böckmann, B.L. de Groot, S. Kakorin, E. Neumann, H. Grubmüller, Kinetics, Statistics, and Energetics of Lipid Membrane Electroporation Studied by Molecular Dynamics Simulations, Biophys. J. 95 (2008) 1837-1850.

[29] A.A. Gurtovenko, J. Anwar, I. Vattulainen, Defect-Mediated Trafficking across Cell Membranes: Insights from in Silico Modeling, Chem. Rev. 110 (2010) 6077-6103.

[30] Z. A. Levine, and P. T. Vernier, Life cycle of an electropore: Field dependent and field-indepedent steps in pore creation and annihilation, J. Membr. Biol. 236 (2010) 27-36.

[31] M.L. Fernández, G. Marshall, F. Sagués, R. Reigada, Structural and Kinetic Molecular Dynamics Study of Electroporation in Cholesterol-Containing Bilayers, J. Phys. Chem. B. 114 (2010) 6855-6865.

[32] L. Delemotte, and M. Tarek, Molecular dynamics simulations of lipid membrane electroporation, J. Membr. Biol. 245 (2012) 531-543.

[33] M. Breton, L. Delemotte, A. Silve et al., Transport of siRNA through lipid membranes driven by nanosecond electric pulses: An experimental and computational study, J. Am. Chem. Soc. 134 (2012) 13938-13941.

[34] M. Tokman, J.H. Lee, Z.A. Levine, M.-C. Ho, M.E. Colvin, P.T. Vernier, Electric Field-Driven Water Dipoles: Nanoscale Architecture of Electroporation, PLoS ONE. 8 (2013) e61111.

[35] M.-C. Ho, M. Casciola, Z.A. Levine, P.T. Vernier, Molecular Dynamics Simulations of Ion Conductance in Field-Stabilized Nanoscale Lipid Electropores, J. Phys. Chem. B. 117 (2013) 11633-11640.

[36] A. Polak, D. Bonhenry, F. Dehez, P. Kramar, D. Miklavčič, M. Tarek, On the Electroporation Thresholds of Lipid Bilayers: Molecular Dynamics Simulation Investigations, J. Membr. Biol. 246 (2013) 843-850.

[37] F. Dehez, L. Delemotte, P. Kramar, D. Miklavčič, M. Tarek, Evidence of Conducting Hydrophobic Nanopores Across Membranes in Response to an Electric Field, J. Phys. Chem. C. 118 (2014) 6752-6757.

[38] M. Casciola, D. Bonhenry, M. Liberti, F. Apollonio, M. Tarek, A molecular dynamic study of cholesterol rich lipid membranes: comparison of electroporation protocols, Bioelectrochemistry. 100 (2014) 11-17.

[39] A. Polak, M. Tarek, M. Tomsic, J. Valant, N.P. Ulrih, A. Jamnik, et al., Electroporation of archaeal lipid membranes using MD simulations, Bioelectrochemistry. 100 (2014) 18-26.

[40] F. Salomone, M. Breton, I. Leray, F. Cardarelli, C. Boccardi, D. Bonhenry, et al., High-Yield Nontoxic Gene Transfer through Conjugation of the CM18-Tat11 Chimeric Peptide with Nanosecond Electric Pulses, Mol. Pharm. 11 (2014) 2466-2474.

[41] Y. Sun, P.T. Vernier, M. Behrend, L. Marcu, M.A. Gundersen, Electrode microchamber for noninvasive perturbation of mammalian cells with nanosecond pulsed electric fields, IEEE Trans. NanoBioscience. 4 (2005) 277-283.

[42] P. Krishnaswamy, A. Kuthi, Meng-Tse Chen, Shih-Jui Chen, P.T. Vernier, M.A. Gundersen, Compact high voltage subnanosecond pulsed power delivery system for biological applications, in: Pulsed Power Conf. 2007 16th IEEE Int., 2007 pp 476-480

[43] C. Dalmay, J. Villemejane, V. Joubert, O. Français, L.M. Mir, B. Le Pioufle, Design and realization of a microfluidic device devoted to the application of ultra-short pulses of electrical field to living cells, Sens. Actuators B Chem. 160 (2011) 1573-1580.

[44] C. Dalmay, J. Villemejane, V. Joubert, A. Silve, D. Arnaud-Cormos, O. Français, et al., A microfluidic biochip for the nanoporation of living cells, Biosens. Bioelectron. 26 (2011) 4649-4655.

[45] D. Arnaud-Cormos, P. Leveque, Y.-H. Wu, J.M. Sanders, M.A. Gundersen, P.T. Vernier, Microchamber Setup Characterization for Nanosecond Pulsed Electric Field Exposure, IEEE Trans. Biomed. Eng. 58 (2011) 1656-1662.

[46] Y.-H. Wu, D. Arnaud-Cormos, M. Casciola, J.M. Sanders, P. Leveque, P.T. Vernier, Moveable Wire Electrode Microchamber for Nanosecond Pulsed Electric-Field Delivery, IEEE Trans. Biomed. Eng. 60 (2013) 489-496.

[47] R. Garg, I. Bahl, M. Bozzi, Microstrip Lines and Slotlines, Third Edition, Artech House, 2013.

Chapter 2

Electroporation: Treatments, Models and Devices / Électroporation: Traitements, Modèles et Dispositifs

En 1959, Richard Feynman [1], en pionnier, a évoqué la promesse de miniaturisation des matériaux jusqu'à l'échelle nanométrique, introduisant ainsi le concept de nanosciences. A ce jour, il y a eu des progrès extraordinaires dans les nanotechnologies, avec des rôles pivots multidisciplinaires dans l'électronique, la biologie et la médecine. Tel que rapporté par le Livre blanc relatif à la "contribution de la nanomédecine au projet Horizon 2020" [2], la nanotechnologie est l'une des six technologies clés qui a un impact significatif sur de nombreux développements médicaux notamment dans trois domaines principaux: Thérapeutique, Diagnostique/Imagerie et Médecine régénérative. L'importance de la nanomédecine dans la recherche actuelle est également manifestée par son rôle de premier plan joué dans le domaine de "Biomédecine et biosciences moléculaires" [3] une des actions COST (Coopération européenne dans le domaine de la recherche scientifique et technique), l'un des premiers et plus large cadre européen pour la coordination transnationale des activités de recherche financées au niveau national.

Des soins personnalisés de santé, la conception rationnelle de médicaments, et la vectorisation ciblée de médicaments sont quelques-uns des avantages des thérapies basées sur une approche fondée sur la nanomédecine [4]. Ce nouveau domaine se concentre sur l'imagerie, le diagnostic précoce [5,6], l'analyse de tissus pathologiques, et la vectorisation de médicaments [7]. Les Systèmes dits "intelligents" (SMART) de vectorisation sont des vecteurs multi-cibles, sensibles à des stimuli, qui peuvent re-larguer les médicaments à des concentrations désirées dans le corps et éviter la nécessité de doses fréquentes et massives, réduisant ainsi les effets secondaires systémiques [8,9]. Le but ultime des technologies intelligentes d'administration de médicaments consiste à administrer des médicaments au bon moment, avec la bonne dose partout dans le corps avec une spécificité et efficacité, ce qui peut aider les patients à mieux adhérer à leur schéma thérapeutique. Deux principaux défis concernent l'utilisation sûre et efficace de ces techniques: tout d'abord l'ingénierie

: le support fonctionnalisé contenant le soluté donné (par exemple les composés pharmaceutiques, les médicaments, le matériel génétique, ...) doitêtre biocompatible, petit (quelques dizaines à quelques centaines de nm de diamètre), stable et résistant capable de surmonter plusieurs obstacles physiologiques à travers le corps pour atteindre le site d'intérêt et, finalement,être "bon marché" pour réduire les coûts de soins de sant [10]; d'autre part, ayant atteint le site à traiter, il est souhaitable que le médicament puisseêtre libéré en réponse à un stimuli [11-14]. Les vésicules (liposomes), composés amphiphiles avec un noyau lipophile et une interface hydrophile, sont les vecteurs les plus largement employés pour plusieurs raisons [15]: i) Ces vecteurs sont relativement faciles à préparer, ii) ils ont des dimensions minimales qui varient jusqu'à quelques dizaines de nm, iii) Ils peuvent transporter un large éventail de médicaments, iv) ils peuvent offrir une charge utile relativement élevée, v) la plupart d'entre eux sont non-toxiques et biocompatibles, vi) leur surface peutêtre facilement modifiée de façon à cibler spécifiquement certaines cellules, vii) ils sont susceptibles de répondre à des stimuli externes. Dans l'ensemble, ils sont donc de bons candidats pour adapter les conditions énumérées auparavant.

Les vecteurs sont d'une préoccupation majeure dans les technologies nanométriques émergentes et l'intérêt pour les systèmes particulièrement sensibles à un stimuli a persisté au cours de nombreuses décennies: beaucoup de travail a été dédiée à leur développement. Dans tous les cas, le paramètre clé définissant le comportement réactif ou "intelligent" du système est une réponse non-linéaire à un signal externe. Cependant, la grande majorité des rapports dans la littérature décrivent des systèmes qui sont sensibles à seulement quelques déclencheurs courants comme des changements de pH et / ou de température [16,17], champs magnétiques [18] ultrasons [19] et concentration d'électrolyte [20].

Plus récemment, l'attention a été portée sur des stimuli qui ne sont pas encore aussi largement considérés en dépit de leur potentiel unique [12]. Une des perspectives très intéressante pour la livraison contrôlée de médicaments est basée sur l'adaptation des transporteurs intelligents sensibles aux champs électriques externes, en particulier les domaines d'impulsions électriques ultra courtes (ucPEF) de forte intensité (quelques à plusieurs KV / cm) et très courte durée (milliseconde à quelques nanosecondes), semblables à ceux qui produisent l'électroporation réversible (EP) sur des cellules [21].

Comme décrit dans la Section 2.1 les changements structurels que ces impulsions induisent dans les cellules vivantes se produisent principalement à la membrane plasmique. Etant donné que les principaux constituants de la membrane cellulaire sont les lipides, c'est à dire ceux la même qui composent les vésicules, l'hypothèse que les champs électriques de forte intensité et de courte durée, produisent des effets similaires (electroporation) est très plausible.

L'objectif principale de la présente thèse est l'étude des effets des ucPEFs sur bicouches lipidiques. Une partie de ce travail se concentre sur la description atomistique de l'interaction entre ce champ électrique pulsé avec ces modèles de membranes cellulaires. Une autre partie importante porte sur la conception de dispositifs d'exposition capables de fournir

des ucPEFs pour l'expérimentation *in vitro*, ce qui permettraient de valider nos prédictions théoriques. Ce chapitre donne un aperçu sur principales applications de l'électroporation à des fins médicales (Section 2.1), un bref rappel des méthodes théoriques atomistiques et en continuum (Section 2.2) et une description brève des systèmes d'exposition communément utilisés (Section 2.3).

Electroporation: Treatments, Models and Devices / Électroporation: Traitements, Modèles et Dispositifs

In 1959 Richard Feynman [1], with a pioneering view, discussed the promise of miniaturization of materials down to the nanoscale, giving life to the inception of the concept of nanoscience. Up to now there has been extraordinary progress in nanotechnology, with pivotal multidisciplinary roles in electronics, biology and medicine. As reported by the White Paper relative to the "Contribution of Nanomedicine to Horizon 2020" [2], nanotechnology is one of the six Key Enabling Technologies that has a significant impact on many different medical developments in three main areas: Therapeutics, Diagnostics/Imaging, and Regenerative Medicine. The tremendous importance of nanomedicine in actual research is also proved by its primary role played in the domain "Biomedicine and Molecular Biosciences" [3] of the COST Actions (European Cooperation in Science and Technology), one of the first and widest European framework for the transnational coordination of nationally funded research activities.

Personalized health care, rational drug design, and targeted drug delivery are some of the benefits of a nanomedicine-based approach to therapy [4]. This emerging area focuses on imaging, early diagnosis [5,6], pathological tissue analysis, and drug delivery [7]. Smart drug delivery systems are multi-targeted, stimuli sensitive, delivery carriers that can keep drugs at desirable levels in the body and avoid the need for frequent and massive doses, reducing systemic side effects [8,9]. The ultimate goal of smart drug delivery technologies is to administer drugs at the right time, with the right dose anywhere in the body with specificity and efficiency, which can help patients to better adhere to their therapy regimen.

Two main challenges concern the efficient and safe use of such techniques: firstly the engineered, functionalized carrier loaded with the given solute (e.g. pharmaceutical compounds, drugs, genetic material, ...) needs to be biocompatible, small (tens to hundreds of nm in diameter), stable and resistant to overcome several physiological barriers through the body to rich the site of interest and ultimately to be "inexpensive" to reduce health-care costs [10]; secondly upon entering the site to be treated, it is desirable that the therapeutic agent is released in a controlled fashion in order to reach cytotoxic levels and therefore to

achieve a stimuli-response release [11-14].

Liposome vesicles (Fig. 2.1), amphiphilic compounds with a lipophilic core and a hydrophilic interface, are the most widely employed carrier among the available systems for several reasons [15]: i) they are relatively easy to prepare, ii) they have dimensions down to tens of nm, iii) can carry a broad variety of drugs in their aqueous core, iv) can offer a relatively high drug payload, v) most of them are non-toxic and biocompatible, vi) their surface can easily modified with specific cell-targeted ligands, vii) they are prone to respond to external stimuli. As a whole they are therefore good candidates to fit the prerequisites listed before.

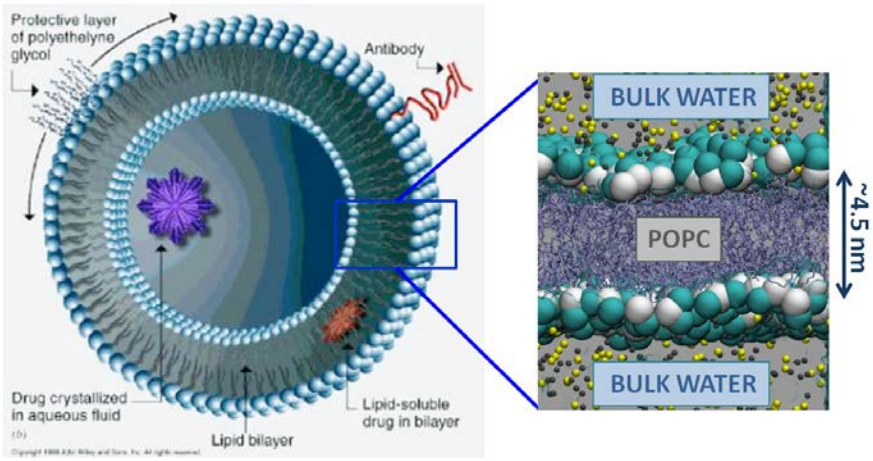

Figure 2.1: Liposome vesicle, with the detail of the amphiphilic bilayer main component: the hydrophilic polar head groups are reported in cyan and white spheres, the hydrophobic fatty acid tails in violet sticks, the water is transparent for simplicity of representation, the sodium ions in yellow balls and the chloride ones in gray

Responsive carriers are a major focus in emerging nanoscale technologies, in fact interest in stimuli-responsive systems has persisted over many decades and a great deal of work has been dedicated to developing environmental sensitive macromolecules. In all the cases the key parameter defining the responsive or 'smart' behavior of the system is a non-linear response to an external signal. However, the overwhelming majority of reports in the literature describe stimuli-responsive systems that are sensitive to only few common triggers, including changes in pH and/or temperature [16,17], magnetic [18] and sonic [19] fields and electrolyte concentration [20].

More recently attention has been focused on stimuli that have not yet been as heavily considered despite their unique potential and which may represent clear opportunities for making advances in biomedical fields [12]. In this scenario, an extremely interesting perspective for controlled drug delivery is based on tailoring smart carriers sensitive to external electric fields, in particular ultra short pulsed electric fields (usPEF) of high magnitude (few to several KV/cm) and extremely short duration (millisecond to nanoseconds), similar to those which produce reversible electroporation (EP) on cells [21]. As described in Section 2.1 the occurrence of structural changes in living cell following the application of

usPEFs take place primarily at the plasma membrane. Since the main constituent of the cell membrane are amphiphilic macromolecules of the same nature of those that compose liposome vesicles, the assumption that electric fields of high intensity and short duration, such as those employed for EP techniques, can also have similar effects on liposomes is plausible.

The main core of the present thesis is the study of the effects of usPEFs, on lipid bilayers. One part of this work focuses on the atomistic description of the interaction between such pulsed electric fields with models of cell membranes and liposomes, i.e. lipid bilayers. Another important part, on the design of exposure devices able to deliver usPEFs for *in vitro* experiments, to eventually validate our theoretical predictions. Therefore, in this Chapter an overview of the main applications of electroporation for medical purposes (Section 2.1), of the continuum and atomistic descriptions (Section 2.2) and of the common exposure systems (Section 2.3) is given.

2.1 Electroporation effects and applications

Electroporation (EP) of living cells and tissues is a widely used technique to enhance the permeabilization of these structures through their exposure to exogenous pulsed electric fields [22-25]. Indeed, numerous biological and medical applications to be efficacious require a local uptake of low-permeant molecules [26-29] (e.g. dyes, disaccharides, vitamins, anticancer drugs, pharmaceutical compounds, proteins, and genes).

Interestingly, the effects of usPEFs on tissues in general and on living cells in particular strongly depend on the pulse characteristics, as duration, amplitude and repetition frequency (see Fig. 2.2). Based on their effects, and therefore on their characteristics, the utilization of usPEFs on biological targets results in various biological and medical applications.

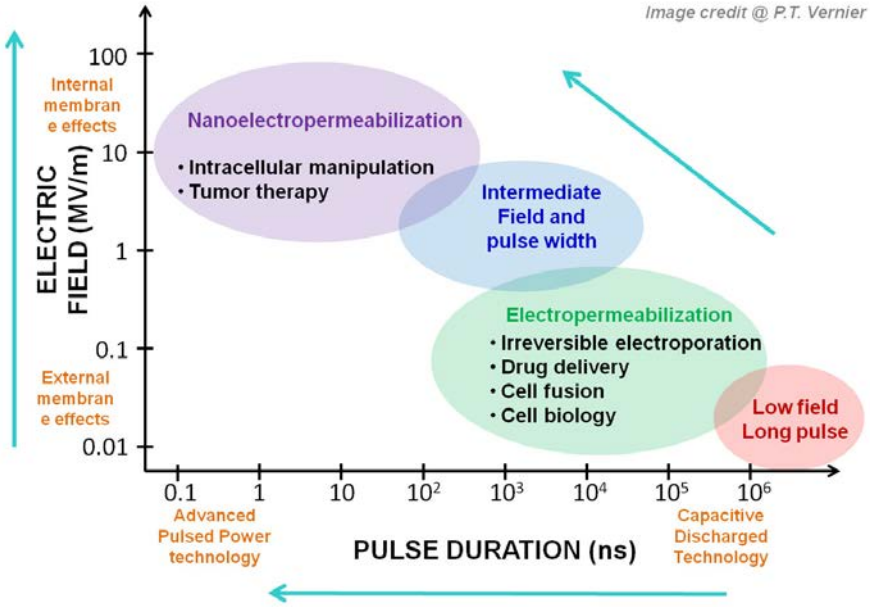

Figure 2.2: Applications of usPEFs over the pulse characteristics

In the past three decades traditional EP, which implies rather long pulses (duration from hundreds of microseconds to milliseconds) of low intensity (0.1-10 kV/cm) known as μs-msPEFs, has been efficiently used in biotechnologies and in various biomedical applications that range from calcium EP [30], electrochemotherapy (ECT) [31-33], DNA vaccination [34,35], gene therapy [36,37], and irreversible EP (IRE) [38]. More recently, developments in devices able to deliver shorter and more intense voltage signals allow the use of electric pulses with durations of less than 1 μs (down to few ns) of magnitude in the order of several hundred kV/cm, termed nsPEFs.

The principal difference between classic and nano-EP resides in the effects induced at the cellular and intracellular level: long, low magnitude pulses affect primarily the plasma membrane (Fig. 2.3), whereas can nsPEFs pass through the outer of the cell resulting in the

permeabilization of organelles. However, due to their concomitant effects on the plasma membrane these nanosecond, high intense electric pulses can also affect cell functions and are employed to promote phosphatidylserine externalization, apoptosis and cancer cell killing [39-41].

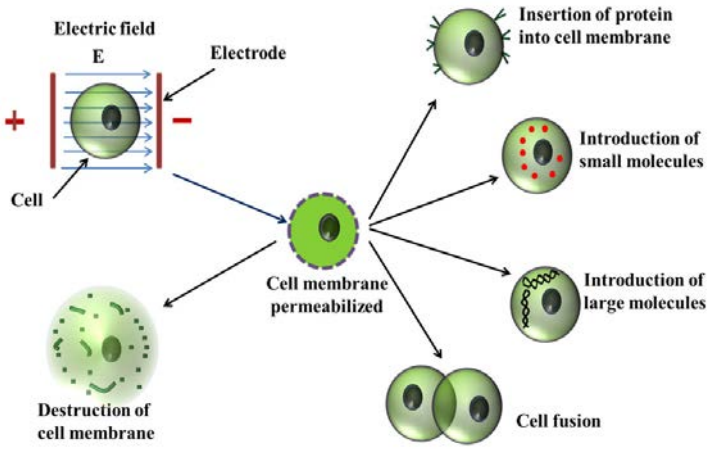

Figure 2.3: Effects on cells following the exposure to μs-msPEFs

2.1.1 μs-msPEFs: Traditional electroporation

The research on non-surgical and minimally invasive treatments of tumors or cardiac diseases has led to the development of new local ablation techniques based on electromagnetic fields. The aim of these non-invasive treatments is to limit surgery and reduce the pain, scarring and mortality of the patients while remaining cost-effective and safe. Initially developed for gene transfer, EP is now in use for delivery of a large variety of molecules: from ions to drugs, dyes, tracers, antibodies, and oligonucleotides to RNA and DNA [29]. Traditional EP has proven to be useful both *in vitro*, *in vivo* and *in patients*, where drug delivery to malignant tumors has been performed [26,21,32,35,42]. Whereas initial EP procedures caused considerable cell damage, developments over the past decades have led to sophistication of equipment and optimization of protocols.

Among the applications of EP in medicine we will briefly describe: i) ECT [31-33], ii) gene therapy [36,37], iii) IRE [38].

i) ELECTROCHEMOTHERAPY

ECT is a safe and efficacious technique for the treatment of solid tumors that couples electricity with anticancer drugs [31].

The chemical injected in ECT protocols are non-permeant or low permeant chemicals with a very high intracellular cytotoxicity. ECT uses electrical pulses to permeabilize the cells and enhance the activity of the anticancerous drug. Currently, the most commonly used drugs in ECT are bleomycin (non-permeant) and cisplatin (low permeant). One of the

most interesting features of ECT is its ability to selectively kill dividing cells, and therefore tumor cells, without harming normal quiescent surrounding tissue [32,33].

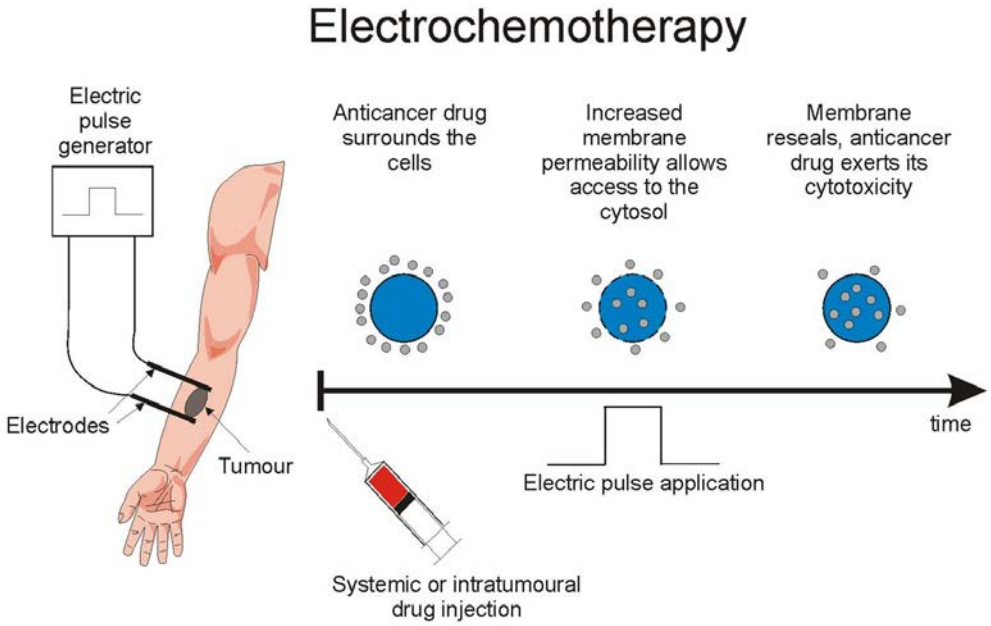

Figure 2.4: Schematic of the ECT procedure

ECT can only be efficient if all tumor cells are permeabilized, so the lesion needs to be entirely submitted to an electric field of sufficient amplitude. However, the electric field has to be as low as possible to ensure the safety of the procedure. Therefore, the design of the electrical parameters, of the electrodes and of their positioning must be accurately chosen such that recently patient specific treatments planning are available [43].

In 2005 and 2006, four of the leading centers in EP conducted a European clinical study on ECT called ESOPE (European Standard Operating Procedures of Electrochemotherapy) [44]. This study was necessary because of the need for a non-randomized, multi-institutional study. These clinical trials proved the efficiency of ECT with bleomycin or cisplatin for the treatment of cutaneous and subcutaneous tumors. According to standard operating procedures validated in the ESOPE project monopolar, direct current electric pulses are used. As shown in Fig. 2.4 the protocol consists in an injection of the antitumor drugs followed by the application of 8 monopolar 100 μs pulses with a repetition frequency ranging from 1 Hz to 5 kHz. Pulses are delivered through needle or plate electrodes with a fixed geometry (Fig. 2.5), the electric field is applied to each electrode couple in order to obtain an electric field in the tumor roughly equals to 400 V/cm [33]. The application of the pulses determines the membrane electropermeabilization with the insertion of the drugs into the cytosol of the cell. After the treatment, the cell recovers its previous state with the drugs trapped inside, expressing locally their cytotoxicity.

ii) GENE THERAPY

Plasmid vectors are composed entirely of covalently closed circles of double-stranded

Figure 2.5: Cliniporator, clinical equipment for ECT: pulse generator and series of standard electrodes for the local treatment of cutaneous and sub-cutaneous tumors

DNA with no associated proteins and therefore allow to avoid neutralizing effects of antibodies [36]. However, gene delivery with plasmid vectors is highly inefficient unless the DNA is either associated with other molecules and/or physical energy is applied to aid cell entry. The use of liposomes and dendrimer complexes has enhanced gene delivery to some tissues *in vivo*, but the most important improvement has been the use of physical delivery systems that enable plasmid-based gene delivery to reach efficiencies close to that achieved with viral vectors. The most substantial change in the efficiency of plasmid based gene transfer has been observed when delivery of plasmid is followed by the application of a series of electrical pulses as a form of *in vivo* EP with an increased gene expression by 100- to 1000-fold compared to injection of naked plasmid DNA [45]. The related mechanism hypnotized of uptake is pore-mediated which permits the insertion of the gene material inside the cell thanks to electrophoresis effects, thus occurring only when the electric field is applied. Given the above mentioned advantages of electrotransfer, it is likely that this method will soon be put to use also in the clinical setting.

iii) IRREVERSIBLE EP

By setting parameters of the pulses as suggested by Davalos et al. [46] and inducing a transmembrane potential high enough it is possible to ensure permanent permeabilization. The membrane is compromised to such an extent that cell death is inevitable. This technique has been used industrially for decades to sterilize food and liquids [47] and only recently considered as a potential ablation technique to treat several diseases in humans

[48,49]. The main advantage on current ablation technologies is that IRE does not need Joule heating or any thermal effect to destroy cells. Moreover, these pulses induce irrecoverable structural changes in the cell membranes only of the targeted tissue, with a sharp transition between normal and necrotic tissue, while preserving important components such as the extracellular matrix, major blood vessels, myelin sheaths and nerves.

2.1.2 nsPEFs: Recent applications and perspectives

The nsPEF experiments were made possible because of major improvements in the design of nanopulsers. Their fabrication is highly complicated due to the high voltages (several hundred kV/cm) and ultrashort duration (ns) needed, being the main challenge the delivery of a repeatable pulse with a minimum of oscillations and reflections in the waveform. For a detailed discussion on this technological issue see Section 2.3. These extremely short electrical pulses have attracted much attention during the last 10 years because they could represent a purely electrical cancer therapy that does not require drugs, hyperthermia, or local pH changes. It must be noted that the shorter the pulses, the higher the field strength necessary to observe the biological effects of nsPEFs. However, the energy transmitted to the treated area by the electric pulses is very low and leads to a very weak heating [50]. Despite the great deal in understanding the pore dimension, its lifetime and transport properties through the plasma cell membranes [40,51-53] caused by nsPEFs, they have been extensively investigated to trigger other effects. Indeed, nsPEFs allow the targeting of intracellular organelles, the initiation of apoptosis in cells, and the inhibition of tumor growth [41,54].

Among the effects of nsPEFs on living cells we will briefly describe: i) effect at the plasma membrane level, ii) intracellular effects, iii) impact on cell viability [55-57].

i) EFFECT AT THE PLASMA MEMBRANE LEVEL

Effects of electric field pulses on membrane permeabilization are are usually investigated indirectly through uptake of fluorescent molecules, which are able to pass or not this cell barrier. However, the molecules used in the early studies were too large for the porated membrane to allow their crossing in the case of submission of a reduced numbers of nsPEFs.

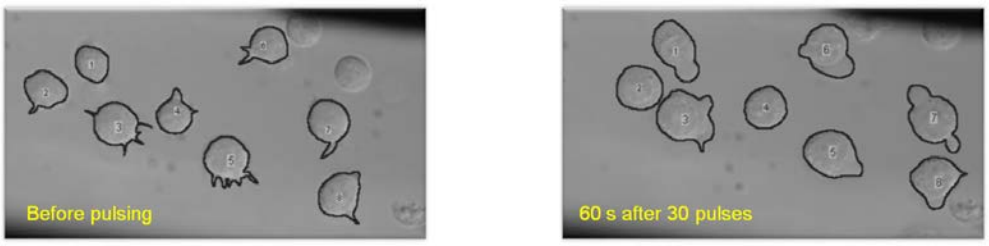

Figure 2.6: Images of Jurkat cells before (left) and 60 s after electric pulses exposure (right) in cell swelling experiment. Images were obtained from [61]

Since 2003 the possibility of nsPEFs to affect the plasma membrane has been supported by experimental observations [58,59], among which the phosphatidylserine (PS) externalization from the inner leaflet of the lipid bilayer to the outer leaflet, a marker of cell apoptosis [60]

Moreover, cell swelling (Fig. 2.6) and small molecules uptake (Fig. 2.7) were proved [40,51,53], showing that the mechanism undergoing μs-msPEFs permeablization takes place also under nsPEFs exposure. Nevertheless the debate on the pore size, its duration and uptake properties under this condition is still open.

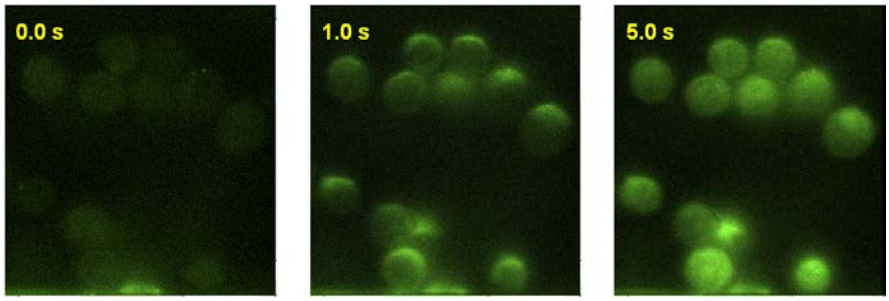

Figure 2.7: High-field, nanosecond pulses at high repetition rates permeabilize cell membranes, permitting entry of the small molecule YO-PRO-1 into the cell. Fluorescence microscopic images of Jurkat cells in growth medium containing YO-PRO-1 (5.0 μM) at 0.0, 1.0, and 5.0 s after exposure of the cells to 100, 4 ns, 8 MV/m pulses at a repetition rate of 1 kHz. Influx of YO-PRO-1 occurs primarily at the anode pole of the cells. Images were obtained from [40]

ii) INTRACELLULAR EFFECTS

nsPEFs were first considered for their potential selective effect on the inner organelles of the cell, e.g. endoplasmic reticulum and mitochondria, nuclei, Golgi vacuoles and secretory or endocytic vesicles [41]. Few studies have targeted the effect of nanosecond pulses on the cytoskeleton. Actin has been shown to stabilize the plasma membrane of plant cells during the application of nsPEFs and to act on its permeabilization [41].

The release of intra-cytoplasmic calcium (Fig. 2.8) has been specifically studied since it is present in organelles, mainly in the endoplasmic reticulum (ER) and mitochondria. Several works have shown a release of calcium independently of intra-cytoplasmic membrane calcium channels, which was thus directly linked to the destabilization of organelle envelopes by pulses shorter than 100 ns [56].

Effects of the nuclear envelope were reported indirectly by the ability to increase the level of plasmid expression following electrotransfection only when the intensity of the pulse is high enough [62]. However, so far there are no experiments that show the destabilization of the nuclear envelope itself by nsPEFs. This can be explained first by the size of the nucleus, which is much larger than that of other intracellular organelles and could prevent any effect of the nsPEFs on the nuclear envelope; second by the complexity of the envelope; and finally by the technical limitations of detection of this expected destabiliza-

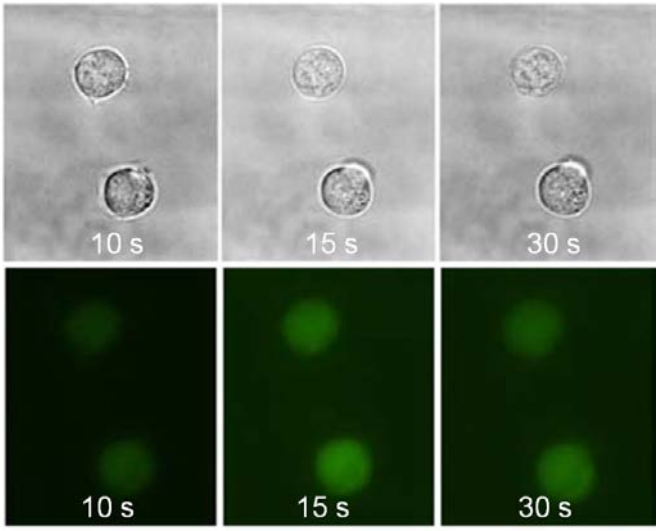

Figure 2.8: e
lectroperturbation]Real-time imaging of [Ca^{2+}] electroperturbation following the application of 10 pulses 30-ns, 2.5 MV/m [56]

tion

iii) IMPACT ON CELL VIABILITY

Because of their very short duration, nsPEFs do not transfer a large amount of energy to the sample and thus the observed effects are probably non-thermal. However, any impact on the external or internal membranes of the cell can profoundly affect its performance and therefore can cause its death. As previously described, nsPEFs could induce the destabilization of the internal membranes and cause the release of important intracellular mediators of cell signaling, or second messengers such as calcium.

Weaver el at. [63] reported that the initial effect of the application of the pulse could be the release of the calcium from the ER and also a flow of the Ca^{2+} from the external to the internal medium due to the EP of the external membrane. This determines calcium redistribution inside the cell. The calcium could enter in the mitochondria and cause the mitochondria destruction with the release of the cytochrome c and other molecules such as SMAC/Diablo, EndoG, and AIF that are signal for cell death.

However, the inability to systematically connect the release of these molecules to apoptosis prevents setting the direct involvement of nanosecond pulses in apoptosis.

Interestingly, it was suggested [41] that a precise adjustment of electrical parameters could help to destabilize cell membranes (internal and external) without causing cell death, using very short pulses (less than 10 ns) and moderate intensity (tens of kV/cm).

2.2 Theoretical descriptions of the electoporation process

Despite the large use of these techniques, the exact molecular description of the pore formation process, of its dimensions, shape, morphology, electrical and mechanical prosperities and molecules uptake remains not fully clarified because of the limitation in time and spatial resolution of the today experimental tools. One hypothesis regarding the molecular mechanism of EP is that the application of electrical pulses induces rearrangements of the membrane components (water and lipids) that ultimately lead to the formation of aqueous hydrophilic pores [64-67], whose presence increases substantially the ionic and molecular transport through the otherwise impermeable membranes. The pore existence was recently confirmed by [68]. In this work the authors showed for the first time the direct imaging of the ionic flux through individual electropores employing total internal reflection fluorescence. This approach yet does not allow straight visualization of the pore needed for a thorough characterization of the pore formation, of its dimensions, and of the mechanisms molecular transport.

Aside the experimental observations, atomistic and continuum models provided a dual and complementary view of the EP phenomena with different levels of spatial and temporal resolution.

Theoretical continuum models (see Subsection 2.2.1) of single cells or cell clusters neglect the molecular structure and the membrane is simply viewed as a thin homogenous dielectric layer surrounded by an electrolyte solution [24,69-73]. Such models constitute an important part of EP research as they enable the exploration on length scales (more than hundreds of micrometers) and time scales (seconds and more) currently not achievable by molecular dynamics (MD) simulations [74] or molecular models based on the mean field theory [75]. On the other hand, MD descriptions have proven to be effective in providing atomic insights (nanometer length range, hundreds of nanosecond time scale) into both the structure and the dynamics of model lipid membrane models. This tool can be used to investigate physiological [76-89] and exposure to usPEFs conditions, hence to study the following cascade of events taking place at the membrane level and providing perhaps the most complete molecular model of the EP process of complex bilayers (see Subsection 2.2.2 for a detailed review of the related state-of-the-art).

2.2.1 Continuum models

The general physical concept embedded in continuum EP models is rather simple: the transmembrane (TM) voltage, which is induced across the membrane by an electric pulse, reduces the energetic barrier for nucleation of small water pores in the lipid bilayer [24]. The induced TM voltage (more specifically the corresponding induced electric field in the membrane) provides a force which tends to expand the formed pores [90]. As the expanding pores start to conduct more and more ions, the voltage across the membrane effectively

reduces, which in turn limits further pore creation and expansion [91].

Going in the direction of a unified global comprehensive model integrating separate mechanisms, the multiple stages that follow the submission of cells and tissues to pulse electric fields, hence, must be taken into account to properly describe the EP phenomenon. More specifically, system-level model comprises separate mechanistic models for pore creation and destruction, pore expansion and contraction, electrical and electrodiffusive molecular transport in bulk electrolyte and through pores. Although the numerous model proposed to describe one or more of these aspects relay on assumptions and simplifications, they provide a means of breaking the complex process of EP of help to the interpretation of experimental findings. It is not the scope of the present work to review the works reported in the field, yet in the following an example of possible estimation of the pore energy and of the pore conductance will be briefly described.

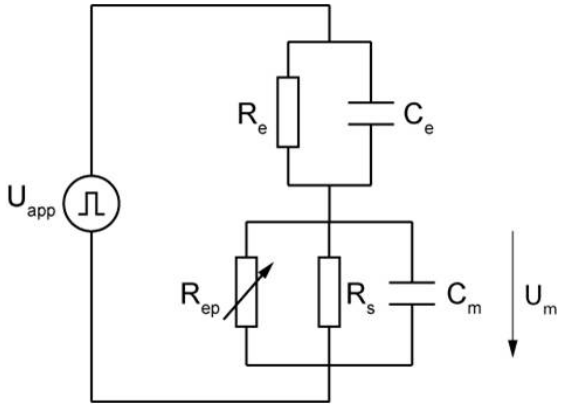

Figure 2.9: Equivalent electrical circuit of the membrane model [92]

The continuum model of EP reported below is taken from our work [92]. The membrane, surrounded by electrolyte solution, is represented by the equivalent circuit shown in Fig. 2.9, where R_e and C_e are the resistance and capacitance of the electrolyte, respectively, R_s and C_m are the static (passive) resistance and capacitance of the membrane, respectively, R_{ep} is the resistance of the electroporated areas of the membrane, U_{app} is the voltage of the applied electric pulse, and U_m is the TM voltage.

Using circuit analysis, the TM voltage can be expressed in terms of an ordinary differential equation:

$$(C_e + C_m)\frac{dU_m}{dt} = -(G_e + G_s + G_e p)U_m + C_e\frac{dU_{app}}{dt} + G_e U_{app}, \tag{2.1}$$

where the inverse of the resistance (the conductance) is denoted by G and the corresponding subscript.

The population of pores in the membrane is described by a distribution function n in the space of the pore radii such that $n\,dr_p$ corresponds to the number of pores between radii r_p and $r_p + dr_p$. The size dynamics of the population of pores n is described by the Smoluchowski equation.

$$\begin{aligned} \frac{\partial n}{\partial t} &= -\frac{\partial J_p}{\partial r_p} \\ J_p &= -D_p \frac{\partial n}{\partial r_p} - \frac{D_p}{kT} n \frac{\partial \Delta W}{\partial r_p}, \end{aligned} \tag{2.2}$$

where J_p denotes the flux of pores in the space of their radii, D_p the pore diffusion coefficient, k the Boltzmann constant, and T the temperature. ΔW is the change in the pore energy when the pore changes its size, with the reference energy given to the energy of a pore with the minimum possible pore radius $r_{p,min}$. The pore energy has two contributions $\Delta W = \Delta W_m + \Delta W_e$. The first is the mechanical contribution:

$$\Delta W_m = 2\pi\gamma(r_p - r_{p,min}) - \frac{\pi\Gamma}{2}(r_p^2 - r_{p,min}^2), \tag{2.3}$$

where γ and Γ denote the pore edge tension and the membrane surface tension, respectively. The second is the electrical contribution, which derives from the Maxwell stress tensor at the lipid-water interface and is calculated as the integral of the radial force acting to expand the pore.

$$\Delta W_e = -F_{max} U_m^2 \left[r_p - r_{p,min} + r_k \ln\left(\frac{r_{p,min} + r_t + r_k}{r_p + r_t + r_k} \right) \right]. \tag{2.4}$$

The Smoluchowski equation is solved in the space of pore radii where we define the maximum allowed pore radius at $r_{p,max} = 50$ nm.

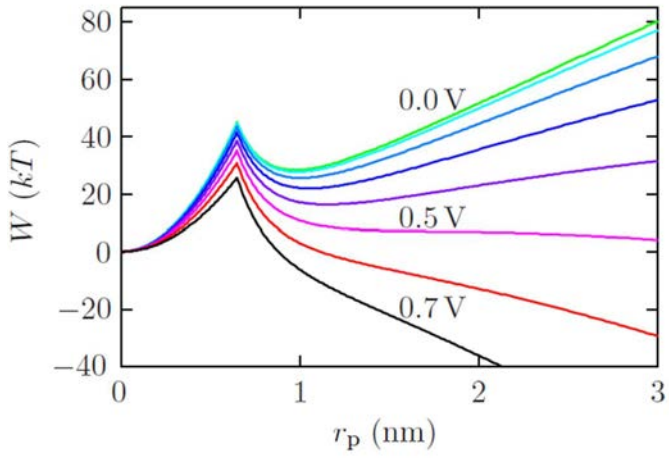

Figure 2.10: Energy functions of a transmembrane pore in different phases [93]. The trend from 0 to the local maximum in 0.8 nm corresponds to the energy function of a hydrophobic pore, the one from 0.8 to 3 nm corresponds to the energy function of a hydrophilic pore. The combined solid curves represents the overall energy function of a pore at different TM voltages (from 0 to 7 mV)

Figure 2.10 illustrates this energy landscape in the pore radius space. There are three

critical radii in the pore energy function W(kT): the first critical radius is located at the point where the energy of an hydrophobic pore equals the one for its hydrophilic (0.8 nm) state, thus this is the point where the phase transition occurs between the hydrophobic pore and the hydrophilic pore state; the second critical radius is located at the local minima (1 nm) and this being the equilibrium radius of the metastable hydrophilic pore state, i.e. for some voltages there are stable pores with fixed diameter; the third critical radius, not shown in the figure, is located at the local maximum and if the pore overcomes this threshold then the pore will keep expanding and eventually the rupture of the membrane (a process known as irreversible breakdown) will occur. Figure 2.10 also show how the value of the TM applied influences the pore stability and evolution.

Another relevant aspect of EP is the ability of the pore to conduct ions. The descriptions of pore conductance used in continuum EP models are more or less simplified analytical expressions which in their core derive from coupled Nernst-Planck and Poisson's equations. The Nernst-Planck equations describe the electro-diffusion of ions in terms of ionic concentration, where the driving force for the electrophoretic drift - the gradient in the electric potential - is given by the Poisson's equation, termed Poisson-Nernst-Planck (PNP).

The changes in the distribution of the population of pores in the membrane influence the conductance of the membrane. In the equivalent circuit in Fig. 2.9, the change in membrane conductance due to pores is represented by $G_{ep} = R_{ep}^{-1}$. G_{ep} is obtained by integrating the product of the distribution n and the conductance of a single pore G_p, which varies with the pore radius.

$$G_e p = -\int_{r_{p,min}}^{r_{p,max}} n G_p \, d\, r_p. \tag{2.5}$$

The general analytical description for conductance of cylindrical pores is:

$$\begin{aligned} G_p &= \frac{1}{R_{spd} + R_{int}} = \frac{2\pi\sigma_e r_p^2}{\pi r_p + 2d_m} \\ R_{spd} &= \frac{1}{2\sigma_e r_p} \\ R_{int} &= \frac{d_m}{\sigma_e \pi r_p^2}, \end{aligned} \tag{2.6}$$

where r_p is the pore radius, and σ_e is the conductance of the electrolyte inside the pore. When the conductivities of the electrolyte solutions on either side of the membrane are different, σ_e needs to be replaced by effective conductivity of the solution inside the pore. $R_s pd$ is the spreading (also access or input) resistance and accounts for the voltage drop at the pore entrance, whereas R_{int} is the resistance of the pore interior region and accounts

for the voltage drop across the central region of the pore.

Figure 2.11 shows and example of pore conductance as a function of the radius evaluated with the PNP model and compared to MD results. For more details and discussions we refer to our work [92].

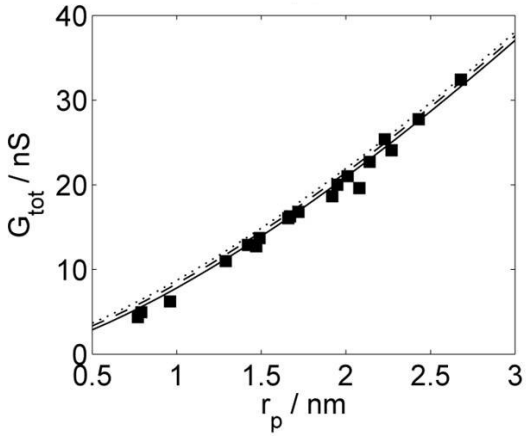

Figure 2.11: Results obtained with PNP model with surface charge and fluid flow [92]. Results on total pore conductance from MD are shown in black squares

The latter results are also indicative of the fact that MD simulations and continuum models are complementary descriptions of the same phenomenon. If on one hand direct comparison of atomistic simulation results at the bilayer level with experimental EP observation is challenging [94,95], on the other analytical and numerical approaches are often based on assumption and simplifications, or on empirical estimation of the parameters used to describe EP phenomena [96-99]. Hence, to generate better cell level models it is crucial to use atom level insights from MD simulations of membrane models and vice versa, to access experimental scale results, MD observations need as intermediate step cell descriptions.

Therefore MD simulations and continuum models should be coupled to give not only qualitative but also quantitative insights and predictions on many aspects of EP, such as estimation of cell electrical parameters (e.g. permittivity of the bilayer and of the water/lipid interface), variation of TM voltage due to pore formation, recovery of the kinetic coefficients used in the equations describing pore evolution, electropore transport of ions and molecules, quantification of pore dimension and density distribution, ... Recently, few works [92,100-102] addressed some of these aspects with a bottom up approach initiating a line of research that will be of fundamental importance in the near future to build a complex, robust, reliable, quantitative and predictive multi-scale model of EP.

2.2.2 Atomic representations

Molecular dynamic (MD) simulations are an extremely powerful tool of accompaniment and support to continuum models and experimental observations, providing inaccessible atomic insights that allow to shed light on molecular mechanisms and to suggest improvement to related technologies. MD simulation methods, see Chapter 3 for more information, have been devised to perform *in silico* experiments of membranes subject to nanosecond megavolt-per-meter pulsed electric fields and of membranes subject to charge imbalance, mimicking therefore the application of low voltage and relative long duration pulses.

2.2.2.1 Modeling membrane electroporation

As biological membranes have a very complex structure and can contain hundreds of different lipid species and proteins, most MD studies have focused their attention on lipid bilayers in their biologically relevant liquid-crystalline state [76]. From both a theoretical and an experimental perspective, zwitterionic phosphatidylcholine (PC) lipid bilayers constitute the best characterized systems (see Fig. 2.12). Despite their simplicity, bilayers built from PC lipids represent remarkable test systems to probe the computation methodology and to gain additional insight into the physical properties of membranes.

The effects of an electric field on a cell may be described considering the latter as a dielectric layer (cell surface membrane) embedded in conductive media (internal: cytoplasm and external: extracellular media). When relatively low-field (kV/cm) pulses of microsecond or millisecond duration (μs-msPEFs) are applied to this cell (by placing for instance the cell between two electrodes and applying a constant voltage pulse) the resulting current causes accumulation of electrical charges at both sides of the cell membrane. The time required to charge the surface membrane is dependent upon the electrical parameters of the medium in which it is suspended. For a spherical cell it is estimated using equivalent network RC circuits in the hundred of ns time scale [39,54,103-105]. If on the other hand, the intense (100s kV/cm) pulse has a duration short enough (typically few nanosecond long) relative to the charging time constant of the resistive-capacitive network formed by the conductive intracellular and extracellular fluids and the cell membrane dielectric, which is the case for nanosecond pulses (nsPEFs), then the electric field acts directly and mainly on the interface of cell membrane.

Simulations allow to perform *in silico* experiments under both conditions, i.e. submitting the system either to nanosecond, megavolt-per-meter pulsed electric fields (2.2.2.1) or to charge imbalance, mimicking therefore the application of low voltage - long duration pulses (2.2.2.1) [106].

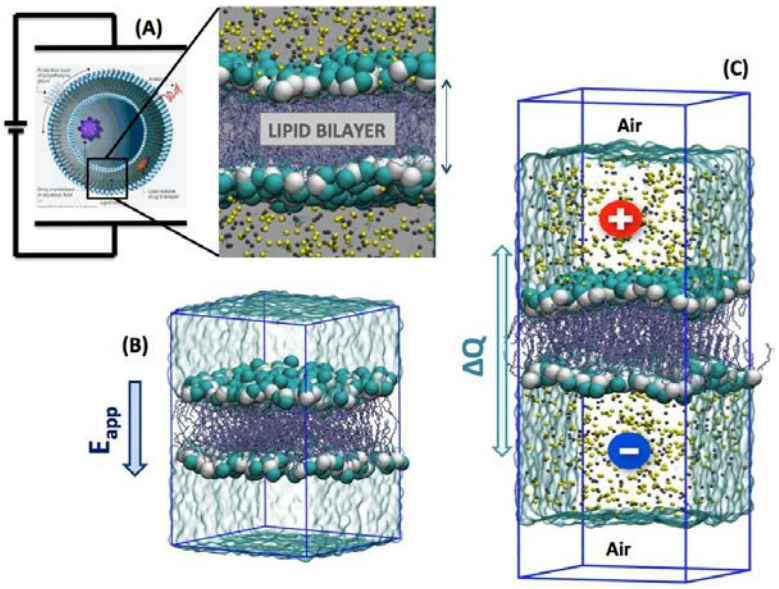

Figure 2.12: Protocols for atomistic modeling of cell membranes or liposomes lipid bilayers (A) electroporation. (B) To model the nsPEFs, the bilayer is considered without salt concentration and subject to an electric field (force acting on the charged particles). (C) For the μ-msPEFs, the bilayer, at a given salt concentration is set at a constant charge imbalance ΔQ, induced by a net difference between the charges located at both sides of the lipid leaflets. The simulation box (in blue) is in this case extended to include an air slab preventing ions from migrating through the periodic boundary conditions

Mimicking nsPEFs: EP induced by the direct application of an electric field

The protocol used to model the application of nsPEFs in simulations is to apply "directly" a constant electric field E_{app} perpendicular to the lipid bilayer plane [107-109]. Usually, the lipid bilayers in this conditions are modeled without consideration of a salt concentration. Indeed, the applied electric field acts primarily on the interfacial water dipoles. Within a very short time scale - typically few picoseconds [110] - the transverse field E_{app} induces an overall TM voltage across the bilayer (Fig. 2.13 b [106]).

This can be characterized by evaluating the electrostatic potential Φ(z) along the normal to the bilayer z (Fig. 2.13 a), usually evaluated by solving Poisson's equation (2.7), i.e. the double integral of the volume charge density distribution ρ, being ϵ_0 the vacuum permittivity:

$$\phi(z) = \phi(z) - \phi_0 = -\frac{1}{\epsilon_0} \int_0^z \rho(z'') dz'' dz' \tag{2.7}$$

U_m is defined as the difference between the electrostatic potential at the lower and the upper baths of the bilayer.

Note that, the E_{app}, because of the MD simulation setup and the use of PBCs, induces a voltage difference $U_m = L_z|E_{app}|$over the whole system, where L_z is the size of the simu-

lation box in the field direction [109-111].

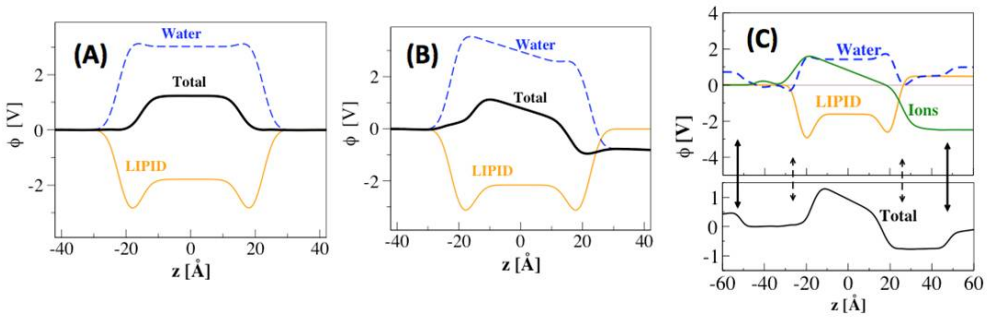

Figure 2.13: Electrostatic potential profiles ϕ(z) along the membrane normal z of a POPC lipid bilayer (A) at rest and (B) subject to a transverse electric field E_{app} and (C) bilayer set with a charge imbalance (μs-msPEF protocol). z = 0 represents the centre of the lipid bilayer. Are shown the contributions to the electrostatic profile from water (blue), lipid (yellow), ions (green) and total (black). The dashed arrows indicate the positions of the lipid/water interfaces and the solid arrows the position of the water/air interfaces. Note that the TM voltage U_m (potential difference between the upper and lower water baths) in the nsPEF protocol is mainly due to water dipoles reorientation, while it is mainly due to the charge (ions) distribution in the μsmsPEF protocol

The E_{app} can be either constant, as most of the works reported, or can vary over time [102,103,113-115].

Mimicking μs-msPEFs: EP induced by ionic salt concentration gradients

The charge imbalance method [117-120,106] is usually employed to model low magnitude ms or μs pulses on the bilayers, building a $U_m$across the lipid bilayer by displacing a net difference of charges form one bath to the other.

In order to ensure the charge imbalance between the two sides of the membrane and avoid ion translocation through the 3d-PBCs two solutions have been proposed: a double bilayer scheme [117-119,121,122], and single bilayer scheme [106,120]. The first method generates potential gradients by a charge imbalance across lipid bilayers by considering a MD unit cell composed of three salt-water baths separated by two bilayers and 3d-PBCs, resulting in a quite expensive setup in terms of computer power. On the contrary, the latter method is less consuming and requires modeling the bilayer surrounded by a slab of vacuum so that the upper and lower water baths are separated.

In both cases, the system can then be subject to voltage (Fig. 2.13 C) by setting a charge imbalance ΔQ between lower and upper baths (typically by displacing individual ions between the baths). Note that the minimum voltage that can be generated using this protocol (by setting a +2e charge imbalance) depends on the size ($L_x \cdot L_y$) of the system.

Using the charge imbalance setup, it was possible for the first time to directly demon-

strate *in silico* that the simulated lipid bilayer behaves as a capacitor [106,123-126]. Simulations at various charge imbalances ΔQ show a linear variation of U_m from which the capacitance can be estimated as $C_{sp} = Q_s/U_m$, where Q_s is the charge imbalance per unit area. The capacitance values extracted from simulations are expected to depend on the lipid composition (charged or not) and on the force field parameters used and as such constitutes a supplementary way of checking the accuracy of lipid force field parameters used in the simulation. In Table 2.1 are reported values of C_{sp} from different works.

System	Salt concentration	T/K	C_{sp}
POPC [106]	1.00 M - NaCl	300	0.85
POPS [123]	0.25 M - NaCl	300	0.41
DPPC [124]	0.45 M - KCl	323	0.94
DPhPC-ester [124]	0.45 M - KCl	323	0.93
DPhPC-ether [124]	0.45 M - KCl	323	0.90
Archaeal [125]	0.45 M - KCl	298, 323	0.67, 0.72
DPPC + 50 mol % Archaeal [125]	0.45 M - KCl	298, 323	0.68, 068
POPC + 10 mol % $C_{12}E_8$ [126]	0.10 M - KCl	298	0.63

Table 2.1: Specific capacitance of different bilayers, evaluated as $C_{sp} = Q_s/U_m$, with A/Å^2 the area of the bilayer patch, and Q_s the charge imbalance per unit area

For large enough induced TM voltages, the two protocols lead to EP of the lipid bilayer. Qualitatively, in both methods, the cascade of events following the application of a high enough TM voltage is similar [106,127]. Using these two approaches it was possible to investigate the mechanisms of pore formation [87,94,95,111,110,118,128-134], the so called pore life cycle [135,136], the role of interfacial water [112,137,138], of different lipids [111,112,123-125,139-143] and different permeation properties [110,144-146], complex bilayer compositions [126,147-152], the pore characterization in terms of size and conductance [61,153-155], and the transport small molecules [42,60,127,156,157].

2.2.2.2 Pore creation and evolution

From the precursory MD studies on EP, the pore formation and evolution have been studied by several groups [110,111,118], and its detailed life cycle was proposed by [135]. All these works suggested that pore creation time strongly depends on gradient of the electric field across the membrane interface, which increases with the increase of the TM voltage applied [131,135,138,143].

Indeed, pores form from small water bumps, which occur more commonly near head group defects, where the choline group of the lipid is located nearer the glycerol backbone region than normal. Hence, water molecules initially restrained to the interfacial region are subject to a high electric field (Fig. 2.14 [106]) and therefore inclined to orient their dipole along this local field in order to minimize the total free energy of the system [138].

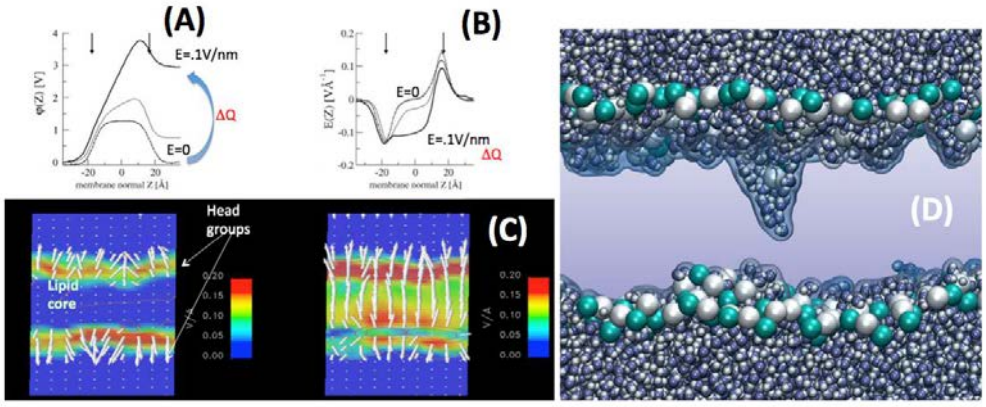

Figure 2.14: (A) Electrostatic potential profiles across a lipid bilayer subject to electric fields of 0 V/nm (dotted line) 0.06 V/nm (thin line) and 0.30 V/nm (bold line), or to a charge imbalances ΔQ. (B) Corresponding electric field profiles. (C) 2d (out of plane) maps of the electric field distribution. The local electric field direction and strength are displayed as white arrows. Note that at 0 mV, due to the bilayer dipole potential at rest, the larger electric fields are located at the lipid water interfaces and are oriented toward the solvent, and no electric field is present in the lipid core. When the bilayer is subject to a TM potential, a net electric field appears in the hydrocarbon region. The latter promotes dipolar orientation and penetration of water molecules (D) inside the bilayer

These molecules can easily hydrogen bond among themselves, which results in the creation of single water files. Such fingers protrude through the hydrophobic core from both sides of the membrane. Finally, these fingers merge to form water columns (often termed pre-pores or hydrophobic pores) that span the membrane (Fig. 2.15). As the TM voltage is maintained, these water wires appear to be able to overcome the free energy barrier associated to the formation of a single file of water molecules spanning the bilayer (estimated to be 108 kJ/mol in the absence of external electric field [158]). As the electrical stress is maintained, lipid head groups migrate along the water column and participate in the formation of larger and more stable "hydrophilic pores", able to conduct ions and larger molecules as they expand.

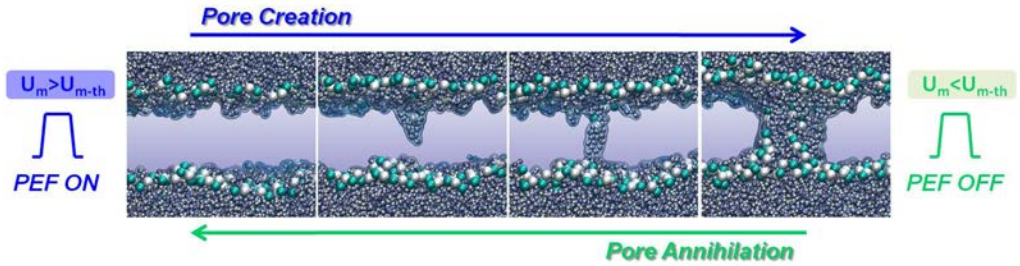

Figure 2.15: Pore evolution in a POPC bilayer: the POPC head groups are shown as cyan and white beads, the tails are shown as purple sticks or transparent; sodium and chloride ions are colored in yellow and gray; water is transparent

An added information coming from the charge imbalance schemes is the ion conduction through the hydrophilic pores that occurs as a consequence of the pore opening. The

MD simulations of the double bilayer system [118,119], and the results for the single bilayer setup [106] show that both cations and anions exchange through the pore between the two baths, with an overall flux of charges directed toward a decrease of the charge imbalance. Ions translocation through the pores from one bulk region to the other leads to a decrease of the charge imbalance and hence to the collapse of U_m. Hence, when the charge imbalance reaches a level where the TM voltage is down to a couple of hundred mV, the hydrophilic pores "close" in the sense that no more ionic translocation occurs.

The process of pore resealing from MD simulations [110,119,135] is reported to be the opposite mechanism as opening, with the head groups exiting the pore first, leaving shortly a water wire across the hydrophobic core, which then collapses. The resealing process is almost independent on the magnitude of the pore initiation electric fields and in general the complete recovery of the original bilayer structure requires a much longer time scale [135,143]. The molecular mechanism for pore closure is as much relevant as pore initiation. Indeed, to minimize leakage from non-targeted cells and to maximize the delivery of charged molecules into the targeted ones is fundamental the understanding of the pore lifetime which spans from nanoseconds to hundreds of nanoseconds and depend critically on the structure of the bilayer [134].

Finally addition of salt to systems undergoing the nsPEF protocol has been shown, quite interestingly, to modulate the characteristic time scales of the whole life cycle [136,159].

Role of the interfacial water and of the lipds head groups

It is evident how the driving component for pore formation is the orientation and motion of dipoles, water molecules and lipid head groups, in the intense field gradients at the interface [110,111] shown in Fig. 2.16 B.

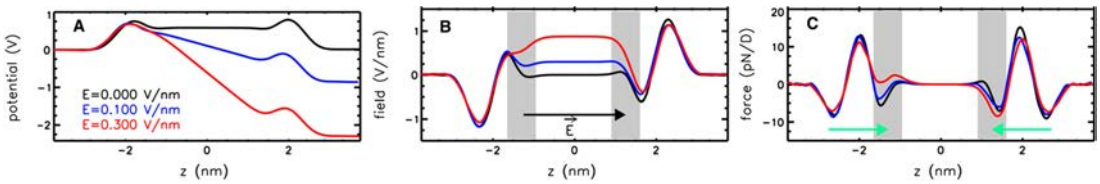

Figure 2.16: Electrostatic potential (A), field strength (B), and force on a dipole of strength 1 Debye (C) across the lipid bilayer for three different field strengths [94]

This gradient is always present at the interface, even in rest conditions, yet it is balanced by other forces that guaranties stability to the interface [94,112], as shown in Fig. 2.16 C black curve. Conversely, when the pulsed electric field is applied the system of forces acting at the interface is not balance and pore formation allows to minimize the total free energy of the system when subject to an exogenous electric field [138].

From several studies [94,110-112,137] it emerges that the key role in the pore creation is played by the interfacial water, and a detailed discussion on the energy minimization

of water orientation in high electric field at membrane interface can be found in [138]. At rest condition water dipoles at the two sides of the interface oriented through opposite directions (Fig. 2.17) with their hydrogen atoms pointing to the membrane interior.

When the charge imbalance or the electric field are applied the water dipoles reorient fast (ps) at the two leaflets of the interface in a different manner (Fig. 2.17): at the anode side of the bilayer ($z < 0$) the dipolar orientation is reinforced, where as is randomized at the cathode one ($z > 0$), since water at this leaflet is forced to reverse its orientation according to the applied field. Therefore the water at the cathode are dielectrophoretically drag towards the bilayer interior by a force F_z (Fig. 2.16) proportional to the electric field gradient (∇E_z/V/m^2) and to the dipole moment (M_z/Cm), $F_z = M_z \cdot \nabla E_z$.

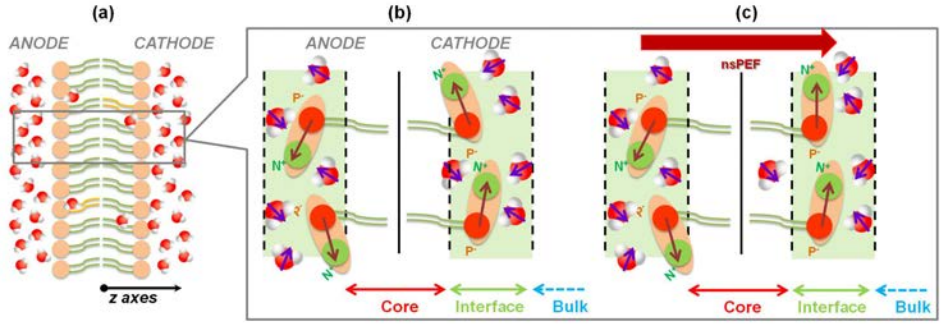

Figure 2.17: Dipolar orientation of the lipid head groups and interfacial water. (a) Schematic of an hydrated lipid bilayer, (b) of the dipolar orientation at rest ad (c) after the application of an electric field in the direction perpendicular to the bilayer (z)

To further support the importance of water orientation in EP recent coarse-grained models, that take into account the dipolar behavior of these molecules, have proven to be able to capture EP of lipid bilayers [122,147]. Ziegler et al. [112] also suggest that head groups tilt is not a determinant factor in the EP process. They calculated the head group dipole tilt angle distribution for different lipid bilayers rest and at minimum porating field conditions reporting a change in the mean head group dipole angle of few degrees in the field direction. This observation was also supported by other studies [94,149]. The general assumption that the lipid head groups have a marginal role in the electropore formation is also suggested by studies on octane slabs EP [111,141] and even vacuum slabs [143]. In this latter case it was shown that the dynamics of water bridge formation in a water-vacuum-water system is similar to water-lipid-water schemes, and both exhibit an exponential decrease in water bridge initiation time with increasing external electric field.

Nevertheless the nature of the lipid is extremely important when looking at other factors than pore formation. From what reported, one can draw the following conclusions regarding the roles played by the hydrophobic core of the bilayer and by its polar head groups: i) when other molecules are present the may lead to formation of defects that prompt pore formation [146] or to stable complexes that inhibit it [110], as discussed in Subsection 2.2.2.3-*EP thresholds*; ii) tune the EP threshold [112,124-126,149], see Subsection 2.2.2.3-*EP thresholds*; iii) stabilize or destabilize water columns resulting in hydrophilic

or hydrophobic pores [123,125], as reported in Subsection 2.2.2.3-*Pore features*; iv) slow down the process of resealing [131,143], as previously described.

2.2.2.3 Complex membrane models

To tune EP applications in biotechnologies and in other areas such as smart drug delivery it is required to characterize the EP threshold in terms of filed magnitude to be applied. Indeed, on one hand it is desirable to maintain a high cell viability in reversible EP applications by maintain the electric field intensity as low as possible, on the other it would be also advantageous for instance to create stable carries (higher EP threshold) for drug delivery applications where the release of their load mediated by EP takes place in the proper location and the electric field applied must be high enough to grantee such targeting.

EP thresholds

From the pioneering works of Tieleman [111] and Tarek [110], which considered simple lipid double layers of 1,2-dioleoyl-sn-glycero-3-phosphocholine (DOPC) and dimyristoylphosphatidylcholine (DMPC) respectively, a variety of bilayers have been considered.

Among the parameters that influences the EP threshold the thickness of the bilayer was one of the first to be reported. In 2007 Ziegler and Vernier [112] observed that the minimum porating external field to be applied increased with the increasing of the bilayer thickness, suggesting that the thinner the lipid slab the more probable the formation of water wire bridges.

The rise of the threshold due to the cholesterol condensing effect was suggested in 2004 [111], than confirmed in [149]. A steady increase of threshold with the cholesterol concentration was observed using the nsPEF protocol: two folds higher electric field was necessary for poration of bilayers with a cholesterol content of 50 mol% with respect to pure lipid one.

The addition of particular chemicals such as dimethyl sulfoxide (DMSO) to the medium halves the minimum electric field required to electroporate both pure lipid and cholesterol reach bilayers [146]. The authors, to explain this favorable effect, suggested a synergy of three cofactors: i) the amphiphilic character and small dimension of DMSO molecules permit to be located at the lipid-water interface, therefore decreasing the negative lateral pressure peak that compacts the bilayer structure and facilitating the intrusion of water fluctuations into the lipid membrane; ii) DMSO strongly alters the electrostatic membrane profile due to its intrinsic dipole moment facilitating the initial stages of EP; iii) DMSO acts as a surfactant and relaxes the surface tension when the hydrophobic water pore is formed.

In a series of three papers [124-126] Tarek's group also investigated the effect on the EP threshold of surfactants, ester and ether links, of branched tails, and of bulky head groups reporting respectively an increasing in the electric field threshold, respectively. The ability

of surfactants, in the particular case of polyoxyethylene glycol ($C_{12}E_8$) molecules [126], to lower the electric field intensity for pore creation are related to the high mobility of such compounds and to their hydrophilic head group moiety which affect the intrinsic properties of the host bilayer, facilitating water intrusion. The authors have found that the EP threshold of a lipid bilayer depends not only on the "electrical" properties of the membrane, i.e. its dipole potential, or membrane capacitance, but also on the properties of its components' hydrophobic tails. Specifically, the lateral pressure in the region of the hydrophobic was shown to somehow correlate with the increase in the EP threshold: An increase of the later pressure hinders the local diffusion of water molecules toward the interior of the hydrophobic core in the branched lipid membrane compared with the simple lipid bilayers, increasing therefore the electroporation threshold.

Simulations of bacteria like membranes EP [151] also show that bilayer with smaller head groups (S. aureus) are less resistant to poration than the one with reduced mobility due to the hindrance effect of massive head groups moieties (E. coli).

Reigada in 2014 [152] extended these findings by looking at the EP of heterogeneous bilayers, considering patches containing liquid order and liquid disordered domains. The main findings can be summarized as follows: the electric field mainly affects the properties of the disordered phases, so that EP takes place in these membrane regions without affecting the edges between the two phases; secondly, the smaller the disordered domains are, the faster they become electroporated, due to their ability to form conical water defects which are favorable nucleation sites for EP.

Generally, one can say that an increase of the stiffness of the bilayer results in rise of the EP threshold. This was further supported by Sun et al. [142] by artificially constrain the head groups moieties and the lipid tails independently. It was observed that only constraints on lateral motions of lipid tails prohibited EP while non-tail parts had little effects. Moreover, the effect of thermal motion of lipids was reported to induce initial defects in the hydrophobic core of membrane, again considered sites of high probability of pore creation. Their simulations also suggested that an increase in temperature will be followed by a reduction in the time taken to the initial pore formation.

Finally the presence of impurities, chemical agents and compounds can modify the permeation properties of membrane models acting on their stability. In 2005 Tarek [110] showed that a peptide nanotube channel stabilizes the lipids in its proximity with strong hydrogen bonds, thus no pore formation close to the peptide channel was observed. In contrast, if the bilayer is pre-embedded with water, that could be an effect of sonoporation, a decrease in the EP threshold was registered [145]. The same favorable trend follows the oxidation of membrane components [144] which enhances the susceptibility of the membrane to electropermeabilization.

Pore features

The stages of pore evolution following the application of the exogenous electric field, described in detail in Subsection 2.2.2.2, support the hypothesis that the cell membrane is permeabilized by the formation of conducting hydrophilic pores, then stabilized by the lipid head groups which surround the water column in a wall like feature. Vernier's group [143] showed that interactions between the water and the surrounding lipids and among the pore lipids themselves contribute to the stabilization of the pore. Therefore, the properties of the lipids play a determinant role in the lifetime and in the structural characteristic (e.g. size, shape, morphology) of electropores.

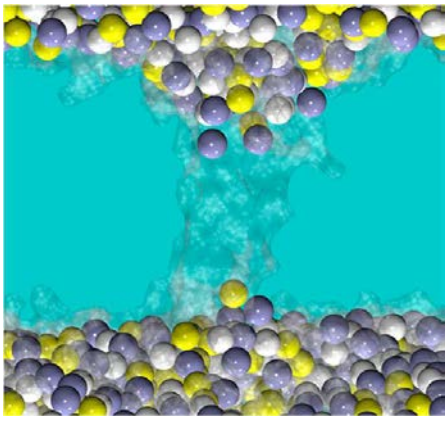

Figure 2.18: Hydrophilic pores in a POPS bilayer [123]: the headgroups do not stabilize the water column for several nanoseconds

Few other studies considering various lipid bilayers challenged the standard representation of pore formation. Indeed, Tarek and coauthors [123,125] pointed out that a peculiar EP process may be possible in which large long living ion-conducting water columns not stabilized by lipid head groups dwell in the bilayer's interior. These "hydrophobic" conducting pores originate from constrains of different nature in the lipid bilayer hypobaric core. The first report [123] concerned a palmitoyl-oleyl-phosphatidylserine (POPS) bilayer characterized by negatively charged head groups. When these system was subject to a charge imbalance high enough to electroporate the bilayer the migration of lipids along the initial water wires turn out to be largely hindered (Fig. 2.19). Similar conclusions were drown when archaeal lipids [125] were modeled.

This peculiar morphology was ascribed to the repulsion of negatively charged head groups in the first case [123] and to the steric hindrance of the bulky head groups coupled with the branched tails in the latter [125]. In 2004 Tieleman [111] already predicted that cumbersome moieties (e.g. coating polymers) would still allow the bridge of water fingers across the core, but that the movement of lipid head groups along the water column would be frustrated. This scenario appears to hold for many "stiff" molecule embedded in the membrane.

One other aspect of electropores morphology was recently outlined by Gurtovenko et

al. in 2014 [148] who carried out simulations of asymmetric model membranes to simulate the outer and inner leaflets of plasma membranes composed by of phosphatidylcholine (PC) and phosphatidylethanolamine (PE) lipid monolayers. The initial step of water bridge formation appears to be asymmetric taking place on the PC side of the PC/PE double layer. The authors reported that changes in the lateral pressure profile induced by the eclectic field were more significant in the PC leaflet, and meaningful of a decrease in its cohesion thus showing a more robust response of the PE leaflet most probably thanks to interlipid hydrogen bonding.

Remarkably, the EP of cell membranes and of liposomes used as drug delivery agents, appears to be possibly tuned by the specific lipid composition, including the nature of the lipids, addition of surfactants, polymers, disaccharides ... The characterization of such morphologies and as well as the evaluation of electroporation thresholds, is a requisite to the understanding and tuning of different biotechnological or biomedical applications.

2.2.2.4 Transport through electropores

The ultimate goal of most EP applications is the efficient transport of ions and molecules, e.g. drugs, genetic material, dyes, ... through cell membranes electropores [29]. In spite of the great interest in understanding the mechanism underlying the passage of different compounds in and out cells, little is known with atomic resolution. In the following, we report on the main insights provided by MD simulations.

Pore stabilization

When dealing with the characteristics of electropores (e.g. size, conductance, transport of molecules) one would expect the pore to be in this energetically favorable state, that could correspond to a stable configuration. In order to first understand if for a given TM voltage the pore can be considered in a steady state and second to quantify its size and conductance the two MD procedure explained in Subsection 2.2.2.1 need to be improved.

The main drawback of the these protocols resides in the impossibility of maintaining a steady pore: in the nsPEF method the pore tends to expand above the dimension of the simulation cell box leading in the brake down of the bilayer; while the μs-msPEF one results in pore resealing once the ions flow through the water bridge with a consequent TM voltage drop below the threshold. To enhance the nsPEF protocol, Fernandez et al. [154] proposed a new simulation procedure where an initially high porating field is reduced after pore creation to lower stabilizing values resulting in stable, size-controlled electropores. In the following Subsections MD results will be illustrated on independent measurements of the pore size, ion conductance and transport of small charged molecules caused by electric pulses mimicked using the standard charge imbalance schemes, as well the canonical and enhanced direct electric field application procedures.

Pore Characterization

A first attempt of to link experimental evidences of pore conductance and radius estimation using linear rising current technique combined with MD simulations performed under similar conditions was carried out by Kramar et al. [153]. Their findings suggested that the opening and closing of a single pore of conductance in the 100-nS scale would be possible for a pore diameter of 5 nm. More systematic investigations, conducted with the enhanced nsPEF [154,155] protocol, allowed to address the question regarding the possible stability of the water pores formed in lipid bilayers: under constant TM voltages the pore formed could be stabilized to different radii for tens of ns. The value of the radius obtained at a given sustaining voltage was shown to be independent from the porating one [154]. For "high" voltages applied the pore eventually expand leading to instability of the bilayer while for "low" voltages pore closure is observed. Notice that the values of the TM voltages are purely indicative since they are system dependent and, as explained in Subsection 2.2.2.3-*Pore Features*, the pore lifetime and structural characteristics are strictly related to the composition of the bilayer.

Quite interestingly the relation between the voltage applied and the pore dimension and therefore between the radius and the conductance is almost linear: in [155] (pure POPC bilayer in a salt solution of 0.1 M NaCl) for a voltage ranging from 0.56 to 1.12 V the pore radius is 0.68-1.50 nm and the conductance 5.48-27.88 nS/M.

Moreover, the pores were found to be more selective to cations than to anions [29,38]. This selectivity arises from the nature of the lipid molecules constituting the pore: the negatively charged phosphate groups that form the walls of the pore attract sodium ions, which hinders their passage across the bilayer, but also makes the pore interior electrostatically unfavorable for other sodium ions [89].

This, already, suggests that the pore transport is sensitive to the type of solutes, showing a different affinity for different charged species.

Transport of molecules

Although numerous bioactive molecules are involved in EP of living cells and in its applications (e.g. ions, drugs, genetic material, dyes, ATP, ...), among them only few where studied with MD.

Starting from lipid molecules, it was shown that under nsPEF they can translocate by diffusion through water-filled nanopores [157], that is of profound interest if one thinks about the cascade of events that can follow the intern/externalization of specific molecules such as phosphatidylserine (PS). Externalization PS [60], a phospholipid usually confined to the inner leaflet of the plasma membrane, that can trigger several recognition, binding and signaling functions, among which cell apoptosis. For this reason a lot of attention was

focused on the MD study of PS translocation in electroporated bilayers [103,113,127,140], that showed how PS externalization is a pore-mediated event since requires pore formation occurring exclusively though it with an electrophoretic drag at the anode side.

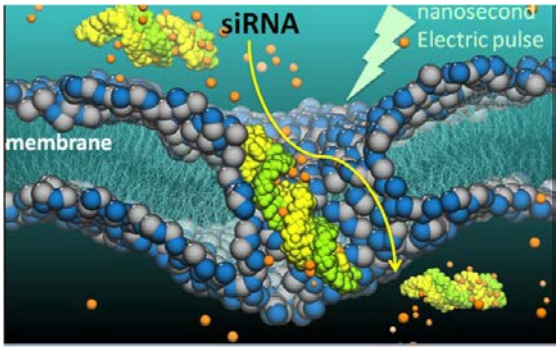

Figure 2.19: Molecular snapshots of the mechanism of electrotransfer of a double-stranded siRNA (shown as yellow and green spheres) through an aqueous pore (water omitted for clarity) within a POPC membrane (head groups shown as blue and gray spheres and hydrophobic tails as cyan lines) [42]

A decade ago, Tarek in 2005 [110] reported the first MD simulation on the transport of a short DNA double strand using high intensity electric fields. It was shown that the uptake occurred only in presence of the pore by electrophoretic drag to overcome the unexpected stable complex formed with the bilayer. Since then, to our knowledge, only two MD studies have been reported on the transport of molecules under nsPEFs.

In 2012 Breton et al. [42] showed, coupling experimental and *in silico* observations, that a single 10 ns high-voltage electric pulse can permeabilize giant unilamellar vesicles (GUVs) and allows the delivery of a double-stranded siRNA through the formed pore by an electrophoretic drag (Fig. 2.19). Comparing experimental evidences with MD simulations they could show in particular that: (i) no transport is detected for electric fields applied below an EP threshold; (ii) following the application of an electric field, the siRNA is pushed toward the lipid head groups forming a stable siRNA-headgroups of phospholipids complex that remains even when the pulse is switched off; (iii) when the E_{app} is above an EP threshold the siRNA is electrophoretically dragged through the electropore and may translocate within a 10 ns time scale; (iv) if the E_{app} is turned off before the complete transition the pore collapses around the molecule trapping the latter.

Recently, Salomone et al. [156] demonstrated the possibility to use a combination of nsPEFs and the chimeric peptides (CM_{18}-Tat_{11}) as efficient delivery vectors for plasmid DNA using the endocytic vesicles. In particular they showed that while Tat_{11}, a small cationic peptide can translocate through an electroporated bilayer within few nanoseconds without interacting with the phospholipids head groups, the amphipatic peptide CM_{18} even when located near a preformed pore, remains anchored to the lipid head-groups and does not translocate during a 12 ns high electric field pulse.

2.2.2.5 psPEFs and terahertz applications

Over the past few years as terahertz technologies have become more accessible an increasing number of studies have been focused on understanding the biological responses to terahertz electromagnetic radiation [115] and thus to picoseconds electric pulses [114], which have a non negligible amount of energy in the GHz and THz spectral content due to their extremely fast rise and fall times.

In order to investigate if these family of electric signals can induce similar effect to nsPEFs and μs-msPEFs Vernier et al [115] reported MD simulations of sinusoidal electric field in the THz spectrum and Petrishia et al. [114] of ps pulsed electric fields.

They suggested that if the magnitude of the field is high enough (hundreds of MV/m) permeabilization can be induced in lipid bilayers. Vernier et al. [115] showed how water dipoles in the membrane interior orient in permeabilizing electric fields on a picosecond time scale, consistent with a mechanism involving energy minimizing intrusions of interfacial water leading to membrane permeabilization by picosecond electric pulses and terahertz electromagnetic fields.

2.3 Exposure setups for *in vitro* electroporation

Biological and medical electroporation applications require proper apparatus to be performed in safe, repeatable and efficient conditions.

Generally, aside a series of measurement equipment (e.g. oscilloscopes, microscopes, ...), two main components are needed to deliver pulsed electric fields: a pulse generator and a delivery chamber. Nevertheless, a variety of these devices are available for *in vitro*, *in vivo* and *in patient* applications [160-166]. Despite a review of these equipment is beyond the scope of the present work, a summary of the *in vitro* apparatus for traditional and nano EP follows.

2.3.1 μs-msPEFs technology

For what concerns conventional EP, both generators and delivery systems require no special features. Indeed, these pulses are characterized by a relative low magnitude and long duration (microseconds to milliseconds, 0.1-10 kV/cm) that can be easily produced with either custom or commercial products.

Indeed, in bench-top sized electrical systems involving signals with frequencies below 1 MHz, or with durations longer than 1 μs, propagation related phenomena (see Subsection 2.3.2) through the electrical connections can be considered negligible and all points in a good electrical conductor can be assumed to reach the same voltage simultaneously ensuring a good matching between the source and the load, which simplify the experimental setup.

One of the common ways of doing macroscale *in vitro* experiments is to use commercial electroporation cuvettes (Fig. 2.20 A) filled with cell suspensions [160], often termed "bulk EP" or "volume EP". On the other hand, when microscale exposure conditions are desirable, e.g. to include microfluidic features and increase cell viability and/or to achieve single cell treatments, *in-house* more complex electrode systems (Fig. 2.20 B) are usually manufactured [165,166].

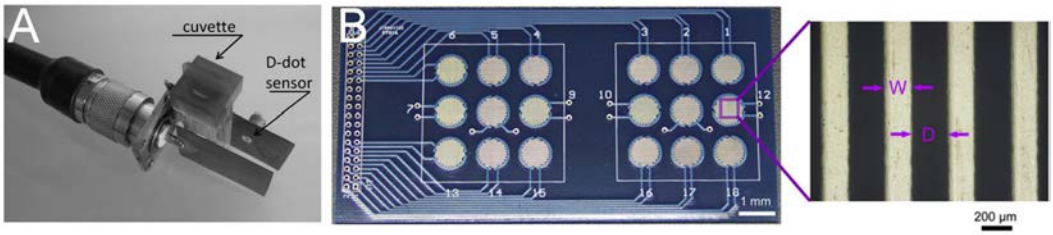

Figure 2.20: Delivery systems for standard EP: A) cuvette enclosed in a couple of planar electrodes [52]; B) interdigitated microelectrode array [167]

A discrete effort has been devoted to microscale engineering in developing tools for bi-

ological applications by miniaturizing devices and providing controllable microenvironments for *in vitro* cell research [165]. Miniaturized devices offer numerous benefits in comparison to their macroscale counterparts, such as lower use of expensive reagents, biomimetic environments, ability to manipulate single cells and to directly see their response during the experiment, spatial and temporal control of various electrical parameters, increase of the electric field applied to the sample for lower voltages produced by the generator. Microscale EP devices can be used to reduce limitations associated with conventional approaches such as variations in the local pH, electric field distortion, sample contamination, and the difficulties in transfecting and maintaining the viability of desired cell types.

Category	# of ref	Shape	Cell line
Extra small	177	Ellipsoidal	HeLa
	120	Globular	B cell
	107	Globular	U937
	65	Globular	K562
	62	Globular	JURKAT T
	1	Ellipsoidal	PC12, Yeast
Small	203(+2)	Ellipsoidal	CHO (CHO-K1)
	66	Ellipsoidal	HEK293
	61	Globular	A431
	49	Globular	HCT116
	1		buccal cell, COS7, C2C12, DC20-3F, DC3F, HEK293,HL60, HUVECS, MCF7, T1080
Medium	141	Ellipsoidal	A549
	37	Ellipsoidal	SW480
	1		HepG2, MDCK
Large	121	Ellipsoidal	NIH3T3
	56 (+28,+12)	Ellipsoidal	MSC (bmMSC, hMSC)
	40	Ellipsoidal	3T3-L1
	29		Atrocities
	1		Neuro2a, 3T3-LA

Table 2.2: Cell lines used in microscale EP experiments categorized in four groups: extra small (<20 μm), small (20-50 μm), medium (50-100 μm) and large (>100 μm)

One possible limitation of this technology is the low throughput of the exposed cells with respect to "bulk EP" achievable with conventional cuvettes. Therefore the choice of the device is also related to the amount of cells one want to expose during one experiment. Another possible limit to take in consideration is the dimension of the cell line that should expose and fit, completely or partially, the gap between the electrodes. In Table 2.2 we report the number of references for different cell lines used for microscale EP experiments from the review of Lee et al. [165] of 2009.

In Table 2.2 we categorized the cell lines reported by [165] through their dimensions in

four groups: extra small (<20 μm), small (20-50 μm), medium (50-100 μm) and large (>100 μm). This could help in the choice of the spacing between electrodes (L_{GAP}) and in general of the volume of treatment. With a L_{GAP} of 100-150 μm most of cell lines usually employed can be fully exposed; while large cells, such as the excitable ones, require a wider gap (>200 μm), in that cases where a partial exposure is not desired.

2.3.2 nsPEFs technology

Since the early 2000s, the emergence of nanosecond electric pulses paves the attention of the scientific community working on electroporation. The emergence of nsPEFs is related to the ability to reliably generate and deliver load these short pulses to the biological.

2.3.2.1 Pulse generators for nsPEFs

Specifically, the main features that such kind of generators mast own are related with the length and the intensity of the pulses produced.

As described in Subsection 2.1.2, the effect of nsPEFs is induced directly on the interfacial water at the cell/organelle membrane level meaning that the charge membrane build up can be neglected. As a consequence, the targeting of subcellular structures with unipolar pulses requires the pulse rise time to be much less than the charging time of the plasma membrane. Furthermore, depending on the application, the pulse duration itself should be kept shorter than the time required for the onset of EP of the outer membrane.

In addition to a shorter pulse length, the electric field needs to be much higher than field strengths provided with μs-msPEFs in order to target cell organelles or their plasma membranes. The required electric field for the poration of organelle membranes scales inversely with the organelle diameter and the pulse length. Based on the results of experiments, for instance, electric field strengths on the order of 5 MV/m are deemed necessary for a single 10 ns pulse to induce subcellular effects [168].

Figure 2.21: Pulse generator commercially available from Transient Plasma Systems, INC. http://www.transientplasmasystems.com/

Therefore, the realization of high-peak-power, low-total-energy pulses generator is not

trivial, and only recently are commercially available (Fig. 2.21). For this reason, in the early studies of nsPEFs effects on biological medium, various nanosecond pulse generators able to deliver very high intensity (beyond kV/cm) and extremely short (nanosecond) pulses have been designed and manufactured *in-house* [169-176].

2.3.2.2 Delivery systems and monitoring devices for nsPEFs

A reliable nsPEFs generator is a necessary but not sufficient prerequisite for reproducible experimentation. There are different aspects that can have a significant impact on the experimental conditions and that will be addressed in this Section, among which: i) signal propagation, ii) breakdown of dielectric components, iii) monitoring devices.

In recent years, thanks to the great improvements in micro and nano-fabrication techniques, a number of devices has been conceived for microscale cell analysis, identification, screening, and manipulation also in combination with chemical or physical agents (e.g. fluorescent dyes, electromagnetic (EM) fields, temperature) [177,178]. Microchamber devices, able to discriminate single cell dielectric properties in real-time and integrated with microfluidic techniques, have been given increasing consideration, being an accurate low-cost and label-free approach for cell status identification, essential for different *in vitro* biological studies [179]. The main benefits of these technologies consist in their miniaturization and parallelization capabilities, as well as real-time observation of cell behaviour when transparent materials are used for the device fabrication.

From the combination of the recent developments in microtechnologies/microfluidics techniques and the requirements of penetrating cells down to fine intracellular structures using nsPEFs, the design and fabrication of new innovative devices for biological applications has come out.

In the following, first we will describe how the development of miniaturized applicators allow both a better transmission of the signal from the generator to the load and the production of very high voltage per centimetre, enhancing the electrical conditions to trigger biological effects. Secondly, we will give an overview of the microchamber available for nsPEFs experiments, comparing their performances.

The delivery of nsPEF signals to the cells is quite hard: the signal has to be provided to the biological sample without deformation of spectral and temporal contents, hence it requires a careful design of the microchamber applicator. Indeed, the large spectral components of the most used nsPEFs, available in literature, span from MHz (hundred of ns of pulse duration with tens of ns for rise and fall time) up to GHz (single ns of pulse duration with fractions of ns for rise and fall time), as reported in Fig. 2.22 [72,180]. Hence, the impedance of the loaded exposure chamber must be as close as possible, i.e. matched, to the one of the generator, usually 50 Ω, for a wide frequency range to avoid reflections (see Fig. 2.23).

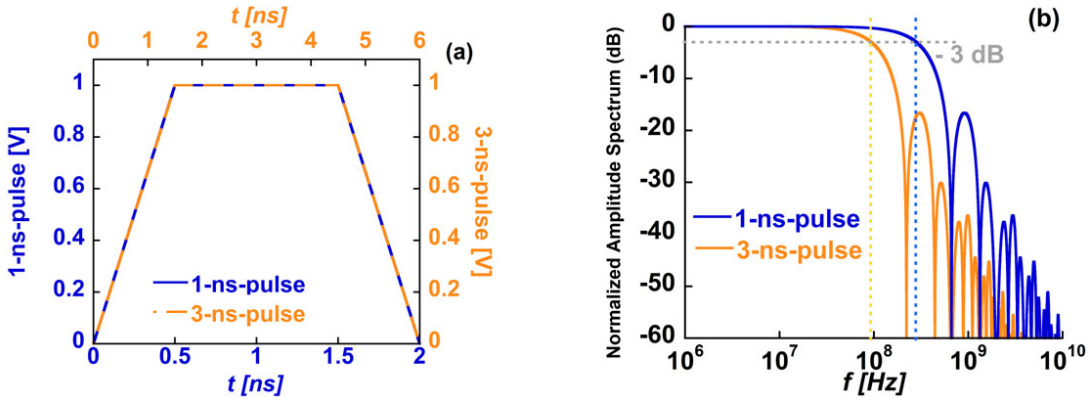

Figure 2.22: Example of two extremely short electric pulses. (a) Temporal distribution, (b) spectral content of a 1 ns pulse with a rise and fall time of 0.5 ns in blue solid line, a 3 ns pulse with a rise and fall time of 1.5 ns in orange dashed line. The shorter the pulse duration and the rise/fall times the higher the pulse content of energy at high frequencies

As far as the time duration of the pulses decreases, traditional electroporation devices are no more adequate to be used [181]. In the case of cuvettes loaded with biological cells, for instance, their usual impedance is between 10-20 Ω [170,181]. Although it is possible to improve the matching of the load impedance to the one of the generator by the adjustment of the geometry of the cuvette and/or the conductivity of the buffer [52,173,175,176,182-186], the experimental requirements limit the degrees of freedom of these modifications. For example, the reduction of the conductivity of a cell solution it is possible if non ionic agents are added to maintain its osmolarity, yet just to a certain point to avoid ambiguity in the interpretation of the results caused by salt depletion.

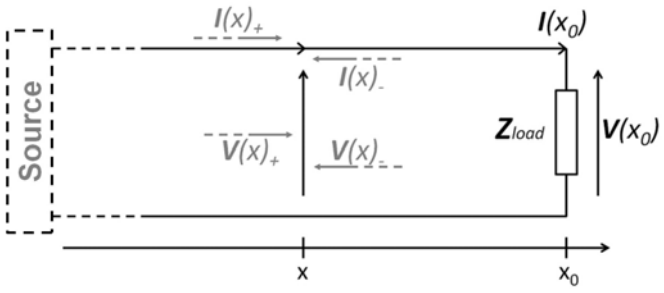

Figure 2.23: Reflection on the termination of a transmission line (delivery system laded with the biological medium). When the voltage and current signals propagating in the positive x-direction ($V(x)^+$; $I(x)^+$) reach a mismatched load, they are partially reflected. The reflected signals ($V(x)^-$; $I(x)^-$) propagate in the opposite direction. This phenomenon induces an attenuation and distortion of the signal applied to the cell sample and an eventual damage of the generator if the reflected power is too high

Another way adopted in several cases [59,169,172,185,187], independently from the reservoir hosting the cells, is to insert impedances in parallel or in series to the load obtaining an improvement of the matching with the characteristic impedance of the cable connected to the generator.

However, even when all the issues aforesaid are carefully addressed the distortion of the voltage signal cannot be fully avoided. Consequently, broadband devices in the radiofrequency and microwave (MW) range seem unavoidable and designing rules typical of MW propagating systems [181,188-190] become the guidelines for the implementation of new micro-scale devices, suitable for nsPEF applications.

The other relevant aspect, for which micro-scale devices are suitable for nsPEF applications, is related to the intensity of the electric field to be generated in the sample. In fact the reduced duration of the pulse requires in parallel a very high intensity of the electric field (MV/m), usually obtained by placing in close proximity the conductors between which the cell sample is located. Therefore, a particular attention must be dedicated to optimize the efficiency, both in terms of intensity of electric field inside region of interest (ROI) and as the ratio of the measured voltage at the sample over the voltage applied by the generator (V_{out}/V_{in}), to guarantee a decrease of the needed output voltage from the generator.

Increasing the efficiency of the setup entail two benefits: first, a decrease of the power consumption through a lowering of generator output power that imply an easier and less expensive realization; second, the decrement of risks of electrical breakdown of the chamber components, i.e. the maximum electric field that dielectric materials can withstand without experiencing an abrupt failure of its insulating properties, either reversible or irreversible.

Another aspect that should not be neglected is the real-time monitoring of the cell sample and of the signal transmission. Indeed, miniaturized devices for biological applications are often realized with transparent components, to allow direct control of the investigated sample, e.g. by inverted microscopy, and are frequently equipped with instrumentation to capture and record the signals that are actually applied to the exposure chamber. As well as the voltage signal, it can be convenient to monitor also the current that flows through the sample.

The most employed acquisition devices are the so-called probes. A high-voltage probe scales down the voltage to levels tolerable by the next stage in the acquisition chain (e.g. a 50 Ω oscilloscope input typically tolerates voltage amplitudes of about 1 V) whereas a current probe transforms the current signal into a voltage signal. A fundamental limitation of high-voltage and current probes is their bandwidth. Typically these probes behave as first-order low-pass filters and their cut-off frequency will determine to a large extent the fidelity of the whole acquisition system. As an alternative to high-voltage probes it is possible to employ tap-offs, also known as power dividers or splitters, inserted in the transmission line. These components are particularly interesting as they allow a direct visualization of the reflections.

In this scenario, an overview of the state of the art of microchambers for *in vitro* experiments of nsPEFs is therefore important to understand which pulses can be currently transmitted. However, with the exception of few works [187,191-193], the characteriza-

tion of the frequency behavior in terms of Scattering parameters, i.e. reflection ($|S_{11}|$) and transmission ($|S_{21}|$) coefficients, of the microchambers has not been explicitly described, which makes more difficult a comparison of the performances of the devices. Indeed to our knowledge, most of the articles simply show the generated and/or measured voltage pulses, providing only a partial and qualitative information on the quality of the transmission of the signal [59,169,170,172,174,182,183,185,194-199].

Several microchambers for microscale EP are composed by couples or arrays of strip electrodes, 10 to 100 μm in height, distant 80-150 μm one from each other and optical paths to enable real-time imaging to study cells exposed to nsPEFs [169,170,172,174,182,183,185,194-197,199]. Biocompatible electrodes are often in gold, deposited over transparent glass substrates and plugged by plastic or glass cover slips. More versatile setups developed for the exposure of individual and small groups of cells on a glass cover slip to subnanosecond and nanosecond pulses were used by [59,198]. In this case the versatility is given by the possibility to move the microchamber during the experiment since it is composed by pairs of thin tungsten wire electrodes detached from the substrate.

Despite the accuracy in the devices realization, the records of the pulse, with duration from 2.5 to hundred of ns, over time show how in almost all cases the delivered signal is attenuated and distorted, with unwanted ripples and fluctuations probably consequence of mismatch. However, since it is not provided any frequency characterization of these setups, it is not possible to quantify the mismatch between the source and the load.

As we can see from Table 2.3, only few papers addressed the issue of delivering to few cells nsPEF with duration down to 3 ns taking into account the frequency behavior of the proposed microchambers [187,191-193], or cuvettes [173,175]. In Table 2.3 the following relevant performances are summarize: the equivalent MW structure when possible; the distance between the electrodes (L_{GAP}); the volume treated; the conductivity of the buffer medium; the frequency at which the module of the reflection coefficient is equal -10 dB, i.e. less than 10% of the incident power is reflected; the intensity of the electric field between the electrodes in kV/cm for 1 kV provided by the generator and estimated by numerical modeling or measurements of the delivered signal; the efficiency (η) of the shorter pulsed studied defined as the maximum value of the voltage pulse delivered (V_{out}) and measured at the load over the maximum voltage pulse generated (V_{in}), e.g. the plateau in a trapezoidal pulse and the maximum peak in a Gaussian like pulse.

Among them, Dalmay et al. [191,192] realized a biochip based on a coplanar wave guide design, i.e. three coplanar strips distant 130 μm on a transparent substrate. The loaded channel is defined by thick gold electrodes (25 μm), resulting in higher final walls (47 μm) increased by a patterned SU8 layer. From a frequency characterized of its impedance, the module of the reflection coefficient equals -10 dB at the frequency of 100 MHz. The voltage pulses tested are a trapezoidal signal of 10 ns duration and a Gaussian like signal of 3 ns duration. Because of the frequency properties of this device, the first pulse is transmitted with a mild distortion of the rise and fall time, while the 3 ns pulse is subject to a stronger

Ref	Structure	L_{GAP}	V	σ	$f_{(\|S_{11}\|=-10db)}$	E_{GAP}	η
[173]	cuvette	4000	800	1.5	∼50	-	0.4
[175]	cuvette	4000	1764	0.31	70	2.5	0.5
[191,192]	CWG	130	0.2	1.0	110	-	0.77
[193]	SL	100	0.03	1.0	99	10	0.44
[187]	BFL	100	0.3	1.5	300	83	-

Table 2.3: Performances of published microchambers and cuvettes for nsPEF experiments
CWG - Coplanar waveguide
SL - Slot line
BFL - Bifilar line
LGAP - Distance between the electrodes in μm
V - Total volume treated in mm^3
σ - Buffer conductivity in S/m
$f_{(|S_{11}|=-10dB)}$ - Frequency at which the module of the reflection coefficient is equal -10 dB
$|E_{GAP}|$ - Intensity of the electric field between the electrodes in kV/cm for 1 kV input
η - Efficiency as V_{out}/V_{in}

modification of its shape; in both cases an efficiency of 0.77 can be estimated.

Using a slot line like guiding structure Vernier's group [193] proposed a two parallel strip design printed on a circuit board incorporating a 50 Ω resistor in parallel with the microchamber and a voltage divider stage for pulse measurements. The 100 μm wide microchamber is a rectangular channel (12 mm long) formed between two gold-plated electrode walls (25 μm deep) on a glass microscope slide. The $|S_{11}|$ at -10 dB is at 99 MHz, the electric field in the channel evaluated is to be 100 kV/cm for 1 kV input and the efficiency 0.54. Two pulse generators were tested with measured pulse durations of 3.0 and 4.2 ns respectively, transmitted with not negligible distortion and attenuation.

From the same group [187] better performances were obtained using a bifilar line composed by two tungsten wire electrodes spaced by 100 μm and designed to be adapted with a microscope and connected to an automated micromanipulator. This setup allowed to have a higher frequency, 300 MHz, at which the $|S_{11}|$ equals -10 dB and an electric field intensity between the wires of 100 kV/cm for 1.2 kV input.

For comparison we show in Table 2.3 also the studies performed with cuvettes that have been characterized electromagnetically [173,175]. Clear advantages follow the use of micro-devices when dealing with the intensity of the electric field in the ROI. In fact, in [193] the electric field magnitude for 1 kV generated is 40 times higher than for [175]. Microchambers also show a better transmission of shorter pulses. The $|S_{11}|$ at -10 dB does not overcome 70 MHz [175], while the best performance of the microcambers is 300 MHz obtained by Wu et al. [187]. In other words, taking into account only the biological sample impedance as criterion for generator/load matching, cuvettes filled with suspension having 0.31 S/m and dimensions reported in Table 2.3 can be used to deliver 10 ns trapezoidal pulses with rise and fall time of 1.5 ns and bifilar line microchambers loading biological

medium of 1.5 S/m, distant 100 μm and long 3 mm can deliver gaussian pulses of 3 ns.

In these papers [173,175,187,191-193] it has been proven that the requisite to provide an undistorted signal, with duration longer than 3 ns, can be respected quite easy without strict problems of impedance matching of the structure by dimensioning the device only on the basis of the biological sample impedance. However, despite the effort made in the direction of the optimization of the exposure conditions, a standard protocol in designing cell reservoir for nsPEF *in vitro* experiments is not currently established.

2.4 References

[1] R.P. Feynman, There's Plenty of Room at the Bottom, Am. Phys. Soc. Meet., Caltech, (1959).

[2] White Paper 'Contribution of Nanomedicine to Horizon 2020' available - ETP Nanomedicine.

[3] COST | Biomedicine and Molecular Biosciences (BMBS).

[4] G.A. Hughes, Nanostructure-mediated drug delivery, Nanomedicine Nanotechnol. Biol. Med. 1 (2005) 22-30.

[5] T. Lammers, S. Aime, W.E. Hennink, G. Storm, F. Kiessling, Theranostic nanomedicine, Acc. Chem. Res. 44 (2011) 1029-1038.

[6] Z. Fan, P.P. Fu, H. Yu, P.C. Ray, Theranostic nanomedicine for cancer detection and treatment, J. Food Drug Anal. 22 (2014) 3-17.

[7] T.M. Allen, P.R. Cullis, Drug Delivery Systems: Entering the Mainstream, Science. 303 (2004) 1818-1822.

[8] A.Z. Mirza, F.A. Siddiqui, Nanomedicine and drug delivery: a mini review, Int. Nano Lett. 4 (2014) 1-7.

[9] M.I. Yatoo, A. Saxena, M.H. Malik, M.K. Sharma, U. Dimri, Nanotechnology Based Drug Delivery at Cellular Level: a Review, J. Anim. Sci. Adv. 4 (2014) 705-709.

[10] L. Zhang, F. Gu, J. Chan, A. Wang, R. Langer, O. Farokhzad, Nanoparticles in Medicine: Therapeutic Applications and Developments, Clin. Pharmacol. Ther. 83 (2008) 761-769.

[11] D.A. LaVan, T. McGuire, R. Langer, Small-scale systems for in vivo drug delivery, Nat. Biotechnol. 21 (2003) 1184-1191.

[12] D. Roy, J.N. Cambre, B.S. Sumerlin, Future perspectives and recent advances in stimuli-responsive materials, Prog. Polym. Sci. 35 (2010) 278-301.

[13] Y. Qiu, K. Park, Environment-sensitive hydrogels for drug delivery, Adv. Drug Deliv. Rev. 64, Supplement (2012) 49-60.

[14] A.S. Hoffman, Stimuli-responsive polymers: Biomedical applications and challenges for clinical translation, Adv. Drug Deliv. Rev. 65 (2013) 10-16.

[15] T.M. Allen, P.R. Cullis, Liposomal drug delivery systems: From concept to clinical applications, Adv. Drug Deliv. Rev. 65 (2013) 36-48.

[16] R.M. Sawant, J.P. Hurley, S. Salmaso, A. Kale, E. Tolcheva, T.S. Levchenko, et al., "SMART" Drug Delivery Systems: Double-Targeted pH-Responsive Pharmaceutical Nanocar-

riers, Bioconjug. Chem. 17 (2006) 943-949.

[17] D. Schmaljohann, Thermo- and pH-responsive polymers in drug delivery, Adv. Drug Deliv. Rev. 58 (2006) 1655-1670.

[18] L. Li, D. Chen, Y. Zhang, Z. Deng, X. Ren, X. Meng, et al., Magnetic and fluorescent multifunctional chitosan nanoparticles as a smart drug delivery system, Nanotechnology. 18 (2007) 405102.

[19] H.J. Kim, H. Matsuda, H. Zhou, I. Honma, Ultrasound - Triggered Smart Drug Release from a Poly (dimethylsiloxane)-Mesoporous Silica Composite, Adv. Mater. 18 (2006) 3083-3088.

[20] C. de las H. Alarcon, S. Pennadam, C. Alexander, Stimuli responsive polymers for biomedical applications, Chem. Soc. Rev. 34 (2005) 276-285.

[21] J. Gehl, Electroporation: theory and methods, perspectives for drug delivery, gene therapy and research, Acta Physiol. Scand. 177 (2003) 437-447.

[22] E. Neumann, A.E. Sowers, C.A. Jordan, Electroporation and Electrofusion in Cell Biology, Springer Science and Business Media, 1989.

[23] J.A. Nickoloff, Animal Cell Electroporation and Electrofusion Protocols, Humana Press,NJ, 1995.

[24] J.C. Weaver, Y.A. Chizmadzhev, Theory of electroporation: A review, Bioelectrochem. Bioenerg. 41 (1996) 135-160.

[25] S. Li, Electroporation Protocols: Preclinical and Clinical Gene Medicine, Humana press: Totowa, NJ., 2008.

[26] L.M. Mir, S. Orlowski, J. Belehradek Jr., J. Teissie, M.P. Rols, G. Sersa, et al., Biomedical applications of electric pulses with special emphasis on antitumor electrochemotherapy, Bioelectrochem. Bioenerg. 38 (1995) 203-207.

[27] J. Teissie, N. Eynard, B. Gabriel, M.P. Rols, Electropermeabilization of cell membranes, Adv. Drug Deliv. Rev. 35 (1999) 3-19.

[28] J. Teissie, Electrically Mediated Gene Delivery: Basic and Translational Concepts., INTECH Open Access Publisher, 2013.

[29] M.S. Venslauskas, S. Satkauskas, Mechanisms of transfer of bioactive molecules through the cell membrane by electroporation, Eur. Biophys. J. 44 (2015) 277-289.

[30] E.L. Hansen, E.B. Sozer, S. Romeo, S.K. Frandsen, P.T. Vernier, J. Gehl, Dose-dependent ATP depletion and cancer cell death following calcium electroporation, relative effect of calcium concentration and electric field strength, PloS One. 10 (2015) e0122973.

[31] M. Breton, L.M. Mir, Microsecond and nanosecond electric pulses in cancer treatments, Bioelectromagnetics. 33 (2012) 106-123.

[32] D. Miklavčič, B. Mali, B. Kos, R. Heller, G. Sersa, Electrochemotherapy: from the drawing board into medical practice, Biomed. Eng. OnLine. 13 (2014) 29.

[33] R. Cadossi, M. Ronchetti, M. Cadossi, Locally enhanced chemotherapy by electroporation: clinical experiences and perspective of use of electrochemotherapy, Future Oncol. 10 (2014) 877-890.

[34] M. Sallberg, L. Frelin, G. Ahlen, M. Sallberg-Chen, Electroporation for therapeutic DNA vaccination in patients, Med. Microbiol. Immunol. (Berl.) 204 (2014) 131-135.

[35] G. Sersa, J. Teissie, M. Cemazar, E. Signori, U. Kamensek, G. Marshall, et al., Electrochemotherapy of tumors as in situ vaccination boosted by immunogene electrotransfer, Cancer Immunol. Immunother. CII. 64 (2015) 1315-1327.

[36] L.C. Heller, R. Heller, In Vivo Electroporation for Gene Therapy, Hum. Gene Ther. 17 (2006) 890-897.

[37] S. Chabot, J. Teissié, M. Golzio, Targeted electro-delivery of oligonucleotides for RNA interference: siRNA and antimiR, Adv. Drug Deliv. Rev. 81 (2015) 161-168.

[38] C. Jiang, R.V. Davalos, J.C. Bischof, A Review of Basic to Clinical Studies of Irreversible Electroporation Therapy, IEEE Trans. Biomed. Eng. 62 (2015) 4-20.

[39] J. Deng, K.H. Schoenbach, E. Stephen Buescher, P.S. Hair, P.M. Fox, S.J. Beebe, The Effects of Intense Submicrosecond Electrical Pulses on Cells, Biophys. J. 84 (2003) 2709-2714.

[40] P.T. Vernier, Y. Sun, M.A. Gundersen, Nanoelectropulse-driven membrane perturbation and small molecule permeabilization, BMC Cell Biol. 7 (2006) 37.

[41] L. Chopinet, M.-P. Rols, Nanosecond electric pulses: a mini-review of the present state of the art, Bioelectrochemistry Amst. Neth. 103 (2015) 2-6.

[42] M. Breton, L. Delemotte, A. Silve, L.M. Mir, M. Tarek, Transport of siRNA through Lipid Membranes Driven by Nanosecond Electric Pulses: An Experimental and Computational Study, J. Am. Chem. Soc. 134 (2012) 13938-13941.

[43] A. Zupanic, B. Kos, D. Miklavčič, Treatment planning of electroporation-based medical interventions: electrochemotherapy, gene electrotransfer and irreversible electroporation, Phys. Med. Biol. 57 (2012) 5425.

[44] M. Marty, G. Sersa, J.R. Garbay, J. Gehl, C.G. Collins, M. Snoj, et al., Electrochemotherapy - An easy, highly effective and safe treatment of cutaneous and subcutaneous metastases: Results of ESOPE (European Standard Operating Procedures of Electrochemother-

apy) study, Eur. J. Cancer Suppl. 4 (2006) 3-13.

[45] D.J. Wells, Gene Therapy Progress and Prospects: Electroporation and other physical methods, Gene Ther. 11 (2004) 1363-1369.

[46] R.V. Davalos, L.M. Mir, B. Rubinsky, Tissue Ablation with Irreversible Electroporation, Ann. Biomed. Eng. 33 (2005) 223-231.

[47] J.R. Beveridge, K. Wall, S.J. MacGregor, J.G. Anderson, N.J. Rowan, Pulsed electric field inactivation of spoilage microorganisms in alcoholic beverages, Proc. IEEE. 92 (2004) 1138-1143.

[48] P.A. Garcia, J.H. Rossmeisl, J. Robertson, T.L. Ellis, R.V. Davalos, Pilot study of irreversible electroporation for intracranial surgery, in: Annu. Int. Conf. IEEE Eng. Med. Biol. Soc. 2009 EMBC 2009, 2009: pp. 6513-6516.

[49] L.M. Mir, The Place of the Electroporation-Based Antitumor Therapies in the Electrical Armamentarium against Cancer, in: B. Rubinsky (Ed.), Irreversible Electroporation, Springer Berlin Heidelberg, 2010: pp. 223-233.

[50] K.H. Schoenbach, S. Xiao, R.P. Joshi, J.T. Camp, T. Heeren, J.F. Kolb, et al., The Effect of Intense Subnanosecond Electrical Pulses on Biological Cells, IEEE Trans. Plasma Sci. 36 (2008) 414-422.

[51] O.M. Nesin, O.N. Pakhomova, S. Xiao, A.G. Pakhomov, Manipulation of cell volume and membrane pore comparison following single cell permeabilization with 60- and 600-ns electric pulses, Biochim. Biophys. Acta. 1808 (2011) 792-801.

[52] A. Silve, I. Leray, L.M. Mir, Demonstration of cell membrane permeabilization to medium-sized molecules caused by a single 10 ns electric pulse, Bioelectrochemistry. 87 (2012) 260-264.

[53] A.G. Pakhomov, E. Gianulis, P.T. Vernier, I. Semenov, S. Xiao, O.N. Pakhomova, Multiple nanosecond electric pulses increase the number but not the size of long-lived nanopores in the cell membrane, Biochim. Biophys. Acta. 1848 (2015) 958-966.

[54] S.J. Beebe, K.H. Schoenbach, Nanosecond Pulsed Electric Fields: A New Stimulus to Activate Intracellular Signaling, J. Biomed. Biotechnol. 2005 (2005) 297-300.

[55] S.J. Beebe, P.M. Fox, L.J. Rec, K. Somers, R.H. Stark, K.H. Schoenbach, Nanosecond pulsed electric field (nsPEF) effects on cells and tissues: apoptosis induction and tumor growth inhibition, IEEE Trans. Plasma Sci. 30 (2002) 286-292.

[56] P.T. Vernier, Y. Sun, L. Marcu, S. Salemi, C.M. Craft, M.A. Gundersen, Calcium bursts induced by nanosecond electric pulses, Biochem. Biophys. Res. Commun. 310 (2003) 286-295.

[57] K.H. Schoenbach, R.P. Joshi, J.F. Kolb, N. Chen, M. Stacey, P.F. Blackmore, et al., Ultrashort electrical pulses open a new gateway into biological cells, Proc. IEEE. 92 (2004) 1122-1137.

[58] P.T. Vernier, A. Li, L. Marcu, C.M. Craft, M.A. Gundersen, Ultrashort pulsed electric fields induce membrane phospholipid translocation and caspase activation: differential sensitivities of Jurkat T lymphoblasts and rat glioma C6 cells, IEEE Trans. Dielectr. Electr. Insul. 10 (2003) 795-809.

[59] A.G. Pakhomov, J.F. Kolb, J.A. White, R.P. Joshi, S. Xiao, K.H. Schoenbach, Long-lasting plasma membrane permeabilization in mammalian cells by nanosecond pulsed electric field (nsPEF), Bioelectromagnetics. 28 (2007) 655-663.

[60] P.T. Vernier, M.J. Ziegler, Y. Sun, W.V. Chang, M.A. Gundersen, D.P. Tieleman, Nanopore Formation and Phosphatidylserine Externalization in a Phospholipid Bilayer at High Transmembrane Potential, J. Am. Chem. Soc. 128 (2006) 6288-6289.

[61] S. Romeo, Y.-H. Wu, Z.A. Levine, M.A. Gundersen, P.T. Vernier, Water influx and cell swelling after nanosecond electropermeabilization, Biochim. Biophys. Acta BBA - Biomembr. 1828 (2013) 1715- 1722.

[62] S.J. Beebe, P.F. Blackmore, J. White, R.P. Joshi, K.H. Schoenbach, Nanosecond pulsed electric fields modulate cell function through intracellular signal transduction mechanisms, Physiol. Meas. 25 (2004) 1077-1093.

[63] J.C. Weaver, K.C. Smith, A.T. Esser, R.S. Son, T.R. Gowrishankar, A brief overview of electroporation pulse strength-duration space: a region where additional intracellular effects are expected, Bioelectrochemistry Amst. Neth. 87 (2012) 236-243.

[64] I.G. Abidor, V.B. Arakelyan, L.V. Chernomordik, Y.A. Chizmadzhev, V.F. Pastushenko, M.P. Tarasevich, Electric breakdown of bilayer lipid membranes: I. The main experimental facts and their qualitative discussion, J. Electroanal. Chem. Interfacial Electrochem. 104 (1979) 37-52.

[65] R. Benz, F. Beckers, U. Zimmermann, Reversible electrical breakdown of lipid bilayer membranes: A charge-pulse relaxation study, J. Membr. Biol. 48 (1979) 181-204.

[66] J.C. Weaver, Electroporation of biological membranes from multicellular to nano scales, IEEE Trans. Dielectr. Electr. Insul. 10 (2003) 754-768.

[67] C. Chen, S.W. Smye, M.P. Robinson, J.A. Evans, Membrane electroporation theories: a review, Med. Biol. Eng. Comput. 44 (2006) 5-14.

[68] M. Szabo, M.I. Wallace, Imaging potassium-flux through individual electropores in droplet interface bilayers, Biochim. Biophys. Acta. (2015).

[69] J.C. Neu, W. Krassowska, Asymptotic model of electroporation, Phys. Rev. E. 59

(1999) 3471-3482.

[70] R.P. Joshi, K.H. Schoenbach, Electroporation dynamics in biological cells subjected to ultrafast electrical pulses: A numerical simulation study, Phys. Rev. E. 62 (2000) 1025-1033.

[71] M.E. Mezeme, G. Pucihar, M. Pavlin, C. Brosseau, D. Miklavčič, A numerical analysis of multicellular environment for modeling tissue electroporation, Appl. Phys. Lett. 100 (2012) 143701.

[72] C. Merla, A. Denzi, A. Paffi, M. Casciola, G. D'Inzeo, F. Apollonio, et al., Novel Passive Element Circuits for Microdosimetry of Nanosecond Pulsed Electric Fields, IEEE Trans. Biomed. Eng. 59 (2012) 2302-2311.

[73] J. Li, W. Tan, M. Yu, H. Lin, The effect of extracellular conductivity on electroporation-mediated molecular delivery, Biochim. Biophys. Acta BBA - Biomembr. 1828 (2013) 461-470.

[74] N.J. English, C.J. Waldron, Perspectives on external electric fields in molecular simulation: progress, prospects and challenges, Phys. Chem. Chem. Phys. 17 (2015) 12407-12440.

[75] H. Pera, J.M. Kleijn, F. a. M. Leermakers, On the edge energy of lipid membranes and the thermodynamic stability of pores, J. Chem. Phys. 142 (2015) 034101.

[76] D.P. Tieleman, S.J. Marrink, H.J.C. Berendsen, A computer perspective of membranes: molecular dynamics studies of lipid bilayer systems, Biochim. Biophys. Acta BBA - Rev. Biomembr. 1331 (1997) 235-270.

[77] D.J. Tobias, K. Tu, M.L. Klein, Atomic-scale molecular dynamics simulations of lipid membranes, Curr. Opin. Colloid Interface Sci. 2 (1997) 15-26.

[78] L.R. Forrest, M.S. Sansom, Membrane simulations: bigger and better?, Curr. Opin. Struct. Biol. 10 (2000) 174-181.

[79] S.E. Feller, Molecular dynamics simulations of lipid bilayers, Curr. Opin. Colloid Interface Sci. 5 (2000) 217-223.

[80] R.J. Mashl, H.L. Scott, S. Subramaniam, E. Jakobsson, Molecular simulation of dioleoylphosphatidylcholine lipid bilayers at differing levels of hydration, Biophys. J. 81 (2001) 3005-3015.

[81] L. Saiz, M.L. Klein, Computer Simulation Studies of Model Biological Membranes, Acc. Chem. Res. 35 (2002) 482-489.

[82] C. Anézo, A.H. de Vries, H.-D. Höltje, D.P. Tieleman, S.-J. Marrink, Methodological Issues in Lipid Bilayer Simulations, J. Phys. Chem. B. 107 (2003) 9424-9433.

[83] M.L. Berkowitz, D.L. Bostick, S. Pandit, Aqueous Solutions next to Phospholipid Membrane Surfaces: Insights from Simulations, Chem. Rev. 106 (2006) 1527-1539.

[84] E. Lindahl, M.S. Sansom, Membrane proteins: molecular dynamics simulations, Curr. Opin. Struct. Biol. 18 (2008) 425-431.

[85] O. Edholm, Chapter 3 Time and Length Scales in Lipid Bilayer Simulations, in: S.E. Feller (Ed.), Curr. Top. Membr., Academic Press, 2008: pp. 91-110.

[86] A.A. Gurtovenko, I. Vattulainen, Calculation of the electrostatic potential of lipid bilayers from molecular dynamics simulations: Methodological issues, J. Chem. Phys. 130 (2009) 215107.

[87] S.J. Marrink, A.H. de Vries, D.P. Tieleman, Lipids on the move: Simulations of membrane pores, domains, stalks and curves, Biochim. Biophys. Acta BBA - Biomembr. 1788 (2009) 149-168.

[88] T.J. Piggot, A. Pineiro, S. Khalid, Molecular Dynamics Simulations of Phosphatidylcholine Membranes: A Comparative Force Field Study, J. Chem. Theory Comput. 8 (2012) 4593-4609.

[89] A. Schlaich, B. Kowalik, M. Kanduc, E. Schneck, R.R. Netz, Physical mechanisms of the interaction between lipid membranes in the aqueous environment, Phys. Stat. Mech. Its Appl. 418 (2015) 105- 125.

[90] V.F. Pastushenko, Y.A. Chizmadzhev, Stabilization of conducting pores in BLM by electric current. Gen. Physiol. Biophys 1 (1982): 43-52.

[91] M. Hibino, M. Shigemori, H. Itoh, K. Nagayama, K. Kinosita, Membrane conductance of an electroporated cell analyzed by submicrosecond imaging of transmembrane potential., Biophys. J. 59 (1991) 209-220.

[92] L. Rems, M. Tarek, M. Casciola, D. Miklavčič, Properties of lipid electropores II: Comparison of continuum-level modeling of pore conductance to molecular dynamics simulations, Bioelectrochemistry Submitt.

[93] K.C. Smith, A unified model of electroporaition and molecular transport, Harvard-Massachusetts Institute of Technology, 2011.

[94] R.A. Böckmann, B.L. de Groot, S. Kakorin, E. Neumann, H. Grubmüller, Kinetics, Statistics, and Energetics of Lipid Membrane Electroporation Studied by Molecular Dynamics Simulations, Biophys. J. 95 (2008) 1837-1850.

[95] A.A. Gurtovenko, J. Anwar, I. Vattulainen, Defect-Mediated Trafficking across Cell Membranes: Insights from in Silico Modeling, Chem. Rev. 110 (2010) 6077-6103.

[96] A. Barnett, The current-voltage relation of an aqueous pore in a lipid bilayer mem-

brane, Biochim. Biophys. Acta BBA - Biomembr. 1025 (1990) 10-14.

[97] S. Kakorin, E. Neumann, Ionic conductivity of electroporated lipid bilayer membranes, Bioelectrochemistry Amst. Neth. 56 (2002) 163-166.

[98] J. Li, H. Lin, The current-voltage relation for electropores with conductivity gradients, Biomicrofluidics. 4 (2010).

[99] K.C. Smith, R.S. Son, T.R. Gowrishankar, J.C. Weaver, Emergence of a large pore subpopulation during electroporating pulses, Bioelectrochemistry. 100 (2014) 3-10.

[100] R.P. Joshi, V. Sridhara, K.H. Schoenbach, Microscopic calculations of local lipid membrane permittivities and diffusion coefficients for application to electroporation analyses, Biochem. Biophys. Res. Commun. 348 (2006) 643-648.

[101] M. Deminsky, A. Eletskii, A. Kniznik, A. Odinokov, V. Pentkovskii, B. Potapkin, Molecular Dynamic Simulation of Transmembrane Pore Growth, J. Membr. Biol. 246 (2013) 821-831.

[102] S. Kohler, Z.A. Levine, M.A. Garcia-Fernandez, M.-C. Ho, P.T. Vernier, P. Leveque, et al., Electrical Analysis of Cell Membrane Poration by an Intense Nanosecond Pulsed Electric Field Using an Atomistic-to-Continuum Method, IEEE Trans. Microw. Theory Tech. 63 (2015) 2032-2040.

[103] Q. Hu, S. Viswanadham, R.P. Joshi, K.H. Schoenbach, S.J. Beebe, P.F. Blackmore, Simulations of transient membrane behavior in cells subjected to a high-intensity ultrashort electric pulse, Phys. Rev. E. 71 (2005) 031914.

[104] Z. Vasilkoski, A. Esser, T. Gowrishankar, J. Weaver, Membrane electroporation: The absolute rate equation and nanosecond time scale pore creation, Phys. Rev. E. 74 (2006) 021904.

[105] R. Sundararajan, Nanosecond Electroporation: Another Look, Mol. Biotechnol. 41 (2009) 69-82.

[106] L. Delemotte, M. Tarek, Molecular Dynamics Simulations of Lipid Membrane Electroporation, J. Membr. Biol. 245 (2012) 531-543.

[107] D.P. Tieleman, H.J.C. Berendsen, M.S.P. Sansom, Voltage-Dependent Insertion of Alamethicin at Phospholipid/Water and Octane/Water Interfaces, Biophys. J. 80 (2001) 331-346.

[108] B. Roux, The Membrane Potential and its Representation by a Constant Electric Field in Computer Simulations, Biophys. J. 95 (2008) 4205-4216.

[109] J. Gumbart, F. Khalili-Araghi, M. Sotomayor, B. Roux, Constant electric field simulations of the membrane potential illustrated with simple systems, Biochim. Biophys. Acta

BBA - Biomembr. 1818 (2012) 294-302.

[110] M. Tarek, Membrane Electroporation: A Molecular Dynamics Simulation, Biophys. J. 88 (2005) 4045-4053.

[111] D.P. Tieleman, The molecular basis of electroporation, BMC Biochem. 5 (2004) 10.

[112] M.J. Ziegler, P.T. Vernier, Interface Water Dynamics and Porating Electric Fields for Phospholipid Bilayers, J. Phys. Chem. B. 112 (2008) 13588-13596.

[113] Q. Hu, R.P. Joshi, K.H. Schoenbach, Simulations of nanopore formation and phosphatidylserine externalization in lipid membranes subjected to a high-intensity, ultrashort electric pulse, Phys. Rev. E. 72 (2005) 031902.

[114] A. Petrishia, M. Sasikala, Molecular Simulation of Cell Membrane Deformation by Picosecond Intense Electric Pulse, J. Membr. Biol. (2015) 1-6.

[115] P.T. Vernier, Z.A. Levine, M.-C. Ho, S. Xiao, I. Semenov, A.G. Pakhomov, Picosecond and Terahertz Perturbation of Interfacial Water and Electropermeabilization of Biological Membranes, J. Membr. Biol. 248 (2015) 837-847.

[116] S. Kohler, M.-C. Ho, Z.A. Levine, P.T. Vernier, P. Leveque, D. Arnaud-Cormos, Electrical analysis of cell membrane poration induced by an intense nanosecond pulsed electric field, using an atomistic- to-continuum method, in: Microw. Symp. IMS 2014 IEEE MTT- Int., 2014: pp. 1-4.

[117] J.N. Sachs, P.S. Crozier, T.B. Woolf, Atomistic simulations of biologically realistic transmembrane potential gradients, J. Chem. Phys. 121 (2004) 10847-10851.

[118] A.A. Gurtovenko, I. Vattulainen, Pore Formation Coupled to Ion Transport through Lipid Membranes as Induced by Transmembrane Ionic Charge Imbalance: Atomistic Molecular Dynamics Study, J. Am. Chem. Soc. 127 (2005) 17570-17571.

[119] A.A. Gurtovenko, I. Vattulainen, Ion Leakage through Transient Water Pores in Protein-Free Lipid Membranes Driven by Transmembrane Ionic Charge Imbalance, Biophys. J. 92 (2007) 1878-1890.

[120] L. Delemotte, F. Dehez, W. Treptow, M. Tarek, Modeling Membranes under a Transmembrane Potential, J. Phys. Chem. B. 112 (2008) 5547-5550.

[121] S.K. Kandasamy, R.G. Larson, Cation and anion transport through hydrophilic pores in lipid bilayers, J. Chem. Phys. 125 (2006) 074901.

[122] Z. Wu, Q. Cui, A. Yethiraj, A New Coarse-Grained Force Field for Membrane-Peptide Simulations, J. Chem. Theory Comput. 7 (2011) 3793-3802.

[123] F. Dehez, L. Delemotte, P. Kramar, D. Miklavčič, M. Tarek, Evidence of Conduct-

ing Hydrophobic Nanopores Across Membranes in Response to an Electric Field, J. Phys. Chem. C. 118 (2014) 6752- 6757.

[124] A. Polak, D. Bonhenry, F. Dehez, P. Kramar, D. Miklavčič, M. Tarek, On the Electroporation Thresholds of Lipid Bilayers: Molecular Dynamics Simulation Investigations, J. Membr. Biol. 246 (2013) 843-850.

[125] A. Polak, M. Tarek, M. Tomsic, J. Valant, N.P. Ulrih, A. Jamnik, et al., Electroporation of archaeal lipid membranes using MD simulations, Bioelectrochemistry. 100 (2014) 18-26.

[126] A. Polak, A. Velikonja, P. Kramar, M. Tarek, D. Miklavčič, Electroporation Threshold of POPC Lipid Bilayers with Incorporated Polyoxyethylene Glycol (C12E8), J. Phys. Chem. B. 119 (2015) 192-200.

[127] P.T. Vernier, M.J. Ziegler, Y. Sun, M.A. Gundersen, D.P. Tieleman, Nanopore-facilitated, voltage-driven phosphatidylserine translocation in lipid bilayers-in cells and in silico, Phys. Biol. 3 (2006) 233.

[128] D.P. Tieleman, Computer Simulations of Transport Through Membranes: Passive Diffusion, Pores, Channels and Transporters, Clin. Exp. Pharmacol. Physiol. 33 (2006) 893-903.

[129] T. Kotnik, P. Kramar, G. Pucihar, D. Miklavčič, M. Tarek, Cell membrane electroporation-Part 1: The phenomenon, IEEE Electr. Insul. Mag. 28 (2012) 14-23.

[130] Q. Hu, Z. Zhang, H. Qiu, M.G. Kong, R.P. Joshi, Physics of nanoporation and water entry driven by a high-intensity, ultrashort electrical pulse in the presence of membrane hydrophobic interactions, Phys. Rev. E. 87 (2013) 032704.

[131] W.F.D. Bennett, N. Sapay, D.P. Tieleman, Atomistic Simulations of Pore Formation and Closure in Lipid Bilayers, Biophys. J. 106 (2014) 210-219.

[132] D.P. Tieleman, H. Leontiadou, A.E. Mark, S.-J. Marrink, Simulation of Pore Formation in Lipid Bilayers by Mechanical Stress and Electric Fields, J. Am. Chem. Soc. 125 (2003) 6382-6383.

[133] A. Venturini, F. Zerbetto, Dynamics of a lipid bilayer induced by electric fields, Phys. Chem. Chem. Phys. 13 (2011) 9216-9222.

[134] W.F.D. Bennett, D.P. Tieleman, The Importance of Membrane Defects-Lessons from Simulations, Acc. Chem. Res. 47 (2014) 2244-2251.

[135] Z.A. Levine, P.T. Vernier, Life cycle of an electropore: field-dependent and field-independent steps in pore creation and annihilation, J. Membr. Biol. 236 (2010) 27-36.

[136] Z.A. Levine, P.T. Vernier, Calcium and phosphatidylserine inhibit lipid electropore formation and reduce pore lifetime, J. Membr. Biol. 245 (2012) 599-610.

[137] P.T. Vernier, M.J. Ziegler, Nanosecond Field Alignment of Head Group and Water Dipoles in Electroporating Phospholipid Bilayers, J. Phys. Chem. B. 111 (2007) 12993-12996.

[138] M. Tokman, J.H. Lee, Z.A. Levine, M.-C. Ho, M.E. Colvin, P.T. Vernier, Electric Field-Driven Water Dipoles: Nanoscale Architecture of Electroporation, PLoS ONE. 8 (2013) e61111.

[139] U. Pliquett, R.P. Joshi, V. Sridhara, K.H. Schoenbach, High electrical field effects on cell membranes, Bioelectrochemistry. 70 (2007) 275-282.

[140] Q. Hu, V. Sridhara, R.P. Joshi, J.F. Kolb, K.H. Schoenbach, Molecular Dynamics Analysis of High Electric Pulse Effects on Bilayer Membranes Containing DPPC and DPPS, IEEE Trans. Plasma Sci. 34 (2006) 1405-1411.

[141] S.O. Yesylevskyy, L.V. Schafer, D. Sengupta, S.J. Marrink, Polarizable Water Model for the Coarse-Grained MARTINI Force Field, PLoS Comput Biol. 6 (2010) e1000810.

[142] S. Sun, G. Yin, Y.-K. Lee, J.T.Y. Wong, T.-Y. Zhang, Effects of deformability and thermal motion of lipid membrane on electroporation: By molecular dynamics simulations, Biochem. Biophys. Res. Commun. 404 (2011) 684-688.

[143] M.-C. Ho, Z.A. Levine, P.T. Vernier, Nanoscale, Electric Field-Driven Water Bridges in Vacuum Gaps and Lipid Bilayers, J. Membr. Biol. 246 (2013) 793-801.

[144] P.T. Vernier, Z.A. Levine, Y.-H. Wu, V. Joubert, M.J. Ziegler, L.M. Mir, et al., Electroporating Fields Target Oxidatively Damaged Areas in the Cell Membrane, PLoS ONE. 4 (2009) e7966.

[145] S. Sun, J.T.Y. Wong, T.-Y. Zhang, Atomistic Simulations of Electroporation in Water Preembedded Membranes, J. Phys. Chem. B. 115 (2011) 13355-13359.

[146] M.L. Fernández, R. Reigada, Effects of Dimethyl Sulfoxide on Lipid Membrane Electroporation, J. Phys. Chem. B. 118 (2014) 9306-9312.

[147] E.K. Peter, I.V. Pivkin, A polarizable coarse-grained water model for dissipative particle dynamics, J. Chem. Phys. 141 (2014) 164506.

[148] A.A. Gurtovenko, A.S. Lyulina, Electroporation of Asymmetric Phospholipid Membranes, J. Phys. Chem. B. 118 (2014) 9909-9918.

[149] M.L. Fernández, G. Marshall, F. Sagués, R. Reigada, Structural and Kinetic Molecular Dynamics Study of Electroporation in Cholesterol-Containing Bilayers, J. Phys. Chem. B. 114 (2010) 6855-6865.

[150] R. Reigada, M.L. Fernandez, Structure and electroporation of lipid bilayers: A Molecular Dynamics study, in: Gen. Assem. Sci. Symp. 2011 XXXth URSI, 2011: pp. 1-4.

[151] T.J. Piggot, D.A. Holdbrook, S. Khalid, Electroporation of the E. coli and S. Aureus Membranes: Molecular Dynamics Simulations of Complex Bacterial Membranes, J. Phys. Chem. B. 115 (2011) 13381-13388.

[152] R. Reigada, Electroporation of heterogeneous lipid membranes, Biochim. Biophys. Acta BBA - Biomembr. 1838 (2014) 814-821.

[153] P. Kramar, L. Delemotte, A.M. Lebar, M. Kotulska, M. Tarek, D. Miklavčič, Molecular-Level Characterization of Lipid Membrane Electroporation using Linearly Rising Current, J. Membr. Biol. 245 (2012) 651-659.

[154] M.L. Fernández, M. Risk, R. Reigada, P.T. Vernier, Size-controlled nanopores in lipid membranes with stabilizing electric fields, Biochem. Biophys. Res. Commun. 423 (2012) 325-330.

[155] M.-C. Ho, M. Casciola, Z.A. Levine, P.T. Vernier, Molecular Dynamics Simulations of Ion Conductance in Field-Stabilized Nanoscale Lipid Electropores, J. Phys. Chem. B. 117 (2013) 11633-11640.

[156] F. Salomone, M. Breton, I. Leray, F. Cardarelli, C. Boccardi, D. Bonhenry, et al., High-Yield Nontoxic Gene Transfer through Conjugation of the CM18-Tat11 Chimeric Peptide with Nanosecond Electric Pulses, Mol. Pharm. 11 (2014) 2466-2474.

[157] V. Sridhara, R.P. Joshi, Numerical study of lipid translocation driven by nanoporation due to multiple high-intensity, ultrashort electrical pulses, Biochim. Biophys. Acta BBA - Biomembr. 1838 (2014) 902-909.

[158] S.J. Marrink, F. Jahnig, H.J. Berendsen, Proton transport across transient single-file water pores in a lipid membrane studied by molecular dynamics simulations., Biophys. J. 71 (1996) 632-647.

[159] V. Sridhara, R.P. Joshi, Evaluations of a mechanistic hypothesis for the influence of extracellular ions on electroporation due to high-intensity, nanosecond pulsing, Biochim. Biophys. Acta BBA - Biomembr. 1838 (2014) 1793-1800.

[160] M. Fromm, L.P. Taylor, V. Walbot, Expression of genes transferred into monocot and dicot plant cells by electroporation, Proc. Natl. Acad. Sci. 82 (1985) 5824-5828.

[161] R.A. Gilbert, M.J. Jaroszeski, R. Heller, Novel electrode designs for electrochemotherapy, Biochim. Biophys. Acta BBA - Gen. Subj. 1334 (1997) 9-14.

[162] Cliniporator, IGEA http://www.igeamedical.com/oncology/cliniporator

[163] M. Rebersek, S. Corovic, G. Sersa, D. Miklavčič, Electrode commutation sequence for honeycomb arrangement of electrodes in electrochemotherapy and corresponding electric field distribution, Bioelectrochemistry Amst. Neth. 74 (2008) 26-31.

[164] S. Mazéres, D. Sel, M. Golzio, G. Pucihar, Y. Tamzali, D. Miklavčič, et al., Non invasive contact electrodes for in vivo localized cutaneous electropulsation and associated drug and nucleic acid delivery, J. Control. Release Off. J. Control. Release Soc. 134 (2009) 125-131.

[165] W.G. Lee, U. Demirci, A. Khademhosseini, Microscale electroporation: challenges and perspectives for clinical applications, Integr. Biol. 1 (2009) 242-251.

[166] N. Hu, J. Yang, S.W. Joo, A.N. Banerjee, S. Qian, Cell electrofusion in microfluidic devices: A review, Sens. Actuators B Chem. 178 (2013) 63-85.

[167] Y. Xu, S. Su, C. Zhou, Y. Lu, W. Xing, Cell electroporation with a three-dimensional microelectrode array on a printed circuit board, Bioelectrochemistry. 102 (2015) 35-41.

[168] K.H. Schoenbach, S. Katsuki, R.H. Stark, E.S. Buescher, S.J. Beebe, Bioelectrics-new applications for pulsed power technology, IEEE Trans. Plasma Sci. 30 (2002) 293-300.

[169] A. Kuthi, P. Gabrielsson, M.R. Behrend, P.T. Vernier, M.A. Gundersen, Nanosecond Pulse Generator Using Fast Recovery Diodes for Cell Electromanipulation, IEEE Trans. Plasma Sci. 33 (2005) 1192-1197.

[170] J.F. Kolb, S. Kono, K.H. Schoenbach, Nanosecond pulsed electric field generators for the study of subcellular effects, Bioelectromagnetics. 27 (2006) 172-187.

[171] A. de Angelis, J.F. Kolb, L. Zeni, K.H. Schoenbach, Kilovolt Blumlein pulse generator with variable pulse duration and polarity, Rev. Sci. Instrum. 79 (2008) 044301.

[172] J.M. Sanders, A. Kuthi, Y.-H. Wu, P.T. Vernier, M.A. Gundersen, A linear, single-stage, nanosecond pulse generator for delivering intense electric fields to biological loads, IEEE Trans. Dielectr. Electr. Insul. 16 (2009) 1048-1054.

[173] C. Merla, S. El Amari, M. Kenaan, M. Liberti, F. Apollonio, D. Arnaud-Cormos, et al., A 10- High-Voltage Nanosecond Pulse Generator, IEEE Trans. Microw. Theory Tech. 58 (2010) 4079-4085.

[174] S. Romeo, M. Sarti, M.R. Scarfí, L. Zeni, Modified Blumlein pulse-forming networks for bioelectrical applications, J. Membr. Biol. 236 (2010) 55-60.

[175] M. Kenaan, S. El Amari, A. Silve, C. Merla, L.M. Mir, V. Couderc, et al., Characterization of a 50- Ω exposure setup for high-voltage nanosecond pulsed electric field bioexperiments, IEEE Trans. Biomed. Eng. 58 (2011) 207-214.

[176] S. Romeo, C. D'Avino, O. Zeni, L. Zeni, A Blumlein-type, nanosecond pulse generator with interchangeable transmission lines for bioelectrical applications, IEEE Trans. Dielectr. Electr. Insul. 20 (2013) 1224-1230.

[177] H. Li, R. Bashir, Dielectrophoretic separation and manipulation of live and heat-

treated cells of Listeria on microfabricated devices with interdigitated electrodes, Sens. Actuators B Chem. 86 (2002) 215-221.

[178] G. Mernier, N. Piacentini, T. Braschler, N. Demierre, P. Renaud, Continuous-flow electrical lysis device with integrated control by dielectrophoretic cell sorting, Lab. Chip. 10 (2010) 2077-2082.

[179] H.-L. Gou, X.-B. Zhang, N. Bao, J.-J. Xu, X.-H. Xia, H.-Y. Chen, Label-free electrical discrimination of cells at normal, apoptotic and necrotic status with a microfluidic device, J. Chromatogr. A. 1218 (2011) 5725-5729.

[180] C. Merla, A. Paffi, F. Apollonio, P. Leveque, G. D'Inzeo, M. Liberti, Microdosimetry for Nanosecond Pulsed Electric Field Applications: A Parametric Study for a Single Cell, IEEE Trans. Biomed. Eng. 58 (2011) 1294-1302.

[181] A. Silve, J. Villemejane, V. Joubert, A. Ivorra, L.M. Mir, Nanosecond pulsed electric field delivery to biological samples: Difficulties and potential solutions, Adv. Electroporation Tech. Biol. Med. Boca Raton FL CRC Press Taylor Francis Group. (2011).

[182] E.S. Buescher, K.H. Schoenbach, Effects of submicrosecond, high intensity pulsed electric fields on living cells - intracellular electromanipulation, IEEE Trans. Dielectr. Electr. Insul. 10 (2003) 788-794.

[183] T. Tang, F. Wang, A. Kuthi, M.A. Gundersen, Diode Opening Switch Based Nanosecond High Voltage Pulse Generators for Biological and Medical Applications, IEEE Trans. Dielectr. Electr. Insul. 14 (2007) 878-883.

[184] W.H. Baldwin, B.W. Gregory, C.J. Osgood, K.H. Schoenbach, J.F. Kolb, Membrane Permeability and Cell Survival After Nanosecond Pulsed-Electric-Field Exposure;Significance of Exposure-Media Composition, IEEE Trans. Plasma Sci. 38 (2010) 2948-2953.

[185] S. Xiao, S. Guo, V. Nesin, R. Heller, K.H. Schoenbach, Subnanosecond Electric Pulses Cause Membrane Permeabilization and Cell Death, IEEE Trans. Biomed. Eng. 58 (2011) 1239-1245.

[186] P. Lamberti, S. Romeo, A. Sannino, L. Zeni, O. Zeni, The Role of Pulse Repetition Rate in nsPEF-Induced Electroporation: A Biological and Numerical Investigation, IEEE Trans. Biomed. Eng. 62 (2015) 2234-2243.

[187] Y.-H. Wu, D. Arnaud-Cormos, M. Casciola, J.M. Sanders, P. Leveque, P.T. Vernier, Moveable Wire Electrode Microchamber for Nanosecond Pulsed Electric-Field Delivery, IEEE Trans. Biomed. Eng. 60 (2013) 489-496.

[188] M. Liberti, F. Apollonio, A. Paffi, M. Pellegrino, G. d'Inzeo, A coplanar-waveguide system for cells exposure during electrophysiological recordings, IEEE Trans. Microw. Theory Tech. 52 (2004) 2521-2528.

[189] A. Paffi, M. Pellegrino, R. Beccherelli, F. Apollonio, M. Liberti, D. Platano, et al., A Real-Time Exposure System for Electrophysiological Recording in Brain Slices, IEEE Trans. Microw. Theory Tech. 55 (2007) 2463-2471.

[190] E. Piuzzi, C. Merla, G. Cannazza, A. Zambotti, F. Apollonio, A. Cataldo, et al., A Comparative Analysis Between Customized and Commercial Systems for Complex Permittivity Measurements on Liquid Samples at Microwave Frequencies, IEEE Trans. Instrum. Meas. 62 (2013) 1034-1046.

[191] C. Dalmay, J. Villemejane, V. Joubert, O. Français, L.M. Mir, B. Le Pioufle, Design and realization of a microfluidic device devoted to the application of ultra-short pulses of electrical field to living cells, Sens. Actuators B Chem. 160 (2011) 1573-1580.

[192] C. Dalmay, J. Villemejane, V. Joubert, A. Silve, D. Arnaud-Cormos, O. Français, et al., A microfluidic biochip for the nanoporation of living cells, Biosens. Bioelectron. 26 (2011) 4649-4655.

[193] D. Arnaud-Cormos, P. Leveque, Y.-H. Wu, J.M. Sanders, M.A. Gundersen, P.T. Vernier, Microchamber Setup Characterization for Nanosecond Pulsed Electric Field Exposure, IEEE Trans. Biomed. Eng. 58 (2011) 1656-1662.

[194] N. Chen, K.H. Schoenbach, J.F. Kolb, R. James Swanson, A.L. Garner, J. Yang, et al., Leukemic cell intracellular responses to nanosecond electric fields, Biochem. Biophys. Res. Commun. 317 (2004) 421-427.

[195] Y. Sun, P.T. Vernier, M. Behrend, L. Marcu, M.A. Gundersen, Electrode microchamber for noninvasive perturbation of mammalian cells with nanosecond pulsed electric fields, IEEE Trans. NanoBioscience. 4 (2005) 277-283.

[196] W. Frey, J.A. White, R.O. Price, P.F. Blackmore, R.P. Joshi, R. Nuccitelli, et al., Plasma Membrane Voltage Changes during Nanosecond Pulsed Electric Field Exposure, Biophys. J. 90 (2006) 3608-3615.

[197] P. Krishnaswamy, A. Kuthi, Meng-Tse Chen, Shih-Jui Chen, P.T. Vernier, M.A. Gundersen, Compact high voltage subnanosecond pulsed power delivery system for biological applications, in: Pulsed Power Conf. 2007 16th IEEE Int., 2007: pp. 476-480.

[198] I. Semenov, S. Xiao, D. Kang, K.H. Schoenbach, A.G. Pakhomov, Cell stimulation and calcium mobilization by picosecond electric pulses, Bioelectrochemistry. 105 (2015) 65-71.

[199] Z. Ji, S.M. Kennedy, J.H. Booske, S.C. Hagness, Experimental Studies of Persistent Poration Dynamics of Cell Membranes Induced by Electric Pulses, IEEE Trans. Plasma Sci. 34 (2006) 1416-1424.

Chapter 3

Methods: Classical Molecular Dynamics / Méthodes de modélisation: Dynamique Moléculaire Classique

La modélisation moléculaire est un terme générique qui fait référence à des méthodes théoriques et techniques de calcul, qui sont appliquées pour modéliser et simuler le comportement de molécules, afin de déterminer des structures macromoléculaires tridimensionnelles, ou l'organisation tridimensionnelle de complexes au niveau atomique. La modélisation moléculaire pour l'étude des membranes est une pratique courante de nos jours. D'une part, tout comme la cristallographie aux rayons X, la résonance magnétique nucléaire (RMN) et la microscopie électronique, les méthodes de modélisation moléculaire fournissent un aperçu des propriétés structurelles. D'autre part, certaines méthodes de modélisation moléculaire permettent d'accéder à la dynamique et ceci à des échelles de temps allant de la picoseconde à la microseconde.

En dynamique moléculaire (DM), le système est représenté par un ensemble de particules (généralement des atomes) en interaction. En appliquant les lois de la mécanique classique, à partir de conditions initiales, on est en mesure de prédire l'évolution du système en fonction du temps (générer les coordonnées et les vitesses des atomes, i.e. une trajectoire). Les interactions entre les atomes sont décrites par plusieurs termes d'énergie (non liées: Type Van der Waals et électrostatiques et liés: énergies de valence et de déformation d'angles et de dièdres, etc), spécialement conçus pour reproduire les propriétés structurales des biomolécules et paramétrés en conséquence. Basé sur les trajectoires de DM, on est en mesure d'avoir accès à des informations pertinentes liées aux propriétés structurales, dynamiques et thermodynamiques du système, capables d'être confrontées aux expériences.

Un algorithme de dynamique moléculaire est structuré de la manière suivante. Les

paramètres définissants les conditions dans lesquelles la dynamiques aura lieu sont d'abord donnés en début de simulation, comme la température, le pas de temps d'intégration, la durée de la simulation ... La simulation s'initialise alors en donnant les positions initiales des atomes, définissant la configuration du système au temps t_0, ainsi que les vitesses initiales, v_0 de chaque atome. L'étape suivante consiste à calculer les forces agissantes sur chaque atome en utilisant l'énergie potentielle décrite par le champs de force. Viens ensuite la résolution des équations du mouvement : connaissant les positions, les vitesses et les forces au temps t, les positions et vitesses des atomes sont calculées au temps suivant puis les forces sont de nouveaux évaluées. Cette dernière étape est répétée autant de fois que nécessaire pour calculer la trajectoire sur le temps de simulation désiré. Finalement notons que dans ces simulations, pour étudier les systèmes macroscopiques réalistes, on impose dans ces calculs des conditions périodiques (à deux ou trois dimensions) aux limites. Les artefacts peuvent être introduits par les images de la période si la condition à la limite ne soit pas manipulé avec soin (voir 3.3).

En simulations dites classiques, les degrés de liberté électroniques sont négligés, ce qui est valable en supposant que l'approximation de Born-Oppenheimer [2]. En conséquence, les densités électroniques sont prédéfinies dans les paramètres de champ de force, et les charges sur les atomes sont fixées au cours de la simulation avec l'hypothèse selon laquelle des électrons sont dans leurs états fondamentaux. Cette limitation exclut des effets quantiques et des effets tels que le transfert d'électrons, l'excitation d'électrons et une réaction chimique entre les molécules pendant la simulation. Par ailleurs, bien que les effets de polarisabilité peuvent être introduits par diverses méthodes telles que l'ajout de sites virtuels (particules Drude) ou un potentiel de paire efficace, le traitement de la polarisabilité est souvent ignorée dans le but de réduire les coûts informatiques. Néanmoins plusieurs phénomènes physiques peuvent être décrits avec une bonne approximation tout en négligeant cette dernière.

Une autre limitation découlant de l'utilisation de champs de force empiriques et leur capacité à bien décrire les interactions atomiques. Il est à noter que les champs de force disponibles pour les modèles de membranes développés au cours des dernières décennies se sont révélés être suffisamment précis en termes de propriétés cinétiques et thermodynamiques lorsqu'ils sont utilisés à des conditions normales de température (environ 300 K) et de pressions (environ 1 bar).

A côté de ces limites méthodologiques, la limite en ressources informatiques introduit également des restrictions supplémentaires. Par exemple, les interactions de Lennard-Jones sont habituellement évalués avec un rayon de coupure au-delà duquel elles sont négligées, et les interactions électrostatiques à longue portée sont généralement calculés en utilisant les sommation Ewald afin de réduire les calculs. Le remplacement des méthodes de troncature électroniques avec la méthode Ewald de maille de particules (PME) a amélioré sensiblement la stabilité et la convergence des simulations, en réduisant les coûts de calcul pour calculer les interactions à longue portée. En particulier, une fois que les

instabilités dues aux méthodes d'approximation dans le traitement de l'électrostatique à longue portée et une précision limitée dans les champs de force ont été surmontés, des dynamiques stables de plusieurs centaines de nanosecondes de modèles membranaires peuvent être obtenues. Notons qu'à ce jour, on a pu simuler les processus de micro et millisecondes pour des système de plusieurs millions d'atomes (par exemple [3]).

Methods: Classical Molecular Dynamics / Méthodes de modélisation: Dynamique Moléculaire Classique

Theoretical methods and computational approaches applied to reproduce and predict the behavior of molecules at the atomic level are all part of the general category of molecular modeling.

Molecular Dynamics (MD) simulations provide atomic details of the structures and motions of a classical many-body scheme and hence allow for computing its structural, dynamic and thermodynamic properties. In this context, the word classical means that the nuclear motion of the constituent particles obeys the laws of classical mechanics. By applying the Newton's equation of motion, from given initial conditions the evolution of the system in time can be predicted.

MD methods produce a so called trajectory, i.e. coordinates and velocities, of the simulated set of interacting particles (e.g. atoms). The behavior and energetics of molecules are fundamentally quantum mechanical. However, quantum mechanical models are computationally demanding with a sever limitation of the system size and time scale of the simulation. Approximating atomic and molecular interactions with classical mechanics, based on the classical motion of nuclei (treated as point charges in a framework that totally neglects electrons), allows to increase simulation size and time scale limits, while preserving accuracy for the description of a number of properties that do not depend on the electronic distribution in a molecule.

In classical MD the potential energy of and forces acting on a many body system are calculated from an empirical force field. Empirical force fields, indeed, are collective of several energy terms to describe the interactions between atoms (bonded: energy of bonds, valence and dihedral angles, etc.; non bonded: electrostatic and van der Waals terms), implemented to reproduce the structural properties of biomolecules and parameterized accordingly.

MD simulations are becoming an increasingly powerful tool for the prediction of molecular properties: based on the MD trajectories, one can access information related to structural, dynamical and thermodynamics properties of the modeled system complementary and of support to experimental observations. It was originally conceived within theoretical physics in the late 1950's [1], but is nowadays applied to various areas of science such as materials science and biochemistry.

Like any other analytical tool, there are limitations for MD simulation.

First, by using Newton's Second Law, the nature of MD simulation is purely classical. The electronic degrees of freedom are neglected, which is valid assuming the Born-Oppenheimer approximation [2]. The latter is the assumption that the motion of atomic nuclei and electrons in a molecule can be separated and, thus, the energy of a molecule can be represented in terms of nuclear coordinates only. Consequently the electron densities of molecules are predefined in the force field parameters, and the charges on the molecules are fixed during the simulation with the assumption that electrons are in their ground states. This limitation excludes quantum effects (e.g. tunneling) and effects such as electron transfer, electron excitation and chemical reaction between molecules during the simulation. Molecules in MD simulation by default also lack polarizability. Although the effects of polarizability can be introduced by various methods such as adding virtual sites (Drude particles) or effective pair potential, the treatment of polarizability is often ignored in order to reduce computing cost. Nevertheless several physical phenomena can be described with a good approximation neglecting the electron wave functions.

Another limitation arise from the use of empirical force fields and their ability to properly describes atomic interactions. Luckily, the available force fields for membrane models developed over the past decades have proved to be sufficiently accurate in terms of kinetic and thermodynamics properties when used at normal temperatures (around 300 K) and normal pressures (around 1 bar).

Beside these methodological limitations, the restriction of computing resources also introduces additional limitations. For instance, Lennard-Jones interactions are usually being cutoff beyond certain range and the long-range electrostatic interactions are usually approximated by Ewald summation in order to reduce computations. The replacement of electronic truncation methods with the particle mesh Ewald (PME) method improved substantially the stability and the convergence of the simulations, reducing the computational costs to calculate the long-range interactions of many-body schemes. In particular, once the instabilities due to approximation methods in the treatment of long range electrostatics and limited accuracy in the force fields have been overcome, stable hundred-ns MD simulations of membrane models are feasible. Nevertheless many biologically relevant processes may occur at timescales from nanoseconds to seconds and may involve more than billions of atoms at a time. Up today, using the MD methods, one was able to simulate micro- and milliseconds processes in the system of millions of atoms (e.g. [3]) and to reach the seconds time scale more than one decade is needed.

Moreover, in order to facilitate MD simulation to study molecular structures that resemble macroscopic systems, periodic boundary condition is often imposed. Artifacts can be introduced by the period images if the boundary condition is not handled carefully (see 3.3).

Challenges to these limitations are currently topics in scientific computing research.

This chapter is dedicated to the description of the MD method, which we applied to investigate the effect of pulse electric fields on membrane models.

3.1 Newtonian dynamics

The time evolution of a N particles molecular system, starting from a known configuration (potions and velocities), during MD simulations is described by Newton's equation of motion [4]:

$$\mathbf{F}_i = m_i \frac{d^2\mathbf{r}_i}{dt^2}, \quad i = 1,2,\ldots,N. \tag{3.1}$$

where $\mathbf{F}_i$ is the force acting on the i^{th} particle (e.g. an atom), with mass m_i and position $\mathbf{r}_i$.

The forces are the negative derivatives of a potential function $U(\mathbf{r}_1,\ldots,\mathbf{r}_N)$: one can compute the interactions among atoms through the potential function, which represents the potential energy of N interacting particles as a function of their positions $\mathbf{r}_i$.

Namely, a force field is an empirical potential characterized by a distinct functional form, representing the interactions of the system of interest, i.e. its physics and chemistry.

The force acting on the particle i is given by the gradient of the know potential with respect to the displacements of this particle:

$$\mathbf{F}_i = -\nabla_{\mathbf{r}_i} U(\mathbf{r}_1,\mathbf{r}_2,\ldots,\mathbf{r}_N) = -\left(\frac{\partial U}{\partial \mathbf{x}_i} + \frac{\partial U}{\partial \mathbf{y}_i} + \frac{\partial U}{\partial \mathbf{z}_i}\right), \quad i = 1,2,\ldots,N, \tag{3.2}$$

therefore

$$m_i \frac{d^2\mathbf{r}_i}{dt^2} = -\nabla_{\mathbf{r}_i} U, \quad i = 1,2,\ldots,N. \tag{3.3}$$

Computing the classical trajectory exactly would require to solve a system of $3N$ second order differential equations, where N is the number of atoms. In practice, these equations are never solved exactly but rather approximated by a suitable algorithm (i.e. integrators) based on time discretization. The size of the time step must be chosen small enough to avoid discretization errors, i.e. much smaller than the fastest vibrational frequency in the system (see 3.2).

The system is propagated for some time, taking care that the temperature and pressure remain at the required values. After initial changes, the system will usually reach an *equilibrium state*. By averaging over an equilibrium trajectory many macroscopic properties can be extracted (see 3.6).

3.2 Integration algorithms

The Verlet algorithm [5] is the most common integrator to propagate the equation of motion in MD simulation: staring from the positions $\mathbf{r}_i$ at time t and velocity $\mathbf{v}_i$ at time $t-\Delta t$ it updates positions and velocities using the forces $\mathbf{F}_i(t)$ acting upon the N particles at time t. Considering the Taylor expansion of a particle position at $\pm\Delta t$:

$$\mathbf{r}_i(t+\Delta t)=\mathbf{r}_i+\Delta t\mathbf{v}_i(t)+\frac{\Delta t^2}{2m_i}\mathbf{F}_i(t)+\frac{\Delta t^3}{3!}\dddot{\mathbf{r}}_i(t)+\mathscr{O}\Delta t^4, \tag{3.4}$$

$$\mathbf{v}_i(t+\Delta t)=\mathbf{v}_i+\frac{\Delta t}{m_i}\mathbf{F}_i(t)+\frac{\Delta t^2}{2}\ddot{\mathbf{v}}+\frac{\Delta t^3}{3!}\dddot{\mathbf{v}}_i(t)+\mathscr{O}\Delta t^4. \tag{3.5}$$

From eqq. 3.4 and 3.5 an important consideration can be made: the Taylor expansion includes a high-order term $\mathscr{O}\Delta t^4$ which can be minimized choosing a Δt small enough, leading to an overall better approximation of the whole integration process. Nevertheless, as previously stated, one subtle aspect of MD simulation is the computational cost required to study long dynamics: hence a convenient time-step has to be chosen. As lower limit one can consider highest frequency proper of the system, namely the vibrations of bonds involving hydrogen atoms in solvated biological macromolecules. The bond stretching frequency of an O-H bond is typically about 10^{14} Hz, so the average period would be of the order of 10 fs [6]. This limits the time-step to be taken in MD simulations to about 0.5 fs (a rule of thumb exists that states that for a reasonable sampling of a periodic function, samples should be taken at least twenty times per period). To increase the time step to a typical value of 2 fs usually algorithms (SHAKE [7], RATTLE [8], LINCS [9], SETTLE [10],...) are employed to constrain all covalent bonds, i.e. the distance between mass points is maintained constant. In general, the algorithm is constructed by following procedures; (i) choosing novel unconstrained coordinates (internal coordinates), (ii) introducing explicit constraint forces, (iii) minimizing constraint forces implicitly by the technique of Lagrange multipliers or projection methods. These approximations are plausible insofar as these bond vibrations can be considered uncoupled from all other vibrations in the system, and therefore the rest of the dynamics of the system are not altered.

One can obtain a numerically stable, efficient and time-reversible integrator by summing eq. 3.4 and 3.5, for $\mathbf{F}_i = m_i\ddot{\mathbf{r}}_i$:

$$\mathbf{r}_i(t+\Delta t)=2\mathbf{r}_i-\mathbf{r}_i(t-\Delta t)+\frac{\Delta t^2}{m_i}\mathbf{F}_i(t)+\mathscr{O}\Delta t^4, \tag{3.6}$$

$$\mathbf{v}_i=\frac{\mathbf{r}_i(t+\Delta t)-\mathbf{r}_i(t-\Delta t)}{2\Delta t}+\mathscr{O}\Delta t^3. \tag{3.7}$$

Notice that the velocities are not needed to calculate the trajectories, yet are useful for the extraction of observables (e.g. kinetic energy).

In our simulations a direct extension of such an algorithm is adopted, the so-called leap-frog algorithm, which minimize numerical imprecision:

$$\mathbf{r}_i(t+\Delta t) = \mathbf{r}_i + \Delta t \mathbf{v}_i\left(t+\frac{\Delta t}{2}\right), \tag{3.8}$$

$$\mathbf{v}_i\left(t+\frac{\Delta t}{2}\right) = \mathbf{v}_i\left(t-\frac{\Delta t}{2}\right) + \frac{\Delta t}{m_i}\mathbf{F}_i(t). \tag{3.9}$$

The name *leapfrog* comes from one of the ways to write this algorithm, where positions and velocities 'leap over' each other. The velocities are updated at half time steps and "leap" ahead the positions. The current velocities can be obtained from:

$$\mathbf{v}_i = \frac{\mathbf{v}_i\left(t-\frac{\Delta t}{2}\right)+\mathbf{v}_i\left(t+\frac{\Delta t}{2}\right)}{2}. \tag{3.10}$$

In the present work, in all the MD simulations chemical bonds between hydrogen and heavy atoms were constrained to their equilibrium values. The integration time-step was chosen to be 2 fs.

3.3 Force fields and potential energy function

As described in 3.1, in order to compute forces MD simulations require a potential energy function, which describes the interactions among all the atoms in the system. If the potential energy of the system is known, given the coordinates of a starting structure and a set of velocities, the force acting on each atom can be calculated. The accuracy and the efficiency of the simulations is directly related to the potential energy function used to describe the interactions among particles. A force field is characterized by a specific functional, implemented to reproduce the structural properties of biomolecules and parameterized accordingly. In other words it is composed by a set of equations, the so-called potential functions, which are used to generate the potential energies and their derivatives (i.e. the forces) correlated with a set of parameters empirically tuned to reproduce the properties of biomolecules.

Within one set of equations various consistent sets of parameters can be used. It is in general dangerous to make *and hoc* changes in a subset of parameters, because the various contributions to the total force are usually interdependent. The basic functional form of a force field includes both bonded terms relating to atoms that are linked by covalent bonds (see Fig. 3.1), and non-bonded (or non-covalent) terms describing the long-range electrostatic and Van der Waals forces (see Fig. 3.2).

A general potential energy function, commonly used in the most know force fields, is:

$$U_{total} = U_{bond} + U_{angles} + U_{dihedrals} + U_{nb}. \tag{3.11}$$

These four contributions account for bonded and non-bonded interactions. The first three terms of eq. 3.11 define the bonded interactions corresponding to two (stretching), three (bending), and four (torsion) body interactions, respectively.

$$U_{bond} = \frac{k_b}{2}(l - l_0)^2, \tag{3.12}$$

$$U_{angles} = \frac{k_\theta}{2}(\theta - \theta_0)^2, \tag{3.13}$$

$$U_{dihedral} = \sum_n \frac{v_n}{2}(1 + (-1)^{n+1}\cos(n\phi - \psi_n)). \tag{3.14}$$

These interactions are represented by harmonic potentials for the bond lengths b (see eq. 3.12), for the bond angle θ (see eq. 3.13) with k_b and k_θ their harmonic force constants, for the dihedral angle ϕ (see eq. 3.14) with n, ψ_n and v_n the torsion, multiplicity, phase angle and barrier height respectively.

The bond term counts each covalent bond in the system (Fig. 3.1 (a) right), angles are the angles between each pair of covalent bonds sharing a single atom at the vertex (Fig. 3.1 (a) left), and the dihedral term describes atoms pairs separated by exactly three covalent bonds with the central bond subject to the torsion angle (Fig. 3.1 C). An improper dihedral term governing the geometry of four planar covalently bonded atoms may be also included.

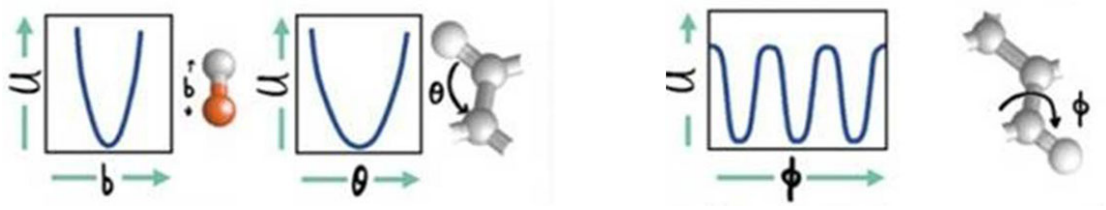

(a) *Bonds, angles.* **(b)** *Torsion angles.*

Figure 3.1: The principles and potentials of short range interactions

The final term of the eq. 3.14 is meaningful of the interaction between non-bonded atom pairs. This term is split into 1-body, 2-body, 3-body, ...subterms. Interactions between particles separated by more than three covalent bonds are usually represented by two components: by Coulomb's law for the electrostatic interactions (eq. 3.15) and by a Lennard-Jones potential for the Van der Waals interactions (eq. 3.16).

The Coulomb potential (Fig. 3.2 (a)) is described by:

$$U_{qq} = \sum_{i<j}\sum_j \frac{q_i q_j}{4\pi\epsilon_{ij} r_{ij}}, \tag{3.15}$$

where the q_i is i^{th} atomic charge, r_{ij} is the distance between the i^{th} an j^{th} point charges, and epsilon is the permittivity of the medium between this two. In more sophisticated force fields the central multipole expansion is considered, which is based upon the electric moments or multipoles: the charge, dipole, quadrupole, octopole, ...

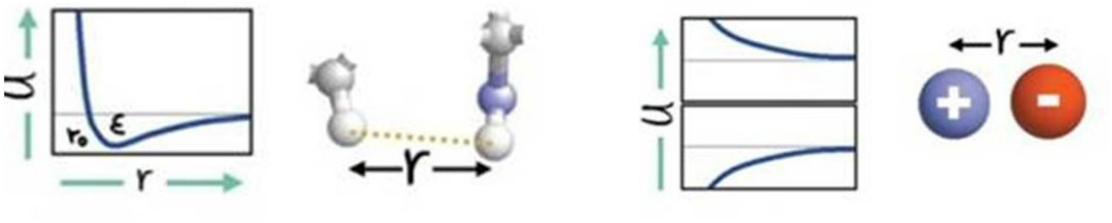

(a) *Non bonded pairs.* **(b)** *Partial charges.*

Figure 3.2: The principles and potentials long range interactions

The Lennard-Jones potential (Fig. 3.2 (b)) can be written as:

$$U_{vdW} = \sum_{i<j}\sum_{j} 4\epsilon_{ij}\left[\left(\frac{\sigma_{ij}}{r_{ij}}\right)^{12} - \left(\frac{\sigma_{ij}}{r_{ij}}\right)^{6}\right], \tag{3.16}$$

where σ_{ij} and ϵ_{ij} are the collision diameter (the finite distance at which the inter-particle potential is zero) and the well depth respectively.

The Lennard-Jones potential is one of the most common empirical function to describe the van der Waals (vdW) interactions, that differ from covalent and ionic bonding in that they are caused by correlations in the fluctuating polarizations of nearby particles. The latter account for two types of forces: the dispersive and exchange/overlap forces. Dispersion (usually named after Fritz London) is the attractive interaction between any pair of molecules, including non-polar atoms, arising from the interactions of instantaneous multipoles. The repulsive component resulting from the Pauli exclusion principle that prevents the collapse of molecules. Induction (also known as polarization), which is the attractive interaction between a permanent multipole on one molecule with an induced multipole on another, is usually neglected.

In addition to the functional form of the potentials, a force field defines a set of parameters for each type of atom. The typical parameter set includes values for atomic mass, Van der Waals radius, partial charge for individual atoms, equilibrium values of bond lengths, bond angles, dihedral angles for pairs, triplets, quandruplets of bonded atoms, and values corresponding to the effective spring constant for each potential. Most current force fields use a fixed-charge model by which each atom is assigned a single value for the atomic charge that is not affected by the local electrostatic environment. All-atom force fields provide parameters for every atom in a system, including hydrogen, while coarse-grained force fields, which are frequently used in long-time simulations of proteins, provide even more abstracted representations for increased computational efficiency [11]. Although many molecular simulations involve biological macromolecules such as proteins, the parameters for given atom types are generally derived from observations on small organic molecules that are more tractable for experimental studies and quantum calculations.

Finally, we would like to notice that special potentials are used for imposing restraints on the motion of the system (position restraint, angle restraint or distance restraint) either

to avoid disastrous deviations, or to include knowledge from experimental data. In either cases they are not really part of the force field and the reliability of the parameters is not important.

The parameters used in the force field can be determined in different ways. The first one is to fit them with results obtained from *ab-initio* calculations on small molecular clusters. The alternative way is to fit the force field parameters to experimental data, like crystal structures, energy and lattice dynamics, infrared or X-ray data on small molecules, liquid properties like density and enthalpy of vaporization, free energy of solvation, nuclear magnetic resonance data, etc. Whatever method is used, the resulting model is far to be universal, and never completely correct. It is worth to note that every force field is usually well suited for specific general conditions, i.e. particular thermodynamic conditions (temperature, density, pressure, etc.) and also boundary conditions. Moreover, they are optimized for specific classes of molecules, such as inorganic molecules, organic molecules, biomolecules (DNA, proteins, lipids), etc.

Popular force fields for MD simulations of biomolecular systems are AMBER [12], CHARMM [13], GROMOS [14] and OPLS-AA [15]. In this work, we considered CHARMM36 force fields [16] to model lipid bilayer, as membrane model. These force field is compatible with the MD software used GROMACS [17].

3.4 Periodic boundary conditions

An important characteristic of the molecular dynamics simulations is the way in which the boundaries are treated. Due to computational limits, a typical simulated system contains hundreds of thousand of atoms, and hence is quite small compared to macroscopic matter. This means that, if the molecules are arranged in a cubic box, a relatively great part of them will lie on the surface and will experience quite different forces from molecules in the bulk. The consequence of the finite size of the system is that the boundary conditions may affect seriously the results of the simulations, especially when the system of interest is a homogeneous liquid or a solution. Usually, periodic boundary conditions (PBCs) (Fig. 3.3) are adopted to reduce the surface effects. PBCs are a set of boundary conditions which are often chosen for approximating a large (infinite) system by using a small part called a unit cell.

This technique consists on simulating the system in a central cubic box surrounded by an infinite number of copies of itself. During the simulation, the molecules in the original box and their periodic images move exactly in the same way. Hence, when a molecule leaves the central box one of its images will enter through the opposite side. As a result, there are no physical boundaries neither surface molecules. Note that other shapes of the box can be used as the truncated octahedron or the rhombic dodecahedron.

Additionally, to avoid redundant interactions the minimum image convention is adopted

(Fig. 3.3), namely each atom interacts with just one image, the closest one, of every other atom in the system.

Nevertheless the size of the simulation box must also be large enough to prevent periodic artifacts from occurring due to the unphysical topology of the simulation: in a box that is too small, a macromolecule may interact with its own image in a neighboring box, which is functionally equivalent to a molecule's "head" interacting with its own "tail". This produces highly unphysical dynamics in most macromolecules, although the magnitude of the consequences and thus the appropriate box size relative to the size of the macromolecules depends on the intended length of the simulation, the desired accuracy, and the anticipated dynamics.

PBCs can be used in conjunction with Ewald summation methods (e.g. the particle mesh Ewald method, 3.5) to calculate electrostatic forces in the system. In such case the net electrostatic charge of the system must be zero to avoid summing to an infinite charge when PBCs are applied.

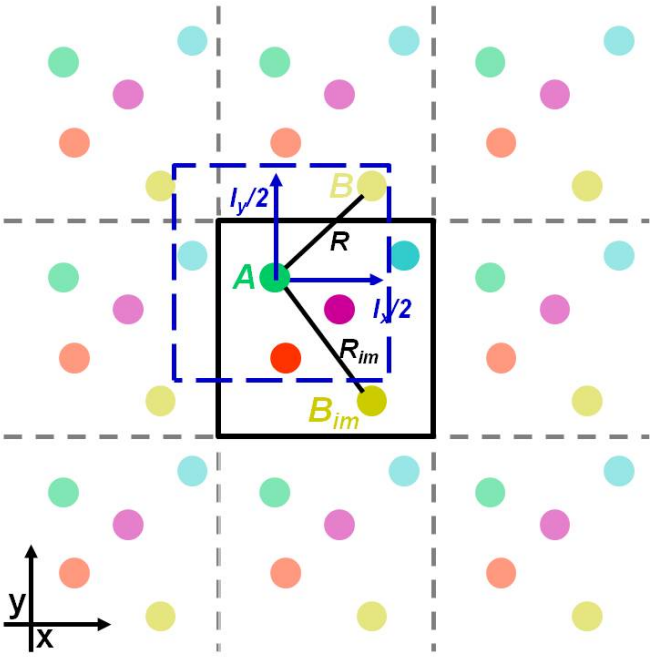

Figure 3.3: Schematic of periodic boundary conditions in two dimensions (x,y). The simulation cell (central) is replicated throughout the space, forming an infinite lattice with images of atoms. For instance, B_{im} is an image of the atom B of the simulation cell. In such scheme each atom interacts with all the other atoms of its cell and also with their images, thus this interaction is limited to the closest image of other atoms as shown by the green dashed box

3.5 Long-range interactions

The treatment of long-range interactions, which usually correspond to the electrostatic forces between molecules, is of enormous importance in MD simulations since they represented the most time-consuming calculations (non-bonded terms increase as the square of the number of atoms N^2). Since experimental evidences have demonstrated the relevance of long range electrostatic interactions in biological molecules, they must be taken into account in MD and many different methods were developed to reduce their computational consumption. Among those, two common techniques are the use of a cut-off radius and the Ewald sum.

The cut-off method is based on the truncation of the forces when the distance between the interacting particles is greater than a specified value, called the cut-off radius, r_c. In this way, the only interactions felt by the i^{th} particle are those due to the particles contained in a sphere of radius r_c and centered at r_i. In MD usually certain cut offs are determined by connectivity, rather than by distance alone. For example, particular potentials may only act between those atoms that are bonded, such as a harmonic force constant, whereas others may specifically only act between those that aren't covalently linked.

The cut-off method is correct only if the intermolecular forces decay rapidly with the distance. In fact, when the forces are negligible at a distance $\leq r_c$, the main structural and dynamical properties are correctly reproduced. Otherwise deviations from the correct bulk behavior are expected.

The use of functions to eliminate the discontinuities in the potential at the cutoff leads to a significant improvement in the accuracy. To deal with with these discontinuities one can employ shifted potentials, switching functions, and tapering. In the first approach, a constant shift can be added to the potential so that the energy at the cut-off boundary becomes zero, it disappears when the potential is differentiated and so does not affect the force calculation in MD. The second multiplies the potential energy function by smoothly switching function ranging from 1 at $r = 0$ to 0 at $r = r_c$, the cutoff distance. The third, the potential is multiplied by a smooth taper function that goes to zero, both for its value and its derivatives typically up to second order. This is usually applied over a short range from an inner radius r_{taper}, to the cut-off distance.

However, this is not one of the most efficient method to reduce the computational costs, since $N(N-1)$ distances among atoms are computed. Verlet [5] proposed to collect neighbor atoms in a pair-list, which significantly reduces the computational cost since this list needs to be updated each 10 or 20 MD time steps only.

Another approach, in MD simulations, is the use of a periodic lattice method in which all the interactions between the molecular system in the central cubic cell and its virtual replica are included. Taking in mind that long-range van der Waals interactions are often neglected, it is particularly important to properly model long-range Coulomb interactions

decaying as $\frac{1}{r}$ because their range is usually greater than the half of the box length. The latter in a periodic system of N charged particles is obtained by a sum over all pairs of which one atom lies in the central box and the other is its periodic image:

$$E = \frac{1}{8\pi\epsilon_0} \sum_{|\mathbf{n}|=0}^{\infty} \sum_{i=1}^{N} \sum_{j=1}^{N} \frac{q_i q_j}{|\mathbf{r}_{ij} + \mathbf{n}|}. \tag{3.17}$$

The sum over n is a summation over all simple cubic lattice points $\mathbf{n} = (x\mathbf{l}_x;\ y\mathbf{l}_y;\ z\mathbf{l}_z)$, with $(\mathbf{l}_x, \mathbf{l}_y, \mathbf{l}_z)$ the unit cell vectors and x, y and z the integers defining the side length of the cubic cell. The case $i = j$ is omitted for n = 0. It was shown that the sum over n for such kind of potential r^{-1} is only conditionally convergent, then its limit may vary or even diverge if the order of terms in the sum is changed.

A solution to this problem was developed following a physical idea [18]: each point charge is surrounded by a charge distribution of equal magnitude and opposite sign, which spreads out radially from the charge, $\rho^G(r)$. This distribution has the effect to screen the interactions between the neighbouring point charges and hence the interaction energy becomes short-ranged. Commonly, the screening charges have a Gaussian form. The total charge distribution is given by:

$$\rho_i(r) = \rho_i^q(r)\rho_i^G(r), \tag{3.18}$$

where $\rho^q(r)$ is the distribution of the point charge of the i^{th} particle and $\rho^G(r)$ is the corresponding Gaussian distribution.

First, the interaction energy due to the distribution eq. 3.18 is calculated in the real space, then, in order to recover the original charge distribution, a canceling function is added in the reciprocal space, which is equal to $-\rho_i^G(r)$, realized by means of a Fourier transform. Hence the final form of the total interaction energy is given by:

$$\begin{aligned}\mathbf{E} = &\frac{1}{8\pi\epsilon_0} \sum_{i=j}^{N} \sum_{j=1}^{N} \left(\sum_{|n|=0}^{\infty} q_i q_j \frac{erfc(\alpha|\mathbf{r}_{ij} + \mathbf{n}|)}{|\mathbf{r}_{ij} + \mathbf{n}|} + \frac{1}{\pi L^3} \sum_{k\neq 0} \frac{4\pi q_i q_j}{k^2} e^{-\frac{k^2}{4a^2}} \cos(\mathbf{k}\cdot\mathbf{r}_{ij}) \right) \\ &- \frac{\alpha}{4\pi^{\frac{3}{2}}\epsilon_0} \sum_{i=1}^{N} q_i^2 + \frac{|\sum_{i=1}^{N} q_i \mathbf{r}_i|^2}{2\epsilon_0 L^3(2\epsilon+1)}.\end{aligned} \tag{3.19}$$

Here $erfc(x)$ is the complementary error function, which falls to zero with increasing its argument. Thus, if the parameter α is large enough, the sum over n in the first term reduces to the only term $n = 0$. The second term is a sum over the reciprocal vectors $k = 2\pi\frac{\mathbf{n}}{L}$. Again, if α is large, a lot of terms in the k-space sum are needed to get a convergence of the energy. The last two terms are, respectively, a correction function, due to the fact

that a self-interaction of the canceling distribution is included in the recipe, and the energy contribution of the depolarizing field, which is compensated by the effect of the external dielectrics. Note that in the Ewald sum the virtual cubic cells are ordered as concentric spherical layers starting from the central box. Clearly the infinite sum is truncated at a certain point and the resulting spherical system is immersed in a continuum dielectrics with dielectric constant ϵ'. The last term in eq. 3.19 is the sum of the contributions of the depolarizing field and the reaction field due to the external dielectrics. If the sphere is embedded in a medium with an infinite dielectric constant, this term vanishes because of a perfect compensation of the two effects. Other periodic lattice methods are often used in computer simulations for their computational stability and efficiency. These methods, like the Particle Mesh Ewald (PME) method [19], can be considered of the same family of the method shown here.

3.6 Thermodynamic ensembles

A thermodynamic ensemble is a specific variety of statistical ensemble that, among other properties, is in statistical equilibrium, and is used to derive the properties of thermodynamic systems from the laws of classical or quantum mechanics. The study of thermodynamics is concerned with systems which appear to human perception to be ”static” (despite the motion of their internal parts), and which can be described by statistical ensembles that depend simply on a set of macroscopically observable variables in statistical equilibrium.

In experiments, a thermodynamic state of a system is usually defined by a small set of parameters, for example, the temperature T, the pressure P, and the number of particles N. In MD simulations, a microscopic state of a system is defined by the atomic positions q, and momenta p; these can also be considered as coordinates in a multidimensional space called phase space. For a system of N particles, this space has $6N$ dimensions. A single point in phase space, denoted by G, describes the state of the system. An ensemble is a collection of points in phase space satisfying the conditions of a particular thermodynamic state. Therefore, a MD simulation generates a sequence of points in phase space as a function of time; these points belong to the same ensemble, and they correspond to the different conformations of the system and their respective momenta.

An experiment is usually made on a macroscopic sample that contains an extremely large number of atoms or molecules sampling an enormous number of conformations. In statistical mechanics, averages corresponding to experimental observables are defined in terms of ensemble averages.

Different macroscopic constraints lead to different types of ensembles, with particular statistical characteristics and, in statistical mechanics, three important thermodynamic ensembles can be considered [20]:

- Microcanonical ensemble or NVE ensemble, a statistical ensemble where the total energy E of the system, its volume V and the number N of particles in the system are each fixed to particular values. The system must remain totally isolated (unable to exchange energy or particles with its environment) in order to stay in statistical equilibrium.

- Canonical ensemble or NVT ensemble, a statistical ensemble where the energy is not known exactly but the number of particles N, its volume V, and the temperature T are maintained constant. The canonical ensemble is appropriate for describing a closed system which is in, or has been in, weak thermal contact with a heat bath. In order to be in statistical equilibrium the system must remain totally closed (unable to exchange particles with its environment), and may come into weak thermal contact with other systems that are described by ensembles with the same temperature.

- Grand canonical ensemble or μVT ensemble, a statistical ensemble where neither the energy nor particle number are fixed. In their place, the chemical potential μ, the volume V and the temperature T and are specified. The grand canonical ensemble is appropriate for describing an open system: one which is in, or has been in, weak contact with a reservoir (thermal contact, chemical contact, radiative contact, electrical contact, ...). The ensemble remains in statistical equilibrium if the system comes into weak contact with other systems that are described by ensembles with the same temperature and chemical potential.

An alternative relevant ensemble often used in MD simulations is the isobaric-isothermal ensemble *NPT*, were the number of atoms N, pressure P and temperature T are constrained. The latter can be extended to allow for a nonzero surface tension γ, the so-called $NP\gamma T$ ensemble extremely useful when modeling lipid bilayer membranes, which require additional considerations when simulating at constant pressure due to the existence of a surface tension at the boundary between two phases.

One should know that these macroscopic description (comparable with experiment observations) from a microscopic state is plausible if a large number of observables is considered simultaneously. In practice the MD systems are often much smaller compared to experiments, thus instead of calculating an ensemble average, a time average over a large number of the system's configurations is calculated, evolving sequentially in time. In other words, if the ergotic hypothesis [20] is satisfied one can consider the properties (e.g. structural, dynamical and thermodynamics) extracted by MD comparable with macroscopic experimental measurements. This hypothesis states that over long periods of time, the time spent by a system in some region of the phase space of microstates with the same energy is proportional to the volume of this region, i.e., that all accessible microstates are equiprobable over a long period of time. Therefore, it is usually satisfied for MD simulations long enough, that allows the system to explore the configuration space.

While the choice of ensemble is usually one of convenience at the macroscopic level

since (away from the critical point) thermal fluctuations are small, for the microscopic systems studied by MD the fluctuations of non-regulated quantities can be sufficiently large to make precise measurement difficult. Modifying the dynamics allows MD to model the equilibrium behavior of such ensembles directly. One approach to the problem ensures that the controlled parameter is maintained constant, apart from numerical drift, by augmenting the equations of motion with suitable mechanical constraints. Below, we will discuss the control mechanism applied to two parameters: the temperature (3.6.1), and the pressure (3.6.2).

3.6.1 Controlled temperature

Several methods for performing MD at constant temperature have been proposed, ranging from *ad hoc* rescaling of atomic velocities in order to adjust the temperature, to consistent formulation in terms of modified equations of motion that force the dynamics to follow the desired temperature constraint. The central idea is to simulate in such a way that we obtain a canonical distribution: this means fixing the average temperature of the system under simulation, but at the same time allowing for a fluctuation of the temperature with a distribution typical for a canonical distribution. In experiments one usually control the temperature of the system and the volume can be considered constant, thus the canonical ensemble (NVT) seems the more appropriated in several situations.

Recalling that in statistical mechanics, the temperature of the system T is defined via the average kinetic energy (K^*) [20]:

$$k_b T = \frac{2K^*}{s}, \tag{3.20}$$

$$K^* = \frac{1}{\tau}\int_0^t K(t)dt, \tag{3.21}$$

with s the number of the degrees of freedom of the system, in MD simulations, in order to switch from microcanonical to canonical ensembles, the equations of motion have to be modified to keep the average kinetic energy at a constant level through the so called thermostat.

In the following we will describe the Nosé-Hoover thermostat [21] employed in the present work.

In the approach of Nosé-Hoover, a Hamiltonian with an extra degree of freedom for heat bath, s, is introduced. The equations of motion for this additional degree of freedom are integrated together with those for atomic coordinates and velocities, as shown in eqq. 3.22-3.25.

$$\mathbf{v}_i = \frac{d\mathbf{r}_i}{dt}, \tag{3.22}$$

$$m_i \frac{d\mathbf{v}_i}{dt} = -\frac{\partial U}{\partial \mathbf{r}_i} - \zeta m_i \mathbf{v}_i, \tag{3.23}$$

$$\zeta = \frac{\partial ln(s)}{\partial dt}, \tag{3.24}$$

$$\frac{\partial \zeta}{\partial t} = \frac{1}{M_s}\left(\sum_{i=1}^{N} \frac{\mathbf{v}_i^2}{2} - g k_B T\right), \tag{3.25}$$

where, ζ is defined in terms of an additional degree of freedom s, M_s is a thermal inertia parameter, which regulates the rate of heat transfer between the system and the heat reservoir, and g is the number of the system's degrees of freedom considering s.

3.6.2 Controlled pressure

In some cases, it is important to simulate a system at constant pressure (e.g. condensed phase system). As with temperature control, there are different classes of pressure control for MD simulation. The only ones we consider here are the length-scaling technique of Berendsen [22], the Andersen [23] and the Parriniello-Raman [24] barostats.

The first thing to start of is an expression for the pressure of a simulated system. Recalling that the most general definition of pressure is an average force F per unit area S to which the force is applied:

$$p = -\frac{1}{S} \cdot \frac{1}{t} \int_0^t \mathbf{F}(t) dt, \tag{3.26}$$

and thus considering eq. 3.26 in all the sections of a periodic system we obtain:

$$p = -\frac{1}{3V}\left(2\langle K \rangle + \langle \sum_{i<j} (\mathbf{r}_j - \mathbf{r}_i)\mathbf{F}_{ij} \rangle\right), \tag{3.27}$$

with $\langle K \rangle$ average kinetic energy, and F_{ij} is the interaction force between the atoms i^{th} and j^{th}.

A barostat is a MD procedure which implements a correction of the pressure by rescaling the distance among atoms.

With the Berendsen barostat [22] the system is weakly coupled to an external bath using the principle of least local perturbation and, by adding an additional term descriptive of pressure changes (eq. 3.28), obeys the following equation of motion (eq. 3.29):

$$\frac{dp}{dt} = \frac{p_0 - p}{\tau_p}, \tag{3.28}$$

$$\frac{d\mathbf{r}_i}{dt} = \mathbf{v}_i - \frac{\beta(p_0 - p)}{3\tau_p}\mathbf{r}_i, \tag{3.29}$$

where p_0 is the pressure of the external bath, τ_p is the coupling time constant used to rescale the atomic positions and β is the isothermal compressibility.

Length scaling at each time step using a global scale factor can lead to violent oscillations of pressure in more ordered systems, and is therefore not recommended for production MD runs.

A simple proportional coordinate scaling, concomitant with volume scaling, minimizes local disturbances.

Other barostats, as Andersen and Parinello-Rahman, are able to model the dynamics of the system in order to reproduce known thermodynamics ensembles.

The Andersen method [23] was developed to adjust the pressure in a simulation of interacting particles. In the following description, only systems of pairwise interacting particles are treated. The method was later extended to anisotropic coupling by Parrinello et al [24]. Andersen proposed to replace the coordinates $\mathbf{r}_i$ by scaled coordinates p_i defined as:

$$\rho_i = \frac{\mathbf{r}_i}{V^{1/3}}. \tag{3.30}$$

Consider the new Lagrangian, in which a new variable Q appears:

$$L(\rho, \dot{\rho}_i, Q, \dot{Q}) = \frac{1}{2}Q^{\frac{2}{3}}\sum_{i=1}^{N} m_i\dot{\rho}_i^2 - \sum_{i<j=1}^{N} U(Q^{1/3}\rho_{ij}) + \frac{1}{2}M\dot{Q} - p_0 Q. \tag{3.31}$$

The interpretation of Q as the volume V, leads the first two terms on the right simply to be the Lagrangian of the unscaled system; the third term is a kinetic energy for the motion of Q, and the fourth represent a potential energy associated with it. Here, p_0 and M are constants to be chosen with particular attention. A physical interpretation of the additional terms would be equivalent to considering the simulated system as in a container that can be compressed by a piston. Thus, Q, whose value is the volume V, is the coordinate of the piston, $p_0 Q$ is the potential derived from an external pressure p_0 acting on the piston and M is the mass of the piston.

Then the equations of the motion with the Q variable may be defined as:

$$\frac{d\mathbf{r}_i}{dt} = \mathbf{v}_i + \frac{1}{3}\mathbf{r}_i\frac{d\ln(V)}{t}, \tag{3.32}$$

$$m_i\frac{d\mathbf{v}_i}{dt} = -\frac{\partial U}{\partial \mathbf{r}_i} - \frac{1}{3}m_i\mathbf{v}_i\frac{d\ln(V)}{dt}, \tag{3.33}$$

$$\frac{Md^2V}{dt^2} = -p_0 + \frac{\frac{2}{3}\sum_{i=1}^{N}\frac{\mathbf{v}_i^2}{2} - \frac{1}{3}\sum_{i<j=1}^{N}\frac{\partial U(\mathbf{r}_{ij})}{\partial \mathbf{r}_{ij}}\cdot\mathbf{r}_{ij}}{v} = p(t) - p_0. \tag{3.34}$$

The Andersen barostat yields trajectories in an isobaric-isoenthalpic ensemble (*NPH*).

Parinello and Rahman [24] extended the method proposed by Andersen, which scales the volume, permitting to the simulation box to adjust also its shape. One of the main advantage of this barostat is the anisotropic coupling, critical for lipid bilayer schemes.

In the present work, we used either Berendsen barostat if the simulations were performed with the $NP\gamma T$ ensemble (see 4.2 and 4.3) or the Parinello- Rahman barostat if the simulations were performed with the standard *NPT* and *NVT* ensembles (see 4.1).

3.7 References

[1] B.J. Alder, T.E. Wainwright, Studies in Molecular Dynamics. I. General Method, J. Chem. Phys. 31 (1959) 459-466.

[2] I. Mayer, Simple Theorems, Proofs, and Derivations in Quantum Chemistry, Springer Science and Business Media, 2013.

[3] D.S.D. Larsson, L. Liljas, D. van der Spoel, Virus Capsid Dissolution Studied by Microsecond Molecular Dynamics Simulations, PLoS Comput Biol. 8 (2012) e1002502.

[4] A.R. Leach, Molecular Modelling: Principles and Applications, Pearson Education, 2001.

[5] L. Verlet, Computer "Experiments" on Classical Fluids. I. Thermodynamical Properties of Lennard-Jones Molecules, Phys. Rev. 159 (1967) 98-103.

[6] Tamar Schlick, Eric Barth, M. Mandziuk, BIOMOLECULAR DYNAMICS AT LONG TIMESTEPS:Bridging the Timescale Gap Between Simulation and Experimentation, Annu. Rev. Biophys. Biomol. Struct. 26 (1997) 181-222.

[7] J.-P. Ryckaert, G. Ciccotti, H.J.C. Berendsen, Numerical integration of the cartesian equations of motion of a system with constraints: molecular dynamics of n-alkanes, J. Comput. Phys. 23 (1977) 327-341.

[8] H.C. Andersen, Rattle: A "velocity" version of the shake algorithm for molecular dynamics calculations, J. Comput. Phys. 52 (1983) 24-34.

[9] B. Hess, H. Bekker, H.J.C. Berendsen, J.G.E.M. Fraaije, LINCS: A linear constraint solver for molecular simulations, J. Comput. Chem. 18 (1997) 1463-1472.

[10] S. Miyamoto, P.A. Kollman, Settle: An analytical version of the SHAKE and RATTLE algorithm for rigid water models, J. Comput. Chem. 13 (1992) 952-962.

[11] Q. Hu, S. Viswanadham, R.P. Joshi, K.H. Schoenbach, S.J. Beebe, P.F. Blackmore, Simulations of transient membrane behavior in cells subjected to a high-intensity ultrashort electric pulse, Phys. Rev. E. 71 (2005) 031914.

[12] W.D. Cornell, P. Cieplak, C.I. Bayly, I.R. Gould, K.M. Merz, D.M. Ferguson, et al., A Second Generation Force Field for the Simulation of Proteins, Nucleic Acids, and Organic Molecules, J. Am. Chem. Soc. 117 (1995) 5179-5197.

[13] A.D. MacKerell, D. Bashford, M. Bellott, R.L. Dunbrack, J.D. Evanseck, M.J. Field, et al., All-Atom Empirical Potential for Molecular Modeling and Dynamics Studies of Proteins, J. Phys. Chem. B. 102 (1998) 3586-3616.

[14] C. Oostenbrink, A. Villa, A.E. Mark, W.F. Van Gunsteren, A biomolecular force field

based on the free enthalpy of hydration and solvation: The GROMOS force-field parameter sets 53A5 and 53A6, J. Comput. Chem. 25 (2004) 1656-1676.

[15] W.L. Jorgensen, D.S. Maxwell, J. Tirado-Rives, Development and Testing of the OPLS All-Atom Force Field on Conformational Energetics and Properties of Organic Liquids, J. Am. Chem. Soc. 118 (1996) 11225-11236.

[16] J.B. Klauda, R.M. Venable, J.A. Freites, J.W. O'Connor, D.J. Tobias, C. Mondragon-Ramirez, et al., Update of the CHARMM all-atom additive force field for lipids: validation on six lipid types, J. Phys. Chem. B. 114 (2010) 7830-7843.

[17] B. Hess, C. Kutzner, D. van der Spoel, E. Lindahl, GROMACS 4: Algorithms for Highly Efficient, Load Balanced, and Scalable Molecular Simulation, J. Chem. Theory Comput. 4 (2008) 435-447.

[18] M.P. Allen, D.J. Tildesley, Computer Simulation of Liquids, Clarendon Press, 1989.

[19] U. Essmann, L. Perera, M.L. Berkowitz, T. Darden, H. Lee, L.G. Pedersen, A smooth particle mesh Ewald method, J. Chem. Phys. 103 (1995) 8577-8593.

[20] D. Chandler, Introduction to Modern Statistical Mechanics, 1987.

[21] W.G. Hoover, Canonical dynamics: Equilibrium phase-space distributions, Phys. Rev. A. 31 (1985) 1695-1697.

[22] H.J.C. Berendsen, J.P.M. Postma, W.F. van Gunsteren, A. DiNola, J.R. Haak, Molecular dynamics with coupling to an external bath, J. Chem. Phys. 81 (1984) 3684-3690.

[23] H.C. Andersen, Molecular dynamics simulations at constant pressure and/or temperature, J. Chem. Phys. 72 (1980) 2384-2393.

[24] M. Parrinello, A. Rahman, Polymorphic transitions in single crystals: A new molecular dynamics method, J. Appl. Phys. 52 (1981) 7182-7190.

Chapter 4

Properties of Electropores, a Molecular Characterization / Propriétés des Électropores, une Caractérisation Moléculaire

Dans l'EP standard (μs-msPEF) [1-2] la longueur des impulsions électriques est dans l'échelle de la micro à milliseconde et l'amplitude de l'ordre de quelques kV/cm. Ceci provoque une accumulation de charges électriques des deux côtés des membranes de cellules, qui prend un temps dependant des paramètres électriques du système, souvent de l'ordre de centaines de ns. Comme la membrane se comporte comme un condensateur, cette accumulation de charge donne lieu à une tension transmembranaire. Des améliorations dans cette technique ont été réalisés au cours des dernières décennies pour permettre une délivrance ciblée et sûre des composés aux cellules et tissus aboutissant à des applications cliniques et précliniques [3-9].

Récemment, des dispositifs électriques ont été développés qui ont permis l'utilisation d'impulsions d'intensité beaucoup plus élevé (MV/m) et de très courte (nanoseconde) durée, nommés nsPEFs [10]. De telles impulsions sont trop courtes pour charger la membrane (condensateur) mais agissent directement sur elle. De tels pulses électriques sont capables de perméabiliser les membranes des organelles internes ainsi que la membrane de la cellule plasmique et présentent l'avantage d'éviter des effets thermiques indésirables.

L'effet de ces deux familles d'impulsions est l'augmentation locale de la tension (voltage) transmembranaire (de la cellule et / ou des organelles) qui, quand elle dépasse un certain seuil, produit un champ électrique local intense au niveau de la membrane conduisant à la formation de pores [11]. Ceci entraîne une augmentation de la perméabilité de la membrane non seulement à l'eau et à des ions [12], mais également à des molécules chargées et ou non [13,14]. Les caractéristiques des pores formés à la suite de l'EP (par exemple la taille, la morphologie et les propriétés conductrices) sont d'une importance capitale dans

la détermination de la perméabilité et la sélectivité des membranes à différentes espèces ioniques et moléculaires, et par conséquent l'efficacité potentielle d'une application de la technique.

Malgré les travaux expérimentaux sur des cellules et des membranes lipidiques modèles (par exemple des bicouches lipidiques planes ou des vésicules lipidiques) consacrés à la caractérisation structurale de ces pores [15-21], les données émergents jusqu'à présent sont très rares et fragmentaires. Plusieurs études expérimentales indirectes [15-21] et investigations *in silico* [22-24] confirment la présence de pore, mais leur observation directe est presque impossible au vu de leur taille (de l'ordre du nanomètre) et de leur temps de formation (ns). Expérimentalement, par conséquent, on est capable d'estimer la dimension des nanopore que de manière indirecte par la mesure soit la perméabilité des membranes à des molécules de tailles différentes, soit par la mesure de conductance estimées à partir de la relation courant/tension, avec les limitations non négligeables dans la précision et la fiabilité des résultats.

Un autre aspect crucial qui manque encore de caractérisation à l'échelle moléculaire est le transport de composés bioactifs (colorants, médicaments, matériel génétique, ...) à travers la membrane plasmique suite à l'application d'impulsions électriques. Bien de quelques travaux expérimentaux on tenté de décrire le processus de translocation sous μs-msPEF [26,27] ou nsPEFs [28] de molécules telles que l'ADN ou l'ARN, par déduction indirecte employant des techniques de fluorescence, les mécanismes de vectorisation de nombreux composés ne sont pas encore élucidés.

Pour appuyer et confronter les hypothèse émanant des investigations expérimentales et de faire la lumière sur les mécanismes moléculaires de l'EP, plusieurs simulations de dynamique moléculaire de modèles de membranes soumises à des champs électriques ont été réalisées ces dix dernières années [22-24,29-33].

Dans ce travail, en utilisant des simulations de MD, nous avons tenté de répondre aux questions suivantes:

- Comment la composition d'une bicouche lipidique influence le seuil d'EP ?
- Quelle est la morphologie des pores formés par nsPEFs ou μs-msPEFs, qu'elles sont leur dimension et leur conductance ?
- Quel sont les mécanismes et l'échelle de temps de translocation de petites molécules aux travers des électropores. Ces mécanismes varient ils selon le d'impulsion (nsPEFs vs μs-msPEFs)?

Les résultats de nos simulations sont présentés dans ce Chapitre et sont divisés en quatre sections. Dans la Section **4.1**, dans le cadre de l'étude du comportement des membranes complexes, nous présentons les résultats concernant la modulation des caractéristiques de bicouches lipidiques contenant 30% de cholestérol. En particulier, nous décrivons les

propriété structurelles et électriques des interfaces lipides/eau. Dans la Section **4.2** nous quantifions les seuils d'EP de bicouches lipidiques contenant des concentrations croissantes de cholestérol (0, 20, 30 à 50 mole%) lorsqu'elles sont soumises à des impulsions nsPEFs et μs-msPEFs. Dans la Section suivante, **4.3**, nous développons une procédure, modélisant l'application des μs-msPEFs, qui permet de stabiliser les électropores sous différentes tensions transmembranaires suffisamment longtemps pour déterminer leur dimension, leur conductance et leur sélectivité aux ions. Dans la dernière Section, **4.4**, nous utilisons cette même méthode pour étudier le transport de petites molécules chargées (Tat_{11} et brins d'ARN), et comparons nos résultats à des études similaires menées dans les conditions des nsPEFs [33,40] afin de caractériser la vectorisation moléculaire par PEFs.

Properties of Electropores, a Molecular Characterization / Propriétés des Électropores, une Caractérisation Moléculaire

In standard EP [1-2], the length of the pulses is in the μs - ms scale and the amplitude in the order of kV/cm, termed μs-msPEF. The resulting current causes an accumulation of electrical charges at both sides of the cell membrane, over a time that depends on the electrical parameters of the system, often in the order of 100s of ns. As the membrane behaves as a capacitance, this charge accumulation gives rise to a transmembrane voltage. Improvements in this technique have been achieved in the past decades to allow for a targeted and safe delivery of compounds to cells and tissues resulting in pre clinical and clinical applications [3-9].

Recently, electric devices have been developed that have enabled the use of pulses of much higher magnitude (MV/m) over very short time scale (nanosecond), named nsPEFs [10]. Such pulses are too short to charge the membrane but act directly on it and they were shown to permeabilize the membranes of internal organelles as well as the plasma cell membrane, and present the advantage of avoiding undesired thermal effects.

The effect of these two families of pulses is the local increase in the transmembrane (i.e. of the cell and/or organelles) voltage that, when it overcomes a certain threshold, produces an intense local electric field at the membrane level leading to pore formation [11]. Such a process induces a rise in the permeability of the plasma cell membrane not only to water and ions [12], but also to charged and uncharged small as well as large molecules [13,14]. The characteristics of pores formed as a result of EP (e.g. size, morphology and conductive properties) are of tremendous importance in determining the permeability and selectivity of the membranes to different ionic and molecular species and consequently the potential efficacy of a given EP application.

Despite extensive experimental work on cells and model lipid membranes (e.g. planar lipid bilayers and lipid vesicles) has been devoted to the structural characterization of these pores [15-21], the data emerging so far is very scarce and fragmented. Indirect experimen-

tal evidences [15-21] and *in silico* investigations [22-24] confirm the electropore presence, however their direct observation by conventional techniques is limited by the nanometer-range size of the pores and by the short dynamics of their formation (ns). Experimentally, therefore, one is able to estimate the nanopore dimension only indirectly by measuring either membrane permeability to molecules of different sizes, or membrane conductance recovered from the current/voltage relationship, with not negligible limitations in the accuracy and reliability of the results. Only very recently, time resolved visualization of pores in droplet interface bilayers was made possible using total internal reflection fluorescence microscopy [25]. Nevertheless, currently such fluorescence imaging does not allow a straight visualization of the pore needed for a thorough measurement of the pore size and of the transport process.

Another crucial aspect that still lack molecular insights is the transport of bioactive compounds (dyes, drugs, genetic materials,...) across the plasma membrane into the cell successive the application of electric pulses. In spite of some experimental work attempted to describe the exact translocation process of charged genetic material (siRNA), by indirect deduction employing fluorescent dye techniques, either under μs-msPEF [26,27] or when nsPEFs are applied [28], the characterization of the uptake of many other compounds is not yet fully elucidated. Remarkably, the authors of [28] coupled experimental evidences with *in silico* modeling to gain advantage from its atomic description. Systematic studies should be carried out following the latter approach in presence of other relevant drugs (e.g. bleomycin) or dyes (e.g. propidium iodide, YO-PRO,...) to broaden the understanding of the transport dynamics, eventually providing further insights that may improve the related experimental techniques and therapeutic effectiveness.

To advocate experimental findings and to shed light on the molecular mechanisms of EP, molecular dynamics (MD) simulations of membrane models subject to electric fields have been carried out in the past ten years [22-24,29-33]. Using the two protocols to mimic nsPEFs or μs-msPEFs, a considerable amount of work have been carried out to describe some of the aspects of EP, nevertheless many relevant questions remain opens:

- What is the effect of complex, physiologically relevant, bilayer on the EP threshold when using the two MD protocols?
- What is the pore morphology, the dimension and the conductance of pores formed under nsPEFs or μs-msPEFs?
- What is the mechanism and the time scale of translocation of small molecules though these electropores and how the characteristic of the pulse influences the transport?

Here, using MD simulations and comparing our results to other findings from our group, we attempted to address some of these questions. Chapter **4** is divided in four Sections. In Section **4.1** we present our results regarding the modulation of the lipid bilayer characteristic when 30 mol % of cholesterol is added. In particular, we describe structural and

electric effects at the lipid headgroups/water interface. In Section **4.2** we quantify the EP threshold of libid bilayes with increasing concentration of cholesterol (0, 20, 30 , 50 mol %) when the two MD protocols aforesaid described are used. Additionally we identify the hydrophobic/hydrophilic putative nature of the pore formed under these conditions. In the successive Section, **4.3**, we developed a procedure, mimicking μs-msPEFs, to stabilize electropores under different transmembrane voltages for long enough to determine the pore dimension, its conductance and selectivity to ion species. In the last Section, **4.4**, we employed the same method to investigate the transport of small charged molecules, used in drug delivery, comparing our findings with similar studies conducted under nsPEFs conditions with attempt to rationalize the molecular up take.

References

[1] E. Neumann, A.E. Sowers, C.A. Jordan, Electroporation and Electrofusion in Cell Biology, Springer Science & Business Media, 1989.

[2] J.A. Nickoloff, Animal Cell Electroporation and Electrofusion Protocols, Humana Press,NJ, 1995.

[3] M. Breton, L.M. Mir, Microsecond and nanosecond electric pulses in cancer treatments, Bioelectromagnetics. 33 (2012) 106-123.

[4] D. Miklavčič, B. Mali, B. Kos, R. Heller, G. Serša, Electrochemotherapy: from the drawing board into medical practice, Biomed. Eng. OnLine. 13 (2014) 29.

[5] M. Sällberg, L. Frelin, G. Ahlen, M. Sällberg-Chen, Electroporation for therapeutic DNA vaccination in patients, Med. Microbiol. Immunol. (Berl.). 204 (2014) 131-135.

[6] G. Serša, J. Teissie, M. Cemazar, E. Signori, U. Kamensek, G. Marshall, et al., Electrochemotherapy of tumors as in situ vaccination boosted by immunogene electrotransfer, Cancer Immunol. Immunother. CII. 64 (2015) 1315-1327.

[7] L.C. Heller, R. Heller, In Vivo Electroporation for Gene Therapy, Hum. Gene Ther. 17 (2006) 890-897.

[8] S. Chabot, J. Teissié, M. Golzio, Targeted electro-delivery of oligonucleotides for RNA interference: siRNA and antimiR, Adv. Drug Deliv. Rev. 81 (2015) 161-168.

[9] C. Jiang, R.V. Davalos, J.C. Bischof, A Review of Basic to Clinical Studies of Irreversible Electroporation Therapy, IEEE Trans. Biomed. Eng. 62 (2015) 4-20.

[10] L. Chopinet, M.P. Rols, Nanosecond electric pulses: a mini-review of the present state of the art, Bioelectrochemistry Amst. Neth. 103 (2015) 2-6.

[11] T. Kotnik, G. Pucihar, D. Miklavčič, Induced Transmembrane Voltage and Its Correlation with Electroporation-Mediated Molecular Transport, J. Membr. Biol. 236 (2010) 3-13.

[12] I.G. Abidor, V.B. Arakelyan, L.V. Chernomordik, Y.A. Chizmadzhev, V.F. Pastushenko, M.P. Tarasevich, Electric breakdown of bilayer lipid membranes: I. The main experimental facts and their qualitative discussion, J. Electroanal. Chem. Interfacial Electrochem. 104 (1979) 37-52.

[13] J. Teissié, N. Eynard, B. Gabriel, M.P. Rols, Electropermeabilization of cell membranes, Adv. Drug Deliv. Rev. 35 (1999) 3-19.

[14] L.M. Mir, S. Orlowski, J. Belehradek Jr, C. Paoletti, Electrochemotherapy potentiation of antitumour effect of bleomycin by local electric pulses, Eur. J. Cancer Clin. Oncol.

27 (1991) 68-72.

[15] S. Kalinowski, G. Ibron, K. Bryl, Z. Figaszewski, Chronopotentiometric studies of electroporation of bilayer lipid membranes, Biochim. Biophys. Acta BBA - Biomembr. 1369 (1998) 204-212.

[16] S. Koronkiewicz, S. Kalinowski, Influence of cholesterol on electroporation of bilayer lipid membranes: chronopotentiometric studies, Biochim. Biophys. Acta BBA - Biomembr. 1661 (2004) 196-203.

[17] M. Kotulska, Natural Fluctuations of an Electropore Show Fractional Lévy Stable Motion, Biophys. J. 92 (2007) 2412-2421.

[18] H. Krassen, U. Pliquett, E. Neumann, Nonlinear current-voltage relationship of the plasma membrane of single CHO cells, Bioelectrochemistry. 70 (2007) 71-77.

[19] O.M. Nesin, O.N. Pakhomova, S. Xiao, A.G. Pakhomov, Manipulation of cell volume and membrane pore comparison following single cell permeabilization with 60- and 600-ns electric pulses, Biochim. Biophys. Acta. 1808 (2011) 792-801.

[20] A. Silve, I. Leray, L.M. Mir, Demonstration of cell membrane permeabilization to medium-sized molecules caused by a single 10 ns electric pulse, Bioelectrochemistry. 87 (2012) 260-264.

[21] A.G. Pakhomov, E. Gianulis, P.T. Vernier, I. Semenov, S. Xiao, O.N. Pakhomova, Multiple nanosecond electric pulses increase the number but not the size of long-lived nanopores in the cell membrane, Biochim. Biophys. Acta. 1848 (2015) 958-966.

[22] D.P. Tieleman, The molecular basis of electroporation, BMC Biochem. 5 (2004) 10.

[23] M. Tarek, Membrane Electroporation: A Molecular Dynamics Simulation, Biophys. J. 88 (2005) 4045-4053.

[24] Z. A. Levine, and P. T. Vernier, Life cycle of an electropore: Field dependent and field-indepedent steps in pore creation and annihilation, J. Membr. Biol. 236 (2010) 27-36.

[25] M. Szabo, M.I. Wallace, Imaging potassium-flux through individual electropores in droplet interface bilayers, Biochim. Biophys. Acta. (2015).

[26] S. Li, Electroporation Protocols: Preclinical and Clinical Gene Medicine, Humana press: Totowa, NJ., 2008.

[27] A. Paganin-Gioanni, E. Bellard, J.M. Escoffre, M.P. Rols, J. Teissié, M. Golzio, Direct visualization at the single-cell level of siRNA electrotransfer into cancer cells, Proc. Natl. Acad. Sci. 108 (2011) 10443-10447.

[28] M. Breton, L. Delemotte, A. Silve et al., Transport of siRNA through lipid membranes

driven by nanosecond electric pulses: An experimental and computational study, J. Am. Chem. Soc. 134 (2012) 13938-13941.

[29] J. Gumbart, F. Khalili-Araghi, M. Sotomayor, B. Roux, Constant electric field simulations of the membrane potential illustrated with simple systems, Biochim. Biophys. Acta BBA - Biomembr. 1818 (2012) 294-302.

[30] L. Delemotte, and M. Tarek, Molecular dynamics simulations of lipid membrane electroporation, J. Membr. Biol. 245 (2012) 531-543.

[31] M.J. Ziegler, P.T. Vernier, Interface Water Dynamics and Porating Electric Fields for Phospholipid Bilayers, J. Phys. Chem. B. 112 (2008) 13588-13596.

[32] M. Tokman, J.H. Lee, Z.A. Levine, M.-C. Ho, M.E. Colvin, P.T. Vernier, Electric Field-Driven Water Dipoles: Nanoscale Architecture of Electroporation, PLoS ONE. 8 (2013) e61111.

[33] A. Polak, D. Bonhenry, F. Dehez, P. Kramar, D. Miklavčič, M. Tarek, On the Electroporation Thresholds of Lipid Bilayers: Molecular Dynamics Simulation Investigations, J. Membr. Biol. 246 (2013) 843-850.

4.1 Water-lipid Interface characterization

As explained in detail in Chapter 3, molecular dynamics refers to a family of computational methods aimed at simulating macroscopic behavior through the numerical integration of the Newton's equations of motion of a microscopic many-body system. Thanks to MD simulations one can access various structural and dynamic properties of a system, including thermodynamic properties. Indeed, macroscopic properties are expressed as functions of particle coordinates and/or momenta, which are computed along a phase space trajectory generated by classical dynamics [1]. When performed under conditions corresponding to laboratory scenarios, MD simulations can provide a detailed view of the structure and dynamics of a macromolecular system.

As biological membranes have a very complex structure and can contain hundreds of different lipid species and proteins, most MD studies have focused their attention on lipid aggregates such as bilayers, in their biologically relevant liquid-crystalline state, to investigate *in silico* structural and dynamical properties. From both a theoretical and an experimental perspective, zwitterionic phosphatidylcholine (PC) lipid bilayers (Fig. 4.1) constitute the best characterized systems [2-4]. Several studies have considered a variety of alternative lipids, featuring different, possibly charged, head groups [5-9], and even mixed bilayer compositions [10-16]. Despite their simplicity, bilayers built from PC lipids represent remarkable test systems to probe the computation methodology and to gain additional insight into the physical properties of membranes [17-19].

For such double layers, the average structure of the lipid water interface at the atomic-scale may be provided by the density distributions of different atom types along the bilayer normal, which can be measured experimentally on multilamellar stacks by neutron and X-ray diffraction techniques [20], as well as calculated from MD simulations (Fig. 4.1 b). These distributions highlight the composition and properties of the membrane that appears as a broad hydrophilic interface, with only a thin slab of pure hydrocarbon fluid in the middle. Fig. 4.1 b indicates clearly the roughness of the lipid headgroup area and how water density decays smoothly from the bulk value and penetrates deeply into the bilayer at a region delimiting the membrane/water interface.

The MD studies carried out so far to shed light on the basic mechanisms of EP concern manly lipid and complex bilayer. In Chapter 2 we already mentioned that since the EP phenomenon takes place primarily at the interface of the plasma cell membranes it seems reasonable, to a first approximation, to model the dynamic (hundreds of ns) of small patch of bilayers (tens of nm^2), accessible by today computational resources.

As aforesaid, many properties of bilayers (e.g. local electric field, electric potential, electric permittivity, ...[21-23]) are hardly measurable experimentally with nm scale and ns time resolutions and in such cases MD is not only an endorsement of experimental evidences, but a substitute providing estimations of observables otherwise overly inaccu-

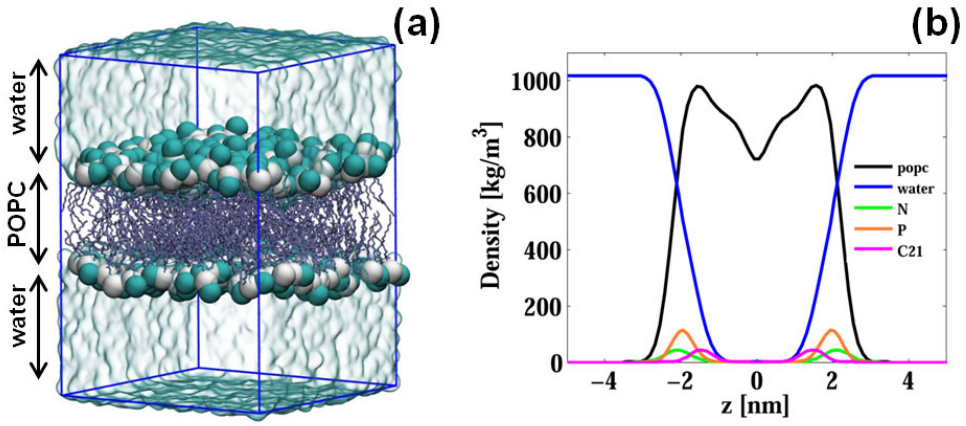

Figure 4.1: (a) POPC scheme: two solution baths are separated by a lipid bilayer. The POPC head groups are shown as cyan and white beads, the tails are shown as iceblue sticks; water is transparent. (b) Density profiles (kg/m^3) along the bilayer normal z, averaged over 10 ns of MD trajectory. The total POPC density and water contributions are indicated in black and blue solid lines respectively, the phosphorus and nitrogen atoms of the head groups in orange and green solid lines, and the carbon atoms of the glycerol groups in pink solid line. The bilayer center is located at z = 0

rate. In this Section we characterize lipid and cholesterol containing bilayers (4.1.2-*Systems and Methods*) in terms of structural (4.1.3.1-*Density profile*) and electric properties (4.1.3.2-*Electric field distribution*, 4.1.3.3-*Dipole Moment*) both not exposed and subject to preporating static electric fields to describe relevant features of these systems that will help understanding the EP process.

4.1.1 Choice of the bilayers

Phosphatidylcholine (PC-head groups) simple zwitterionic lipids and cholesterol are the most common components of cell membranes and standard liposomes employed in drug delivery.

Phospholipid molecules are characterized by the presence of a phosphate headgroup and a glycerol backbone that joins two fatty acid tails together (Fig. 4.2 a). Furthermore the phosphate in the lipid headgroup region is joined together with an additional organic molecule which can create positive, negative, or zwitterionic (dipolar) headgroup charge densities [24]. In contrast to the polar lipid headgroup region, lipid tails are composed of cis- or trans- oriented hydrocarbon chains which are electrostatically neutral and characterized primarily by their length or degree of saturation (where single bonds join saturated atoms and double bonds join unsaturated atoms). This ampiphilic property means that their uncharged tails are hydrophobic, namely an energetic barrier to charged and polar species forced to cross the membrane through specific pathways [25,26], while their headgroups are hydrophilic, in other words polar and able to produce a local electric field that

influences surrounding polar and charged particles, resulting in unique aggregate structures (micelles, bilayers, vesicles) when multiple lipids are mixed together in an aqueous or cytosolic solution. These structures can take on a variety of forms based on the solvent temperature or the average lipid size.

Cholesterol (Fig. 4.2 b) is a ubiquitous component of mammalian cells usually present in high concentrations (~40 mol %). This sterol, composed of a semi-rigid tetracyclic ring system with a hydroxyl group and a short 8-carbon atom chain attached to carbon C17 (as shown in Fig. 4.2 b), sits in the hydrophobic core of bilayers and influences profoundly the behavior of membranes as it tunes their permeability, fluidity and mechanical properties [16,27-31]. The main attribute that makes cholesterol a unique lipid molecule is its ability to condense fluid lipid bilayers since increases the order of fluid-phase phospholipid acyl chains, giving rise to the formation of the liquid-ordered phase. This can be traced back in several membrane properties as for instance a decrease of the area per molecule (4.2.4-*Contrasting results for the electroporation thresholds of the nsPEF and the µs-msPEF protocols*) and an increase in the bilayer thickness (4.1.3.1-*Density profile*).

For these reasons cholesterol is commonly added to the composition of liposomes used in drug delivery since it tends to stabilize their structure, thereby generating more resistant carriers [32]. A stable composition is highly desirable in order to allow the carrier to reach intact the specific site of treatment and to release a pharmacologically active molecule solely in this area in response of an external stimuli, leaving the healthy tissues unexposed.

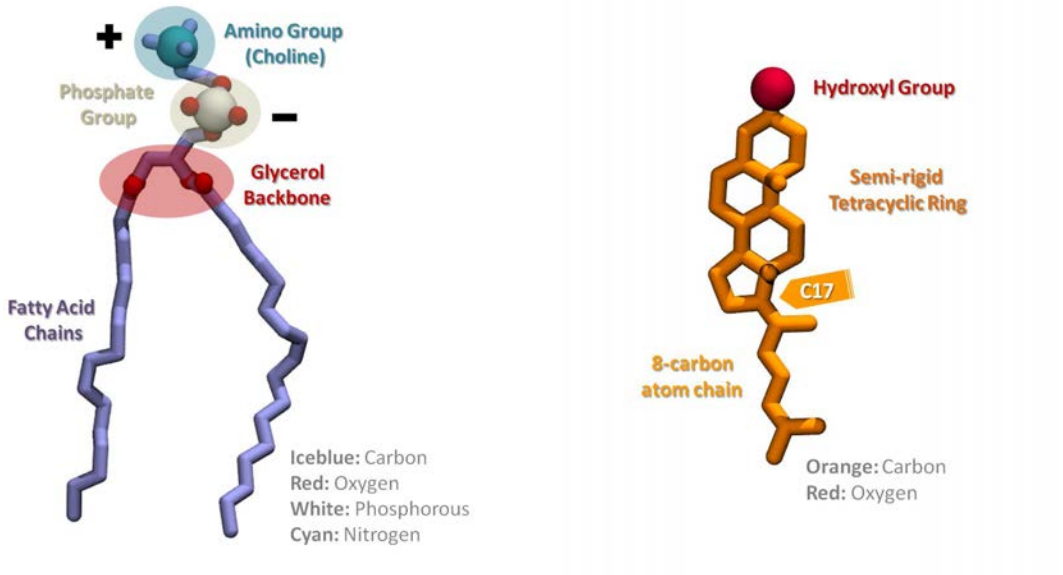

(a) *POPC.* **(b)** *Cholesterol.*

Figure 4.2: Diagram of a typical zwitterionic phospholipid POPC (a) and of a cholesterol (b) molecule

In Section 4.2-*Electroporation of pure lipid and cholesterol rich bilayers* EP thresholds and consequent pore formation will be studied in detail. To identify eventual changes in

the properties of the bilayer, the concentrations we will investigate are 0, 20, 30 and 50 mol %; we will show how leveling off is observed in correspondence of 30 mol % for crucial characteristics, i.e. area per lipid, capacitance and transmembrane voltage EP threshold, that can therefore be considered a critical value.

The aim of the present Section is to develop and test a methodological procedure to characterize membrane models exposed to different intensities of electric field. We focused our attention on the effect of static E fields on POPC and POPC with 30 mol % of cholesterol bilayers (see 4.1.2-*Systems and Methods* for a detailed summary of the exposure conditions).

4.1.2 Systems and Methods

The reference scheme is a bilayer composed of 256 1-palmitoyl-2-oleoyl-sn-glycero-3-phosphatidylcholine (POPC) units, and about 17000 water molecules resulting in a box of dimensions 8.8 x 8.8 x 12.6 nm^3. The other system is composed by a POPC bilayer with a 30 mol % of cholesterol (7.4 x 7.4 x 12.2 nm^3). All the systems were considered at no salt concentration.

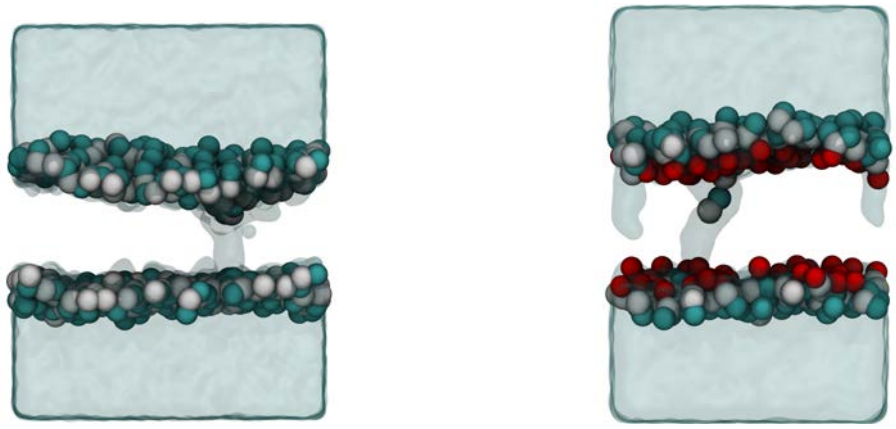

(a) *POPC.* **(b)** *Cholesterol.*

Figure 4.3: Representative frames of the pre-pore state: one can see water merging from the two leaflets in the POPC (a) and cholesterol rich (b) bilayers. POPC head groups are shown as cyan and white beads, cholesterol hydroxyl groups in red spheres, tails and water are transparent

The lipid and cholesterol force fields were derived from CHARMM36 all-atom parameters [33]. The TIP3P water model was used [34]. Bond lengths were constrained using the LINCS algorithm [35]. Short-range electrostatic and Lennard-Jones interactions were cut off at 1.0 nm. Long-range electrostatic interactions were calculated by the PME algorithm [36], with a direct space sum tolerance of 10^{-6} and a spherical truncation of 1.2 nm.

All simulations were performed using GROMACS.4.5.5 [37]. All the systems were first equilibrated at constant pressure (1 atm) and constant temperature (300 K) for at least 100

ns. They were then extended to study the effects of electric fields. Note that at the temperature set for the study, the POPC bilayer is in the biologically relevant liquid crystal L_α phase.

To model the effect of nanosecond pulsed electric field (nsPEFs) an exogenous E_{app} can be applied "directly" perpendicular to bilayer plane by adding a force $F = E_{app} \cdot q_i$ to all the atoms bearing a charge q_i [38,39]. This is possible because the applied electric field acts primarily on the interfacial water dipoles (polarization of bulk water molecules). In few picoseconds [40] a transverse field induces an overall transmembrane voltage $U_m = E_{app} \cdot L_z$ over the whole system [39], where L_z is the size of the simulation box in the field direction.

Table 4.1 summarizes the exposure conditions. Three trials of 50 ns for each electric field applied were run to increase the statistics. If a pore is formed the trajectories are analyzed until t_{water}, i.e. the time a t which the merging of the water fingers percolating from the two leaflets occurs (pre-pore state). Notice that this is only an indicative value of pore formation in a certain time scale (few ns).

$\mathbf{E}_{app}$	**Pure POPC**			**30% chol.**		
V/nm	*Trials*	t_{sim}/ns	t_{water}/ns	*Trials*	t_{sim}/ns	t_{water}/ns
0.00	3	50	-	3	50	-
0.16	3	50	-	3	50	-
0.20	3	20	17.9±4.0	3	50	-
0.40	-	-	-	1	5	2.9

Table 4.1: Conditions of exposition for the POPC and the cholesterol rich bilayers
E_{app} - electric field applied
t_{sim} - MD simulation duration
t_{water} - time when the first wire of water is formed in the hydrophobic core of the bilayer

4.1.3 Results and Discussions

4.1.3.1 Density profile

When describing lipid double layers, how the system is disposed in space can be represented as the average structure of the various components and at the atomic-scale can be provided by the density distributions of different atom types..

The latter can be calculated solving the equation 4.1 discretizing the simulation cell box in voxels of wanted dimensions as shown in Figure 4.4.

$$\rho = \frac{1}{V_j} \sum_{i=1}^{N} m_i, \quad j = i, ..., N \tag{4.1}$$

with ρ the density in kg/m^3 and V_j the j^{th} voxel containing N atoms of a given species with mass m_i.

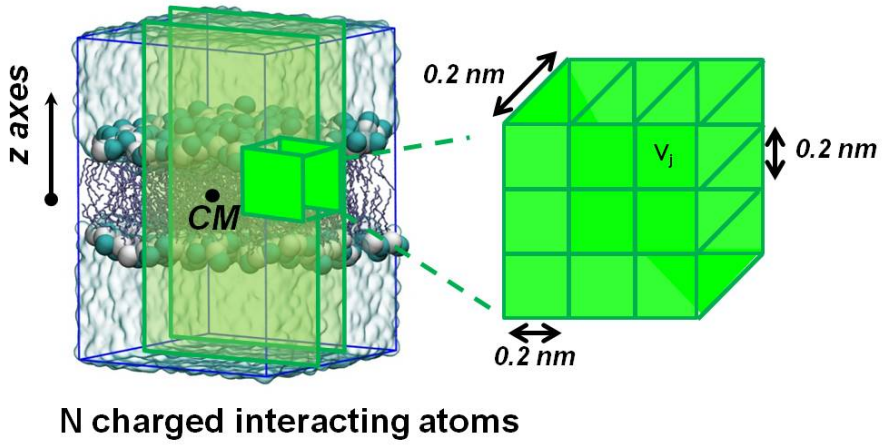

Figure 4.4: POPC scheme: the POPC head groups are shown as cyan and white beads, the tails are shown as iceblue sticks, water is transparent. Graphical representation of the methodological approach used to evaluate the density profile on an arbitrary plane. In each voxels of dimension 0.2x0.2x0.2 nm^2 are counted summing the mass m_i of the i particles of a given species

With this method we calculated 2d representation of the density of the pure POPC scheme (Fig. 4.5) in plane perpendicular to the bilayer for the lipids (a) and the water (b) separately. These distributions clearly indicates how the membrane appears as a thin slab of pure hydrocarbon fluid in the center (z = 0) with with a broad hydrophilic interface. The bulk water (Fig. 4.5 b) from the edge of the cell box smoothly penetrates deeply into the bilayer: the decrease (from 1 to 0 in arbitrary units) of its density value delimits the membrane/water interface.

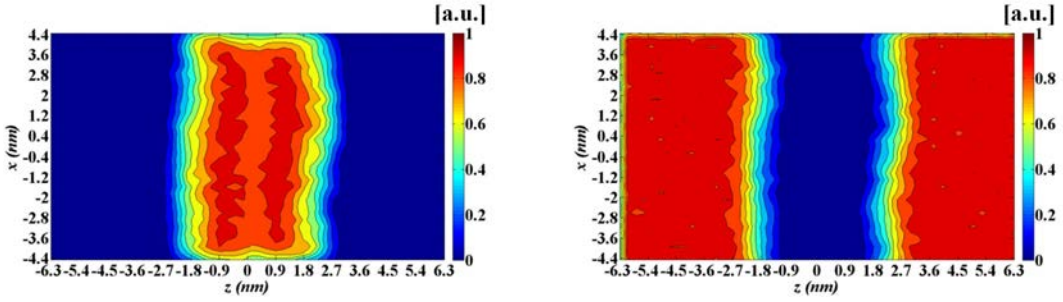

(a) *POPC.* **(b)** *Water.*

Figure 4.5: 2d density maps in xz plane (perpendicular to the bilayer) of the POPC scheme: (a) lipid (b) water in arbitrary units. The bilayer center is located at z = 0

A more quantitative description is given with 1d profiles along the bilayer normal, obtained by averaging 2d maps. In Fig. 4.6 (a) nitrogen (green) and the phosphorus (orange) atoms, that are part of the choline and phosphorus groups of the lipid heads respectively,

are commonly a reference for the definition of bileyer thickness and the C21 (pink) is the linker of one of the two fatty acid tails which points out the position of the glycerol backbone, the very last polar region of the phospholipid which is therefore hydrated. The latter and the value at which the water (blue) reaches the bulk are often used as markers for the interface.

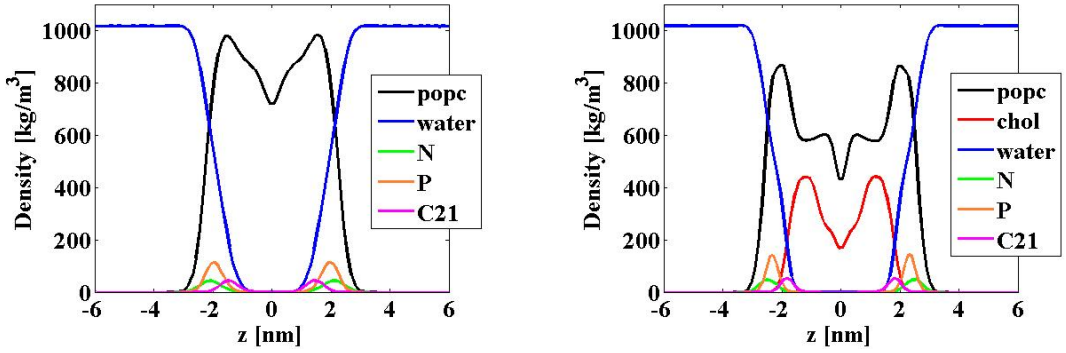

(a) *POPC.* **(b)** *Cholesterol.*

Figure 4.6: Density profiles (kg/m^3) along the bilayer normal z, averaged over 150 ns of MD trajectory. (a) The total POPC density and water contributions are indicated in black and blue solid lines respectively, the phosphorus and nitrogen atoms of the head groups in orange and green solid lines, and the carbon atoms of the glycerol groups in pink solid line; (b) the cholesterol is reported in red solid lines. The bilayer center is located at z = 0

When cholesterol is added (Fig. 4.6 (b)) the thickness of the bilayer increases from 4.0 to 4.7 nm. The water density undergoes to a more abrupt decrease resulting in a sharper interface of almost 1.4 nm compared to the 1.8 of the pure lipid.

When the field is applied the water penetrates in the bilayer hydrophobic core (Fig. 4.7). Panel (a) shows that in the POPC interface when 0.2 V/nm are 23% more water can be found at the level of the phosphorous atoms (orange arrows) and 81% more at the level of the backbones (pink arrows). While at the cholesterol interface (panel b) exposed to 0.4 V/nm only a 15% in correspondence of the phosphorous (orange arrows) and a 53% of the glycerol groups (pink arrows).

The water density profiles show that under the same pre-pore condition (0.2 V/nm vs 0.4 V/nm, see 4.1.2-*Systems and Methods*) in the pure POPC bilayer the water penetrates almost 1.5 times more (backbone level) than in the cholesterol rich system.

The water permeability or diffusion toward the interior of lipid bilayers is the very initial and key step in membrane EP. The reduced diffusion in the cholesterol containing bilayer could be an unfavorable factor in pore formation.

To better understand this intrusion mechanism, which occurs at the water/lipid interface, one should take into account its driving force, i.e. the gradient of the electric field (4.1.3.2-*Electric field distribution*), and its effects, one of the most relevant is the orienta-

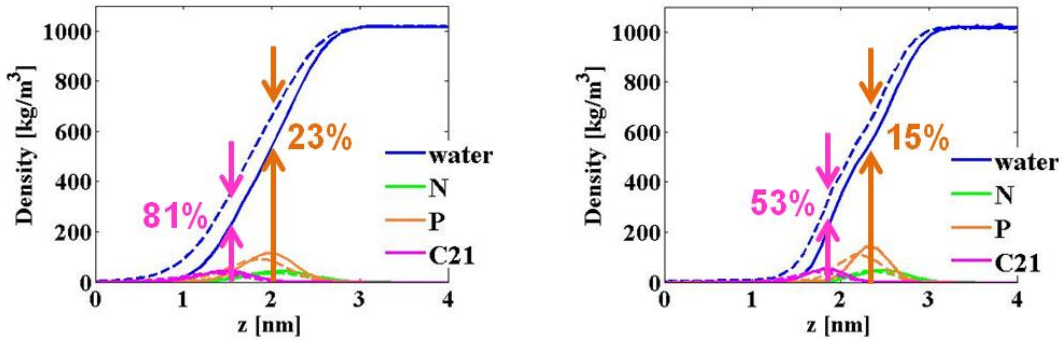

(a) *POPC.* **(b)** *Cholesterol.*

Figure 4.7: Density profiles (kg/m^3) along the bilayer normal z when at rest (solid lines) and in the pre-pore state (dashed lines) equivalent to 0.2 V/nm for the pure POPC and 0.4 for the 30 mol % of cholesterol. In (a) and (b) the water is in blue, the phosphorus and nitrogen atoms of the head groups are in orange and green, and the carbon atoms of the glycerol groups in pink solid line

tion of the dipoles (4.1.3.3-*Dipole moment*).

4.1.3.2 Electric field distribution

The electrostatic interactions of bio-systems play a role in the conformational stability, anchoring of proteins and molecules, and other chemical-physical properties [41]. Electrostatics considers the evaluation of the static electric properties that arise between charged species once a rearrangement of their charge distributions has occurred due to the influence of each other and their local environment.

The local endogenous electric field, which is due to all the charged atoms and groups of the biomolecule plus solvent water molecules, becomes extremely interesting since it points out how a molecular system interacts at distance with charged particles approaching it. The characteristics of this local electric field are a signature of each system, representing a sort of extremely specific fingerprint. The evaluation of such system's property is hardly achievable by experiments, and poorly treated by continuum model that are based on homogenously distributed parameters, neglecting local behaviors.

Atomistic simulations represent a powerful tool, used to follow the many interactions among the polar and/or charged residues. They can provide atomic-scale information on energetic and dynamic contributions of the bio-molecular structure.

Several works have attempted to calculate this endogenous electric field for membrane bilayers alone or for proteins embedded in bilayers, starting from molecular modelling based on microscopic all-atom models and molecular dynamics simulations [42,43] and producing maps of the electrostatic potential profiles. All the data reported are based on the numerical integration of the Poisson equation once given properly boundary condi-

tions [36,44]. An other way to treat the problem is to consider in each point of the simulation domain the contribution of the local electric field as the vector summation of the fields generated by the discrete atomic charge distribution at each time step of the MD simulation [45].

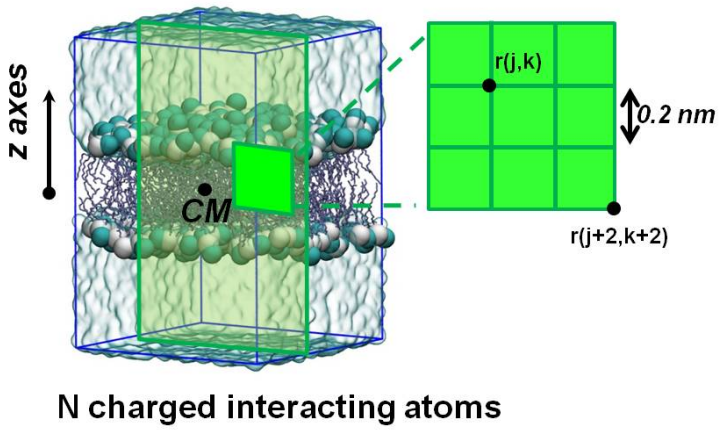

Figure 4.8: POPC scheme: the POPC head groups are shown as cyan and white beads, the tails are shown as iceblue sticks, water is transparent. Graphical representation of the methodological approach used to evaluate the electric field on an arbitrary plane. The Electric field $\mathbf{E}_{j,k}$ is calculated over the N atoms inside the simulation box, at a given point $\mathbf{r}_{j,k}$. Each point $\mathbf{r}_{j,k}$ with [j:0, 1, ..., DIM_X] and [k:0, 1, ..., DIM_Y] coincides with a node of a regular grid with DIM_X x DIM_Y elements, chosen in order to obtain a certain spatial resolution to represent the electrostatic map

We present a methodology [46] able to calculate and map on a three-dimensional space grid the distribution of the electric field of complex biological systems. The methodology proposed is intrinsically general to the extent that it is applicable even to lipid bilayers, trans-membrane proteins, ionic channels and lipidic vesicles, given that the description of the molecular structure is rigorous, as provided by fully-atomistic simulations.

This approach is also quite flexible and capable to separately take into account contributions from different species as well as to represent them as a whole to describe the endogenous electric field in physiological conditions. Moreover, the use of this methodology combined to the application of external intense electric fields allows to understand in which extent the field modify the local electric field profile.

The methodological approach adopted consists in the calculation of the electric field E in a certain number of nodes laying on a plane surface normal to the lipid bilayer (Fig 4.8).

For each node and for all the N atoms of the simulation box we solve equation:

$$\mathbf{E}_{j,k}(\mathbf{r}_1,\ldots,\mathbf{r}_N) = \frac{1}{4\pi\epsilon_0}\sum_{i=1}^{N} q_i \frac{\mathbf{r}_{j,k}-\mathbf{r}_i}{|\mathbf{r}_{j,k}-\mathbf{r}_i|^3}, \tag{4.2}$$

where $E_{j,k}$ is the E field at the node *(j,k)* with position $r_{j,k}$, the ϵ_0 is the permittivity of

the vacuum, q_i and r_i the charge and the position of the i^{th} particle.

In this way, depending on the number of the grid-nodes, one can calculate with the desired spatial resolution the complete electrostatic map as given by all the charged particles within the simulation box. Since the calculation is performed taking into account each charge q_i of the system, contributions due to the different species (lipid molecules, sterols, water molecules) can be calculated separately.

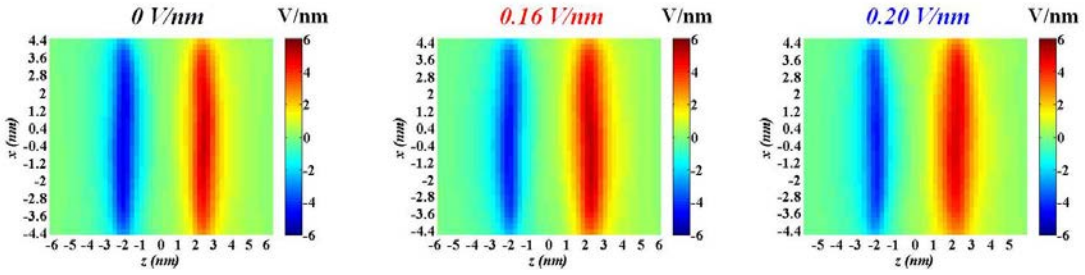

(a) *POPC.*

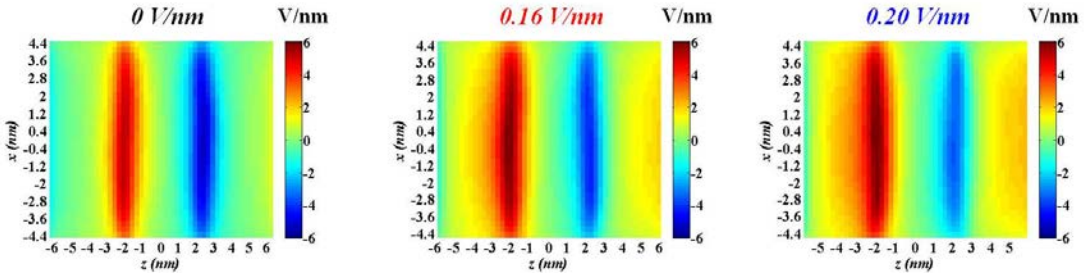

(b) *Water.*

Figure 4.9: Electric field distributions of the POPC scheme in the plane xz (perpendicular to the bilyer) averaged over 3 planes (y = -2, 0 , 2 nm). The contributions of the different species are reported separately: POPC (a) and water molecules (b), both in absence of an exogenous electric field (left panel 0 V/nm) and when 0.16 (central panel) or 0.20 (right panel) V/nm are applied

Here this approach was used to quantify the local electric field distribution at the interface of lipid membrane in absence or presence of static applied electric fields in the order of fractions of V/nm. In Fig. 4.9 and 4.10 we report the endogenous electric field maps due to all system's components separately (POPC, cholesterol and water molecules respectively) in the xz plane perpendicular to the bilayer averaged over 3 planes (y = -2, 0 , 2 nm) and over the three independent trials run (4.1).

In the absence of an applied field, the membrane interior has a zero electric field since water and lipids (both POPC and Chol) balance their dipoles at each leaflet interface region (see 4.1.3.3-*Dipole moment*).

Analyzing the different contribution separately, the POPC molecules produce a local electric field with values of ∼4 V/nm (Fig. 4.9 a, 0 V/nm) in the pure lipid scheme and of ∼3.7 V/nm (Fig. 4.10 a, 0 V/nm) in the cholesterol system, with the sign depending on the

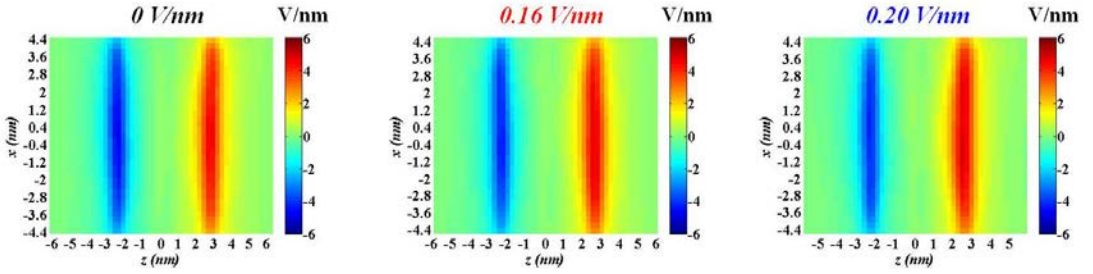

(a) *POPC.*

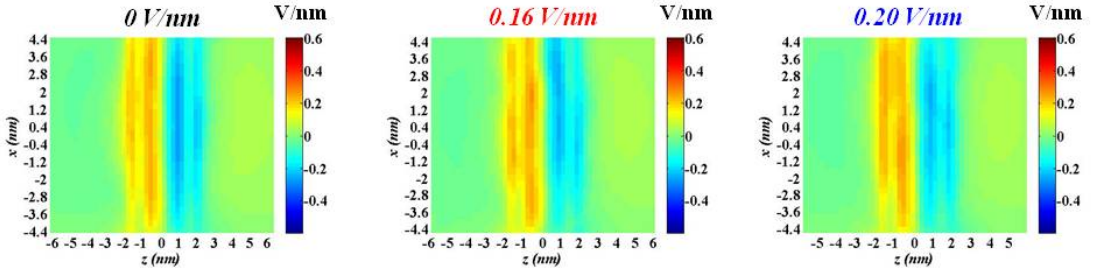

(b) *Cholesterol.*

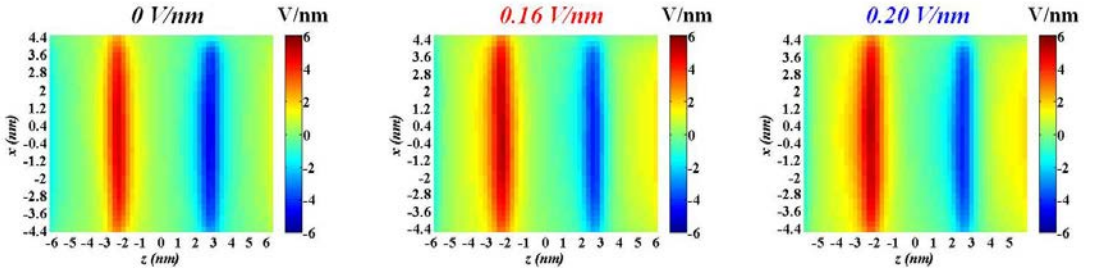

(c) *Water.*

Figure 4.10: Electric field distributions of the cholesterol rich scheme in the plane xz (perpendicular to the bilyer) averaged over 3 planes (y = -2, 0 , 2 nm). The contributions of the different species are reported separately: POPC (a), cholesterol (b) and water molecules (c), both in absence of an exogenous electric field (left panel 0 V/nm) and when 0.16 (central panel) or 0.20 (right panel) V/nm are applied

orientation with respect to z-axis (negative for z < 0 and positive for z > 0). The cholesterol contribution (Fig. 4.10 b, 0 V/nm) is one order of magnitude lower with respect to the other components suggesting that this sterol has a little influence in the membrane electric field profiles [47]. The water molecules counterbalance the local electric field induced by the headgroup dipole reaching values of ∼5 V/nm (Fig. 4.9 b, 0 V/nm) in the pure lipid scheme and of ∼4 V/nm (Fig. 4.10 c, 0 V/nm) in the cholesterol system, and opposite sign with respect to the lipids. The water molecules exhibit an overall zero electric field at 4 nm far from the bilayer center, in correspondence to bulk phase. In this region the water molecules are not affected by the headgroups and thus are randomly distributed.

When an external field is applied, water dipoles at opposite leaflets align to the field (Fig. 4.9 b and 4.10 c, *0.16 V/nm* and *0.20 V/nm*) and do not balance anymore the headgroups contribution (4.1.3.3-*Dipole moment*). Thus a non zero electric field, ∼0.5 V/nm, is present in the membrane interior. This means that water molecules orient at the lipid/water interface in response to the applied electric field and for this reason it is important to characterize the behavior of water orientation in this region.

4.1.3.3 Dipole moment

The driving force for pore formation is the orientation and motion of dipoles [38,40,48,49], primarily water molecules and secondary lipid head groups, in the intense field gradients at the interface shown in Fig. 4.9 and 4.10. This gradient is always present the interface, even in rest conditions, yet it is balanced by other forces that guaranties stability to the interface [48,49], as reported in Fig. 4.10 (panel 0 V/nm) and 4.10 (panel 0 V/nm). Conversely, when the pulsed electric field is applied the system of forces acting at the interface is not balance and pore formation allows to minimize the total free energy of the system when subject to an exogenous electric field [50].

As for the density distribution (4.1.3.1), the electric dipole moment can be calculate in MD as a time average charge distribution in space, carrying each atom i in the system a charge q_i.

$$\mathbf{M}_j = \sum_{1}^{N} q_i \mathbf{r}_i, \tag{4.3}$$

where M_j is the dipole moment of the species j, q_i the charge of the i^{th} particle, $\mathbf{r}_i$ its position. We reported the dipole moment in the CGS unit Debye [D] for clarity, being 1 D $= \sim 3.33564 \cdot 10^{-30}$ C·m. If the simulation cell is discretized in voxel of volume V_k one can obtain 3d and 2d (Fig. 4.11) distributions in a region of interest.

Notice that it is possible to consider the normal (z) and tangential (x, y) components of the dipole separately. In this Section we will discuss only the normal component since the direction of application of the electric field is z, i.e. the effect in the orientation of the dipoles is more evident and significant in this direction.

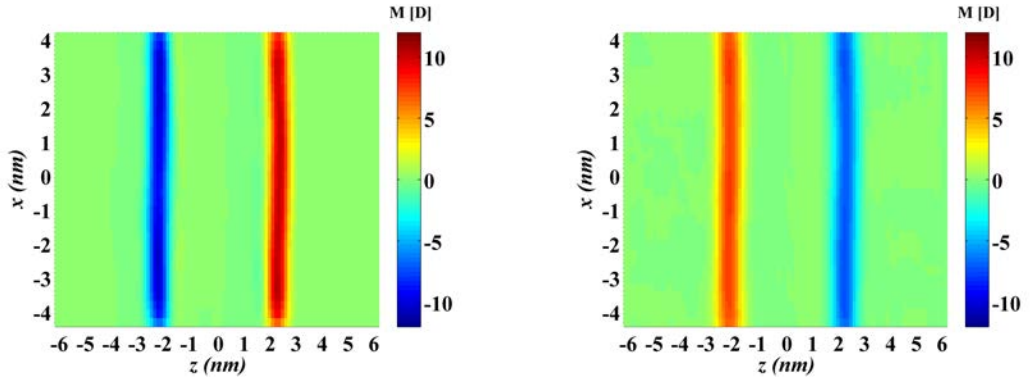

(a) *POPC.* **(b)** *Water.*

Figure 4.11: 2d maps (xz plane - perpendicular to the bilayer) of the dipole moment of lipid head groups (a) and interfacial water (b). In rest conditions ($E_{app} = 0$ V/nm) the dipole moment of the two components almost balance: the water is slightly more oriented, inducing a non null dipole potential (fractions of V) lipid dependent. Dimension of the voxels: 0.2 x 0.2 x L_y nm^3, with L_y the length of the box in the y direction

Taking in mind that for the POPC bilayer the maximum peaks of the head groups distribution are located at -2.1 (lower leaflet) and at 2.1 nm (upper leaflet) as reported in Fig. 4.5 (a), at rest ($E_{app} = 0$ V/nm) the head groups, which have a zwitterionic nature, are oriented in such a way (Fig. 4.11 a) to produce a not negligible local electric field (Fig. 4.9 a, 0 V/nm). The interfacial water feels this local e field and reorients accordingly (Fig. 4.11 b) through opposite directions with their hydrogen atoms pointing to the membrane interior, so that the formation of hydrogen bonds with the lipid head groups is maximized. Interestingly, even at rest condition the dipole moment water counterbalance the head groups orientation, slightly overcoming it and inducing the so called dipole potential with magnitude dependent on the nature of lipids and in the order of fractions of V [51].

In the following we compare the normal component of the dipole moment per molecule along the axis perpendicular to the bilayer z of the pure lipid and cholesterol containing systems when exposed to 0, 0.2 and 0, 0.2, 0.4 V/nm respectively (4.1.2-*Systems and Methods*).

When an high enough electric field is applied the water dipoles reorient fast (ps) at the two leaflets of the interface in a different manner (Fig. 4.12): at the anode side of the bilayer (z < 0) the dipolar orientation is reinforced, where as is randomized at the cathode one (z > 0), since water at this leaflet is forced to reverse its orientation according to the applied field. Therefore the water at the cathode are dielectrophoretically drag towards the bilayer interior by a force F_z proportional to the electric field gradient (∇E_z/V/m^2) and to the dipole moment (μ_z/Cm), $F_z = \mu_z \cdot \nabla E_z$ [48]. The percolation of water toward the hydrophobic core is illustrated by the density profiles (see 4.1.3.1-*Density profiles*) and by Fig. 4.12 (c): in the latter the red curve (corresponding to an exposition of 0.2 V/nm) at 0.7 nm from the bilayer center shows higher values of dipole moment per water molecule at the cathode (∼0.6 D) than at the anode (∼0.25 D) side; from the cathode the water get to the

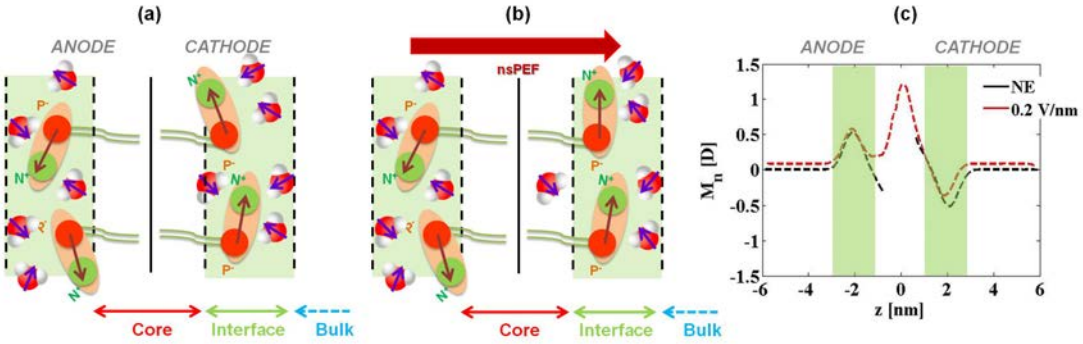

Figure 4.12: Dipole orientation of the lipid head groups and interfacial water. (a) Schematic of the dipolar orientation at rest, (b) after the application of an electric field in the direction perpendicular to the bilayer (z). (c) Dipole moment orientation per water molecule in Debye along z when the bilayer is not exposed (black dashed line) or subject to an exogenous electric field 0.2 V/nm before pore creation (red dashed line) from MD simulations (data over 3 trials: max standard error of 0.2 D); the interfaces of the upper and lower leaflets are highlighted in green

center of the bilayer reaching it maximum orientation (∼1.5 D).

We remind that the trajectories for this analysis are considered up to the merging of the water fingers percolating through the leaflets. The values of water dipole moment present in the lipid core are hence meaningful only of water intrusion and not of pore formation, i.e. during the observed time a statistically non null presence of water in the hydrophobic region is possible when the electric field is applied.

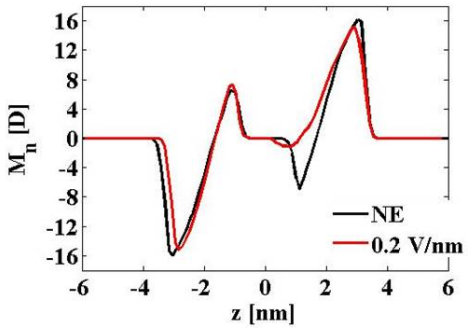

Figure 4.13: POPC scheme: normal component of the headgroups dipole moment per lipid molecule along z of the POPC when the bilayer is not exposed (black solid line) or subject to an exogenous electric field 0.2 V/nm (red line). Data over 3 trials: max standard error of 1.1 D for the head groups and 0.18 for the water molecules

The response of the lipid head groups in the elapsed time observed (50 ns, three independent trials) is mild: only at the cathode side (z > 0) the inner dipoles (Fig. 4.13, 1 nm) are forced to reverse their orientation according to the applied field almost laying in the plane parallel to the bilayer (0 D).

Cholesterol, in sufficient high concentrations, increases the bilayer thickness (4.1.3.1-*Density profiles*) and reduces the area per lipid (4.2.4-*Contrasting results for the electropora-*

tion thresholds of the nsPEF and the µs-msPEF protocols), indication of a condensing effect. Despite this evident effect, at rest we register a negligible change in the dipole moment per molecule of the lipid head groups (Fig. 4.14 a, black curve) compared to the pure POPC (Fig. 4.13, black curve).

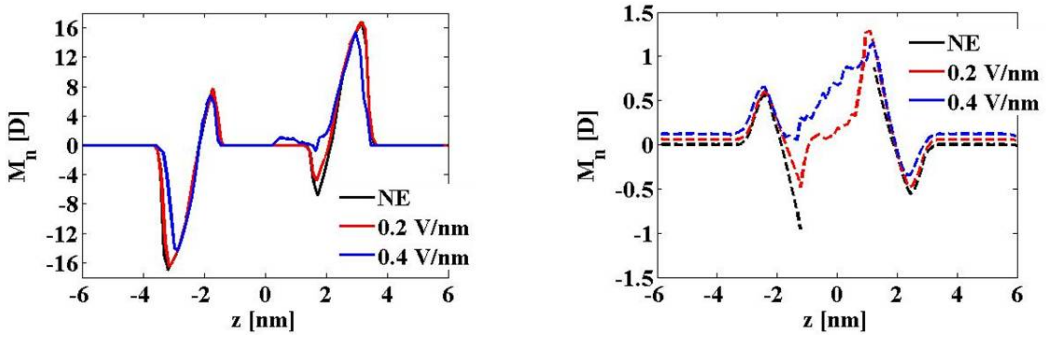

(a) *POPC.* **(b)** *Water.*

Figure 4.14: Cholesterol rich scheme: normal component of the headgroups dipole moment per lipid molecule along z of the POPC head groups (a) and water (b) when the bilayer is not exposed (black solid line) or subject to an exogenous electric field of 0.2 (red line) and 0.4 (blue line) V/nm. Data over 3 trials: max standard error of 1.1 D

On contrary a rise of the water orientation is observed below the glycerol backbones (∼0.5 and ∼1 nm from the center of the bilayer for the POPC and cholesterol rich, respectively) going from ∼0.45 (Fig. 4.12 c, black curve) to ∼0.75 D (Fig. 4.14 b, black curve). This is due to the location of the cholesterol in the hydrophobic core that, as explained in 4.1.3.1-*Density profiles*, resides in the dipper part and tends to align its oxygen with the glycerol groups of the phospholipids locally increasing the electric field (Fig. 4.10 b, 0 V/nm).

For 0.2 V/nm water starts to penetrate the bilayer, oriented almost perpendicular to the z axis. We must apply a two fold higher e filed (0.4 V/nm) to obtain an increase similar to the POPC scheme in the dipole moment of the head groups (cf. Fig. 4.13 and 4.14 a, back curves) and of the interfacial water (cf. Fig. 4.12 c and 4.14 b, back curves).

The only sharp difference is in the distance between the two leaflets that grows when cholesterol is added, and meaningful of a lower probability of encounter between the water fingers protruding in the core upon the application of the electric field. Interestingly enough, these are the e field intensities at which pore formation occurs in the same time scale (few ns).

Based on this consideration the water orientation at the interface of the lipid barrier alone can not be an indicator of how easily the pore forms in a given bilayer.

4.1.4 Conclusions

Insights into membrane hydration, i.e. the interplay between water and membrane molecules, is essential for a complete understanding of biological cell functioning in physiological condition and under exogenous stimuli, e.g. external electric fields. Capturing these characteristics by means of MD simulations can be a support and a complementary insight for experimental findings, since today instrumentation is often not adequate to measure accurately many properties, such as electric fields distributions and molecule orientation, with a molecular definition and a ns time resolution.

The methodology proposed is quite versatile and capable of taking into account separately single subspecies contributions as well as to represent the effects of electric fields externally applied. It is intrinsically general to the extent that it is applicable even to different lipid bilayers, trans-membrane proteins, ionic channels and lipidic vesicles.

We have illustrated how our approach is able to calculate and map on a three-dimensional space grid system the distribution of the density of the system, of the electrostatic potential, and of the electric dipole moment of a complex bio-molecular structure embedded in its water-solvent environment. In particular, the aim of this Section has been to propose a methodology able to quantify with atomic resolution and ns time scale different structural (density profiles) and electrical (local electric field, electric dipole moment) properties of water/headgroups interface in different membrane modes, namely a pure lipid POPC and a 30 mol % cholesterol rich bilayer when different intensity of electric field are applied (0 , 0.16, 0.20 and 0.40 V/nm) in the order of magnitude of the ones employed in electroporation techniques for controlled drug delivery.

The water density profiles showed that when 0.4 V/nm are applied to the cholesterol rich system only the 53% more water can be found at the level of the glycerol groups with respect that to the not exposed condition; while when 0.2 V/nm are applied to the pure POPC bilayer 81% of increase is observed always in correspondence of the glycerol groups, a more favorable condition for pore formation.

The electric field maps, based on the summation of the Coulomb potentials generated by the discrete atomic charge distribution on fixed points in the 3D space, split in the two contributions of the bilayer residues and of the water molecules illustrated that in specific regions on water/lipid interface there is an evident higher electric field gradient, indicating a re-distribution of water. The use of this methodology combined to the application of external intense electric fields allows to understand in which way the field is capable to modify the physiological electric field profile, increasing its intensity in the bilayer core from 0 to almost 1 V/nm giving rise to a dragging force for polar molecule to penetrate in the hydrophobic region.

Comparing the pure lipid and the cholesterol containing schemes the only difference registered in terms of dipolar orientation at rest condition ($E_{app} = 0$ V/nm) is a rise of the

water orientation observed in the latter system below the glycerol backbones going from ∼0.45 to ∼0.75 D. However for the sterol rich bilayer the electric field applied has to be two folds higher than in the pure POPC one to orientate the interfacial dipole moments in a similar manner and, interesting enough, to porate. Therefore based on this consideration the water orientation at the interface with the lipid barrier alone can not be an indicator of how easily the pore forms in a given bilayer and other crucial properties should be considered to interpret the electroporation phenomenon, e.g. the pressure profiles, the interfacial water diffusivity and permittivity of the various components.

4.1.5 References

[1] A.R. Leach, Molecular Modelling: Principles and Applications, Pearson Education, 2001.

[2] L. Saiz, M.L. Klein, Structural Properties of a Highly Polyunsaturated Lipid Bilayer from Molecular Dynamics Simulations, Biophys. J. 81 (2001) 204-216.

[3] T. Róg, K. Murzyn, M. Pasenkiewicz-Gierula, The dynamics of water at the phospholipid bilayer surface: a molecular dynamics simulation study, Chem. Phys. Lett. 352 (2002) 323-327.

[4] S.E. Feller, K. Gawrisch, A.D. MacKerell, Polyunsaturated Fatty Acids in Lipid Bilayers: Intrinsic an Environmental Contributions to Their Unique Physical Properties, J. Am. Chem. Soc. 124 (2002) 318-326.

[5] K.V. Damodaran, K.M. Merz, A comparison of DMPC- and DLPE-based lipid bilayers, Biophys. J. 66 (1994) 1076-1087.

[6] J.J. López Cascales, H.J.C. Berendsen, J. Garcia de la Torre, Molecular Dynamics Simulation of Water between Two Charged Layers of Dipalmitoylphosphatidylserine, J. Phys. Chem. 100 (1996) 8621-8627.

[7] S.W. Chiu, S. Vasudevan, E. Jakobsson, R.J. Mashl, H.L. Scott, Structure of Sphingomyelin Bilayers: A Simulation Study, Biophys. J. 85 (2003) 3624-3635.

[8] P. Mukhopadhyay, L. Monticelli, D.P. Tieleman, Molecular Dynamics Simulation of a Palmitoyl-Oleoyl Phosphatidylserine Bilayer with Na+ Counterions and NaCl, Biophys. J. 86 (2004) 1601-1609.

[9] D.Y. Villanueva, J.B. Lim, J.B. Klauda, Influence of Ester-Modified Lipids on Bilayer Structure, Langmuir. 29 (2013) 14196-14203.

[10] S.A. Pandit, D. Bostick, M.L. Berkowitz, Mixed bilayer containing dipalmitoylphosphatidylcholine and dipalmitoylphosphatidylserine: lipid complexation, ion binding, and electrostatics, Biophys. J. 85 (2003) 3120-3131.

[11] R.Y. Patel, P.V. Balaji, Characterization of Symmetric and Asymmetric Lipid Bilayers Composed of Varying Concentrations of Ganglioside GM1 and DPPC, J. Phys. Chem. B. 112 (2008) 3346-3356.

[12] A.A. Gurtovenko, I. Vattulainen, Membrane Potential and Electrostatics of Phospholipid Bilayers with Asymmetric Transmembrane Distribution of Anionic Lipids, J. Phys. Chem. B. 112 (2008) 4629-4634.

[13] A.A. Gurtovenko, I. Vattulainen, Effect of NaCl and KCl on phosphatidylcholine and phosphatidylethanolamine lipid membranes: insight from atomic-scale simulations for

understanding salt-induced effects in the plasma membrane, J. Phys. Chem. B. 112 (2008) 1953-1962.

[14] T. Róg, H. Martinez-Seara, N. Munck, M. Orešič, M. Karttunen, I. Vattulainen, Role of Cardiolipins in the Inner Mitochondrial Membrane: Insight Gained through Atom-Scale Simulations, J. Phys. Chem. B. 113 (2009) 3413-3422.

[15] R. Vácha, M.L. Berkowitz, P. Jungwirth, Molecular Model of a Cell Plasma Membrane With an Asymmetric Multicomponent Composition: Water Permeation and Ion Effects, Biophys. J. 96 (2009) 4493-4501.

[16] H. Martinez-Seara, T. Róg, M. Karttunen, I. Vattulainen, R. Reigada, Cholesterol Induces Specific Spatial and Orientational Order in Cholesterol/Phospholipid Membranes, PLoS ONE. 5 (2010) e11162.

[17] D.J. Tobias, K. Tu, M.L. Klein, Atomic-scale molecular dynamics simulations of lipid membranes, Curr. Opin. Colloid Interface Sci. 2 (1997) 15-26.

[18] C. Anézo, A.H. de Vries, H.-D. Höltje, D.P. Tieleman, S.-J. Marrink, Methodological Issues in Lipid Bilayer Simulations, J. Phys. Chem. B. 107 (2003) 9424-9433.

[19] C. Chipot, M.L. Klein, M. Tarek, Modeling Lipid Membranes, in: S. Yip (Ed.), Handb. Mater. Model., Springer Netherlands, 2005: pp. 929-958.

[20] M.C. Wiener, S.H. White, Structure of a fluid dioleoylphosphatidylcholine bilayer determined by joint refinement of x-ray and neutron diffraction data. III. Complete structure, Biophys. J. 61 (1992) 434-447.

[21] S. Kohler, Z.A. Levine, M.A. Garcia-Fernandez, M.-C. Ho, P.T. Vernier, P. Leveque, et al., Electrical Analysis of Cell Membrane Poration by an Intense Nanosecond Pulsed Electric Field Using an Atomistic-to-Continuum Method, IEEE Trans. Microw. Theory Tech. 63 (2015) 2032-2040.

[22] K.J. Tielrooij, D. Paparo, L. Piatkowski, H.J. Bakker, M. Bonn, Dielectric Relaxation Dynamics of Water in Model Membranes Probed by Terahertz Spectroscopy, Biophys. J. 97 (2009) 2484-2492.

[23] S. Gekle, R.R. Netz, Nanometer-Resolved Radio-Frequency Absorption and Heating in Biomembrane Hydration Layers, J. Phys. Chem. B. 118 (2014) 4963-4969.

[24] Life - As a Matter of Fat, Springer-Verlag, Berlin/Heidelberg, 2005.

[25] B. Hille, 1940-, Ion channels of excitable membranes, Sinauer, 2001.

[26] E. Gouaux, R. MacKinnon, Principles of Selective Ion Transport in Channels and Pumps, Science. 310 (2005) 1461-1465.

[27] M. Bloom, E. E., and O. G. Mouritsen, Physical properties of the fluid lipid-bilayer component of cell membranes: a perspective, Q. Rev. Bioph. 24 (1991) 293-397.

[28] D. A. Brown, and E. London, Structure and function of sphingolipid- and cholesterol-rich membrane rafts, J. Biol. Chem. 275 (2000) 17221-17224.

[29] Berkowitz, M. L., Detailed molecular dynamics simulations of model biological membranes containing cholesterol, Biochim. Biophys. Acta 1788 (2009) 86-96.

[30] K. Tu, M. L. Klein, and D. J. Tobias, Constant-pressure molecular dynamics investigation of cholesterol effects in a dipalmitoyl phosphatidyl choline bilayer. Biophys. J. 75(5) (1998) 2147-2156.

[31] N. Kucerka, J. D. Perlmutter, J. Pan, S. Tristram-Nagle, J. Katsaras, and J. N. Sachs, The effect of cholesterol on short- and long-chain mono-unsaturated lipid bilayers as determined by molecular dynamics simulations and X-ray scattering, Biophys. J., 95 (2008) 2792-2805.

[32] A. Sharma, U.S. Sharma, Liposomes in drug delivery: Progress and limitations, Int. J. Pharm. 154 (1997) 123-140.

[33] J. B. Klauda, R. M. Venable, J. A. Freites et al., Update of the CHARMM all-atom additive force field for lipids: Validation on six lipid types, J. Phys .Chem. B 114 (2010) 7830-7843.

[34] W. L. Jorgensen, J. Chandrasekhar, J. D. Madura et al., Comparison of simple potential functions for simulating liquid water, J. Chem. Phys. 79 (1983) 926-935.

[35] B. Hess, H. Bekker, H. J. C. Berendsen et al., LINCS: A linear constraint solver for molecular simulations, J. Comp. Chem. 18 (1997) 1463-1472.

[36] U. Essmann, L. Perera, M. L. Berkowitz et al., A smooth particle mesh ewald method, J. Chem. Phys. 103 (1995) 8577-8593.

[37] B. Hess, C. Kutzner, D. van der Spoel et al., GROMACS 4: algorithms for highly efficient, load-balanced, and scalable molecular simulation, J. Comp. Theor. Chem. 4 (2008) 435-447.

[38] D.P. Tieleman, The molecular basis of electroporation, BMC Biochem. 5 (2004) 10.

[39] J. Gumbart, F. Khalili-Araghi, M. Sotomayor, B. Roux, Constant electric field simulations of the membrane potential illustrated with simple systems, Biochim. Biophys. Acta BBA - Biomembr. 1818 (2012) 294-302.

[40] M. Tarek, Membrane Electroporation: A Molecular Dynamics Simulation, Biophys. J. 88 (2005) 4045-4053.

[41] P. Kohel, Electrostatics calculations: latest methodological advances. Current Opinion in Structural Biology (2006) 16:142-1.

[42] L. Delemotte, and M. Tarek, Molecular dynamics simulations of lipid membrane electroporation, J. Membr. Biol. 245 (2012) 531-543.

[43] A. Aksimentiev, K. Schulten, Imaging a-Hemolysin with Molecular Dynamics: Ionic Conductance, Osmotic Permeability, and the Electrostatic Potential Map. Biophysical Journal (2005) 88:3745-3761.

[44] A.A. Gurtovenko, I. Vattulainen, Calculation of the electrostatic potential of lipid bilayers from molecular dynamics simulations: Methodological issues, J. Chem. Phys. 130 (2009) 215107.

[45] M. D'Alessandro, M. Aschi, M. Paci et al. Theoretical Modeling of Enzyme Reaction Chemistry: The Electron Transfer of the Reduction Mechanism in CuZn Superoxide Dismutase. J Phys Chem B (2004) 108:16255-16260.

[46] P. Marracino, M. Casciola, M. Liberti, F. Apollonio, Evaluation of Protein Electrostatic Potential from Molecular Dynamics Simulations in the Presence of Exogenous Electric Fields: The Case Study of Myoglobin, in: W. Rocchia, M. Spagnuolo (Eds.), Comput. Electrost. Biol. Appl., Springer International Publishing, 2015: pp. 255-270.

[47] M.L. Fernández, G. Marshall, F. Sagués, R. Reigada, Structural and Kinetic Molecular Dynamics Study of Electroporation in Cholesterol-Containing Bilayers, J. Phys. Chem. B. 114 (2010) 6855-6865.

[48] R.A. Böckmann, B.L. de Groot, S. Kakorin, E. Neumann, H. Grubmüller, Kinetics, Statistics, and Energetics of Lipid Membrane Electroporation Studied by Molecular Dynamics Simulations, Biophys. J. 95 (2008) 1837-1850.

[49] M.J. Ziegler, P.T. Vernier, Interface Water Dynamics and Porating Electric Fields for Phospholipid Bilayers, J. Phys. Chem. B. 112 (2008) 13588-13596.

[50] M. Tokman, J.H. Lee, Z.A. Levine, M.-C. Ho, M.E. Colvin, P.T. Vernier, Electric Field-Driven Water Dipoles: Nanoscale Architecture of Electroporation, PLoS ONE. 8 (2013) e61111.

[51] A. Polak, D. Bonhenry, F. Dehez, P. Kramar, D. Miklavčič, M. Tarek, On the Electroporation Thresholds of Lipid Bilayers: Molecular Dynamics Simulation Investigations, J. Membr. Biol. 246 (2013) 843-850.

4.2 Electroporation of pure lipid and cholesterol rich bilayers

In this Section, we report on a MD simulation study of the EP of lipid bilayers at different cholesterol contents using protocols mimicking *traditional EP* (μs-msPEF), and nsPEF. The results show that addition of cholesterol in concentrations lipid:sterol ranging from 20 to 50 mol % enhances substantially the membrane cohesion, which is manifested by an increase of the EP threshold (U_{thr}). This increase is steady in the case of the nsPEF protocol, reaching roughly a factor 2 in the 50 mol % samples. In contrast, for the μs-msPEF protocol, U_{thr} increases by 50 % upon addition of 30 mol % cholesterol then levels off. Furthermore, pores formed under μs-msPEF are found to possess morphologies much different from the usually reported hydrophilic *electropores* encountered under the nsPEF protocol, which may have profound consequences on the transport properties of electroporated membranes. Hence, in contrast to what has been found in simple zwitterionic bilayers, this study reveals for the first time quite different responses of cell membranes models containing the ubiquitous cholesterol component to the two EP techniques.

4.2.1 Introduction

Electroporation is a phenomenon which affects the fundamental behavior of cells since it disturbs transiently or permanently the integrity of their membrane [1-12], and is therefore used in several biological and mediacl applications [13-34].

In the last decade several MD simulations have been conducted in order to model membrane EP [35-47] using different protocols to mimic *in silico* the effect of both low magnitude microsecond pulses (μs-msPEF), and of high magnitude nanosecond pulses (nsPEF) on planar bilayers [44,47].

Both protocols have been used to monitor the effect of electric fields on zwitterionic membranes and quite noticeably, despite the differences in the techniques, they have been reported to yield similar results [44,47]. In particular, the two types of pulses induce formation of hydrophilic pores, in which, transmembrane water columns created above an electrtoporation threshold are stabilized by lipid bilayer head groups. This crucial step in the so-called electropore life cycle [43] is prerequisite to ion conduction as most MD simulations studies reported so far [37,40,42,44,45,48].

However, to date, simulations have been exclusively performed on membranes formed by simple zwitteroinic lipids (phosphatidyl choline -PC- head groups) at the exceptions of few that considered also a small fraction of negatively charged lipids to study their externalization [39]. Recently [49], we have found that for some particular lipid compositions, pores formed by imposing a charge imbalance method may not have the same morphology as the commonly created hydrophilic pores. For lipids from archaea for instance, we did not observe rearrangement of lipid headgroups to stabilize the defects in membrane. The

cell membranes of these types of archaea have a unique composition, a high chemical and a high physical stability [50-52] compared to simple phosphatidyl-choline (PC) lipids as they carry head-groups formed by sugar moieties, ether linkages instead of ester linkages between the head group and the carbonyl region, and methyl branches in the lipid tails [51]. These properties appear not only to increase the stability of these bilayers to electrical stress manifested by the increase of EP threshold, but change also the morphology of defect such perturbation creates.

Here we extend on these investigations to study the response of bilayers containing cholesterol. This sterol, a ubiquitous components of mammalian cells, influences as well profoundly the behavior of the membranes as it tunes their permeability, fluidity and mechanical properties [53-58].

Several experimental studies characterized the impact of cholesterol contents on the EP of simple lipid bilayers (egg PC,...) [7,59-61]. Most reported a stabilizing effect. Yet, this seems not to be a universal behavior: in the case of diphytanoyl-glycero-phosphocholine (DPhPC), lipid of which the saturated hydrocarbon chains are functionalized with methyl groups, cholesterol was found to slightly decrease EP threshold [62].

Recently, MD simulations were used to provide a molecular level insight onto EP of zwitterionic lipid membranes containing cholesterol [63]. Using an external E_{app} field, Fernández et al. [63] reported a steady (almost linear) increase of the EP thresholds for bilayers containing 20, 30 and 40 mol %, cholesterol. This behavior seems to contrast with other changes in the physical properties of the lipids bilayers, e.g. the average area per molecule and the bilayers thickness that do change as cholesterol content increases but only up to 30 mol % [56,64,65]. Above such concentration, addition of cholesterol has only a slight effect. Furthermore, all the simulations carried out by Fernández et al. [63] above the EP thresholds led to the formation of hydrophilic pores. However, in another set of seemingly unrelated MD simulations, the presence of cholesterol in lipid bilayers was shown to slow down the rate of lipid flip-flops by orders of magnitude [66,67]. Quite interestingly, hydrophilic pores that mediate such flip flop in pure lipid bilayers [66] were not observed in the bilayers containing concentrations of cholesterol of 20, and 40 mol %.

In order to further investigate the specificity of membranes containing cholesterol in particular their stability, and in complement to the pioneering work by Fernández et al. [63] we have modeled here cholesterol rich Palmitoyl-Oleyl-Phosphatidyl Choline (POPC) lipid bilayers subject to both low magnitude microsecond pulses (μs-msPEF) and to high magnitude nanosecond pulses (nsPEF) considering concentrations up to 50 mol %.

4.2.2 Systems and Methods

Four different systems were studied. The reference one is a bilayer composed of 256 1-palmitoyl-2-oleoyl-sn-glycero-3-phosphatidylcholine (POPC) lipids, and about 17000 water molecules. Such a high number of water molecules allows to consider water slabs on both sides of the bilayer thicker than 25-30 Å ensuring that for the μs-msPEF protocol, the membrane characteristics are those of a bilayer embedded in infinite baths [44,68]. The other three systems were formed by a POPC bilayer containing different molar ratios (fraction): respectively 20, 30, and 50 mol %. All the systems were considered either at no salt concentration for the study of the bilayers under electric fields, or at 0.5 M NaCl concentration for the study of the bilayers under transmembrane voltages created by charge imbalances.

The lipid and cholesterol force fields were derived from CHARMM36 all-atom parameters [69]. The TIP3P water model was used [70]. Bond lengths were constrained using the LINCS algorithm [71]. Short-range electrostatic and Lennard-Jones interactions were cut off at 1.0 nm. Long-range electrostatic interactions were calculated by the PME algorithm [72], with a direct space sum tolerance of 10^{-6} and a spherical truncation of 1.2 nm.

All simulations were performed using GROMACS.4.5.5 [73] on the GENCI-CINES High Performance Computing Linux cluster. All the systems were first equilibrated at constant pressure (1 atm) and constant temperature (300 K) for at least 100 ns. They were then extended to study the effects of electric fields, either at constant pressure and constant temperature (1 atm and 300 K) for the nsPEF protocol or at constant volume and constant temperature (300 K) for the μs-msPEF protocol. Note that at the temperature set for the study, the POPC bilayer is in the biologically relevant liquid crystal L_α phase.

4.2.2.1 nsPEF protocol

As previously stated, in simulations it is possible to apply "directly" a constant electric field E_{app} perpendicular to the membrane (lipid bilayers) plane. Such a protocol is used to model the application of short (typically few nanosecond long) high electric fields pulses (100s kV/cm). In practice, this is done by adding a force $F = E_{app} \cdot q_i$ to all the atoms bearing a charge q_i [74-76]. MD simulations adopting such an approach have been used to study membrane electroporation [35,36,38-40], as well as lipid externalization [39]. The lipid bilayers are modeled without consideration of a salt concentration. The applied electric field acts primarily on the interfacial water dipoles (small polarization of bulk water molecules). Within a very short time scale - typically few picoseconds [39] - a transverse field induces an overall transmembrane potential. Note here that, because of the MD simulation setup, and the use of Periodic Boundary Conditions (PBCs), E_{app} induces a voltage difference $U_m = E_{app} L_z$ over the whole system, where L_z is the size of the simulation box in the field direction [35,38].

4.2.2.2 μs-msPEF protocol

In order to model the effect of low magnitude ms pulses on the bilayers, we have used the charge imbalance method [37,44,68] to induce a U_m across the lipid bilayer systems embedded in 0.5 M NaCl salts. The method requires modeling the bilayer surrounded by vacuum so that the upper and lower water baths are separated, preventing hence ions from migrating from one solution to the other. The system can then be subject to voltage by setting a charge imbalance ΔQ/C between lower and upper baths (typically by displacing individual ions between the baths). As the membrane behaves as a capacitor (of capacitance C_{sp}), this gives rise to $U_m = Q_s/C_{sp}$, where Q_s is the charge imbalance per unit area. All simulations using this protocol are carried out at constant volume starting from well equilibrated bilayers.

4.2.2.3 Electrostatic properties

The electrostatic potential profiles U_z/V along z, the bilayer normal, were obtained from MD simulations using the Poisson's equation 4.4, i.e. derived as double integral of $\rho_z/(C/m^3)$, the volume charge density distribution, being $\epsilon_0/(F/m)$ the vacuum permittivity:

$$U_z = U(z) - U_0 = -\frac{1}{\epsilon_0}\int_0^z \int \rho_z(z'')dz''dz', \tag{4.4}$$

As reference, U_0 was set to zero in the lower bulk solution. The transmembrane voltages U_m were calculated as the difference between the electrostatic potential measured at the lower and the upper baths.

4.2.3 Results

4.2.3.1 nsPEF protocol

This Section reports the results of the simulations of the systems mimicking high intensity nanosecond electric pulses.

The response of the bilayer to high voltages has been investigated by monitoring the formation of pores across the membranes hydrophobic core.

Table 4.2 reports results from simulations carried out under constant electric field for the POPC pure bilayers and bilayers with cholesterol content ranging from 20 to 50 mol %. We consider as EP threshold the transmembrane voltage (U_{thr}) at which no pore is observed for 100 ns length simulations. One replica was run for each condition. The results show clearly that as the concentration of cholesterol increases, the intensity of the E_{app}, and accordingly the transmembrane voltage U_m required to create a pore in the membrane,

System	t_{sim}/ns	E_{app}/(V/nm)	U_m/V	t_{water}/ns
Pure POPC	100	0.16	1.59	-
	15	0.20	1.99	13.6
POPC + 20 mol % chol.	100	0.20	2.05	-
	35	0.25	2.56	33.7
POPC + 30 mol % chol.	100	0.25	2.73	-
	85	0.30	3.28	82.4
POPC + 50 mol % chol.	100	0.30	3.40	-
	40	0.35	3.85	33.5

Table 4.2: Electroporation under transmembrane voltages created by an applied electric field
t_{sim} - MD simulation duration
E_{app} - exogenous electric field applied
U_m - transmembrane voltages created by the applied electric field, with an estimated error of 50 mV
t_{water} - time when the first wire of water is formed in the hydrophobic core of the bilayer

must be higher. At the conditions of the present simulations (system size) and given the force field used, we note that the field EP threshold almost doubles between the bare bilayer and the bilayer containing 50 mol % cholesterol. This is very consistent with the recent simulations of DOPC (di Oleyl PC) bilayers containing cholesterol [63].

As reported in previous simulations [63], above the EP thresholds, in all simulations under the nsPEF protocol, the electric field favors quite rapidly formation of water defects and water wires deep into the membrane hydrophobic core. Ultimately water fingers forming at both sides of the membrane join up to form water channels (often termed pre-pores or hydrophobic pores) that span the membrane. Within nanoseconds, few lipid head-groups start to migrate from the membrane-water interface to the interior of the bilayer stabilizing hydrophilic pores.

4.2.3.2 μs-msPEF protocol

This Section reports the results of the simulations of the systems mimicking classical electroporation. First we determine characteristics of the bilayers, from the simulations carried out under charge imbalance.

4.2.3.2.1 Bilayer characteristics Fig. 4.15 reports the number density profiles of the membrane constituents for a selected system, and shows that in the present setup the 3.0-3.5 nm thickness of the water slab in both sides of the membrane are large enough to allow establishment of a constant electrostatic potential within each slab (Fig. 4.15 B). The setup is therefore adequate for modeling infinite baths surrounding the bilayer.

The increase of charge imbalance then permits to build in an increasing U_m voltage. As

previously found for other lipids and using other force fields [37,44,68], the voltage induced is proportional to the charge imbalance (per unit area of membranes) demonstrating that the bilayer behaves as a capacitor (Fig. 4.15 C).

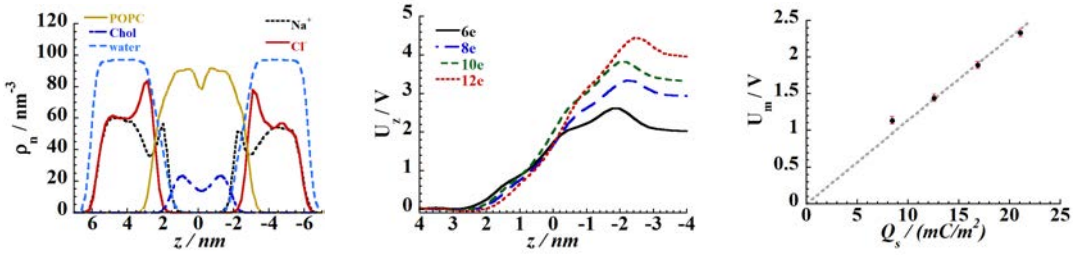

(a) *Number density.* **(b)** *Electrostatic potential.* **(c)** *Electrical capacitance.*

Figure 4.15: Structural and electrostatic characteristics of the POPC-cholesterol (20 mol %) system. (A) Number density profiles along z, for POPC (yellow dotted line), water (light dashed blue), cholesterol (blue dashed line), sodium ion (red solid line), chloride ion (black dashed line), a factor of 102 was applied to sodium and chloride densities for clarity of data; (B) Electrostatic potential along z (error of 50 mV); (C) U_z as a function of the charge imbalance per unit area for the POPC-bilayer; the capacitance can be deduced out of the equation $U_m = Q_s/C$

System	A_m/Å^2	$C_{sp}/(\mu$Fcm$^{-2})$	ΔQ/C	U_m/V	t_{sim}/ns
Pure POPC	59.9 ± 0.2	0.88 ± 0.01	4e	1.13	15
			6e	1.44	35
			8e	1.86	40
			10e	2.33	100
POPC + 20 mol % chol.	46.8 ± 1.0	0.78 ± 0.01	6e	2.02	20
			8e	2.68	100
			10e	3.51	100
POPC + 30 mol % chol.	41.6 ± 0.7	0.70 ± 0.01	8e	3.37	20
			10e	4.4	140
POPC + 50 mol % chol.	40.7 ± 0.4	0.72 ± 0.01	8e	3.26	20
			10e	4.55	100

Table 4.3: Characteristics of the equilibrated bilayers in 0.5 M NaCl salt concentration from the MD simulations

The specific capacitance $C_{sp}/(\mu F/cm^2)$ of the bilayers, deduced out of the equation $U_m = Q_s/C_{sp}$ with $Q_s/(mC/m^2)$ the charge imbalance per unit area, slightly decreases with increasing cholesterol content at least up to 30 mol %, then it levels-off as does the average area per molecule A_m/Å^2 (see Table 4.3, and Fig. 4.18 insert). Even if other approaches were proposed [77], for the scope of this work, the area per molecule was evaluated here simply by dividing the area of the system by the number of molecules (POPC or Chol) per leaflet.

Note that this particular structural characteristic of the bilayers has also been reported for other lipid bilayers [63-65], where the area per molecule as well as the bilayer thickness have been shown to change very mildly as the concentration of cholesterol reaches or is

higher than 30 mol %.

4.2.3.2.2 Membranes electroporation As for the previous protocol, we consider the as EP threshold the transmembrane voltage U_{thr} at which no pore is observed for simulation of 100 ns length. One replica was run for all the conditions. Table 4.4 reports that the U_{thr} does increase from ∼2.3 V for bare bilayers to ∼4.4 V as the cholesterol content reaches the 30 mol % concentration and quite interestingly, as for the capacitance and the bilayer area per molecule, U_{thr} levels-off above 30 mol % cholesterol content.

System	t_{sim}/ns	ΔQ/C	U_m/V	t_{water}/ns
Pure POPC	100	10e	2.33	-
	100	12e	3.01	8.4
POPC + 20 mol % chol.	100	8e	2.68	-
	35	10e	3.51	69.6
POPC + 30 mol % chol.	140	10e	4.44	-
	100	12e	5.30	29.7
POPC + 50 mol % chol.	100	10e	4.55	-
	40	12e	5.35	36.4

Table 4.4: Electroporation under transmembrane voltages created by a net charge imbalance

Perhaps the most peculiar phenomena observed in all simulations performed under the μs-msPEF protocol for large cholesterol content is the formation of conducting pores, which show a morphology (Fig. 4.17 (a) and (b)), that is completely different from the one of pores forming in POPC bilayers (Fig. 4.16). When using the μs-msPEF protocol, the pore formation starts from the intrusion of water molecules toward the hydrophobic core of the bilayer.However, we did not observe major rearrangement of the lipid head-groups to stabilize such defects in membrane.

In none of the simulations performed, we have observed the creation of hydrophilic pores as in the case of simple zwitterionic lipid bilayers. In fact, even if one or two cholesterol, and POPC molecules slightly migrated toward the interior of the bilayer in the pore area, the water columns were never completely stabilized by the lipid head groups (Fig. 4.17 (a) and (b)). Overall, these pores morphologies were maintained while the pore diameter kept increasing, until it became able to conduct ions (Fig. 4.16). Water columns hence formed were always exposed to the apolar and hydrophobic tails of the phospholipids.

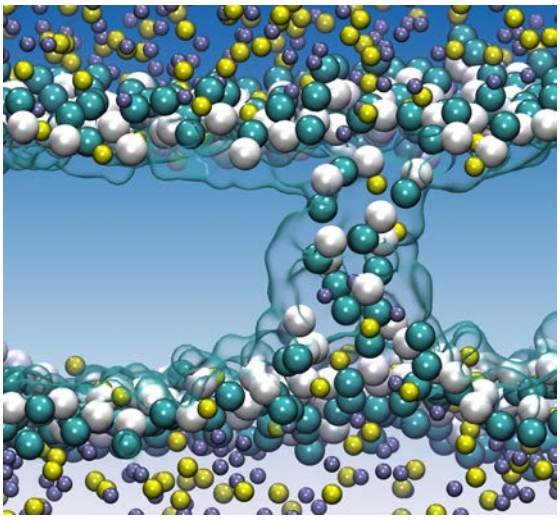

Figure 4.16: Hydrophilic pore in a pure POPC bilayer, when subject to a large TM voltage create by a net charge imbalance: the headgroups stabilize the pore surrounding completely the water column. Water molecules are plotted as transparent fluid, POPC headgroups are in cyan and white beads, cholesterol hydroxyl groups are in red beads, sodium in yellow beads, chloride in ice-blue ones, POPC chain are not shown

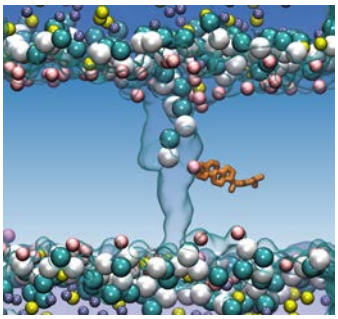

(a) *30 mol % chol.*

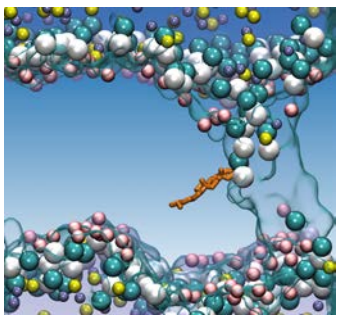

(b) *50 mol % chol.*

Figure 4.17: Representative MD snapshots of the pore morphologies for the system at 30 and 50 mol % cholesterol, in panel (a), and (b) respectively when subject to a large TM voltage create by a net charge imbalance. For legend see 4.16, one representative cholesterol molecule is reported in orange. Hydrophobic pores: even if one or two cholesterol, and POPC molecules migrated toward the interior of the bilayer the water columns is not completely sustained by the polar headgroups of the phospholipids up until the pore closure. This implies that part of the water column is always exposed to the apolar and hydrophobic tail of the phospholipids

4.2.4 Discussions

Addition of cholesterol to lipid membranes is known to alter their structural properties. The main attribute that makes cholesterol a unique lipid molecule is its ability to condense fluid lipid bilayers. This can be traced back in several membrane properties as for instance a decrease of the area per molecule and an increase in the bilayer thickness [56,64]. These condensing effects, which have been reproduced and observed in the present simulations, show a trend in line with previous experimental and theoretical reports [64,65]: the properties of different lipid bilayers are strongly influenced by the addition of cholesterol up to 30 mol %. Above such concentrations, addition of cholesterol has only a slight effect.

Several experimental studies characterized the influence of cholesterol contents in the range of the concentrations studied here on the EP of simple lipid bilayers (egg PC,...) [7,59-61]. Most reported a stabilizing effect. Along the same lines, MD simulations were recently performed to study EP of di-oleyl-phosphatidylcholine (DOPC) lipid patches containing cholesterol, by subjecting the bilayer to high electric fields [63]. In complement to these investigations, we have modeled here the two experimental protocols generally used to trigger electroporation. The first one is based on the direct application of an external E_{app} field on the whole simulation box, and mimics the application of a nanosecond high intensity electric pulse as in [63]; the second one, the charge imbalance method, explicitly includes the accumulation of charges near the lipid head group interface mimicking hence the application of lower intensity pulses for longer duration (leading to a charging of the bilayer). Overall, both methods show that higher applied transmembrane potentials are needed to electroporate bilayers containing increasing amounts of cholesterol (Tables 4.2, and 4.4).

This study however highlights unexpected differences in the results obtained with the two protocols.

4.2.4.1 Contrasting results for the electroporation thresholds of the nsPEF and the μs-msPEF protocols

The results obtained using the external E_{app} field are similar to the ones reported in [63]: essentially, the fields required for bilayer electroporation were larger for higher cholesterol content. The extensive simulations performed by the authors showed a steady (almost linear) increase of the EP threshold for bilayers containing 20, 30 and 40 mol %, and in this study as reported in Fig. 4.18, up to 50 mol %. The lipid bilayer behavior obtained using the charge imbalance method is quite different. The simulations show that bilayers with a 20 mol % cholesterol content requires a mild increase of the EP threshold, while for the sample at 30 mol % this value almost doubles. Overall the EP thresholds obtained with the μs-msPEF protocols are higher then those obtained using the nsPEF protocol. However this increase reaches a sort of saturation for higher concentrations of cholesterol (Fig.

4.18). Interestingly, this is more consistent with the changes in the characteristics of the bilayers i.e. the order parameters, the area per lipid, or the capacitance that level-off above 30 mol % (Fig. 4.18).

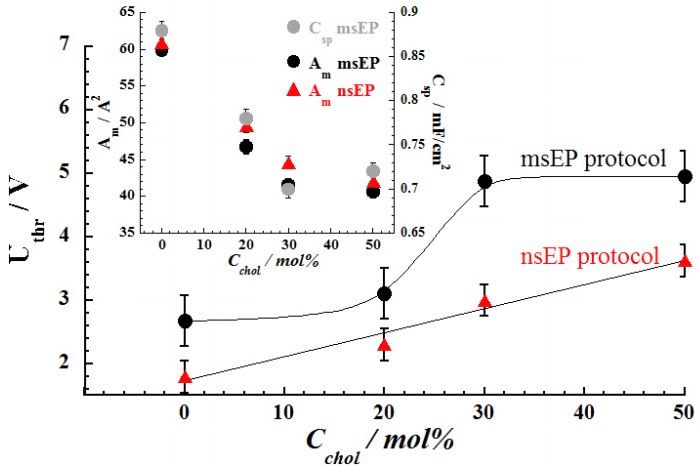

Figure 4.18: U_{thr} as a function of the cholesterol content (C_{chol}/mol%) for the two protocols. Vertical bar limit: the lower limit is the voltage at which no EP is observed in 100 ns, the higher limit is the voltage at which EP is observed within 100 ns. The effective threshold values are in between these limits. Insert: area per molecule A_m calculated for the two protocols and specific capacitances C_{sp} of the bilayers, as functions of C_{chol}

4.2.4.2 Contrasting results for the pores morphologies

The morphologies of the pores formed above the threshold using the two protocols show also significant differences. When nsPEFs are applied, the pores are hydrophilic and stabilized by both lipid head groups and cholesterol hydroxyl groups which is consistent with what reported also by [63]. In the case of the protocol mimicking the μs-msPEF, above 30 mol % concentration of cholesterol, migration of the lipids along the initial water wires appears to be largely hindered (Fig. 4.17 (a) and Fig. 4.17 (b)) for the all pore life. We never observed a large number of lipid molecules following the intrusion of the water molecules in the hydrophobic core as in pure POPC bilayers. In all cases, just one or two cholesterol and a couple of POPC molecules migrated toward the interior of the bilayer resulting in water columns never completely sustained during the all life of the pore. Recent extensive comparative MD simulations studies on simple (POPC based) lipids bilayers [44,47] have shown that, at the molecular level, the two types of pulses induce formation of hydrophilic pores. The present results on cholesterol containing bilayers, seem to challenge this result. Quite interestingly, evidence from experiments [60] suggests that pores formed in simple PC membranes have different characteristics than those of planar lipid membranes containing cholesterol. Indeed, using constant current pulses the authors found that the conductance traces of electroporated bilayers containing cholesterol have very large fluctuations, reaching occasionally 0 nS, not observed in absence of the sterol. The authors

suggest this is an indication that pores in the cholesterol samples do close during electroporation. This is consistent with our finding. Pores not stabilized by the lipid head groups are expected indeed to collapse and reseal much more rapidly once the electric stress is released following ionic transport across the bilayer. What specific characteristics are responsible for the difference in behavior between nsPEF and μs-msPEF? Comparison of the electrostatic potential profiles across the bilayer when the systems are subject to transmembrane potentials using the charge imbalance and the electric field methods do not show a significant difference (data not shown). Accordingly it does not seem that the contrasting behavior stems from a difference in the induced electric field that the membrane components sense between the two protocols. Another hypothesis is that the discrepancy is due to other methodology issues. Indeed, using the charge imbalance method, we constrain the system to a constant volume. The transmembrane voltage may induce in such a case a large surface tension on the system as EP takes place. In contrast, in the nsPEF protocol, since we perform simulations under constant pressure, the surface tension is by definition maintained constant ($\sim$0 mN/m) and the lateral dimensions of the box are allowed to change and fluctuate accordingly. Hence, when subject to high transmembrane voltages, the lateral stress on the bilayer is not relaxing in the same manner under the two protocols. To verify the incidence of these constraints on the results, we performed an additional simulation above the EP threshold using the charge imbalance method (system at 30 mol % cholesterol) but maintaining the lateral tension on the bilayer constant ($\sim$0 nN/m). The system underwent as expected electroporation, and the pores formed were also *hydrophobic* like. This demonstrates that under our conditions, constraining the volume when using the charge imbalance protocol is not at the origin of the different behavior of the membrane, when subject to ms and ns EPs.

The other difference between the two methods is the consideration of a salt concentration. It is required obviously in the charge imbalance method, while modeling the membrane in absence of ions is more appropriate [44] when modeling the effect of nsPEFs. Finally, another aspect that may be considered in conjunction with the previous observations is the release of the electrical stress immediately after few ions go through the pore that occurs only for the charge imbalance setup (the electric field is maintained throughout the simulation for the nsPEF protocol). It would be very informative to follow the bilayer electroporation of these systems under a constant charge imbalance conditions, i.e. maintaining the voltage across the bilayer. At any rate, much more studies are required to shed light on this.

Nonetheless, this study highlights the fact that bilayers and evidently cells response to high electric pulses is far from being a simple and identical molecular process, but rather varies with the lipid composition and the protocol used.

4.2.5 Conclusions

Our simulations and analyses show that at the molecular scale, electroporation of a phospholipid cholesterol rich bilayer is heavily influenced by the presence of this sterol. The results obtained applying two protocols - mimicking *traditional* EP using low intensity pulses (μs-msPEF) and high intensity electric pulses (nsPEF) - indicate that in both cases an increase in cholesterol concentration requires a higher transmembrane voltage to porate the membrane bilayer. Using the first protocol the EP threshold increases steadily with the electric field applied doubling the threshold necessary for poration with respect to the one for pure bilayer when cholesterol content reaches 50 mol %. Under μs-msPEF, the EP threshold, as well as all the other structural characteristics of the bilayer are leveled-off above 30 mol % cholesterol. Moreover in the latter protocol, the morphology of the pores formed above this cholesterol concentration show different characteristics: the migration of the lipids along the initial water wires appears to be largely hindered, resulting in a water column not completely saturated by the headgroups of phospholipids. The nature of such pores should in principle lead to different ionic and molecular transport across electroporated membranes and have a direct effect on pore life time and resealing time.

Experimental studies have yet to confirm our findings, but we anticipate that these notable differences, noticed also for other lipid membranes compositions should impact on the outcome of several biomedical applications of the electroporation. On the biotechnological front, our results should contribute to the development of new protocols that better regulate and exploit the phenomenon of EP by tuning the composition of membranes in applications ranging from cell manipulation such as electro-fusion to the use of electric fields to trigger release of drug from lipid based smart carriers.

4.2.6 References

[1] E. Neumann, The relaxation hysteresis of membrane electroporation, in: Electroporation and Electrofusion in Cell Biology, eds. E. Neumann, A.E. Sowers, C.A. Jordan, Plenum Publ. Corp. 1989, pp.61-82.

[2] J. A. Nickoloff, Animal Cell Electroporation and Electrofusion Protocols, Totowa, NJ: Humana Press (1995).

[3] S. Li, Electroporation Protocols: Preclinical and Clinical Gene Medecine, Totowa, NJ.: Humana press (2008).

[4] E. Neumann, and K. Rosenheck, Permeability changes induced by electric impulses in vesicular membranes, J. Membr. Biol. 10 (1972) 279-290.

[5] U. Zimmerman, G. Pilwat, F. Beckers et al., Effects of external electrical fields on cell membranes, Bioelectrochem. Bioenerg. 3 (1976) 58-83.

[6] R. W. Glaser, S. L. Leiken, L. V. Chernomordik et al., Reversible electrical breakdown of lipid bilayers: Formation and evolution of pores, Biochim. Biophys. Acta. 940 (1988) 275-287.

[7] D. Needham, and R. M. Hochmuth, Electro-mechanical permeabilization of lipid vesicles, Biophys. J. 55 (1989) 1001-1009.

[8] U. Zimmerman, The Effect of High Intensity Electric Field Pulses on Eukaryotic Cell Membranes: Fundamentals and Applications, Boca Raton, Florida: CRC Press (1996).

[9] J. Teissié, N. Eynard, B. Gabriel et al., Electropermeabilization of cell membranes, Adv. Drug Deliv. Rev. 35 (1999) 3-19.

[10] T. Y. Tsong, Electric modification of membrane permeability for drug loading into living cells, Methods Enzymol. 149 (1987) 248-259.

[11] J. C. Weaver, Electroporation Theory, Methods in Molecular Biology, Clifton, New Jersey: Humana Press (1995)3-29.

[12] T. Y. Tsong, Electroporation of cell membranes, Biophys. J. 60 (1991) 297-306.

[13] E. Neumann, M. Schaefer-Ridder, Y. Wang et al., Gene transfer into mouse lyoma cells by electroporation in high electric fields, EMBO J. 1 (1982) 841-845.

[14] R. C. Lee, L. P. River, F. S. Pan et al., Surfactant-induced sealing of electropermeabilized skeletal muscle membrane in vivo, Proc. Natl. Acad. Sci. U.S.A. 89 (1992) 4524-4528.

[15] T. Nishi, K. Yoshizato, S. Yamashiro et al., High-efficiency in vivo gene transfer using intraarterial plasmid DNA injection following in vivo electroporation, Cancer Res. 56 (1996)

1050-1055.

[16] J. A. Lundqvist, F. Sahlin, M. A. Aberg et al., Altering the biochemical state of individual cultured cells and organelles with ultramicroelectrodes, Proc. Natl. Acad. Sci. U.S.A. 95 (1998) 10356-10360.

[17] R. L. Harrison, B. J. Byrne, and L. Tung, Electroporation-mediated gene transfer in cardiac tissue, FEBS Lett. 435 (1998) 1-5.

[18] M. Golzio, J. Teissie, and M.-P. Rols, Direct visualization at the single-cell level of electriclly mediated gene delivery, Proc. Natl. Acad. Sci. U.S.A. 99 (2002) 1292-1297.

[19] T. Y. Tsong, Voltage modulation of membrane permeability and energy utilization in cells, Biosci. Rep. 3 (1983) 487-505. [20] M. R. Prausnitz, V. G. Bose, R. Langer et al., Electroporation of mammalian skin: a mechanism to enhance transdermal drug delivery, Proc. Natl. Acad. Sci. U.S.A. 90 (1993) 10504-10508.

[21] T. Suzuki, B. C. Shin, K. Fujikura et al., Direct gene transfer into rat liver cells by in vivo electroporation, FEBS Lett. 425 (1998) 436-440.

[22] M. Breton, L. Delemotte, A. Silve et al., Transport of siRNA through lipid membranes driven by nanosecond electric pulses: An experimental and computational study, J. Am. Chem. Soc. 134 (2012) 13938-13941.

[23] A. Testori, J. Soteldo, A. Di Pietro et al., The treatment of cutaneous and subcutaneous lesions with electrochemotherapy with bleomycin, Eur. Dermatology 3 (2008) 1-3.

[24] M. Cemazar, Y. Tamzali, G. Serša et al., Electrochemotherapy in veterinary oncology, J. Vet. Int. Med. 22 (2008) 826-831.

[25] J. Villemejane, and L. M. Mir, Physical methods of nucleic acid transfer: general concepts and applications, Brit. J. Pharma. 157 (2009) 207-219.

[26] A. M. Bodles-Brakhop, R. Heller, and R. Draghia-Akli, Electroporation for the delivery of DNA-based vaccines and immunotherapeutics: Current clinical developments, Mol. Therap. 17 (2009) 585-592.

[27] L. G. Campana, S. Mocellin, M. Basso et al., Bleomycin-based electrochemotherapy: clinical outcome from a single institution's experience with 52 Patients, Ann. Surg. Onc. 16 (2009) 191-199.

[28] A. Pakhomov, D. Miklavcic and M. Markov, Advanced Electroporation Techniques in Biology and Medicine, Taylor and Francis/CRC Press (2010).

[29] B. Zorec1, V. Préat, D. Miklavčič, N. Pavšelj, Active enhancement methods for intra- and transdermal drug delivery: a review, Zdrav. Vestn. 82 (2013) 339-356.

[30] S. Chabot, C. Rosazza, M. Golzio, A. Zumbusch, J. Teissie, M. P. Rols, Nucleic acids electro-transfer: from bench to bedside, Curr. Drug. Metab. 14 (2013) 300-308.

[31] C. Chen, S.W. Smye, M.P. Robinson et al., Membrane electroporation theories: a review, Med. Biol. Eng. Comput. 44 (2006) 5-14.

[32] S. J. Beebe, and K. H. Schoenbach, Nanosecond pulsed electric fields: A new stimulus to activate intracellular signaling, J. Biomed. Biotech. 4 (2005) 297-300.

[33] R. Benz, F. Beckers, and U. Zimmerman, Reversible electrical breakdown of lipid bilayer membranes - Charge-pulse relaxation study, J. Membr. Biol. 48 (1979) 181-204.

[34] L. V. Chernomordik, S. I. Sukharev, S. V. Popov et al., The electrical breakdown of cell and lipid membranes: the similarity of phenomenologies, Biochim. Biophys. Acta 902 (1987) 360-373.

[35] D. P. Tieleman, The molecular basis of electroporation, BMC Biochemistry 5 (2004) 10.

[36] Q. Hu, S. Viswanadham, R. P. Joshi et al., Simulations of transient membrane behavior in cells subjected to a high-intensity ultrashort electric pulse, Phys. Rev. E. 71 (2005) 031914.

[37] A. A. Gurtovenko, and I. Vattulainen, Pore formation coupled to ion transport through lipid membranes as induced by transmembrane ionic charge imbalance: Atomistic molecular dynamics study, J. Am. Chem. Soc. 127 (2005) 17570-17571.

[38] M. Tarek, Membrane electroporation: A molecular dynamics simulation, Biophys. J. 88 (2005) 4045-4053.

[39] P. T. Vernier, M. J. Ziegler, Y. Sun et al., Nanopore formation and phosphatidylserine externalization in a phospholipid bilayer at high transmembrane potential, J. Am. Chem. Soc. 128 (2006) 6288-6289.

[40] R. A. Bockmann, B. L. de Groot, S. Kakorin et al., Kinetics, statistics, and energetics of lipid membrane electroporation studied by molecular dynamics simulations, Biophys. J. 95 (2008) 1837-1850.

[41] M. J. Ziegler, and P. T. Vernier, Interface water dynamics and porating electric fields for phospholipid bilayers, J. Phys. Chem. B 112 (2008) 13588-13596.

[42] A. A. Gurtovenko, J. Jamshed Anwar, and I. Vattulainen, Defect-mediated trafficking across cell membranes: Insights from in silico modeling, Chem. Rev. 110 (2010) 6077-6103.

[43] Z. A. Levine, and P. T. Vernier, Life cycle of an electropore: Field dependent and field-indepedent steps in pore creation and annihilation, J. Membr. Biol. 236 (2010) 27-36.

[44] L. Delemotte, and M. Tarek, Molecular dynamics simulations of lipid membrane electroporation, J. Membr. Biol. 245 (2012) 531-543.

[45] M.-C. Ho, M. Casciola, Z. A. Levine, and P. T. Vernier, Molecular dynamics simulations of ion conductance in field-stabilized nanoscale lipid electropores, J. Phys .Chem. B 117 (2013) 11633-11640.

[46] M. Tokman, J. H. Lee, Z. A. Levine, M.-C. Ho, M. E. Colvin, P. T. Vernier, Electric Field-Driven Water Dipoles: Nanoscale Architecture of Electroporation, PLoS ONE 8 (2013) 1-9.

[47] P. T. Vernier, M. J. Ziegler, Y. Sun, M. A. Gundersen, and D. P. Tieleman, Nanopore-facilitated, voltage-driven phosphatidylserine translocation in lipid bilayers - in cells and in silico, Phys. Biol., 3 (2006) 233-247.

[48] P. Kramar, L. Delemotte, A. M. Lebar, et al. Molecular-level characterization of lipid membrane electroporation using linearly rising current, J. Membr. Biol. 245 (2012) 651-659.

[49] A. Polak, M. Tarek, M. Tomšič, J. Valant, N. P. Ulrih, A. Jamnik, P. Kramar, D. Miklavčič, Electroporation of Archaeal Lipid Membranes using MD Simulations, Bioelectrochem. (2014) In press.

[50] T. Benvegnu, M. Brard, D. Plusquellec, Archaeabacteria bipolar lipid analogues: structure, synthesis and lyotropic properties, Curr. Opin. Colloid Interface Sci. 8 (2004) 469-479.

[51] N.P. Ulrih, D. Gmajner, P. Raspor, Structural and physicochemical properties of polar lipids from thermophilic archaea, Appl. Microbiol. Biotechnol. 84 (2009) 249-60.

[52] N.P. Ulrih, U. Adamlje, M. Nemec, M. Sentjurc, Temperature-and pH-induced structural changes in the membrane of the hyperthermophilic archaeon Aeropyrum pernix K1, J. Membr. Biol. 219 (2007) 1-8.

[53] M. Bloom, E. E., and O. G. Mouritsen, Physical properties of the fluid lipid-bilayer component of cell membranes: a perspective, Q. Rev. Bioph. 24 (1991) 293-397.

[54] D. A. Brown, and E. London, Structure and function of sphingolipid- and cholesterol-rich membrane rafts, J. Biol. Chem. 275 (2000) 17221-17224.

[55] Berkowitz, M. L., Detailed molecular dynamics simulations of model biological membranes containing cholesterol, Biochim. Biophys. Acta 1788 (2009) 86-96.

[56] K. Tu, M. L. Klein, and D. J. Tobias, Constant-pressure molecular dynamics investigation of cholesterol effects in a dipalmitoyl phosphatidyl choline bilayer. Biophys. J. 75(5) (1998) 2147-2156.

[57] H. Martinez-Seara, T. Rog , M. Karttunen, I. Vattulainen, R. Reigada, Cholesterol

induces specific spatial and orientational order in cholesterol/phospholipid membranes, PLoS ONE 5 (2010) 1-11.

[58] N. Kucerka, J. D. Perlmutter, J. Pan, S. Tristram-Nagle, J. Katsaras, and J. N. Sachs, The effect of cholesterol on short- and long-chain mono-unsaturated lipid bilayers as determined by molecular dynamics simulations and X-ray scattering, Biophys. J., 95 (2008) 2792-2805.

[59] S. Kakorin, U. Brinkmann, E. Neumann, Cholesterol reduces membrane electroporation and electric deformation of small bilayer vesicles, Biophys. Chem. 117 (2005) 155-171.

[60] S. Koronkiewicz, S Kalinowski, Influence of cholesterol on electroporation of bilayer lipid membranes: chronopotentiometric studies, Biochim. Biophys. Acta 1661 (2004) 196-203.

[61] M. Naumowicz, Z. A. Figaszewski, Pore formation in lipid bilayer membranes made of phosphatidylcholine and cholesterol followed by means of constant current, Cell Biochem. Biophys. 66 (2013) 109-119.

[62] I. van Uitert, S. Le Gac, A. van den Berg, The influence of different membrane components on the electrical stability of bilayer lipid membranes, Biochim. Biophys. Acta 1798 (2010) 21-31.

[63] M.L. Fernáandez, G. Marshall, F. Saguées et al., Structural and kinetic molecular dynamics study of electroporation in cholesterol-containing bilayers, J. Phys Chem. B 114 (2010) 6855-6865.

[64] W. C. Hung, M. T. Lee, F. T. Chen et al., The condensing effect of cholesterol in lipid bilayers, Biophys. J. 92 (2007) 3960-3967.

[65] F. de Meyer and B. Smit, Effect of cholesterol on the structure of a phospholipid bilayer, Proc. Natl. Acad. Sci. U.S.A. 106 (2009) 3654-3658.

[66] S. J. Marrink, , A. H. de Vries, T. A. Harroun, J. Katsaras, and S. R. Wassall, Cholesterol shows preference for the interior of polyunsaturated lipid membranes, J. Am. Chem. Soc., 130 (2008) 10-11.

[67] W. F. Bennett, J. L. MacCallum, and D. P. Tieleman, Thermodynamic analysis of the effect of cholesterol on dipalmitoylphosphatidylcholine lipid membranes, J. Am. Chem. Soc., 131 (2009) 1972-1978.

[68] L. Delemotte, F. Dehez, W. Treptow et al., Modeling membranes under a transmembrane potential, J. Phys. Chem. B 112 (2008) 5547-5550.

[69] J. B. Klauda, R. M. Venable, J. A. Freites et al., Update of the CHARMM all-atom additive force field for lipids: Validation on six lipid types, J. Phys .Chem. B 114 (2010)

7830-7843.

[70] W. L. Jorgensen, J. Chandrasekhar, J. D. Madura et al., Comparison of simple potential functions for simulating liquid water, J. Chem. Phys. 79 (1983) 926-935.

[71] B. Hess, H. Bekker, H. J. C. Berendsen et al., LINCS: A linear constraint solver for molecular simulations, J. Comp. Chem. 18 (1997) 1463-1472.

[72] U. Essmann, L. Perera, M. L. Berkowitz et al., A smooth particle mesh ewald method, J. Chem. Phys. 103 (1995) 8577-8593.

[73] B. Hess, C. Kutzner, D. van der Spoel et al., GROMACS 4: algorithms for highly efficient, load-balanced, and scalable molecular simulation, J. Comp. Theor. Chem. 4 (2008) 435-447.

[74] Q. Zhong, P. B. Moore, D. M. Newns et al., Molecular dynamics study of the LS3 voltage-gated ion channel, FEBS Lett. 427 (1998) 267-270.

[75] D. P. Tieleman, J. H. C. Berendsen, and M. S. P. Sansom, Voltage-dependent insertion of alamethicin at phospholipid/water and octane water interfaces, Biophys. J. 80 (2001) 331-346.Y. Yang.

[76] D. Henderson, P. Crozier et al., Permeation of ions through a model biological channel: effect of periodic boundary condition and cell size, Molec. Phys. 100 (2002) 3011-3019.

[77] C. Hofsšb, E. Lindahl, and O. Edholm, Molecular dynamics simulations of phospholipid bilayers with cholesterol, Biophys. J. 84 (2003) 2192-2206.

4.3 Electropores characterization

In the present Section, we extend MD investigations by modeling for the first time conditions comparable to experiments using long (μs-ms) low intensity (~kV/cm) pulses, by studying the characteristics of pores formed in lipid bilayers maintained at a constant surface tension and subject to constant charge imbalance. This enables the evaluation of structural (size) and electrical (conductance) properties of the pores formed, providing information hardly accessible directly by experiments. Extensive simulations of EP of simple phosphotidylcholine bilayers in 1 M NaCl show that hydrophilic pores with stable radii (1-2.5 nm) form under transmembrane voltages between 420 and 630 mV, allowing for ionic conductance in the range of 6.4-29.5 nS. We discuss in particular these findings and characterize both convergence and size effects in the MD simulations. We further extend these studies in a follow-up paper (Rems et al., Bioelectrochemistry, Submitted), by proposing an improved continuum model of pore conductance consistent with the results from the MD simulations.

4.3.1 Introduction

The size of pores formed as a result of EP [1-24] together with their morphology and conductive properties are crucial in determining the permeability and selectivity of the plasma membrane to different ionic and molecular species and consequently the potential efficacy of a given EP application. While extensive experimental work on cells and model lipid membranes (e.g. planar lipid bilayers and lipid vesicles) has been devoted to the structural characterization of these pores [25-35], the data emerging so far is very scarce. Experimentally, one is able to estimate the nanopore dimension only indirectly by measuring either membrane permeability to molecules of different sizes, or membrane conductance recovered from the current/voltage relationship. Both approaches, however, have their specific limitations.

Estimates of pore size based on monitoring the transmembrane transport of small molecules (e.g. sugars, polyethylene glycols [33], bleomycin [34]) and fluorescent dyes (e.g. thallium ions [32], YO-PRO, propidium iodide [35]) were mostly obtained from *in vitro* experiments on cells after exposing them to nanosecond long (≤600 ns) electric pulses. Results of these studies suggested that nanosecond pulses induce a high number of long-lived yet small pores, most of them with radii of about 0.5-0.7 nm, which allow the transport of larger molecules such as propidium iodide, but prevent the massive flux reported for longer (millisecond) less intense (kV/cm) pulses [35-38]. The direct correlation between the size of a molecule and that of a pore is though debatable for molecules that might interact strongly with the pore walls. Indeed an interacting molecule requires certain time to dissociate from the bilayer and diffuse into the cytosolic milieu where it can be detected. In addition, a charged molecule can significantly perturb the local electrostatic environment in the pore proximity, leading to changes in pore dimensions and pore morphology [39]. Even neutral

sugar molecules can strongly interact with lipid headgroups through hydrogen bonding, consequently modifying the bilayer properties [40]. Such measurements may therefore not reflect properly the properties of pores as directly induced by electric pulses.

Estimates of pore size based on measurements of membrane conductance were on the other hand mostly obtained from planar lipid bilayers when applying a constant current (chronopotentiometry) to the membrane [25,26,29]. The benefit of controlling the current instead of the voltage is that once a pore is formed, the voltage across the membrane can reduce due to ionic transport through the pore, hence stabilizing the pore and preventing membrane rupture. For phosphatidylcholine based planar lipid bilayers, pore radii from 1.9 to 6.0 nm were reported, with larger pores observed when imposing a higher current. Conductance measurements have also been performed on dense cell suspensions during exposures to trains of 100 μs pulses [28] and on single cells using patch clamp techniques [30]. These studies suggested that pore radii can vary from ∼1 to 55 nm, depending on the experimental conditions. However, the major limitation of estimating the pore size from conductance measurements is that the experimental data needs to be fitted to a certain model, which relates the pore conductance with the pore size. For such purpose, analytical models deriving from the continuum Nernst-Planck theory are normally used, which inherently impose simplified assumptions about the pore geometry and the effective conductivity of the electrolyte inside the pore [41-43]. The choice of such parameters and characteristics are in general arbitrary or too approximate, which may casts doubts on the accuracy of the predictions arising from the models. Moreover, continuum theories can fail to properly describe the physics in a molecular-scale system, which was indeed observed for ion channels [44,45]. One way of testing, validating, and if needed improving the continuum models is to compare them with molecular dynamics (MD) simulations, which provide full atomistic details of the entire process of ionic conduction through a pore.

This is precisely the approach we are undertaking hereafter. In a series of papers, we pursue a line of research where we use MD simulations to determine the structural (shape, size) and electrical (conductance, selectivity) properties of electropores formed in a model lipid bilayer in its liquid crystal L_α phase, when subject to increased transmembrane (TM) voltage. In the first (present) paper, we introduce a new MD simulation protocol that allows one to observe stable pores and extract their equilibrium properties under EP conditions. The results from the simulations are then further analyzed in our subsequent paper [46], where they are compared to the predictions of a continuum model constructed based on the model system in MD simulations. As we will demonstrate, improvement of the standard models is required in order to obtain results which are consistent with the molecular modeling.

We extensively described the two common methods that allow the modeling of a TM voltage (trigger of EP) in MD.

For the nsPEF protocol [14,47-50] see 4.2.2.1. It was demonstrated, however, that in simulations with an external electric field, the pores keep expanding in their size while the

field is maintained above the EP threshold, indicating their instability [51]. Stabilization can be reached by lowering the intensity of the external electric field [52,53], but an arbitrary control of the field intensity hardly corresponds to a clear experiment.

The μs-msPEF protocol (see 4.2.2.2) either considering two solution baths separated by two bilayers [54-56] (the double bilayer scheme) or by a bilayer and a vacuum slab [57] (the single bilayer scheme). Unlike the external electric field method, which rather mimics an experiment using high intensity nanosecond pulses [57,58], the charge imbalance method corresponds to the traditional EP setup where low microsecond/millisecond pulses are applied.

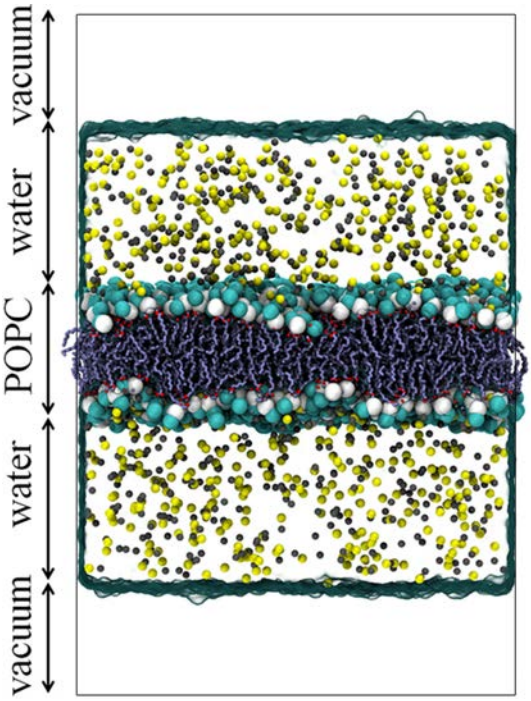

Figure 4.19: The single bilayer scheme used in this study: two solution baths are separated by a lipid bilayer (POPC) and a vacuum slab, which prevent an exchange of ions and, hence, collapse of the charge imbalance. The POPC headgroups are shown as cyan and white beads, the tails are shown as iceblue sticks; sodium and chloride ions are colored in yellow and gray; water is transparent

The charge imbalance protocols used so far in simulations to model EP, suffers from two important shortcomings. First, the charge imbalance is not re-set during the simulation. Thus, in studies with the double [55,56] and single bilayer [57,58] schemes, after the EP occurs, the imposed charge imbalance at the beginning decreases significantly within several tens/hundreds ps (depending on the system size) due to an exchange of ions through the pores in the bilayer. The decrease of the charge imbalance results in a TM voltage drop, which may ultimately leads to the pore collapse or resealing. A procedure to maintain the charge imbalance at a constant level was recently proposed by Kutzner et al.[59] to study the transport in ion channels. In this procedure, named "swapping", the number of ions in the two solution baths is frequently estimated and if the latter differs from the initial setup,

a "swapping" event takes place: an ion of one solution is exchanged by a water molecule of the other solution bath.

The second shortcoming of the charge imbalance method as used so far in MD simulations concerns the membrane lateral expansion: the latter can hardly be controlled in the double bilayer scheme due to the fact that only one bilayer undergoes EP, and is prohibited in the single bilayer scheme because in this case the simulations are carried out at a constant volume. As a result, the pores are not allowed to relax to their equilibrium conformation and the quantitative estimation of their properties (e.g. size, current, selectivity to different ionic species, etc.) becomes unreliable.

In this work, we present a protocol that deals with both shortcomings of the charge imbalance method discussed so far. In particular, we used the "swapping" procedure [59] to maintain the charge imbalance at a constant level. Here, instead of considering the system with two bilayers, as used by Kutzner et al., we adapted the procedure for the single bilayer scheme (see Fig. 4.19). In order to overcome the second shortcoming, which concerns the membrane lateral expansion, we used an assumption that in 'experimental' macroscopic systems (cells, liposomes or planar lipid bilayers) the formation of pores does not lead to any dramatic change in the membrane surface tension due to its dissipation. Hence we performed our simulations at a constant null surface tension. Using this protocol, we were able to model for the first time the EP process in conditions comparable with experiments. We show that in contrast to previous simulations [60-62], the pores relax to a stable conformation, which allow the estimation of their average size, ionic current and selectivity.

4.3.2 Systems and methods

4.3.2.1 System preparation

Two systems with a hydrated Palmitoyl-Oleoyl-PhosphatidylCholine (POPC) bilayer were considered: a small one, composed by 256 POPC molecules (POPC-256), with a total size of 8.9 x 8.9 x 19 nm^3, and a big one, composed by 1024 POPC molecules (POPC-1024), with a total size of 17.8 x 17.8 x 19 nm^3. In both systems, the bilayers were surrounded by 1 M NaCl solution. The CHARMM36 force field [63] was used for POPC, and the TIP3P model was considered for water [64].

4.3.2.2 Parameters of MD

The MD simulations were performed using Gromacs 4.6. [65]. The equations of motion were integrated using the leap-frog algorithm, with a time step of 2.0 fs. The long-range electrostatic was calculated using Particle Mesh Ewald (PME). The cut-off distance of the short-range electrostatic was taken to be 1.2 nm. A switching function was used between 0.8 and 1.2 nm to smoothly bring the van der Waals forces and energies to 0 at 1.2 nm. Dur-

ing the simulations, chemical bonds between hydrogen and heavy atoms were constrained to their equilibrium values using LINCS. Periodic boundary conditions were applied in all directions.

4.3.2.3 Equilibration

The POPC-256 system was equilibrated during 100 ns in the NPT ensemble: pressure and temperature of the system were kept constant at 1 atm (using the Parrinello-Rahman barostat) and 300 K (using the Nose-Hoover thermostat), respectively. Note that at the temperature set for the study, the POPC bilayer is in its biologically relevant liquid crystal L_α phase. To verify the convergence of the equilibration we estimated the area per lipid along the run. The latter rapidly reached the plateau of ~61.8 Å^2, which is in agreement with the previously reported data for bare POPC bilayers [66].

The big system (POPC-1024) was further constructed by replicating the equilibrated POPC-256 in the bilayer plane. The POPC-1024 was additionally equilibrated during 20 ns.

4.3.2.4 Estimation of the total surface tension

During the equilibration, the total surface tension (γ/mN/m) in the system was zero since the lateral and the normal pressure to the solution/bilayer interface are set equal as in the NPT ensemble. However, in our further simulations we considered the scheme with a vacuum slab [57,58], which introduces an additional solution/vacuum interface with a non-zero surface tension. In the system with a vacuum slab, the total surface tension (γ_{tot}/mN/m) is the sum of the surface tension at the solution/bilayer ($\gamma_{bilayer/sol}$/mN/m) and solution/vacuum interfaces ($\gamma_{vacuum/sol}$/mN/m): $\gamma_{tot} = 2\gamma_{vacuum/sol} + \gamma_{bilayer/sol}$. Since the area per lipid was kept constant when switching to the NVT ensemble, the lateral pressure on the lipid bilayer stays at zero. Thus, considering that$\gamma_{bilayer/sol}$ ~0 mN/m, the total surface tension is double the surface tension at the vacuum/solution interface: $\gamma_{tot} = 2\gamma_{vacuum/sol}$. In order to estimate the total surface tension, arising from the solution/vacuum interfaces we fixed its volume and performed short MD simulations (10 ns). Based on the obtained trajectories, a surface tension of ~100 mN/m was obtained from the lateral (P_l/bar) and the normal pressure to the solution/bilayer interface (P_t/bar) as: $\gamma = \int [P_l - P_t] dz$, i.e. the surface tension at each of the two vacuum/solution interfaces was ~50 mN/m, in agreement with the experimental measurements and modeling [67,68].

4.3.2.5 Transmembrane (TM) potential

The electrostatic potential U_z/V along the normal to the bilayer can be calculated by solving Poisson's equation 4.5, i.e. derived as double integral of ρ_z/(C/m^3), the volume

charge density distribution, being ϵ_0/(F/m) the vacuum permittivity:

$$U_z = U(z) - U_0 = -\frac{1}{\epsilon_0} \int \int_0^z \rho_z(z'') dz'' dz'. \tag{4.5}$$

As reference, U_0 was set to zero in the lower bulk solution. Practically, we calculated the electrostatic potential by dividing the system into 0.1 nm slices along Z-axis, summing the charges in each slice and integrating the resulting charge distribution for 10,000 configurations spread out over 20 ns time-windows. The TM voltage U_m/V was calculated as the difference between the electrostatic potential measured at the lower and the upper baths.

4.3.2.6 Swapping protocol

In order to maintain the applied charge imbalance ΔQ/C at a constant value, we used the "swapping" protocol [59] implemented in GROMACS. Briefly, the protocol works the following way: the program estimates the number of ions in the two solution baths and if this number differs from the initial setup, an ion of one solution bath is exchanged by a water molecule of the other solution bath. Here, we adapted the "swapping" protocol for the single bilayer scheme considering the Z-planes separating the two solution baths as the Z-coordinates of the water molecule center of mass placed in vacuum, and of the center of mass of the bilayer. The centers of mass of both groups were restrained during the simulations.

4.3.2.7 Production runs

The production runs of 100 ns each were performed in the NPγT ensemble (constant surface tension) using the single-bilayer scheme [57,58] and the "swapping" protocol [59]. In order to keep the total surface tension of the membrane/water at zero, we considered 100 mN/m as a reference value for the total surface tension γtot (see 4.3.2.4-*Estimation of the total surface tension*). To avoid the collapse of the vacuum slab we changed the compressibility of the system in the Z-direction (perpendicular to the bilayer) to zero, using the Berendsen barostat.

For the POPC-256 and POPC-1024 the following ΔQ/C were applied: $0q_e$, $12q_e$ and $14q_e$, and $0q_e$, $20q_e$, $32q_e$, $40q_e$, $48q_e$ and 56qe respectively (q_e/C is the elementary charge). Notice that the $48q_e$ ΔQ was considered only in our subsequent paper [46] to increase the statistic needed for a more detailed analysis of the pore conductance, carried out over time windows of 20 ns each. In fact, when the ΔQ is too high the bilayer shows a less stable behavior in time in terms of membrane area. This is probably due to the osmotic pressure imposed by the water flow (see 4.3.3.1-*Pore characteristics*) that results in unequal volumes of water in the two baths of the bilayer as well as in a corresponding increase in the ionic concentration where the water volume is reduced. Therefore, like in the case of $48q_e$, if

such not predictable behavior was observed before 80 ns, the simulation was rejected. The $56q_e$ run exhibits this behavior after 80 ns, which allowed us to carry out the analysis until that.

4.3.2.8 Analysis of the pore

Based on the obtained trajectories, the minimum pore radius (R/nm), ionic current (I/nA), conductance (G/nS) and selectivity (S) were analyzed. The pore radius was estimated using HOLE [69] at each 250 ps; the ionic current was evaluated as the slope of the ionic flux at each 0.2 ps; and the conductance was estimated as the ratio between the average ionic current and the TM potential applied. In order to verify the convergence, the cumulative values of the pore radius and ionic current were calculated along the MD runs. The simulations were assumed to converge when the cumulative values reached their plateau values. Accordingly, the average values and their standard deviations were estimated for the plateau regions. The bilayer density (d/a.u.), thickness (t_m/nm) and an average molecular order parameters (P_{CH}) were extracted using the protocol suggested by Castillo et al. [70].

4.3.3 Results and Discussions

Experimentally, when macroscopic systems are exposed to an electric pulse causing EP, the formation of the pores does not lead to dramatic changes in the membrane surface tension, as it is re-distributed along the entire membrane surface. Hence, if one wishes to model the EP process in conditions comparable with the experimental ones, the membrane surface tension should be kept constant (and null). In the single bilayer charge imbalance scheme that we considered in this work, the total surface tension is the sum of the surface tension at the bilayer/solution and the surface tension at the solution/vacuum interfaces ((see 4.3.2.4-*Estimation of the total surface tension*). While the total surface tension is constant when the bilayer is intact, it rises abruptly after the pore formation occurs [14,71]. To avoid such unrealistic increase, we estimated the total surface tension during the equilibration step (no charge imbalance) and used this value to maintain the surface tension constant when the system was exposed to the charge imbalance (see 4.3.2.4-*Estimation of the total surface tension*). In order to prevent the collapse of the vacuum slab, we maintained the compressibility of the system in the Z-direction (perpendicular to the bilayer) to zero (see 4.3.2.7-*Production runs*). Finally, the simulations were performed using the "swapping" procedure proposed by Kutzner et al. [59] which allows to maintain the charge imbalance constant (see 4.3.2.6-*Swapping protocol*).

The protocol that combines the constant surface tension and constant charge imbalance was applied to the big system with 1024 POPC molecules (POPC-1024, see 4.3.2.1-*Systems preparation*). Four different ΔQ were considered ($20q_e$, $32q_e$, $40q_e$, $56q_e$), corre-

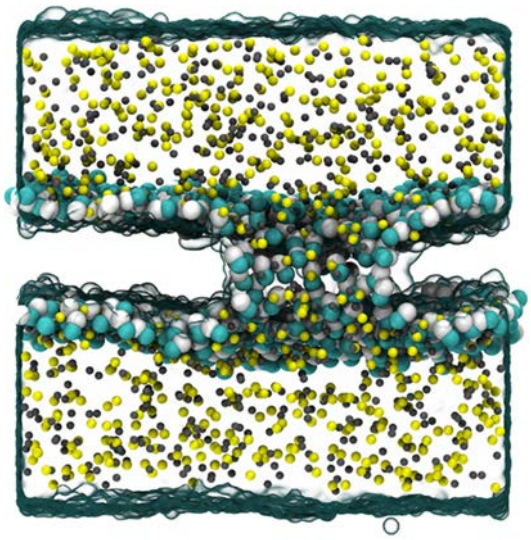

Figure 4.20: Cross section of an electroporated POPC-1024 bilayer. The POPC headgroups are shown as cyan and white beads, the tails are transparent; sodium and chloride ions are colored in yellow and gray; water is transparent

sponding to the TM voltages Um of ∼ 420, 510, 520 and 630 mV, respectively (note that the TM voltages were estimated after the bilayer electroporation, Fig. 4.20).

4.3.3.1 Pore characteristics

Fig. 4.21 reports the cumulative average of the pore radius along the MD run and the average pore profile estimated for the four charge imbalances. The cumulative pore radii (Fig. 4.21A) reach a plateau after 20 ns indicating that the pores are stable and that the corresponding simulations have converged. For each MD run, the average pore radius and the standard deviation were further estimated for the remaining part of the trajectory: from 20 to 80 ns. The average pore radius (Fig. 4.21B), ranging from 1 to 2.5 nm, was shown to be dependent on the charge imbalance applied to the system, thereby being dependent also on the TM voltage; the dependence of the average pore radius on the TM voltage is approximately linear in the investigated range.

Our observation of stable pores at moderate TM voltages is in general agreement with theoretical predictions [6,72-74]. The theory of EP namely predicts that once the energetic barrier for pore formation is overcome, the formed hydrophilic pore will stabilize at certain radius which corresponds to the local minimum in the pore free energy landscape. The position of this minimum with respect to the pore radius is also expected to shift with increasing TM voltage, resulting in larger stable pores. If the TM voltage exceeds a certain value, however, the minimum is expected to disappear leading to irreversible expansion of the pore and ultimate rupture of the bilayer provided that the TM voltage remains constant. We interpret our results as being in the range of TM voltages which allow pores to remain

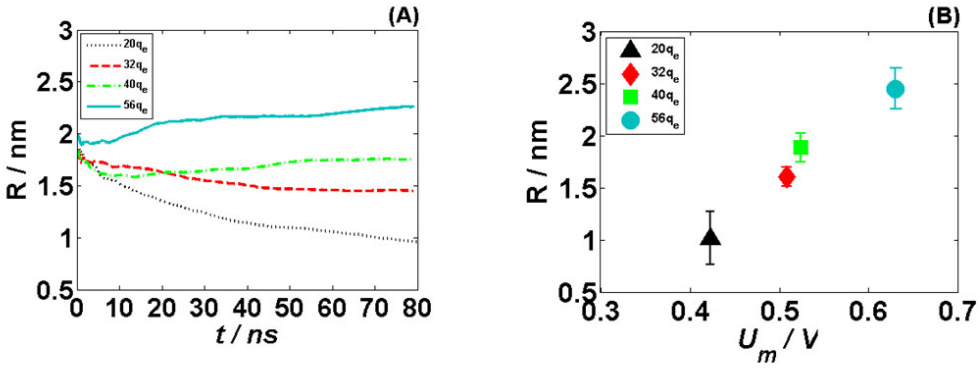

Figure 4.21: (A) Cumulative minimum pore radius R/nm along the elapsed time t/ns, corresponding to the charge imbalances ΔQ/C of $20q_e$ (black dotted line), $32q_e$ (red dashed line), $40q_e$ (green dot-dashed line) and $56q_e$ (cyan solid); (B) Minimum pore radius R/nm versus the TM voltage U_m established at charge imbalances ΔQ/C of $20q_e$ (black triangle), $32q_e$ (red diamond), $40q_e$ (green square) and $56q_e$ (cyan circle)

stable, at least in the time window considered.

The ionic current through the pore was estimated as the slope of the ionic flux. In Fig. 4.22A we report the cumulative average of the ionic current for the four charge imbalances over time. As expected, the currents grow to reach a plateau after less than 10 ns until the end of the runs, which proves the convergence of this observable. The stable currents range from 2.69 to 18.58 nA, when the TM voltages from 420 to 630 mV are maintained.

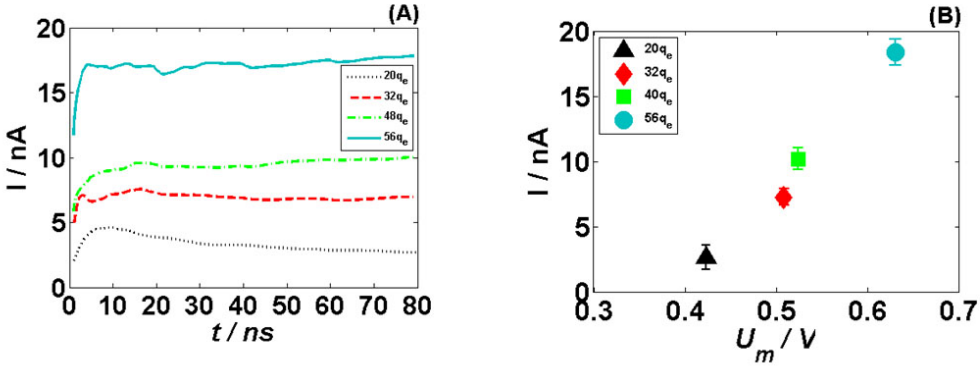

Figure 4.22: (A) Cumulative average of the ionic current I/nA along the elapsed time t/ns, corresponding to the charge imbalances ΔQ/C of $20q_e$ (black dotted line), $32q_e$ (red dashed line), $40q_e$ (green dot-dashed line) and $56q_e$ (cyan solid line); (B) Current/voltage relationship for the charge imbalances ΔQ/C of $20q_e$ (black triangle), $32q_e$ (red diamond), $40q_e$ (green square) and $56q_e$ (cyan circle)

The current/voltage relationship of Fig. 4.22B shows that as the TM voltage applied is increased, the current flowing through the single electropore rises approximately linearly. Note that with increasing TM voltage the pore radius also increases. Since pores with larger size allow the passage of a higher number of ions, the increase in the current is both due

to the increase in the TM voltage by directly increasing the electrophoretic drift of ions, as well as the increase in the pore size.

The conductance (G/nS) of the pore was calculated as the ratio of ionic current (I/nA) and TM voltage (U_m/V); the results are presented in Fig. 4.23A. We reported G as a function of the pore radius (R/nm) to facilitate the correlation of our results with the experimental ones, where the radius is indirectly deduced from the conductance measured. In the range of TM potentials investigated, the conductance changes almost linearly with the pore radius (for further analyses and discussions on the relationship between the pore conductance, pore shape, and pore radius we refer the reader to our subsequent paper [46]).

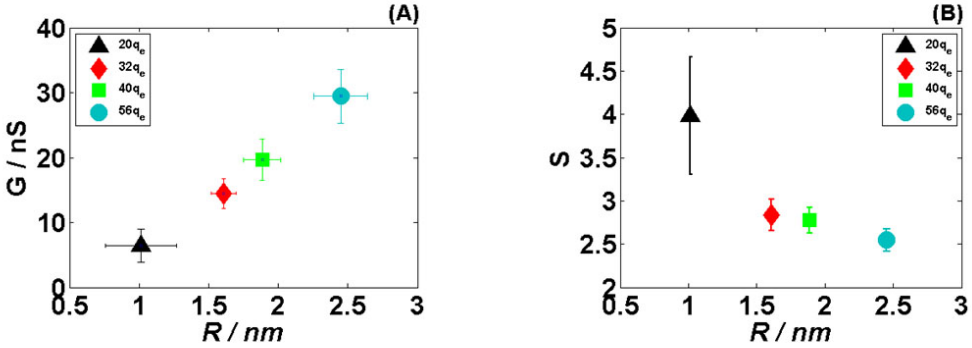

Figure 4.23: Ionic conductance G/nS (A) and ionic selectivity S (B) as a function of the minimum pore radius R/nm, corresponding to the charge imbalances ΔQ/C of $20q_e$ (black triangle), $32q_e$ (red diamond), $40q_e$ (green square) and $56q_e$ (cyan circle)

Finally, we estimated the pore selectivity (S) as the ratio of anionic (I^-_{Cl}/nA) to cationic (I^-_{Na}/nA) current, Fig. 4.23B. In agreement with the previous findings [53], the pore was shown to be more selective to chloride ions than to sodium ions. This selectivity arises from the nature of the lipid molecules constituting the pore: the negatively charged phosphate groups that form the walls of the pore attract sodium ions, which hinders their passage across the bilayer, but also makes the pore interior electrostatically unfavorable for other sodium ions. Consequently, as we show in Fig. 4.23B, the ratio of Cl and Na current decreases as the pore expands. Indeed, the pore expansion results in a higher fraction of those sodium ions that pass the pore without any hindrance as they do not interact with the pore walls. According to the analysis we performed in our subsequent paper [46], the pore selectivity to Cl ions can partially arises also due to electroosmotic flux of water through the pore, which enhances the current of Cl ions and at the same time reduces the current of Na ions.

Indeed, in all performed simulations, we observed a net flux of water in the direction of the flux of Cl ions (i.e., opposite to the direction of the electric potential gradient), which can be attributed to the interactions of water with electrophoretically driven charged ions. The water flux gradually reduces the volume of water on one side of the bilayer and increases the volume of water on the other side. The changes in water volume limit the time

range for which the simulations can be performed (∼100 ns) in the absence of excessive osmotic pressure, which can lead to instability of the simulated system.

4.3.3.2 Simulation cell and size effects

System	U_m/V	R/nm	G/nS
POPC-1024	0.42±0.04	1.0±0.3	6.4±2.5
	0.52±0.05	1.9±0.2	19.6±3.2
POPC-256	0.46±0.06	0.6±0.1	2.3±0.2
	0.54±0.10	0.7±0.2	2.8±1.2

Table 4.5: Pore radius R/nm and conductance G/nS estimated at a specific TM voltages U_m/V
U_m - transmembrane voltage resulting by the charge imbalance
R - minimum pore radius maintained by a given Um_m
G - conductance of the elctropore for the corresponding radius

In MD simulations, the EP of bilayers is commonly studied on relatively small systems composed of 256, 128 and in some cases of 64 lipids. Accordingly, we compared our data discussed so far with a smaller system, containing 256 POPC molecules instead of 1024 (POPC-256, see 4.3.2.1-*Systems preparation*); the results of the comparison are presented in Table 4.5. We found that at similar TM voltages the pore radius in the POPC-256 bilayer is almost twice lower than that in the POPC-1024 bilayer, which results as well in different values of conductance. We hypothesize that the observed inconsistency of the results stems from the size effect. Indeed, once a pore is formed in the POPC-256, the size of the simulation box prevents its adequate expansion, i.e. the bilayer patch is not large enough to allow for the release of tension induced by the pore spanning which consequently induces a constraint on the pore size.

In order to test this hypothesis, we analyzed the density, thickness and order parameters of the electroporated POPC-1024 and POPC-256 bilayers (Fig. 6). The lipid order parameter, defined as $P_{CH} = \frac{1}{2} < 3\cos^2\theta - 1 >$, where θ is the angle between the C-H bond vector and the membrane normal, was calculated for all carbons in the lipid acyl chains and then averaged within each voxel over the ensemble of lipids and over the simulation (see 4.3.2.8-*Analysis of the pore*).

The presence of the pore locally changes the bilayer properties; the headgroups surrounding the pore slide along the water column to stabilize it, resulting in a toroidal shape, and causing: a decrease in the order parameter; a local drop in the lipid density, and in the bilayer thickness. Fig. 4.24A and E show clearly that for the small system, the pore is too large with respect to the cell size. The area affected by the pore (where we register a decrease in the value of the properties mentioned above) almost reaches the patch borders, which probably influences through the periodic boundary condition its own stability

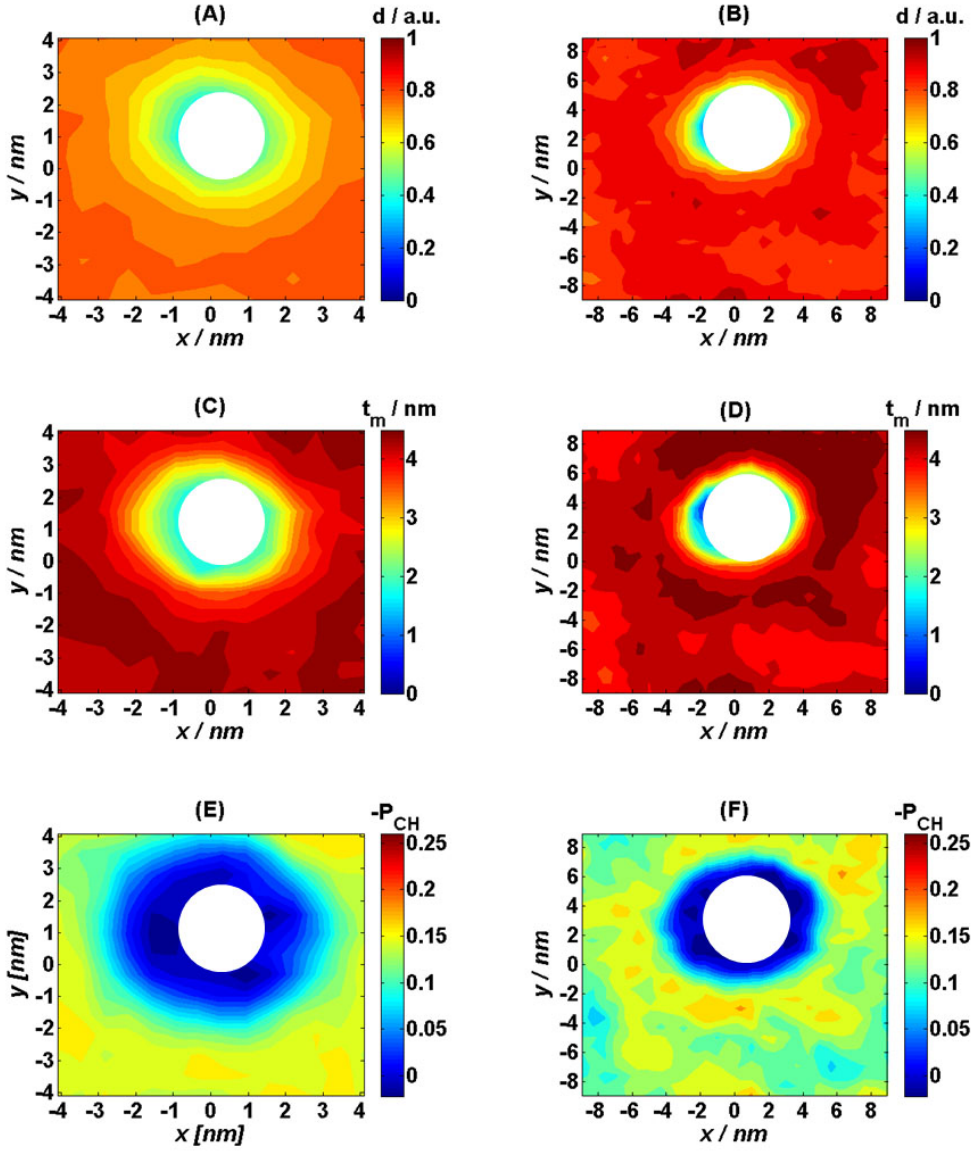

Figure 4.24: 2D spatial maps of the density d/a.u (A and B), thickness t_m/nm (C and D) and order parameter P_{CH} (E and F) estimated for the POPC-256 (A, C, E) and POPC-1024 (B, D, F) bilayers subject to ∼500 mV

and expansion. On the contrary, in the POPC-1024 the values of the density (d/a.u.) and the average molecular order parameter (P_{CH}) (Fig. 4.24B and F respectively) recover when moving away from the water defect.

4.3.3.3 Comparison with the nsPEF protocol

As mentioned in the introduction (4.3.1) there is uncertainty in the determination of the size and the conductance of electropores with the today experimental techniques, both when the effects of nsPEFs and μs-msPEFs are investigate. For instance, it is believed that nsPEFs produce a considerable number of small (∼1 nm radius) electropores and that multiple nanosecond electric pulses increase the number but not the size of long-lived nanopores in the cell membrane [35].

So far we discussed about MD conditions mimicking μs-msPEFs (see 4.3.2). It is, therefore, interesting to compare these results with the MD protocol modeling the response of bilayers to nsPEFs (see 4.2.2-*nsPEF protocol*).

When dealing with the characteristics of electropores one would expect the pore to be in this energetically favorable state, that could correspond to a stable configuration. In the present work we developed a scheme to maintain a certain charge imbalance constant refining the μs-msPEFs approach to produce stable and size-controlled pores. To compare the results (e.i. size, conductance, selectivity) obtained and previously described with the one following the direct application of an exogenous electric field E_{app} (see 4.2.2-*nsPEF protocol*), one must overcome the main drawback of nsPEF protocol which resides in the impossibility of maintaining a steady pore that tends to expand above the dimension of the simulation cell box leading in the brake down of the bilayer when the E_{app} is above a certain threshold.

To enhance the nsPEF approach, Fernández et al. [75] proposed a new simulation procedure where an initially high porating field is reduced after pore creation to lower stabilizing values resulting in stable, size-controlled electropores.

We conducted a systematic investigation [53], following the latter method. Despite a detailed discussion of these results is not within the purpose of the present thesis, we will briefly compare the two MD approaches.

The two methods, indeed, brought to the same conclusion that under constant TM voltages below threshold the pore formed could be stabilized to different radii for tens of ns. The value of the radius obtained at a given sustaining voltage was shown to be independent from the porating one [75]. Moreover, in both cases, for a "high" voltages applied the pore eventually expand leading to instability of the bilayer while for "low" voltages pore closure is observed. Notice that the values of the TM voltages are purely indicative since they are system dependent, and the pore life time and structural characteristics are strictly related

to the composition of the bilayer.

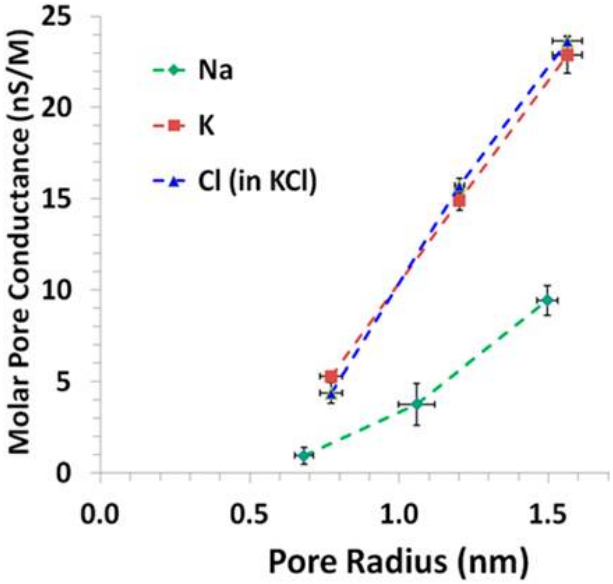

Figure 4.25: Ion conductance versus pore radius. Conductances of K^+ and Cl^- were obtained from the same sets of simulations [53]

Quite interestingly the relation between the voltage applied and the pore dimension and therefore between the radius and the conductance is almost linear: in [53] (pure POPC bilayer in a salt solution of 0.1 M NaCl) for a voltage ranging from 0.56 to 1.12 V the pore radius is 0.68-1.50 nm and the conductance 5.48-27.88 nS/M (Fig. 4.25); while here (pure POPC bilayer in a salt solution of 0.9 M NaCl) when the voltage spans from 0.42 to 0.63 V, the pore radius is 1.01-2.45 nm and its conductance 7.11-32.77 nS/M.

For a more comprehensive discussion about the dependency of these three variables we refer to [46].

Nevertheless, the discrepancy arising from these two works can be easily justified by a finite size effect of the simulation box. Indeed, in (4.3.2-*Simulation cell and size effects*) we compared the pore radius for a similar TM voltage of two bilayers composed by 256 and 1024 units of POPC and we showed how the pore radius almost double in the latter scheme. This is because the area affected by the pore in the 256 units patch almost reaches the cell borders, which affects through the PBCs its own relaxation and expansion.

The pore was found to be selective to different ion species both when nsPEFs [53] and μs-msPEFs (see 4.3.3-*Pore characteristics*). In particular, small positively charge ions, e.g. Na^+, bound more the strongly to the phospholipids interface than K^+ or Cl^-, with restrained Na^+ located deep at the acyl oxygens of the glycerol backbone, resulting in lower values of current for smaller pore radii. This suggests that the pore transport, under the two conditions, is sensitive to the type of solutes, showing a different affinity for different charged species.

4.3.4 Conclusions

Here we introduced a new protocol that enables for the first time to perform MD simulations of electroporated bilayer under conditions similar to those of experiments using low intensity, long (μs-ms) pulses. This is perceived as the most appropriate approach to directly determine the transport of ions and selected molecules across bilayers exposed to electric pulses, which remains a challenge for experimental methods. We proposed the use of an ensemble that allows the membrane surface tension γ_{tot} to be constant, avoiding unrealistic constrains. Then, the establishment of a constant voltage comparable with experimental exposures was guaranteed by the swap procedure. Both these conditions permit the formation of relaxed stable pores that can be characterized geometrically and electrically. The cumulative average of the pore radius and that of the ionic current confirm indeed the convergence of these observables after 20 ns of simulation run.

We found that for TM voltages ranging from 420 mV to 630 mV, the pore radius increases from 1 to 2.5 nm and the conductance from 6.4 to 29.5 nS. Quite interestingly, when the same TM voltage was maintained on the lipid patch of the sizes usually employed in MD simulations (8.8 x 8.8 nm^2, 256 lipids) the pore radius obtained was twice smaller and the conductance almost three times smaller than what we reported for the large system (17.8 x 17.8 nm^2, 1024 lipids), likely a consequence of the constrains imposed by the finite size of the simulation box.

A qualitative comparison between the characteristics of electropores generated *in silico* by μs-msPEFs and nsPEFs lead to the conclusion that, under roughly the same TM voltage, similar values of radius (some nm) and conductance (tens of nS) are obtained. Despite a more detailed and systematic study should be carried out to quantitatively confront the two schemes, one can say that from MD simulations, no matter the type of electric pulse applied, the characteristic of the pore will be similar when the membrane undergoes the same TM voltage.

Simulations along these lines should contribute to a better understanding of phenomenon of electroporation. Two further applications can be considered. First, investigating the EP of more complex membranes, and second investigating the transport of large molecules, e.g. drugs and genetic material to shed light on the uptake mechanisms.

To provide a further insight to the EP process these results need also to be linked with experimental observations. Since the direct comparison is challenging, as stated in the introduction, an intermediate and complementary step could be the use of continuum models. In a following paper, we therefore constructed a numerical model of pore conductance based on the Poisson-Nernst-Planck theory, and found a surprisingly exquisite agreement between the two approaches.

4.3.5 References

[1] E. Neumann, A.E. Sowers, C.A. Jordan, Electroporation and Electrofusion in Cell Biology, Springer Science & Business Media, 1989.

[2] J.A. Nickoloff, Animal Cell Electroporation and Electrofusion Protocols, Humana Press,NJ, 1995.

[3] S. Li, Electroporation Protocols: Preclinical and Clinical Gene Medicine, Humana press: Totowa, NJ., 2008.

[4] I.G. Abidor, V.B. Arakelyan, L.V. Chernomordik, Y.A. Chizmadzhev, V.F. Pastushenko, M.P. Tarasevich, Electric breakdown of bilayer lipid membranes: I. The main experimental facts and their qualitative discussion, J. Electroanal. Chem. Interfacial Electrochem. 104 (1979) 37-52.

[5] R. Benz, F. Beckers, U. Zimmermann, Reversible electrical breakdown of lipid bilayer membranes: A charge-pulse relaxation study, J. Membr. Biol. 48 (1979) 181-204.

[6] J.C. Weaver, Y.A. Chizmadzhev, Theory of electroporation: A review, Bioelectrochem. Bioenerg. 41 (1996) 135-160.

[7] J.C. Weaver, Electroporation of biological membranes from multicellular to nano scales, IEEE Trans. Dielectr. Electr. Insul. 10 (2003) 754-768.

[8] C. Chen, S.W. Smye, M.P. Robinson, J.A. Evans, Membrane electroporation theories: a review, Med. Biol. Eng. Comput. 44 (2006) 5-14.

[9] G. Pucihar, T. Kotnik, D. Miklavčič, J. Teissié, Kinetics of transmembrane transport of small molecules into electropermeabilized cells, Biophys. J. 95 (2008) 2837-2848.

[10] M. Hibino, M. Shigemori, H. Itoh, K. Nagayama, K. Kinosita, Membrane conductance of an electroporated cell analyzed by submicrosecond imaging of transmembrane potential., Biophys. J. 59 (1991) 209-220.

[11] M. Breton, L. Delemotte, A. Silve, L.M. Mir, M. Tarek, Transport of siRNA through Lipid Membranes Driven by Nanosecond Electric Pulses: An Experimental and Computational Study, J. Am. Chem. Soc. 134 (2012) 13938-13941.

[12] L.M. Mir, H. Banoun, C. Paoletti, Introduction of definite amounts of nonpermeant molecules into living cells after electropermeabilization: direct access to the cytosol, Exp. Cell Res. 175 (1988) 15-25.

[13] J. Teissié, N. Eynard, B. Gabriel, M.P. Rols, Electropermeabilization of cell membranes, Adv. Drug Deliv. Rev. 35 (1999) 3-19.

[14] M. Tarek, Membrane Electroporation: A Molecular Dynamics Simulation, Biophys.

J. 88 (2005) 4045-4053.

[15] T. Kotnik, G. Pucihar, D. Miklavčič, Induced Transmembrane Voltage and Its Correlation with Electroporation-Mediated Molecular Transport, J. Membr. Biol. 236 (2010) 3-13.

[16] M. Szabo, M.I. Wallace, Imaging potassium-flux through individual electropores in droplet interface bilayers, Biochim. Biophys. Acta. (2015).

[17] T. Kotnik, P. Kramar, G. Pucihar, D. Miklavčič, M. Tarek, Cell membrane electroporation-Part 1: The phenomenon, IEEE Electr. Insul. Mag. 28 (2012) 14-23.

[18] S. Lakshmanan, G.K. Gupta, P. Avci, R. Chandran, M. Sadasivam, A.E.S. Jorge, et al., Physical energy for drug delivery; poration, concentration and activation, Adv. Drug Deliv. Rev. 71 (2014) 98-114.

[19] J. Villemejane, L.M. Mir, Physical methods of nucleic acid transfer: general concepts and applications, Br. J. Pharmacol. 157 (2009) 207-219.

[20] J. Teissie, Electrically Mediated Gene Delivery: Basic and Translational Concepts., INTECH Open Access Publisher, 2013.

[21] M. Breton, L.M. Mir, Microsecond and nanosecond electric pulses in cancer treatments, Bioelectromagnetics. 33 (2012) 106-123.

[22] M.L. Yarmush, A. Golberg, G. Serša, T. Kotnik, D. Miklavčič, Electroporation-Based Technologies for Medicine: Principles, Applications, and Challenges - Annual Review of Biomedical Engineering, 16(1):295.

[23] R. Cadossi, M. Ronchetti, M. Cadossi, Locally enhanced chemotherapy by electroporation: clinical experiences and perspective of use of electrochemotherapy, Future Oncol. 10 (2014) 877-890.

[24] D. Miklavčič, B. Mali, B. Kos, R. Heller, G. Serša, Electrochemotherapy: from the drawing board into medical practice, Biomed. Eng. OnLine. 13 (2014) 29.

[25] S. Kalinowski, G. Ibron, K. Bryl, Z. Figaszewski, Chronopotentiometric studies of electroporation of bilayer lipid membranes, Biochim. Biophys. Acta BBA - Biomembr. 1369 (1998) 204-212.

[26] S. Koronkiewicz, S. Kalinowski, K. Bryl, Programmable chronopotentiometry as a tool for the study of electroporation and resealing of pores in bilayer lipid membranes, Biochim. Biophys. Acta. 1561 (2002) 222-229.

[27] S. Koronkiewicz, S. Kalinowski, Influence of cholesterol on electroporation of bilayer lipid membranes: chronopotentiometric studies, Biochim. Biophys. Acta BBA - Biomembr. 1661 (2004) 196-203.

[28] M. Pavlin, M. Kandušer, M. Rebersek, G. Pucihar, F.X. Hart, R. Magjareviccacute;, et al., Effect of Cell Electroporation on the Conductivity of a Cell Suspension, Biophys. J. 88 (2005) 4378-4390.

[29] M. Kotulska, Natural Fluctuations of an Electropore Show Fractional Lévy Stable Motion, Biophys. J. 92 (2007) 2412-2421.

[30] H. Krassen, U. Pliquett, E. Neumann, Nonlinear current-voltage relationship of the plasma membrane of single CHO cells, Bioelectrochemistry. 70 (2007) 71-77.

[31] P. Kramar, L. Delemotte, A.M. Lebar, M. Kotulska, M. Tarek, D. Miklavčič, Molecular-Level Characterization of Lipid Membrane Electroporation using Linearly Rising Current, J. Membr. Biol. 245 (2012) 651-659.

[32] A.M. Bowman, O.M. Nesin, O.N. Pakhomova, A.G. Pakhomov, Analysis of plasma membrane integrity by fluorescent detection of Tl(+) uptake, J. Membr. Biol. 236 (2010) 15-26.

[33] O.M. Nesin, O.N. Pakhomova, S. Xiao, A.G. Pakhomov, Manipulation of cell volume and membrane pore comparison following single cell permeabilization with 60- and 600-ns electric pulses, Biochim. Biophys. Acta. 1808 (2011) 792-801.

[34] A. Silve, I. Leray, L.M. Mir, Demonstration of cell membrane permeabilization to medium-sized molecules caused by a single 10 ns electric pulse, Bioelectrochemistry. 87 (2012) 260-264.

[35] A.G. Pakhomov, E. Gianulis, P.T. Vernier, I. Semenov, S. Xiao, O.N. Pakhomova, Multiple nanosecond electric pulses increase the number but not the size of long-lived nanopores in the cell membrane, Biochim. Biophys. Acta. 1848 (2015) 958-966.

[36] J. Deng, K.H. Schoenbach, E. Stephen Buescher, P.S. Hair, P.M. Fox, S.J. Beebe, The Effects of Intense Submicrosecond Electrical Pulses on Cells, Biophys. J. 84 (2003) 2709-2714.

[37] P.T. Vernier, Y. Sun, L. Marcu, S. Salemi, C.M. Craft, M.A. Gundersen, Calcium bursts induced by nanosecond electric pulses, Biochem. Biophys. Res. Commun. 310 (2003) 286-295.

[38] P.T. Vernier, Y. Sun, M.A. Gundersen, Nanoelectropulse-driven membrane perturbation and small molecule permeabilization, BMC Cell Biol. 7 (2006) 37.

[39] F. Salomone, M. Breton, I. Leray, F. Cardarelli, C. Boccardi, D. Bonhenry, et al., High-Yield Nontoxic Gene Transfer through Conjugation of the CM_{18}-Tat_{11} Chimeric Peptide with Nanosecond Electric Pulses, Mol. Pharm. 11 (2014) 2466-2474.

[40] J. Kapla, J. Wohlert, B. Stevensson, O. Engström, G. Widmalm, A. Maliniak, Molecular dynamics simulations of membrane-sugar interactions, J. Phys. Chem. B. 117 (2013)

6667-6673.

[41] A. Barnett, The current-voltage relation of an aqueous pore in a lipid bilayer membrane, Biochim. Biophys. Acta BBA - Biomembr. 1025 (1990) 10-14.

[42] S. Kakorin, E. Neumann, Ionic conductivity of electroporated lipid bilayer membranes, Bioelectrochemistry Amst. Neth. 56 (2002) 163-166.

[43] J. Li, H. Lin, The current-voltage relation for electropores with conductivity gradients, Biomicrofluidics. 4 (2010).

[44] G. Moy, B. Corry, S. Kuyucak, S.-H. Chung, Tests of Continuum Theories as Models of Ion Channels. I. Poisson-Boltzmann Theory versus Brownian Dynamics, Biophys. J. 78 (2000) 2349-2363.

[45] B. Corry, S. Kuyucak, S.-H. Chung, Tests of Continuum Theories as Models of Ion Channels. II. Poisson-Nernst-Planck Theory versus Brownian Dynamics, Biophys. J. 78 (2000) 2364-2381.

[46] L. Rems, M. Casciola, M. Tarek, D. Miklavčič, Properties of lipid electropores II: Comparison of continuum-level modeling of pore conductance to molecular dynamics simulations, Bioelectrochemistry Submitt. Rev.

[47] D.P. Tieleman, The molecular basis of electroporation, BMC Biochem. 5 (2004) 10.

[48] Q. Hu, S. Viswanadham, R. Joshi, K. Schoenbach, S. Beebe, P. Blackmore, Simulations of transient membrane behavior in cells subjected to a high-intensity ultrashort electric pulse, Phys. Rev. E. 71 (2005) 031914.

[49] R.A. Böckmann, B.L. de Groot, S. Kakorin, E. Neumann, H. Grubmüller, Kinetics, Statistics, and Energetics of Lipid Membrane Electroporation Studied by Molecular Dynamics Simulations, Biophys. J. 95 (2008) 1837-1850.

[50] M.J. Ziegler, P.T. Vernier, Interface Water Dynamics and Porating Electric Fields for Phospholipid Bilayers, J. Phys. Chem. B. 112 (2008) 13588-13596.

[51] Z.A. Levine, P.T. Vernier, Life cycle of an electropore: field-dependent and field-independent steps in pore creation and annihilation, J. Membr. Biol. 236 (2010) 27-36.

[52] M.L. Fernández, G. Marshall, F. Sagués, R. Reigada, Structural and Kinetic Molecular Dynamics Study of Electroporation in Cholesterol-Containing Bilayers, J. Phys. Chem. B. 114 (2010) 6855-6865.

[53] M.-C. Ho, M. Casciola, Z.A. Levine, P.T. Vernier, Molecular Dynamics Simulations of Ion Conductance in Field-Stabilized Nanoscale Lipid Electropores, J. Phys. Chem. B. 117 (2013) 11633-11640.

[54] J.N. Sachs, P.S. Crozier, T.B. Woolf, Atomistic simulations of biologically realistic transmembrane potential gradients, J. Chem. Phys. 121 (2004) 10847-10851.

[55] A.A. Gurtovenko, I. Vattulainen, Pore Formation Coupled to Ion Transport through Lipid Membranes as Induced by Transmembrane Ionic Charge Imbalance: Atomistic Molecular Dynamic Study, J. Am. Chem. Soc. 127 (2205) 17570-17571.

[56] S.K. Kandasamy, R.G. Larson, Cation and anion transport through hydrophilic pores in lipid bilayers, J. Chem. Phys. 125 (2006) 074901.

[57] L. Delemotte, F. Dehez, W. Treptow, M. Tarek, Modeling Membranes under a Transmembrane Potential, J. Phys. Chem. B. 112 (2008) 5547-5550.

[58] L. Delemotte, M. Tarek, Molecular Dynamics Simulations of Lipid Membrane Electroporation, J. Membr. Biol. 245 (2012) 531-543.

[59] C. Kutzner, H. Grubmüller, B.L. de Groot, U. Zachariae, Computational Electrophysiology: The Molecular Dynamics of Ion Channel Permeation and Selectivity in Atomistic Detail, Biophys. J. 101 (2011) 809-817.

[60] A. Polak, M. Tarek, M. Tomsic, J. Valant, N.P. Ulrih, A. Jamnik, et al., Electroporation of archaeal lipid membranes using MD simulations, Bioelectrochemistry. 100 (2014) 18-26.

[61] M. Casciola, D. Bonhenry, M. Liberti, F. Apollonio, M. Tarek, A molecular dynamic study of cholesterol rich lipid membranes: comparison of electroporation protocols, Bioelectrochemistry. 100 (2014) 11-17.

[62] F. Dehez, L. Delemotte, P. Kramar, D. Miklavčič, M. Tarek, Evidence of Conducting Hydrophobic Nanopores Across Membranes in Response to an Electric Field, J. Phys. Chem. C. 118 (2014) 6752-6757.

[63] J.B. Klauda, R.M. Venable, J.A. Freites, J.W. O'Connor, D.J. Tobias, C. Mondragon-Ramirez, et al., Update of the CHARMM all-atom additive force field for lipids: validation on six lipid types, J. Phys. Chem. B. 114 (2010) 7830-7843.

[64] W.L. Jorgensen, J. Chandrasekhar, J.D. Madura, R.W. Impey, M.L. Klein, Comparison of simple potential functions for simulating liquid water, J. Chem. Phys. 79 (1983) 926-935.

[65] B.Hess, C. Kutzner, D. van der Spoel, E. Lindhal, GROMACS 4: Algorithms for Highly Efficient, Load-Balanced, and Scalable Molecular Simulation, J. Chem. Theory Comput. 4 (2008) 435-447.

[66] N. Kucerka, S. Tristram-Nagle, J.F. Nagle, Structure of Fully Hydrated Fluid Phase Lipid Bilayers with Monounsaturated Chains, J. Membr. Biol. 208 (2006) 193-202.

[67] J.N. Israelachvili, Intermolecular and Surface Forces: Revised Third Edition, Academic Press, 2011.

[68] T.J. Lewis, A model for bilayer membrane electroporation based on resultant electromechanical stress, IEEE Trans. Dielectr. Electr. Insul. 10 (2003) 769-777.

[69] O.S. Smart, J.G. Neduvelil, X. Wang, B.A. Wallace, M.S.P. Sansom, HOLE: A program for the analysis of the pore dimensions of ion channel structural models, J. Mol. Graph. 14 (1996) 354-360.

[70] N. Castillo, L. Monticelli, J. Barnoud, D.P. Tieleman, Free energy of WALP23 dimer association in DMPC, DPPC, and DOPC bilayers, Chem. Phys. Lipids. 169 (2013) 95-105.

[71] T.V. Tolpekina, W.K. den Otter, W.J. Briels, Nucleation free energy of pore formation in an amphiphilic bilayer studied by molecular dynamics simulations, J. Chem. Phys. 121 (2004) 12060-12066.

[72] V.F. Pastushenko, Y.A. Chizmadzhev, Stabilization of conducting pores in BLM by electric current. Gen. Physiol. Biophys 1 (1982): 43-52.

[73] J.C. Neu, W. Krassowska, Asymptotic model of electroporation, Phys. Rev. E. 59 (1999) 3471-3482.

[74] K.C. Smith, R.S. Son, T.R. Gowrishankar, J.C. Weaver, Emergence of a large pore subpopulation during electroporating pulses, Bioelectrochemistry. 100 (2014) 3-10.9.

[75] M.L. Fernández, M. Risk, R. Reigada, P.T. Vernier, Size-controlled nanopores in lipid membranes with stabilizing electric fields, Biochem. Biophys. Res. Commun. 423 (2012) 325-330.

4.4 Electro-transfer of small molecules through electropores

The transport of chemical compounds across the plasma membrane into the cell is relevant for several biological and medical applications. One of the most efficient techniques to enhance this uptake is reversible electroporation (EP). Nevertheless, the detailed molecular mechanism of transport of chemical species (dyes, drugs, genetic materials,...) following the application of electric pulses is not yet fully elucidated. In the past decade molecular dynamics simulations have been conducted to model the effect of pulsed electric fields on membranes, describing several aspects of this phenomenon. Here we extend these findings to study the electrotransfer across lipid bilayers subject to microsecond pulsed electric fields (μs-msPEFs) of Tat_{11}, a small hydrophilic charged peptide, and of siRNA. We introduce an MD simulation protocol allowing us to characterize the transport of these charged species through stable pores driven by the μs-msPEFs, Unexpectedly, our results show that for an electroporated bilayer subject to transmembrane voltages in the order of 500 mV, i.e. consistent with experimental conditions, both Tat_{11} and siRNA can translocate through nano electropores within tens of ns. We discuss these results in comparison to experiments in order to rationalize the mechanism of drug uptake by cells.

4.4.1 Introduction

Traditional EP (μs-msPEF) [1-15], thanks to its convenience (i.e. ease of procedure, relatively low cost and speed) and safety (only few side-effects have been reported [16]), in the last thirty years was efficiently employed as a non-viral method to transfect into cells and tissues various bioactive poorly permeable molecules such as dyes, disaccharides, vitamins, anticancer drugs, proteins, and genes [17]. The resulting biomedical applications span from calcium electroporation [18], electrochemoterapy (ETC) [19,20], DNA vaccination [21,22] and gene regulation [23,24], for instance by employing RNAi as a mean of targeting and silencing of pathological proteins in specific ways [25].

In spite of the large use of this technique, the exact mechanisms involved at the molecular level of cell and tissue uptake are not fully clarified. Since the understanding of the transport dynamics is important for the transfer optimization, molecular dynamics (MD) simulations can provide a powerful tool to investigate such mechanisms with atomic resolution [26-33].

As mentioned in 4.3, improvements to the MD protocols to mimic the effect of nsPEFs and μs-msPEFs where recently proposed to stabilize the electropores and study their properties. The first one by Fernández et al. [34] to control pores formed with the nsPEFs procedure, and more recently by our group [35] to tune the μs-msPEFs approach (see 4.3).

It has been shown that regardless of the method used, charge imbalance or direct electric field, lipid bilayers electroporation takes place within identical time scales (namely few

nanoseconds), provided the voltages applied are identical [33].

So far only two MD studies have been reported on the transport process of molecules under nsPEFs. In 2012 Breton et al. [36] demonstrated, coupling experimental and *in silico* observations, how a single 10 ns high-voltage electric pulse can permeabilize lipid vesicles and allow the delivery of siRNA to the cytoplasm by electrophoretic drag. More recently, Salomone et al. [37] showed the possibility to use a combination of nsPEFs and a chimeric peptide (CM_{18}-Tat_{11}) as efficient transferection for pDNA administration. Insight onto the molecular mechanism of such synergic effect was possible only thanks to MD evidences.

While both nsPEFs and μs-msPEFs increase membranes permeability [33,38], it is not known whether they lead to similar transport mechanisms. To answer such a question, the transport of different chemical species through electroporated membranes should be investigated with MD techniques using both the proposed protocols. Following this line of research, here we extend our previous MD investigations on the translocation of Tat_{11} and siRNA to clarify some missing aspects of the μs-msPEFs driven transport.

4.4.2 Systems and Methods

4.4.2.1 System preparation

A system composed by 1024 Palmitoyl-Oleoyl-PhosphatidylCholine (POPC) lipids was considered. The bilayer is fully hydrated in a ∼0.9 M NaCl solution, resulting in a cell with total size 17.8 x 17.8 x 19 nm^3. The force field used for the POPC is CHARMM36 [39], and the TIP3P model was considered for water [40].

The 22 base-pair double stranded siRNA molecule coordinates were extracted from the 2F8S PDB structure. The Tat_{11} peptide: YGRKKRRQRRR, residues 47-57 of HIV-1 Tat protein (trans-activating proteins) [41,42].

4.4.2.2 Parameters of MD

The MD simulations were performed using GROMACS 4.6. [43]. The equations of motion were integrated using the leap-frog algorithm. The time step of the simulations was 2.0 fs. The long-range electrostatics was calculated using Particle Mesh Ewald (PME). The cut-off distance of the short-range electrostatics was taken to be 1.2 nm. A switching function was used between 0.8 and 1.2 nm to smoothly bring the van der Waals forces and energies to 0 at 1.2 nm. During the simulations, chemical bonds between hydrogen and heavy atoms were constrained to their equilibrium values using LINCS. 3d Periodic boundary conditions were applied.

4.4.2.3 Equilibration

The scheme studied here was constructed by replicating an equilibrated patch of 256 molecules in the bilayer plane. The system obtained was further equilibrated during 20 ns in the NPT ensemble: the pressure and the temperature were kept constant at 1 atm (using the Parrinello-Rahman barostat) and 300 K (using the Nose-Hoover thermostat), respectively. At the temperature set for the study, the POPC bilayer is in its biologically relevant liquid crystal L_α phase. To verify the convergence of the equilibration we estimated the area per lipid along the run, which rapidly reached the plateau of ∼62 Å^2 [44].

4.4.2.4 Production runs

The production runs, with duration variable depending on the crossing event of the given molecule (see Table 4.7), were performed in the NPγT ensemble using the single-bilayer scheme [33] and the "swapping" algorithm [45], as described in a protocol we recently proposed [35]. The NPγT was chosen to keep the surface tension of the bilayer at zero and to allow the pore to freely adapt its size, considering 100 mN/m as a reference total surface tension of the system including the air-water interfaces. Since 3d boundary conditions are applied, a vacuum layer is present between the two baths to ensure the charge imbalance between the two sides of the membrane, as shown in Fig. 4.26 (a). We therefore changed the compressibility of the system in the Z-direction (perpendicular to the bilayer) to zero, to avoid the collapse of the vacuum slab, using the Berendsen barostat. The swapping algorithm (s.a.) maintains a constant charge imbalance $\Delta Q/C$ across the porated bilayer resulting in relatively steady transmembrane voltage stabilizing the pore at a certain radius. Briefly, the algorithm is developed such that when an ion from the region above the bilayer goes to the region below the bilayer through the pore, a different ion of the same species from the below region is swapped with a water molecule from the above region (or vice versa).

Finally, once the pore was stabilized at a given ΔQ (see Fig. 4.26 (b)), we inserted a siRNA (-42 e, 13.89 kDa) and Tat_{11} (+8 e, 1.50 kDa) molecule in the bulk water of two different patches (see at t = 0 ns Fig. 4.27 and 4.29, respectively).

To save computer time we avoided the bulk diffusion process by placing the molecules in proximity of the pore (roughly 0.5 nm far from its edge in the Z direction) [42]. Notice that, using the s.a. one is not able to establish *a priori* a ΔQ that stabilizes the transmembrane voltage (U_m/V) to a certain value (an therefore the radius to a corresponding size), mainly because the molecule considered are highly charged. These charges are not taken into account by the s.a., resulting in a not negligible decrease in the ΔQ once the molecule crosses the center of the pore in the Z direction. When a transmembrane voltage above 0.5 V was desired, if the drop in Um consequent the crossing of the molecule was considered to high the simulation was restarted with an increased ΔQ. We evaluated eventual changes

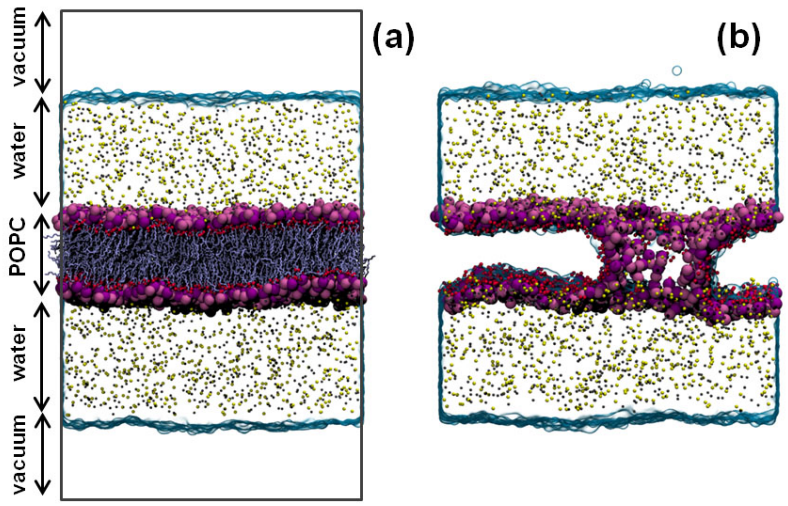

Figure 4.26: (a) The POPC bilayer scheme studied: two solution baths are separated by a lipid bilayer and a vacuum slab, which prevent an exchange of ions from the pbc and collapse of the charge imbalance. (b) Electroporated bilayer. The POPC headgroups are shown as purple and violet beads, the tails as iceblue sticks (a) transparent (b); sodium and chloride ions are colored in yellow and gray; water is transparent

in the Um and R values as explained in 4.4.2.5.

4.4.2.5 Analysis of the trajectories

We analyzed the obtained trajectories in terms of Um and of minimum pore radius (R/nm). The electrostatic potential U_z/V along the normal to the bilayer was evauated by solving Poisson's equation (1), i.e. the double integral of the volume charge density distribution (ρ_z/C/m^3), being ϵ_0/(F/m) the vacuum permittivity:

$$U_z = U(z) - U_0 = -\frac{1}{\epsilon_0} \int \int_0^z \rho_z(z'') dz'' dz'. \tag{4.6}$$

U_0 was set to zero in the lower bulk solution. Um was defined as the difference between the electrostatic potential at the lower and the upper baths of the bilayer.

For a given system configuration *j*, the 3d electrostatic potential U_j(**r**, ΔV) at position **r** was computed using the PME method as implemented in VMD [45]. In this scheme, the potential is obtained by solving the Poisson's equation as follows:

$$\nabla^2 U_j(\mathbf{r}, \Delta V) = -4\pi \sum_j \rho_j(\mathbf{r}), \tag{4.7}$$

where ρ_j is the point charge approximated by a spherical Gaussian of inverse width σ

and the sum running over all atoms in the system. We considered a grid of 1.0 x 1.0 x 1.0 $Å^3$ and $\sigma = 0.25\ Å^{-1}$. The 3d-electric potential was then obtained by averaging 1000 frames of 10 ns trajectory. The electric field (E/V/nm) was evaluated from the gradient of the electric potential distribution $U_j(\mathbf{r},\Delta V)$.

The pore radius was estimated using HOLE [46]. The program HOLE was designed to determine protein channels dimensions along the perpendicular to the bilayer, defining the radius in a given position as the largest possible sphere which can fit the channel without overlapping with van der Waals radii of any atom species previously set. To adapt the algorithm to our case, we chose as reference atoms the phosphorous and nitrogen of the lipid headgroups. Practically we calculated U_m and R over time windows of 2.5-5 ns, depending on the total length of the simulation, to evaluate possible major fluctuations. We therefore defined a mean U_m, indentifying as threshold 0.5 V, which should be considered as an indicative value.

We defined the crossing time t_c/ns as the time needed for the all molecule to translocate from the starting location 0.3 nm above the plane identified by the mean position of the phosphorous and nitrogen atoms of the upper headgroups to 0.3 nm below the mean position of the phosphorous and nitrogen atoms of the lower headgroups.

4.4.3 Results and Discussions

In the present study we investigated using MD simulations the transport of two small molecules (∼1-14 kDa) through elecroporated lipid bilayers subject to a transmembrane voltage, mimicking the uptake through the plasma membrane of cells subject to μs-msPEFs. We focused our attention on a small charged peptide Tat_{11} and an siRNA double strand firstly to compare our results with the one reported on the same solutes under the effect of nsPEFs [36,37]. We further aim at providing a molecular insight on siRNA transport that can rationalize the experiments using μs-msPEFs [47]. In the following paragraph, we briefly describe these works, summarized in Table 4.6.

4.4.3.1 Comparative studies

In 2011, a study conducted by Paganin-Gioanni et al. [47], carried out on mouse melanoma cells (pulse parameters in Table 4.6), investigated the processes of siRNA uptake by localization of fluorescently labeled (AF-546) siRNA at the single-cell level by using time lapse fluorescence confocal microscopy.

This technique allows the quantification of fluorescence intensity due to siRNA inflow in the cytoplasm through the plasma cell membrane following the application of electric pulses (1 Hz). Notice that the technique used quantifies an average transport into the cytoplasm with successive scans of ∼1 s, that hence does not have the temporal resolution

Reference	Target	PEF Frequency Duration Intensity	U_m/V	t_c/ns
[47]	B16F10 mouse melanoma cells	10 pulses, 1Hz 5 ms 300-500 V/cm	0.25*	in the first pulse < 5 ms
[36]	POPC BLM (1152 lipids)	1 pulses 10 ns 140 kV/mm**	1.60	<10 ns
[37]	POPC BLM (256 lipids)	1 pulses 10 ns 200 kV/mm**	1.60	< 10 ns

Table 4.6: a
nd Tat_{11} [37] using nsPEFs, and experimental results of siRNA [47] entrance using μs-msPEFs]Molecular dynamic results from the literature on the transport of siRNA [36] and Tat_{11} [37] using nsPEFs, and experimental results of siRNA entrance using μs-msPEFs [47]
U_m - Estimated transmembrane voltage induced by the electric field applied
t_c - crossing time of the molecule through the electropore
BLM - lipid bilayer membrane
*not measured in [47], yet indirectly deduced from [48]
**from MD simulations

to detect a faster transport if any through membrane electropores. The study suggested that when dealing with high negatively charged RNAs the transport is solely due to an electrophoretic drag against the field direction through the pore taking place during the first electric pulse. As it terminates immediately after the pulse is switched off, siRNA uptake requires both poration of the plasma cell membrane and electrophoretic drag of the molecule. The same group also observed that pulses (0.17 kV/cm, 5 ms) named EGT [49] are more effective in terms of silencing than the more intense less lasting HV pulses (1.3 kV/cm, 0.1 ms). They also showed how a double pulse procedure, consisting in a long below EP threshold pulse after the HV didn't increase the efficiency of the delivery. Therefore, they evidenced that for μs-msPEFs, keeping the voltage above the EP threshold and tuning the duration of the pulse are key factors for an efficient delivery protocol. Nevertheless the reasons why this is needed remain unclear.

Breton et al. [36] demonstrated the feasibility of using a single 10 ns pulse to induce the uptake of siRNA in giant unilamellar vesicles (GUVs), comparing experimental evidences with MD simulations. From the latter, they deduced that: (i) no transport is detected for electric fields applied below the EP threshold (Table 4.6); (ii) a stable complex siRNA-headgroups of phospholipids forms once the molecule is pushed in proximity of the membrane by the E_{app}, which lasts for long after the pulse is switched off; (iii) when the E_{app} is above the EP threshold (E_{th}) the drag of the siRNA is shown to take place in 10 ns in the opposite direction of E_{th}; (iv) if the Eth is turned off before the complete transition the

pore collapses around the molecule, which is therefore trapped. These observations lead to conclusions with respect to the process in line with the results involving low millisecond pulses.

Salomone et al. [37] reported on the process of translocation of a Tat_{11} peptide through porated lipid GUVs, always integrating observations from experiments with MD simulations. Using MD simulations and high electric fields as a method to impose the voltage they showed that the peptide can cross a pore formed in a lipid bilayer in less than 10 ns without interacting with the phospholipids headgroups.

4.4.3.2 Transport of siRNA

In order to investigate the siRNA transfer into cells, we first analyzed its behavior when a transmembrane voltage U_m was kept below 0.5 V (see 4.4.2.5-*Analysis of the trajectories* for the definition of this threshold). Under this condition we observe a strong interaction of the high charged molecule with the zwitterionic headgroups of the bilayer, resulting in the siRNA sliding along the pore wall, without a complete transport in 100 ns of run. Corroborating previous results [36,47] and as expected from the high charge of he plasmid, the drag is indeed due to an electrophoretic force and one expect that the speed of translocation of the molecule will depend strongly on the local electric field strength.

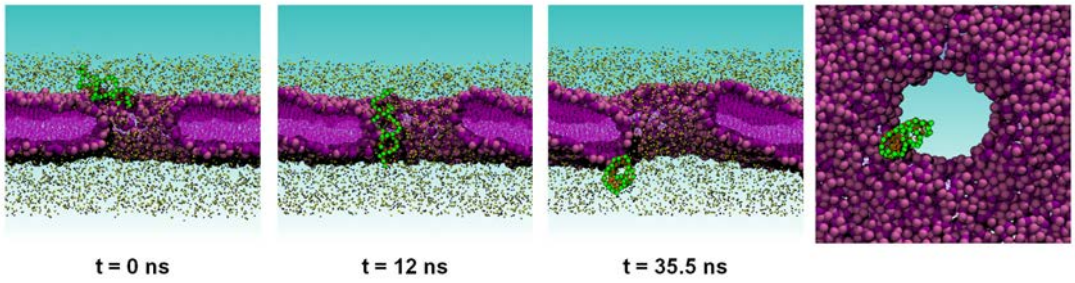

Figure 4.27: The process of siRNA transport, when U_m is above 0.5 V, in three frames corresponding to 0, 12, and 35.5 ns. In the last panel the top view clearly shows the anchoring interaction. The POPC headgroups are shown as mauve and violet beads, the tails as purple lines; sodium and chloride ions are colored in yellow and gray; siRNA is green

Indeed, we observed the complete translocation of the small interfering RNA during when a larger transmembrane voltage was applied (see Fig. 4.27). Despite its anchoring to the lipid headgroups (in Fig. 4.27, t = 12 ns) that are dragged with the molecule during the transport, we registered a complete translocation from the upper to the lower bath in 35.5 ns when the U_m was maintained above 0.5 V. Our MD simulations also showed that once the siRNA reaches the lower leaflet of the membrane it remains bound to the phosphate zwitterionic headgroups without diffusing in the bulk solution even if the U_m is kept (in Fig. 2, t = 35.5 ns).

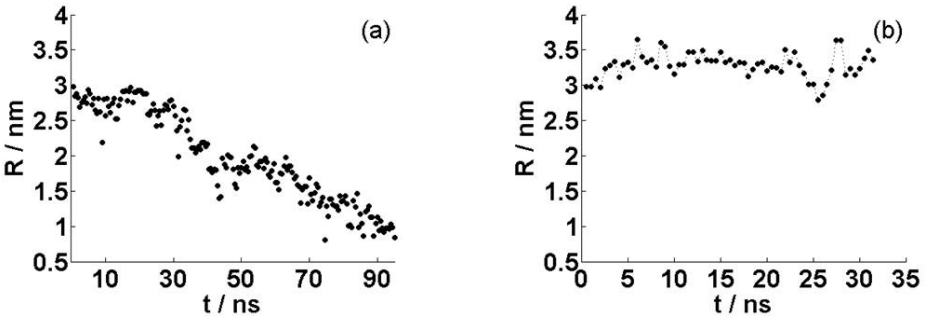

Figure 4.28: Pore radius in time when the U_m is kept below (a) and above (b) 0.5 V

Note here that the pore radius R (in Fig. 4.28) decreased significantly when U_m below 0.5 V was applied, indicating a collapse of the pore around the molecule, while for U_m above 0.5 V it maintained a steady trend and was large enough to allow translocation of the siRNA.

All together the present results interestingly demonstrate that the translocation of SiRNA through the pore driven by the application of transmembrane voltages > 0.5 V mimicking therefore the μs-msPEFs experiments, takes place in the nanosecond time scale, as reported when high electric fields mimicking the nsPEFs experiments are applied (Table 4.6).

4.4.3.3 Transport of Tat_{11}

The translocation for this peptide differs from that of the highly charged siRNA because no specific interactions between Tat_{11} and the lipid headgroups took place during the process, resulting in a faster uptake (see Fig. 4.29).

In the case of U_m above the electroporation threshold, the molecule, initially parallel to the membrane and located near the pore mouth, first rotates 90 degrees to align its dipole along the local electric field (Fig. 4.29, t = 0 ns), than diffuses within 11.3 ns though the center of the pore of R ∼2 nm (Fig. 4.29, t = 7.8 ns), i.e. at the same time scale reported with the nsPEFs procedure [37]. The Tat_{11} reaches the lower bath where it freely diffuses (Fig. 4.29, t = 12 ns).

Contrary to the case of siRNA, when the U_m is below 0.5 V, and above the electroporation threshold (0.7 V) a full Tat_{11} transport still occurs, although with a lag. In fact, under this condition the pore radius decreases of the 20% and the crossing time increases 3 folds (32.8 ns), presumably as a consequence of a higher hindrance of the pore and a reduction of the electrophoretic drag.

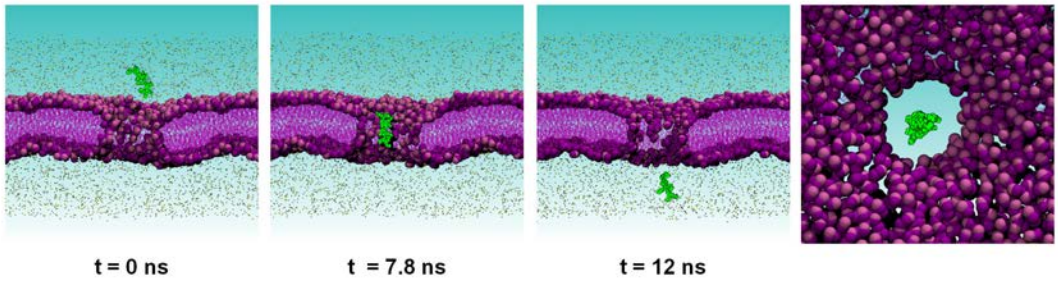

Figure 4.29: The process of Tat_{11} transport in three frames corresponding to 0, 7.8, and 12 ns. In the last panel the top view clearly shows no interactions between the molecule and the pore wall. The POPC headgroups are shown as mauve and violet beads, the tails as purple lines; sodium and chloride ions are colored in yellow and gray; Tat_{11} is green

4.4.3.4 Electric potential and field distributions

In order to investigate the effect of a transmembrane voltage U_m on the transport properties of electropores, we reported in Figure 4.30 and 4.31 the spatial distributions of the electrostatic potential and of the electric field averaged over 10 ns run (see 4.3.2.8-*Analysis of the trajectories*) in the plane xz perpendicular to the bilayer without the presence of solutes (e.i. Tat_{11} and siRNA).

Indeed, a charged species (q/C) subject to an electric field (E/V/m) is subject to a force (F/CV/m) $F = q \cdot E$, that drags the charge along the direction of E. Therefore, understanding the intensity and the direction of the electric field in the pore region, that originates from the imposed U_m, shades light on the process of molecules translocation through porated cell membranes.

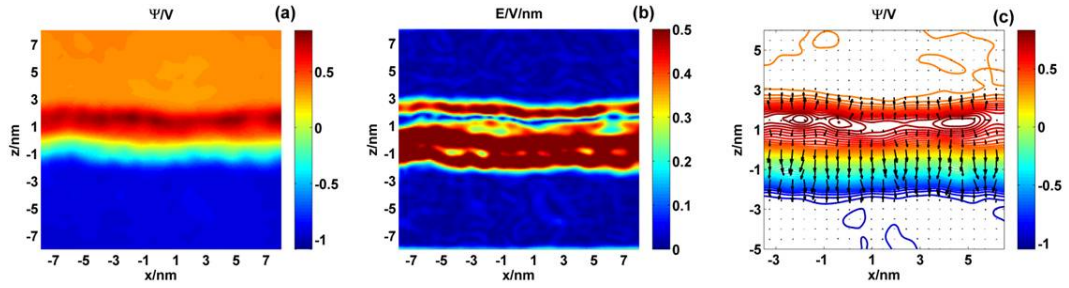

Figure 4.30: Spatial distributions in the plane xz perpendicular to an intact bilayer subject a ΔQ: a) Electrostatic potential, b) Electric field intensity, c) Electrostatic potential and electric filed orientation indicated by arrows

For a whole bilayer (Fig. 4.30 a), the application of a charge imbalance between the two baths, and hence of a U_m 0.9 V, induces an intense electric field across the membrane that in this specific case reaches 0.5 V/nm (Fig. 4.30 b). Figure 4.30 c shows the isolines of the electric potential and the electric field direction indicated by arrows, which are perpendicular to the equipotential lines.

While when poration occurs, and the U_m is maintained, we can observe in the pore region a slight decrease of the electric field intensity (Fig 4.31 b), a distortion of the electric field potential (Fig 4.31 a), and therefore of the normal to its isolines, e.g. of the electric field direction (Fig 4.31 c). In the inner region of the water column the arrows are normal to the bilayer and negatively directed along the all z axis (Fig 4.31 c). In this case the electric force will push a positive charged species from the upper to the lower bath, and vice-versa a negative charged one from the below to the above solution. In the proximity of the pore edges the eclectic field direction is oblique (Fig 4.31 c), this induces a "funnel" effect on nearby charged particles that will be dragged towards its opening, as we observed for the Tat_{11} (see 4.4.3.3-*Transport of* Tat_{11}).

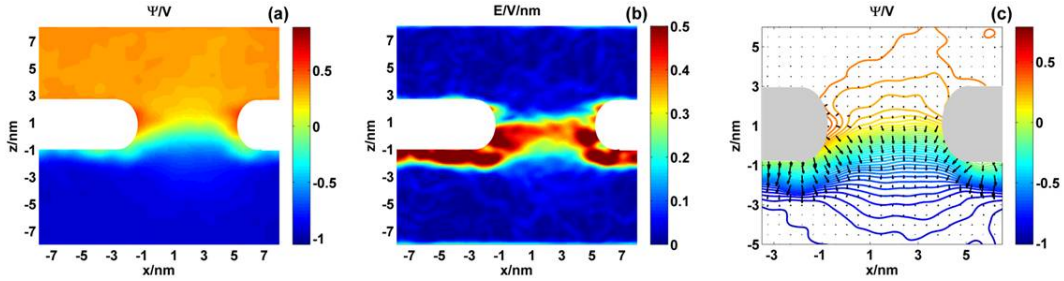

Figure 4.31: Spatial distributions in the plane xz perpendicular to a poreated bilayer: a) Electric potential, b) Electric field intensity, c) Electric potential and electric filed orientation indicated by arrows

4.4.3.5 Comparison with previous findings

Table 4.7 summarizes our results for the two molecules studied. Confronting them with the nsPEF procedure we can unexpectedly conclude that for each of the solutes the translocation processes through electropores are characterized by similar features (binding or not to the lipid head groups) and similar time scales, namely occur within the nanoseconds.

System	t_s/ns	U_m/V	R/nm	t_c/ns
POPC-1024+siRNA	100	0.16 ± 0.16	1.96 ± 0.65	>100
	35	0.55 ± 0.19	3.30 ± 0.21	32.5
POPC-1024+Tat_{11}	40	0.43 ± 0.16	1.62 ± 0.18	32.8
	14	0.70 ± 0.24	2.04 ± 0.13	11.3

Table 4.7: Pore radius R/nm and crossing time t_c/ns estimated at specific TM voltages U_m/V for the two molecules considered
t_s - simulation time
U_m - Estimated transmembrane voltage induced by the electric field applied
R - minimum pore radius maintained by a given U_m
t_c - crossing time of the molecule through the electropore

In the simulations of the Tat_{11}, no interactions were observed with the pore wall, but a lag is recorded for U_m lower than 0.5 V, probably due to both the hindering that follows the

reduction of the pore radius and of the electrophoretic drag. When comparing our results with the ones reported by [37] only a qualitative estimation of the crossing time can be given because of the different simulation conditions (c.v. Table 4.6 and Table 4.7). First, under conditions of an applied electric field, it is difficult to stabilize the pore size when a large field intensity is applied. Second, the size of the patch used in the present simulation (1024 lipids) subject to 0.5 V allows the pore relaxation stabilization around a radius of ∼2.0 nm. Under these conditions, Tat_{11} is translocated within the 10 ns time scale. We also showed how a reduction of the voltage that leads to a 20% reduction of the pore radius induces a 3 fold slowdown of the transport process. Considering a patch of 256 lipids, and applying an electric field that generates a 1.6 V across the bilayer, Salomone et al. reported that Tat_{11} translocated within 10 ns, while one should expect a much faster uptake due to over a 3 fold increase in electrophoretic drag (3 times large electric field). One shall note however that the pore created under the simulations conditions of [37] is ∼1.7 nm in radius, much smaller that what one expect. It is unclear if this is due to the difference in protocols used (e field vs charge imbalance) or to artifacts that may rise from the size effects as we have recently shown [35]. Despite these discrepancies, it is very interesting to note that both when an electric field and a charge imbalance are applied, i.e. under conditions of μs-msPEFs or nsPEFs, the translocation of a small charged molecule such as Tat_{11} occurs on the tens of nanosecond time scale.

When investigating the siRNA behavior, using the two MD protocols, once the molecule is pulled close to the bilayer by the external electric pulse a long lasting complex is established with the lipid headgroups, even after the siRNA crossing to the other leaflet, preventing therefore an electrophoretic driven flow in the inner solution, as previously reported when using the e field method, i.e. under nsPEFs conditions. Mimicking the μs-msPEFs, when we maintain here U_m at 0.5 V using the charge imbalance, tc is 32.5 ns (Table 2) and we expect that for 1.5 V t_c would be around 10.8 ns in agreement again with time scale reported in [36] (Table 4.6).

Experiment performed on mouse melanoma cells applying V/cm ms-long pulses [49] evidenced that tuning the duration of the pulse is essential for an efficient siRNA uptake. In fact they found more effective the EGT (0.17 V/cm, 5 ms) class of pulses than the HV (1.3 V/cm, 0.1 ms) one. Longer pulses means apply the electroporetic force for a longer period. No direct measurement of the TM voltage was carried out during these experiments and the authors assume that it is around 0.25 V, since it was observed that the EP threshold value is always about 0.20 mV for many different cell systems [48].

Our results indicate that that the siRNA transport through electropored lipid bilayers occurs in tens of nanoseconds when roughly the double of transmembrane voltage is maintained (0.25, 0.50 V), which is orders of magnitude faster than the experimental pulse duration. How to explain then differences in the uptake and efficiency (see 4.4.3.1-*Comparative studies*) between EGT and HV protocols that last from a fraction of to few ms? First we recall that these experiments are performed on cells, while our investigation concerns lipid

bilayers. Even then, we have shown that the formation of stable complexes siRNA/lipid head groups prevents the molecule from detaching from the lipids even if the pulse is still on. Estimating from simulations the time scale needed for depletion of siRNA from the lipid bilayer is beyond our capabilities, and does not occur with the 100-ns time scale as we reported earlier [36]. In cells, one should also consider the cytoskeleton and possible interaction of siRNA with its components in its way to the cytosol slowing down the process of transfection.

Corroborated by our findings one can speculate that the transport of the plasmid when subject to longer pulses could be facilitated by a more likely formation of a pore population having higher radii, allowing for siRNAs to flow through the pore without interacting with the lipids and hence to access directly the cytoplasm. It is plausible that this population of large pores would reduce the probability of long lasting complex formation among the siRNAs and the plasma membrane that we observed with MD simulations and which prevents the electrophoretic flow toward the inner of the cell.

Another aspect that should be considered when comparing to experiments are the exact processes taking place during μs-msPEFs experiments. It has been suggested over a decade ago, that under electroporation protocols, membranes may undergo oxidation. It has been experimentally reported indeed that pulsed electric fields can increase the extent at which lipid acyl chain peroxidation occurs. In particular, it has been demonstrated that the application of external electric fields alters the phospholipid composition and the properties of liposomes, vesicles and cells [50-53].

The presence of oxidized lipids within biomembranes is known to alter their physical properties and, in particular, their permeability [54-56]. We cannot therefore exclude that siRNA uptake under μs-msPEFs experiments may be at least partially taking place through diffusion across oxidized/permeabilized lipid bilayers and not uniquely across electropores.

4.4.4 Conclusions

The study of the mechanisms of transport of bioactive compounds through biological cell membranes enhanced by electroporation is important for several biological and medical applications that require a local uptake to be effective. Despite the wide use of this technique little is known regarding the process of transfection at the molecular scale.

Our results are direct observations at the atomic scale of the electrotransfer of small charged molecules, siRNA (-42 charge, 13.89 kDa) and Tat_{11} (+8 charge, 1.50 kDa) thorough a cell membrane model subject to microsecond pulse electric fields (μs-msPEFs). For transmembrane voltages lower than 0.5 V no crossing of siRNA and a lag in the transport of Tat_{11} were observed. When the transmembrane voltage is above this critical value we report for the siRNA a complete crossing in $\sim$30 ns albeit its strong anchoring with the zwitterionic

phospholipids headgroups, and for the peptide in ~10 ns without any interaction with the surrounding pore walls.

Interestingly we found that that the dynamic of the transport process takes place in the same time scale (nanosecond) that for shorter pulses (nsPEFs) we previously reported.

Confronting our findings on the siRNA with experiments conducted maintaining a comparable transmembrane voltage (above the electroporation threshold), the long time (milliseconds) necessary for the pulse to be efficient and observe an increase in uptake can be probably attributed to the formation of stable complexes between the siRNA and lipid headgroups and subsequent interactions with the cytoskeleton that hamper the detachment of the molecule even when the pulse is not switched off. Experimentally it was shown that longer pulses above the threshold (EGT-0.17 kV/cm, 5 ms) are more effective than more intense an shorter ones (HV-1.3 kV/cm, 0.1 ms), thus one can hypnotize that a population of pores with higher radius may form when EGT, and in general longer pulses, are applied permitting to the siRNAs to flow through the pore without interacting with the phospholipids headgroups and hence access directly the cytoplasm.

In conclusion, we have introduced an MD protocol that is suitable to characterize the transport of uncharged and charged species driven by μs-msPEFs, shading light on the understanding of the uptake mechanism of drugs by cell membranes. Systematic studies carried out with this protocol in presence of other relevant drugs (e.g. bleomycin) or dyes (e.g. propidium iodide, YO-PRO,...) are expected to drastically broaden such an understanding eventually providing further insights that may improve the related experimental techniques and therapeutic effectiveness.

It is worth mentioning that another aspect that should be considered when comparing to experiments relates to the exact processes taking place during PEFs experiments. It has been suggested over a decade ago, that under electroporation protocols, membranes may undergo oxidation. It has been experimentally reported indeed that pulsed electric fields can increase the extent at which lipid acyl chain peroxidation occurs. In particular, it has been demonstrated that the application of external electric fields alters the phospholipid composition and the properties of liposomes, vesicles and cells [57-60]. The presence of oxidized lipids within biomembranes is known to modify their physical properties and, in particular, their permeability [61-63]. We cannot therefore exclude that substrates uptake under PEFs experiments may be, at least partially, taking place through diffusion across oxidized/permeabilized lipid bilayers and not uniquely across electropores. Simulations along these lines should improve our characterization of the electro-transport of molecules across membranes driven by electric fields.

4.4.5 References

[1] J.C. Weaver, Y.A. Chizmadzhev, Theory of electroporation: A review, Bioelectrochem. Bioenerg. 41 (1996) 135-160.

[2] T. Kotnik, G. Pucihar, D. Miklavčič, Induced Transmembrane Voltage and Its Correlation with Electroporation-Mediated Molecular Transport, J. Membr. Biol. 236 (2010) 3-13.

[3] I.G. Abidor, V.B. Arakelyan, L.V. Chernomordik, Y.A. Chizmadzhev, V.F. Pastushenko, M.P. Tarasevich, Electric breakdown of bilayer lipid membranes: I. The main experimental facts and their qualitative discussion, J. Electroanal. Chem. Interfacial Electrochem. 104 (1979) 37-52.

[4] J. Teissié, N. Eynard, B. Gabriel, M.P. Rols, Electropermeabilization of cell membranes, Adv. Drug Deliv. Rev. 35 (1999) 3-19.

[5] L.M. Mir, S. Orlowski, J. Belehradek Jr, C. Paoletti, Electrochemotherapy potentiation of antitumour effect of bleomycin by local electric pulses, Eur. J. Cancer Clin. Oncol. 27 (1991) 68-72.

[6] S. Koronkiewicz, S. Kalinowski, Influence of cholesterol on electroporation of bilayer lipid membranes: chronopotentiometric studies, Biochim. Biophys. Acta BBA - Biomembr. 1661 (2004) 196-203.

[7] M. Kotulska, Natural Fluctuations of an Electropore Show Fractional Lévy Stable Motion, Biophys. J. 92 (2007) 2412-2421.

[8] P. Kramar, L. Delemotte, A.M. Lebar, M. Kotulska, M. Tarek, D. Miklavčič, Molecular-Level Characterization of Lipid Membrane Electroporation using Linearly Rising Current, J. Membr. Biol. 245 (2012) 651-659.

[9] D.P. Tieleman, The molecular basis of electroporation, BMC Biochem. 5 (2004) 10.

[10] M. Tarek, Membrane Electroporation: A Molecular Dynamics Simulation, Biophys. J. 88 (2005) 4045-4053.

[11] Z. A. Levine, and P. T. Vernier, Life cycle of an electropore: Field dependent and field-indepedent steps in pore creation and annihilation, J. Membr. Biol. 236 (2010) 27-36.

[12] M. Szabo, M.I. Wallace, Imaging potassium-flux through individual electropores in droplet interface bilayers, Biochim. Biophys. Acta. (2015).

[13] J. Deng, K.H. Schoenbach, E. Stephen Buescher, P.S. Hair, P.M. Fox, S.J. Beebe, The Effects of Intense Submicrosecond Electrical Pulses on Cells, Biophys. J. 84 (2003) 2709-2714.

[14] P.T. Vernier, Y. Sun, M.A. Gundersen, Nanoelectropulse-driven membrane pertur-

bation and small molecule permeabilization, BMC Cell Biol. 7 (2006) 37.

[15] L. Chopinet, M.-P. Rols, Nanosecond electric pulses: a mini-review of the present state of the art, Bioelectrochemistry Amst. Neth. 103 (2015) 2-6.

[16] M. Marty, G. Serša, J.R. Garbay, J. Gehl, C.G. Collins, M. Snoj, et al., Electrochemotherapy - An easy, highly effective and safe treatment of cutaneous and subcutaneous metastases: Results of ESOPE (European Standard Operating Procedures of Electrochemotherapy) study, Eur. J. Cancer Suppl. 4 (2006) 3-13.

[17] M.S. Venslauskas, S. Šatkauskas, Mechanisms of transfer of bioactive molecules through the cell membrane by electroporation, Eur. Biophys. J. 44 (2015) 277-289.

[18] E.L. Hansen, E.B. Sozer, S. Romeo, S.K. Frandsen, P.T. Vernier, J. Gehl, Dose-dependent ATP depletion and cancer cell death following calcium electroporation, relative effect of calcium concentration and electric field strength, PloS One. 10 (2015).

[19] M. Breton, L.M. Mir, Microsecond and nanosecond electric pulses in cancer treatments, Bioelectromagnetics. 33 (2012) 106-123.

[20] D. Miklavčič, B. Mali, B. Kos, R. Heller, G. SerÅ¡a, Electrochemotherapy: from the drawing board into medical practice, Biomed. Eng. OnLine. 13 (2014) 29.

[21] M. Sällberg, L. Frelin, G. Ahlen, M. Sällberg-Chen, Electroporation for therapeutic DNA vaccination in patients, Med. Microbiol. Immunol. (Berl.). 204 (2014) 131-135.

[22] G. Serša, J. Teissie, M. Cemazar, E. Signori, U. Kamensek, G. Marshall, et al., Electrochemotherapy of tumors as in situ vaccination boosted by immunogene electrotransfer, Cancer Immunol. Immunother. CII. 64 (2015) 1315-1327.

[23] L.C. Heller, R. Heller, In Vivo Electroporation for Gene Therapy, Hum. Gene Ther. 17 (2006) 890-897.

[24] S. Chabot, J. Teissié, M. Golzio, Targeted electro-delivery of oligonucleotides for RNA interference: siRNA and antimiR, Adv. Drug Deliv. Rev. 81 (2015) 161-168.

[25] R.W. Carthew, E.J. Sontheimer, Origins and Mechanisms of miRNAs and siRNAs, Cell. 136 (2009) 642-655.

[26] M.-C. Ho, M. Casciola, Z.A. Levine, P.T. Vernier, Molecular Dynamics Simulations of Ion Conductance in Field-Stabilized Nanoscale Lipid Electropores, J. Phys. Chem. B. 117 (2013) 11633-11640.

[27] A. Polak, D. Bonhenry, F. Dehez, P. Kramar, D. Miklavčič, M. Tarek, On the Electroporation Thresholds of Lipid Bilayers: Molecular Dynamics Simulation Investigations, J. Membr. Biol. 246 (2013) 843-850.

[28] R. Reigada, Electroporation of heterogeneous lipid membranes, Biochim. Biophys. Acta BBA - Biomembr. 1838 (2014) 814-821.

[29] F. Dehez, L. Delemotte, P. Kramar, D. Miklavčič, M. Tarek, Evidence of Conducting Hydrophobic Nanopores Across Membranes in Response to an Electric Field, J. Phys. Chem. C. 118 (2014) 6752-6757.

[30] M. Casciola, D. Bonhenry, M. Liberti, F. Apollonio, M. Tarek, A molecular dynamic study of cholesterol rich lipid membranes: comparison of electroporation protocols, Bioelectrochemistry. 100 (2014) 11-17.

[31] A.A. Gurtovenko, A.S. Lyulina, Electroporation of Asymmetric Phospholipid Membranes, J. Phys. Chem. B. 118 (2014) 9909-9918.

[32] A. Polak, A. Velikonja, P. Kramar, M. Tarek, D. Miklavčič, Electroporation Threshold of POPC Lipid Bilayers with Incorporated Polyoxyethylene Glycol (C12E8), J. Phys. Chem. B. 119 (2015) 192-200.

[33] L. Delemotte, M. Tarek, Molecular Dynamics Simulations of Lipid Membrane Electroporation, J. Membr. Biol. 245 (2012) 531-543.

[34] M.L. Fernández, M. Risk, R. Reigada, P.T. Vernier, Size-controlled nanopores in lipid membranes with stabilizing electric fields, Biochem. Biophys. Res. Commun. 423 (2012) 325-330.

[35] M. Casciola, M.A. Kasimova, S. Zullino, F. Apollonio, M. Tarek, Properties of lipid electropores I: Molecular dynamics simulations of stabilized pores by constant charge imbalance, Bioelectrochemistry Submitt. Rev.

[36] M. Breton, L. Delemotte, A. Silve, L.M. Mir, M. Tarek, Transport of siRNA through Lipid Membranes Driven by Nanosecond Electric Pulses: An Experimental and Computational Study, J. Am. Chem. Soc. 134 (2012) 13938-13941.

[37] F. Salomone, M. Breton, I. Leray, F. Cardarelli, C. Boccardi, D. Bonhenry, et al., High-Yield Nontoxic Gene Transfer through Conjugation of the CM_{18}-Tat_{11} Chimeric Peptide with Nanosecond Electric Pulses, Mol. Pharm. 11 (2014) 2466-2474.

[38] P.T. Vernier, M.J. Ziegler, Y. Sun, M.A. Gundersen, D.P. Tieleman, Nanopore-facilitated, voltage-driven phosphatidylserine translocation in lipid bilayers-in cells and in silico, Phys. Biol. 3 (2006) 233.

[39] J. B. Klauda, R. M. Venable, J. A. Freites et al., Update of the CHARMM all-atom additive force field for lipids: Validation on six lipid types, J. Phys .Chem. B 114 (2010) 7830-7843.

[40] W.L. Jorgensen, J. Chandrasekhar, J.D. Madura, R.W. Impey, M.L. Klein, Comparison of simple potential functions for simulating liquid water, J. Chem. Phys. 79 (1983) 926-935.

[41] P. Lundberg, Ü. Langel, A brief introduction to cell-penetrating peptides, J. Mol. Recognit. 16 (2003) 227-233.

[42] H.D. Herce, A.E. Garcia, Molecular dynamics simulations suggest a mechanism for translocation of the HIV-1 TAT peptide across lipid membranes, Proc. Natl. Acad. Sci. 104 (2007) 20805-20810.

[43] B. Hess, C. Kutzner, D. van der Spoel et al., GROMACS 4: algorithms for highly efficient, load-balanced, and scalable molecular simulation, J. Comp. Theor. Chem. 4 (2008) 435-447.

[44] N. Kučerka, S. Tristram-Nagle, J.F. Nagle, Structure of Fully Hydrated Fluid Phase Lipid Bilayers with Monounsaturated Chains, J. Membr. Biol. 208 (2006) 193-202.

[45] C. Kutzner, H. Grubmüller, B.L. de Groot, U. Zachariae, Computational Electrophysiology: The Molecular Dynamics of Ion Channel Permeation and Selectivity in Atomistic Detail, Biophys. J. 101 (2011) 809-817.

[46] O.S. Smart, J.G. Neduvelil, X. Wang, B.A. Wallace, M.S.P. Sansom, HOLE: A program for the analysis of the pore dimensions of ion channel structural models, J. Mol. Graph. 14 (1996) 354-360.

[47] A. Paganin-Gioanni, E. Bellard, J.M. Escoffre, M.P. Rols, J. Teissié, M. Golzio, Direct visualization at the single-cell level of siRNA electrotransfer into cancer cells, Proc. Natl. Acad. Sci. 108 (2011) 10443-10447.

[48] J. Teissié, M.P. Rols, An experimental evaluation of the critical potential difference inducing cell membrane electropermeabilization., Biophys. J. 65 (1993) 409-413. [49] S. Li, Electroporation Protocols: Preclinical and Clinical Gene Medicine, Humana press: Totowa, NJ., 2008.

[50] L.C. Benov, P.A. Antonov, S.R. Ribarov, Oxidative damage of the membrane lipids after electroporation, Gen. Physiol. Biophys. 13 (1994) 85-97.

[51] M. Maccarrone, N. Rosato, A.F. Agro, Electroporation Enhances Cell Membrane Peroxidation and Luminescence, Biochem. Biophys. Res. Commun. 206 (1995) 238-245.

[52] Y. Zhou, C.K. Berry, P.A. Storer, R.M. Raphael, Peroxidation of polyunsaturated phosphatidylcholine lipids during electroformation, Biomaterials. 28 (2007) 1298-1306.

[53] E. Schnitzer, I. Pinchuk, D. Lichtenberg, Peroxidation of liposomal lipids, Eur. Biophys. J. 36 (2007) 499-515.

[54] A.W. Girotti, Mechanisms of lipid peroxidation, J. Free Radic. Biol. Med. 1 (1985) 87-95.

[55] G. Stark, The effect of ionizing radiation on lipid membranes, Biochim. Biophys.

Acta BBA - Rev. Biomembr. 1071 (1991) 103-122.

[56] B. Tavazzi, D. Di Pierro, A.M. Amorini, G. Fazzina, M. Tuttobene, B. Giardina, et al., Energy metabolism and lipid peroxidation of human erythrocytes as a function of increased oxidative stress, Eur. J. Biochem. 267 (2000) 684-689.

[57] L.C. Benov, P.A. Antonov, S.R. Ribarov, Oxidative damage of the membrane lipids after electroporation, Gen. Physiol. Biophys. 13 (1994) 85-97.

[58] M. Maccarrone, N. Rosato, A.F. Agro, Electroporation Enhances Cell Membrane Peroxidation and Luminescence, Biochem. Biophys. Res. Commun. 206 (1995) 238-245.

[59] Y. Zhou, C.K. Berry, P.A. Storer, R.M. Raphael, Peroxidation of polyunsaturated phosphatidylcholine lipids during electroformation, Biomaterials. 28 (2007) 1298-1306.

[60] E. Schnitzer, I. Pinchuk, D. Lichtenberg, Peroxidation of liposomal lipids, Eur. Biophys. J. 36 (2007) 499-515.

[61] A.W. Girotti, Mechanisms of lipid peroxidation, J. Free Radic. Biol. Med. 1 (1985) 87-95.

[62] G. Stark, The effect of ionizing radiation on lipid membranes, Biochim. Biophys. Acta BBA - Rev. Biomembr. 1071 (1991) 103-122.

[63] B. Tavazzi, D. Di Pierro, A.M. Amorini, G. Fazzina, M. Tuttobene, B. Giardina, et al., Energy metabolism and lipid peroxidation of human erythrocytes as a function of increased oxidative stress, Eur. J. Biochem. 267 (2000) 684-689.

Chapter 5

Exposure Devices for nsPEFs / Dispositifs d'Exposition pour les nsPEFs

Les applications précliniques et cliniques de l'électroporation nécessitent des appareils adéquats utilisés dans des conditions sûres, reproductibles et efficaces. Généralement, à part une série d'équipements de mesure (par exemple, des oscilloscopes, des microscopes, ...), deux composantes principales sont nécessaires pour délivrer des champs électriques pulsés: un générateur d'impulsions [1-4] et une chambre (réservoir) de livraison [5-11].

Comme déjà noté, il y a une grande variété d'impulsions utilisées en EP qu'on peut différencier selon leur forme (trapézoïdale monopolaire et bipolaire, exponentielle, gaussienne, ...), mais elles sont classés en deux familles en fonction de leur durée et intensité: l'EP classique (μs-msPEFs) [12] et la nanoseconde EP (nsPEFs) [13]. Cette dernière famille a suscité un intérêt grandissant dans la communauté scientifique, bien que chronologiquement plus récente (années 2000) en raison de la technologie particulière qu'elles nécessitent, à savoir la capacité à générer de manière fiable des impulsions intenses ultra-courtes.

Dans les systèmes électriques classiques impliquant des signaux avec des fréquences inférieures à 1 MHz ou d'une durée plus longue qu'une μs, i.e. μs-msPEFS. Les phénomènes de propagation à travers les connexions électriques peuvent être considérés comme négligeables et on peut supposer que tous les noeuds d'un bon conducteur électrique atteignent la même tension simultanément assurant une bonne correspondance entre la source et la charge, ce qui simplifie le montage expérimental.

A l'inverse, les nsPEFs doivent être générés et transmis suivant les spécifications appropriées. Les principales caractéristiques que les générateurs doivent posséder sont en la durée et l'intensité des impulsions produites [1-4]. L'effet de nsPEFs est induite directement sur l'eau interfaciale au niveau cellulaire et / ou de la membrane des organites impliquant le fait que la montée en charge (dans le sens du condensateur) de la membrane peut

être négligé. Par conséquent, le ciblage des structures subcellulaires nécessite que le temps de montée des impulsions doit être beaucoup plus petit que le temps de charge de la membrane et la durée de l'impulsion elle-même doit être maintenue une durée plus courte que le temps nécessaire à l'apparition de l'EP de cette membrane. En outre, le champ électrique doit être beaucoup plus élevé que dans le cas des μs-msPEFS afin de cibler les organites cellulaires ou de leurs membranes. Basé sur les mesures expérimentales, [14], les intensités de champ électrique de l'ordre de 5 MV/m sont nécessaires pour une seule impulsion de 10 ns pour induire des effets subcellulaires.

Disposer d'un générateur de nsPEF fiable est une condition préalable nécessaire mais non suffisante pour assurer une expérimentation reproductible. Il y a différents aspects qui peuvent avoir un impact significatif sur les conditions expérimentales, parmi lesquelles les conditions de propagation de signal [15]. La tension, une fois correctement générée par une source 50 Ω, doit être livré à la charge biologique généralement de faible impédance (de l'ordre de 10 Ω), ce qui signifie qu'un recouvrement d'une large bande d'impédance est nécessaire pour appliquer le signal à l'échantillon biologique sans déformation de son contenu spectral et temporel. Ainsi une conception adéquate du générateur est nécessaire de réaliser un dispositifs à large bande, étant donné que les grandes composantes spectrales de nsPEFs les plus utilisés vont du MHz au GHz.

Plusieurs dispositifs pour l'application *in vitro* de pulses nsPEF avec la durée 10 ns [16-21] ont été décrits. Il a été montré qu'il était possible de générer un signal non déformé simplement en dimensionnant le micro-dispositif sur la base de l'impédance de l'échantillon biologique. Cependant, dès que la durée de l'impulsion est moins que 5 ns et que les phases de monté et descente en charge sont de l'ordre de la fraction de ns, il devient nécessaire d'adapter l'impédance, sinon un signal distordu est livré pour les cellules.

Par conséquent, deux conditions préalables principales doivent être remplies pour bien concevoir de tels systèmes d'exposition, nommés microchambres, pour les nsPEFs:

- Une bonne efficacité pour atteindre l'intensité nécessaire pour EP des composants intracellulaires
- Un signal pulsé doit se propager sans atténuation du plateau ni distorsion des phases de montée et descente.

Dans la cadre de ce travail de thèse en cotutelle, on a conçu un système de type puce à électrodes pour conduire des expériences *in vitro* en utilisant des impulsions électriques d'ultra courte durée nommés usPEF. Les résultats fondamentaux de ce travail de conception et caractérisation sont reportés dans le Chapitre qui suit.

Dans ce Chapitre, nous présentons les résultats relatifs à ces travaux. Ils sont divisées en quatre sections. Au paragraphe **5.1.1**, nous décrivons les fonctionnalités que notre dispositif devrait avoir pour améliorer l'état d'art actuel de la technique [41-46]. Le paragraphe suivant, **5.1.2**, est consacré à la description de la procédure en termes de modèles

analytiques [47] que nous avons utilisé pour le dimensionnement de notre structure de guidage. Au paragraphe **5.1.3**, nous caractérisons l'efficacité et le comportement fréquentiel de notre microchambre dans deux configurations différentes: pour les expériences sur mono et multi- cellulaires. Enfin, à la section **5.1.4**, nous discutons de nos résultats mettant en évidence les principaux avantages proposés. On montre comment les performances globales de ce dispositif sont une amélioration par rapport à des structures similaires disponibles dans la littérature [41-46].

Exposure Devices for nsPEFs / Dispositifs d'Exposition pour les nsPEFs

Biological, pre-clinical and clinical electroporation (EP) applications require proper apparatuses to be performed in safe, repeatable and efficient conditions. Generally, aside a series of measurement equipment (e.g. oscilloscopes, microscopes, ...), two main components are needed to deliver pulsed electric fields: a pulse generator [1-4] and a delivery chamber [5-11].

As already explained, there is a great variety of pulses used in EP (trapezoidal monopolar and bipolar, exponential, gaussian, ...), yet they are categorized in two families based on their length and intensity: in standard EP (μs-msPEF) [12] and nanosecond EP (nsPEFs) [13]. The latter family has gained grate interest in the scientific community for such capabilities, however they are chronologically more recent (2000's) because of the peculiar technology they require, namely the ability to reliably generate and deliver to the biological load these ultra-short intense pulses.

In bench-top sized electrical systems involving signals with frequencies below 1 MHz or with duration longer than 1 μs, i.e. when dealing with μs-msPEFS, propagation related phenomena through the electrical connections can be considered negligible and it can be assumed that all points in a good electrical conductor reach the same voltage simultaneously ensuring a good matching between the source and the load, which simplify the experimental set-up.

On contrary, nsPEFs must be generated ad transmitted following appropriate specifications. The main features that the generators mast own are related with the length and the intensity of the pulses produced [1-4]. The effect of nsPEFs is induced directly on the interfacial water at the cell and/or organelle membrane level meaning that the charge membrane build up can be neglected. As a consequence, the targeting of subcellular structures requires the pulse rise time to be much less than the charging time of the plasma membrane and the pulse duration itself should be kept shorter than the time required for the onset of EP of the outer membrane. Additionally, the electric field needs to be much higher than field strengths provided with μs-msPEFs in order to target cell organelles or their mem-

branes. The required electric field for the poration of organelle membranes scales inversely with the organelle diameter and the pulse length. Based on the experimental evidences [14], electric field strengths on the order of 5 MV/m are necessary for a single 10 ns pulse to induce subcellular effects.

Reliable nsPEF generator is a necessary but not sufficient prerequisite for reproducible experimentation. There are different aspects that can have a significant impact on the experimental conditions, among which the signal propagation [15]. The voltage signal, once properly generated from a 50 Ω source, must be delivered to the usually low impedance biological load (in the order of 10s Ω), meaning that a broad band impedance matching is required to apply the signal to the biological sample without deformation of spectral and temporal contents. Hence a careful design of the applicator is necessary to realize a broadband devices, considering that the large spectral components of the most used nsPEFs span from MHz up to GHz.

Some papers designed devices to deliver *in vitro* nsPEF with duration down to 10 ns [16-21]. In these works it has been proven that the requisite to provide an undistorted signal can be followed quite easy without strict problems of impedance matching of the structure by dimensioning the micro-device only on the basis of the biological sample impedance. However, as soon as the time duration of the pulse goes down to 5 ns and the rise and fall time of the signal to fractions of ns, the impedance matching proper of a microwave (MW) propagating structure becomes necessary otherwise a distorted signal is delivered to cells.

Therefore two main prerequisites must be met to properly design this exposure systems, named microchambers, for nsPEFs:

- A good efficiency to reach the intensity needed for EP of intracellular components
- A pulsed signal must propagate without attenuation of the plateau and distortion of the rise and fall time

In this Chapter to satisfy these requirements we designed an exposure device, based on MW propagating systems, able to deliver pulses down to 1 ns, with rise an fall time of 1.5 ns and efficiency above the 96%. In Subsection **5.1.1**, we target the features our device should have to improve the current state of the art. The following Subsection, **5.1.2**, is dedicated to the description of the synthesis procedure based on available analytical closed-form expressions we used for the dimensioning of our guiding structure, to the illustration of the numerical model for its optimization and to summarize the measurements of different cell buffers carried out to solve a reliable and realistic model of the cell suspension. In Subsection **5.1.3**, we characterize the efficiency and the frequency behavior of our microchamber in two different configurations: for single- and multi-cell experiments. Finally, in **5.1.4** we discuss our findings highlighting the main advantages proposed.

References

[1] A. Kuthi, P. Gabrielsson, M.R. Behrend, P.T. Vernier, M.A. Gundersen, Nanosecond Pulse Generator Using Fast Recovery Diodes for Cell Electromanipulation, IEEE Trans. Plasma Sci. 33 (2005) 1192-1197.

[2] J.F. Kolb, S. Kono, K.H. Schoenbach, Nanosecond pulsed electric field generators for the study of subcellular effects, Bioelectromagnetics. 27 (2006) 172-187.

[3] J.M. Sanders, A. Kuthi, Y.-H. Wu, P.T. Vernier, M.A. Gundersen, A linear, single-stage, nanosecond pulse generator for delivering intense electric fields to biological loads, IEEE Trans. Dielectr. Electr. Insul. 16 (2009) 1048-1054.

[4] C. Merla, S. El Amari, M. Kenaan, M. Liberti, F. Apollonio, D. Arnaud-Cormos, et al., A 10- High-Voltage Nanosecond Pulse Generator, IEEE Trans. Microw. Theory Tech. 58 (2010) 4079-4085.

[5] M. Fromm, L.P. Taylor, V. Walbot, Expression of genes transferred into monocot and dicot plant cells by electroporation, Proc. Natl. Acad. Sci. 82 (1985) 5824-5828.

[6] R.A. Gilbert, M.J. Jaroszeski, R. Heller, Novel electrode designs for electrochemotherapy, Biochim. Biophys. Acta BBA - Gen. Subj. 1334 (1997) 9-14.

[7] Cliniporator, IGEA http://www.igeamedical.com/oncology/cliniporator.

[8] M. Rebersek, S. Corović, G. Sersa, D. Miklavčič, Electrode commutation sequence for honeycomb arrangement of electrodes in electrochemotherapy and corresponding electric field distribution, Bioelectrochemistry Amst. Neth. 74 (2008) 26-31.

[9] S. Mazéres, D. Sel, M. Golzio, G. Pucihar, Y. Tamzali, D. Miklavcic, et al., Non invasive contact electrodes for in vivo localized cutaneous electropulsation and associated drug and nucleic acid delivery, J. Control. Release Off. J. Control. Release Soc. 134 (2009) 125-131.

[10] W.G. Lee, U. Demirci, A. Khademhosseini, Microscale electroporation: challenges and perspectives for clinical applications, Integr. Biol. 1 (2009) 242-251.

[11] N. Hu, J. Yang, S.W. Joo, A.N. Banerjee, S. Qian, Cell electrofusion in microfluidic devices: A review, Sens. Actuators B Chem. 178 (2013) 63-85.

[12] J.C. Weaver, Y.A. Chizmadzhev, Theory of electroporation: A review, Bioelectrochem. Bioenerg. 41 (1996) 135-160.

[13] L. Chopinet, M.P. Rols, Nanosecond electric pulses: a mini-review of the present state of the art, Bioelectrochemistry Amst. Neth. 103 (2015) 2-6.

[14] K.H. Schoenbach, S. Katsuki, R.H. Stark, E.S. Buescher, S.J. Beebe, Bioelectrics-new applications for pulsed power technology, IEEE Trans. Plasma Sci. 30 (2002) 293-300.

[15] A. Silve, J. Villemejane, V. Joubert, A. Ivorra, L.M. Mir, Nanosecond pulsed electric field delivery to biological samples: Difficulties and potential solutions, Adv. Electroporation Tech. Biol. Med. Boca Raton FL CRC Press Taylor Francis Group. (2011).

[16] Y. Sun, P.T. Vernier, M. Behrend, L. Marcu, M.A. Gundersen, Electrode microchamber for noninvasive perturbation of mammalian cells with nanosecond pulsed electric fields, IEEE Trans. NanoBioscience. 4 (2005) 277-283.

[17] P. Krishnaswamy, A. Kuthi, Meng-Tse Chen, Shih-Jui Chen, P.T. Vernier, M.A. Gundersen, Compact high voltage subnanosecond pulsed power delivery system for biological applications, in: Pulsed Power Conf. 2007 16th IEEE Int., 2007 pp 476-480

[18] C. Dalmay, J. Villemejane, V. Joubert, O. Français, L.M. Mir, B. Le Pioufle, Design and realization of a microfluidic device devoted to the application of ultra-short pulses of electrical field to living cells, Sens. Actuators B Chem. 160 (2011) 1573-1580.

[19] C. Dalmay, J. Villemejane, V. Joubert, A. Silve, D. Arnaud-Cormos, O. Français, et al., A microfluidic biochip for the nanoporation of living cells, Biosens. Bioelectron. 26 (2011) 4649-4655.

[20] D. Arnaud-Cormos, P. Leveque, Y.-H. Wu, J.M. Sanders, M.A. Gundersen, P.T. Vernier, Microchamber Setup Characterization for Nanosecond Pulsed Electric Field Exposure, IEEE Trans. Biomed. Eng. 58 (2011) 1656-1662.

[21] Y.-H. Wu, D. Arnaud-Cormos, M. Casciola, J.M. Sanders, P. Leveque, P.T. Vernier, Moveable Wire Electrode Microchamber for Nanosecond Pulsed Electric-Field Delivery, IEEE Trans. Biomed. Eng. 60 (2013) 489-496.

5.1 A Versatile Microchamber for nsPEFs experiments

The emergence of nanosecond pulsed electric fields (nsPEFs) for intracellular electromanipulation experiments implies the application of extremely short (ns) high intensity (MV/m) electric field pulses. Specific pulse generators and miniaturized applicators are necessary to properly deliver this category of voltage signals to biological loads. In this context we propose a numerical design of a versatile nsPEFs applicator, developed following the guidelines typical of microwave propagating systems, which ensures a reliable propagation of such short pulses from the source to the load. The designed microchamber is suitable for *in vitro* exposure to pulses with duration down to 1-3 ns during single and multi cell experiments. Further features are: low power consumption thanks to its high efficiency (above 0.95), high cell viability by the integration of microfluidic components, real time monitoring of the biological sample and of the pulse propagation, reduced radiation and fringing field to ensure electromagnetic compatibility and compliance with safety standards. These features can be considered as designing rules for new nanosecond and subnanosecond applicators, to ensure experimental repeatability and reproducibility when the impact of propagation on pulse signals is no more negligible.

5.1.1 Introduction

In recent years, thanks to the great improvements in micro and nano fabrication techniques, a number of devices has been conceived for single cell analysis, identification, screening, and manipulation also in combination with chemical or physical agents (e.g. fluorescent dyes, electromagnetic (EM) fields, temperature) [1,2]. Microchamber devices, able to discriminate single cell dielectric properties in real-time and integrated with microfluidic techniques, have been given increasing consideration, being an accurate low-cost and label-free approach for cell status identification, essential for different in vitro biological studies [3]. The main benefits of these technologies consist in their miniaturization and parallelization capabilities, as well as real-time observation of cell behavior when transparent materials are used for the device fabrication.

Another great challenge in the application of micro-devices in biology is related to cell electroporation and nanoporation [4], whose application on cells has proven to increase the cell membrane permeability by means of electric field pulses [5-7]. In particular electric pulses of few nanoseconds (known as nsPEF) due to their large frequency spectrum (up to few GHz), are able to completely penetrate cells down to fine intracellular structures, hence making possible an interaction at both cellular and subcellular level [8-10]. For this reason, applications based on nsPEFs have gained increasing attention being exploitable for a number of alternative medical treatments (e.g. highly-localized and low-energy cancer treatment, wound healing, neuro-stimulations) [11].

From the combination of the recent developments of microtechnologies / microfluidics

techniques and the requirements of penetrating cells down to fine intracellular structures using nsPEFs, the design and fabrication of new innovative devices for biology applications has come out. The delivery of a nsPEF signal to the cells is quite hard: the signal has to be provided to the biological sample without deformation of spectral and temporal contents, hence it requires a careful design of the microchamber applicator. As far as the time duration of the pulses decreases, traditional electroporation devices (e.g. electroporation cuvette) are no more adequate to be used [12,13]. In fact, the large spectral components of the most used nsPEFs, available in literature, span from MHz (hundred of ns of pulse duration with tens of ns for rise and fall time) up to GHz (single ns of pulse duration with fractions of ns for rise and fall time) [14,15]. In such cases broadband devices in the radiofrequency and microwave (MW) range seem unavoidable and designing rules typical of MW propagating systems [16-18] become the guidelines for the implementation of these new micro-scale devices, suitable for nsPEF applications.

Some papers addressed the problem of delivering to few cells nsPEF with duration down to 10 ns [19-24]. In those papers it has been proven that the requisite to provide an undistorted signal can be followed quite easy without strict problems of impedance matching of the structure by dimensioning the micro-device only on the basis of the biological sample impedance. However, as soon as the time duration of the pulse goes down to 3 or even 1 ns, the impedance matching proper of a MW propagating structure becomes necessary otherwise a distorted signal is delivered to cells.

The other relevant aspect, for which micro-scale devices are suitable for nsPEF applications, is related to the intensity of the electric field to be generated on the sample. In fact the reduced duration of the pulse, which guarantees the penetration inside the cell and organelles, requires in parallel a very high intensity of the electric field (MV/m). Moreover there is attention to optimize the efficiency, often defined as the ratio of the measured voltage at the sample over the voltage applied by the generator (V_{out}/V_{in}). The best performances reached in terms of efficiency range from 0.66 [23] to 0.75 [22].

In this Section we propose the design of a versatile nsPEF applicator for in vitro experiments able to deliver pulses with duration down to 1 ns and with an high efficiency. The accomplishment of the following features was taken into account during the design of the delivery system:

- Preservation of the signal integrity through a broadband matching, allowing the propagation of both extremely short signals down to 1 ns as well as long pulses (μs)
- Versatile use for both single cell exposure and multi cell experiments, to answer the need for a flexible experimentation
- High efficiency to limit power consumption
- Real-time monitoring of the biological sample, by using transparent metallic components (e.g. Indium Thin Oxide ITO)

- High cell viability maintenance, thanks to microfluidic channels
- Real-time measurements to monitor the voltage passing through the line by using a four ports device
- Low radiated power to ensure the EM compatibility with the environment to satisfy safety standards

To fulfill these prerequisites a device based on a coupled microstrip line was chosen among different possible EM propagating planar structures [25]. Such an open planar system permits an easy handling of the cells and preserves their viability, by incorporation of microfluidic channels. To make possible the flowing of the cells suspension through the exposure region, a channel can be shaped in the covering of the structure realized in polydimethylsiloxane (PDMS); this allows the exposure of a single cell or multiple cells on the same EM structure only by varying the orientation of the channel in the cover.

The choice of a coupled microstrip line has another major advantage making such structure extremely appealing. In fact being a four-port system, the coupled microstrip line allows multiple and simultaneous access points for measurements, making possible to have a real-time monitoring of the transmitted and reflected electric power.

In our study, the coupled microstrip line system consists of two coplanar strips, a quartz glass substrate and an ITO transparent ground for the real-time monitoring of the biological sample by inverted microscopy. Finally, the efficiency and the broadband matching were ensured by a preparatory analytical synthesis procedure which, starting from a given characteristic impedance and distance between the strips, returns the sizing of the coupled microstrip lines scheme, that was optimized and validated by means of numerical modeling.

5.1.2 Methods

The design of the microchamber was based on the coupling of two transmission lines set close enough to each other such that EM energy passing through one is coupled to the other. The two parallel coupled lines are based on microstrip planar technology in order to obtain: i) a propagating quasi transversal electromagnetic (TEM) mode structure; ii) wide band matching up to one GHz frequency; iii) high performance in terms of E field magnitude within the channels; iv) control and accessibility of the exposure sample; v) an easy integration with microfluidic features. The resulting structure is a parallel coupled microstrip line, thus a four-ports microwave passive device, see Figure 5.1 (a) for a schematic of the structure cross section and Fig. 5.1 (b) for a top view of the device.

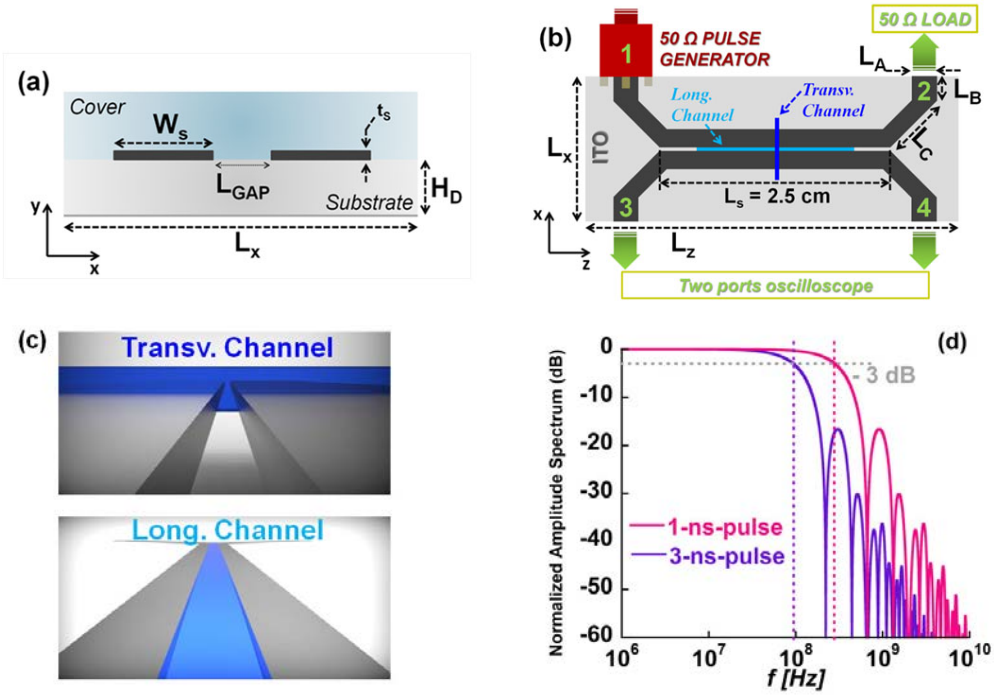

Figure 5.1: Schematic of the device (a, b, and c). a) Cross section, with W_S the width of the strips, L_{GAP} the gap between them, t_s their thickness, H_C height of the PDMS cover, H_S height of the substrate and L_x of the device along the x direction. b) Device top view, showing the connections with the generator, the load and the two ports oscilloscope, as well as the two possible configurations of the loaded channel. c) Details of the loaded channel placed transversal and longitudinal with respect to the device conductors. d) Spectral content of two trapezoidal nanosecond electric pulses: a 1 ns duration, 0.5 ns rise/fall times (named 1-ns-pulse) in magenta solid line, and a 3 ns duration, 1.5 ns rise/fall times (named 3-ns-pulses) in violet solid line

5.1.2.1 Synthesis procedure

The synthesis procedure was based on available analytical closed-form expressions relating the cross section geometry of the device to its characteristic impedance [26]. For a

characteristic impedance (Z_0) of 50 Ω and a gap between the strips (L_{GAP}) of 50 μm, this synthesis procedure determined the height of the substrate (H_D) to be 460 μm and the width of the strips (W_S) to be 750 μm, while thickness of the strip t_S and the one of the ground are negligible (see Fig. 5.1 (a)).

This initial configuration, giving the transversal section in terms of impedance matching of the odd modes, was the starting one for the numerical optimization. Numerical simulations were carried out through the commercial software HFSS ANSYS Academic Research, Release 13.0, the geometry and electrical properties of the different simulated studied structures are summarized in Table 5.1. The scope was to optimize the coupling between the two lines obtaining high values of electric field intensity inside the channel, to ensure a high efficiency of the structure while maintaining low radiation of such an open line.

Units in mm

	Width	**Length**		**Strip**		**Gap**	**Substrate**
	L_x	L_z	W_S	t_S	L_S	L_{GAP}	H_D *Material*
C. μ-S.	5	25	0.631	0.045	25	0.050	0.660 Qtz ($\epsilon_r = 3.78$)
μ-C.	16	52	0.631	0.045	25	0.050	0.660 Qtz ($\epsilon_r = 3.78$)

	Transv.			**Long.**			**Material**
	Width	*Length*	*Thick.*	*Width*	*Length*	*Thick.*	
W. Chan.	5.0	0.1	0.1	0.050	10	0.045	$\epsilon_r = 76$ $\sigma = 1$
Cover	16	52	3.3	16	52	3.3	PDMS ($\epsilon_r = 2.80$)

Transition Branch	**Input tract**	**Right tract**	**Diagonal tract**
	L_A	L_B	L_C
	1.261	0.904	10

Table 5.1: Geometrical and electrical characteristics of the schemes modeled: coupled microstrip lines and microchamber both for single-cell (transversal channel) and for multicell (longitudinal channel) exposures. For each component, dimensions (in mm) and electrical properties are reported
C. μ-S. - Coupled μ-Strip
μ-C. - μ-Chamber
Qtz - Quartz
W. Chan.- Water channel

5.1.2.2 Coupled microstrip line: numerical design

Simulations were performed from 0.1 to 1 GHz using an adaptive solution following the criterion of S-parameters optimization, which resulted in a mesh element minimum size of 7.95 μm and a maximum size 59.76 μm in the loaded channel. The structure was fed in the odd-configuration with 1 W on the waveguide port (Port 1 in Fig.5.1 (b)).

The metallic lines and the ground were modelled as perfect electric conductor (PEC), while the dielectric transparent substrate as quartz. The channel was considered transversal or longitudinal with respect to the direction of propagation (z-direction) of the quasi TEM mode inside the structure (Fig. 5.1 (c)). It was considered loaded with biological solution with relative permittivity (ϵ_r) equal to 76 and conductivity (σ) of 0.1 and 1 S/m measured as described in the 5.1.2.4-*Complex permittivity measurements*.

The final dimensions (see Table 5.1) of the coupled microstrip lines are $L_{GAP} = 50$ μm, $W_S = 631$ μm and $H_D = 660$ μm: while the gap between the lines ($_{GAP}$) remains the same as the analytical dimensioning, the thickness of the quartz glass substrate (H_D) has increased, going in the direction of encouraging odd modes versus the even ones and thus minimizing the risks of a mechanical break; finally the width of the metallic lines (W_S) has decreased favoring the coupling between the two lines.

5.1.2.3 Single-cell and multi-cell microchambers: final design

The design for the final microchamber followed the general approach used for directional couplers based on microstrip technology, with the main line bended and prolonged up to the connector of the coaxial cable feeding the structure (Port 1, Fig. 5.1 (b)). In order to minimize the dispersion due to phase velocities of even and odd modes propagating in the coupled line, the length of the central conductor has been kept well below a quarter-wave length.

Port 1 and Port 2 need to be provided with power connectors, since on the main line a power pulse is traveling (for final use Port 2 will be closed on a matched load). The two remaining ports are used to monitor in real-time the voltage passing through the line; therefore Port 3 and Port 4 can be connected with standard coaxial connectors to an oscilloscope without the need of high performance attenuators. In this way the acquisition of the input and output pulses will be possible during the experiment.

The chosen bending was of 45° and it was realized with the aim of maintaining a good matching to the 50 Ω impedance source, all other dimensions are reported in Table 5.1.

The structure obtained in such a way presents a high level of versatility. In fact, by only varying the position of the channel with respect to the direction of signal propagation, either longitudinal or transversal, it is possible to have our system suitable for two different

kinds of experiments. If the channel is transversal to the power flow (Fig. 5.1 (c) *Transversal Channel*) we obtain a structure useful for single cell exposure: the channel will be equipped with microfluidics control and the cell will be trapped inside the volume of exposure at the center of the conductor slots. Otherwise, if the channel will be placed along the direction of the lines between strips (Fig. 5.1 (c) *Longitudinal Channel*), we will obtain a multi cell exposure since the volume exposed will be the volume of the overall channel. In both cases, to make possible the flowing of the cell solution and to properly shape the channel it has been considered the covering of the structure realized in PDMS. As concerns the single cell exposure system, the effect of the variation in solution conductivity is negligible. When the channel is longitudinal, as in the case of multi cell exposure, the conductivity value has an impact on the performances of the structure. Therefore for the latter case, the channel was loaded with different biological solutions. To characterize our system in the conditions closest to experiments we measured the cell buffers relative permittivity and conductivity, as explained in 5.1.2.4-*Complex permittivity measurements*.

5.1.2.4 Complex permittivity measurements

Briefly, the complex permittivity measurements of buffer solutions were carried out using a vector network analyser (Agilent N5302 A) connected to an open-end coaxial sensor (Agilent slim form probe 85070 E) inserted into the liquids; reflection coefficients ($|S_{11}|$ parameters) as a function of frequency were acquired and the depending complex permittivity was computed using a custom algorithm [27,28]. A suitable calibration using air, acetone, and distilled water (milli Q) was carried out before the buffer measurements to de-embed any type of artefacts due to probe defects (aging, spurious capacitances, geometrical imperfections) as fully detailed by Piuzzi et al. [28]. Phosphate buffer saline (PBS) solution (purchased by EuroClone) and a dilution at 10% of this buffer (named PBS10%) were measured and characterized in terms of permittivity and conductivity being among the most used cellular buffers.

Solution	ϵ_∞	ϵ_s	$\mathbf{f}_r$ **[GHz]**	σ **[S/m]**
PBS	76.8	6.9	18.5	1.0
PBS 10%	78.7	7.0	19.0	0.1

Table 5.2: Cole and Cole parameters for the measured buffer solutions

Measurements were performed between 500 MHz and 5 GHz, the lower limit corresponds to the low operational frequency of the coaxial sensor. An intermediate frequency bandwidth of 1 kHz was used to get accurate results [28]. For each liquid (measured volume 200 mL) five independent measurements at 26 °C were carried out. Complex permittivity averages were computed for Cole and Cole parameters extraction (using a MATLAB routine) and statistical uncertainty evaluated over the repeated acquisitions with a cover factor of 2, resulting within 5%. The obtained Cole and Cole parameters for these liquids, reported in Table 5.2, are the static permittivity (ϵ_s), the residual permittivity at high fre-

quency (ϵ_∞), the frequency of relaxation (f_r), and the conductivity (σ). For the two cellular buffers measured, the difference in static permittivity values is within statistical uncertainty of 5%, therefore a unique value of 76 has been used in simulations.

5.1.3 Results

In the following, the results will be discussed separately for the two configurations: single cell (tranversal channel) and multi cell (longitudinal channel). It will be shown how the final microchamber for single cell exposure has even better performances with respect to the initial coupled microstrip line in terms of structure matching (reflection coefficient $|S_{11}|$), while presents a still acceptable transmission coefficient ($|S_{21}|$ higher than -1.5 dB). For the multi cell microchamber (longitudinal channel), the channel positioning has a not negligible impact on both matching and transmission performances, in fact it travels all along the length of the chamber (Fig. 5.1 (c)). Nevertheless the overall behavior of the chamber confirms its ability to propagate nsPEFs down to 3 ns duration.

5.1.3.1 Single-cell exposure

The goodness of the impedance matching procedure adopted can be seen by the $|S_{11}|$ reported in Fig. 5.2 (a), while the quality of the propagation inside the structure is quantified by the $|S_{21}|$ reported in Fig. 5.2 (b); as a whole Fig. 5.2 demonstrates how the microchamber has a good behavior in frequency, with low reflection and high transmission.

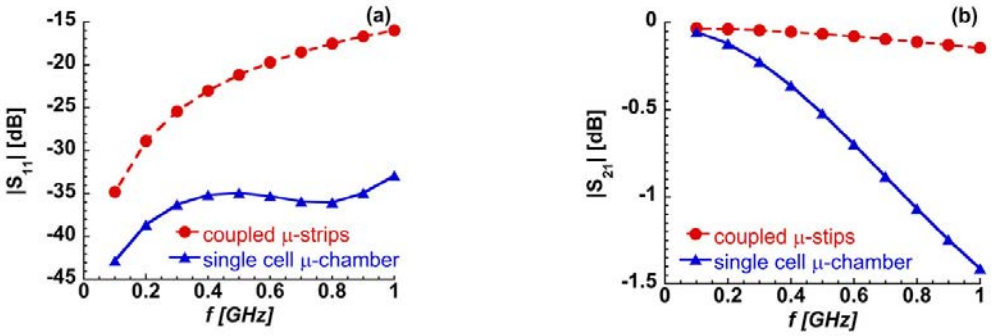

Figure 5.2: Scattering parameters, from 0.1 to 1 GHz, of the single cell microchamber (transversal channel). The reflection (a) and transmission (b) coefficients of the coupled microstrip lines (transversal channel) and the ones of the single cell microchamber are reported in red dashed and blue solid line, respectively

The influence of the conductivity of the buffer, loading the channel in the transversal orientation, is negligible (data not shown). Indeed, the reflection parameters for both the coupled microstrip and the single-cell microchamber are well below -30 dB, ensuring an excellent matching of the signal up to 1 GHz. The transmission coefficient (Fig. 5.2 (b)) of the microchamber for single cell shows a decrease from -0.60 dB at 100 MHz to -1.45 dB at 1

GHz with respect to the more flat trend of the coupled basic design, which never overcomes the -0.15 dB. Nevertheless a power loss of -1.45 dB seems still an acceptable value.

The scattering parameters related to the other two ports were estimated as an average value over the bandwidth: an attenuation of ∼11 dB and ∼41 dB is evaluated at Port 3 and Port 4, respectively. Although the values do not reach the ones of high performances power directional couplers, they are anyway comparable, ensuring a safe use of possible connected devices.

The EM behavior of the single cell microchamber in the considered bandwidth, permits in principle, a good transmission of pulses with duration down to 1 ns, since the most part of the spectral content (first lobe) of such pulses is restricted to 1 GHz (see Fig. 5.1 (d)). To verify this observation a trapezoidal extremely short pulse of 1 ns duration (1-ns-pulse), with a rise and fall time of 0.5 ns, was applied to Port 1 and measured at Port 2 (see Fig. 5.3 (a)).

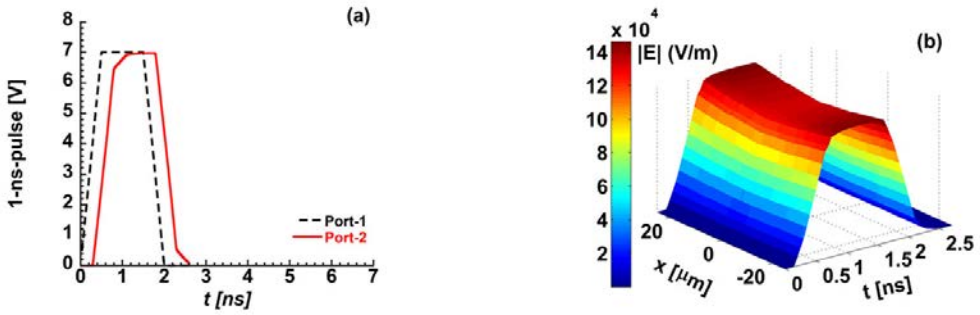

Figure 5.3: a) Electric signal 1-ns-pulse [V] over time, applied at Port 1 (black dashed line) and measured at Port 2 (red solid line). b) E field intensity along the x axis in the center of the channel, between the strips (gap L_{GAP}), at y = 30 μm over time

The applied voltage pulse signal (Port 1) propagates along the line with negligible distortion and almost no amplitude reduction for pulses down to 1 ns. In fact the voltage in time at the two ports (Fig. 5.3 (a)) shows that the signal was transmitted with no attenuation and a mild distortion along the line, ensuring that the biological target is properly exposed. The small delay (∼300 ps) at Port 2 seems acceptable for such applications.

Moreover, we defined the efficiency of the microchamber as the value of the normalized cross correlation between the input signal (at Port 1) and the detected signal (at Port 2) at 0 time lag, which corresponds to 0.98 (data not shown). To quantify the E field in the cell medium, its intensity over time was evaluated along the x axes in the centre of the channel (z = 0 mm) at 30 μm from the quartz substrate (y direction) and reported in Figure 5.3 (b). The E field reaches 140 kV/m in x = 0 mm when 7 V 1-ns-pulse was applied to Port 1. This indicates that to obtain the tens of MV/m needed for nsPEFs applications only 500 V must be applied, avoiding unwished problems such as high power consumption. Figure 5.3 (b) also shows a good homogeneity of the E field that we further evaluated over the region of interest (ROI), defined as the volume between the strips of dimension 50 x 40 x 100 μm^3,

through the Coefficient of Variation (CV), defined as standard deviation over mean value. A CV = 0.038, indicates that all the cells flowing inside the channel will be exposed to almost the same field with inhomogeneity around 3.8%.

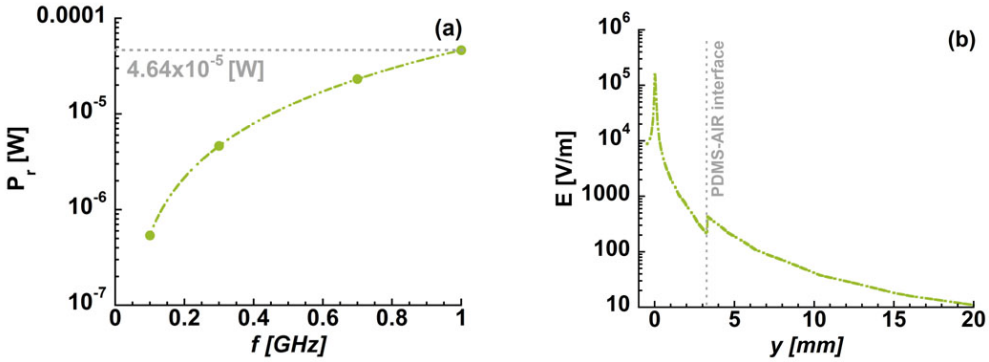

Figure 5.4: a) Radiated power estimated at 0.1, 0.3, 0.7 and 1 GHz. b) Electric field along the y axis perpendicular to the strips plane in the middle of the channel (x = 0) and the center of the structure (z = 0); the origin (y = 0) is taken at the interface between the substrate and the channel

Finally, possible electromagnetic compatibility problems between the intense E field produced during the pulse and external electronic equipments were evaluated in terms of radiated power (P_r) and the electric field (E_y) along the perpendicular to the plane of the strips (Fig. 5.4 (a) and 4 (b), respectively). The P_r was estimated to be $4.6{\cdot}10^{-5}$ W (at 1 GHz) for 1 W of input power, and the field with a decay (D_{dB}) per mm of D_{dB} 17.5 dB/mm, with the origin (y = 0) taken at the interface between the substrate and the channel, thus ensuring an acceptable EM compatibility and safety.

5.1.3.2 Multi cell exposure

To obtain a multi cell exposure the volume treated will be the volume of the overall channel inserted in the gap along the lines for a total length of 10 mm (Fig. 5.1 (c) and Table 5.1). In this case the presence of a conductive medium, where the coupling of the strips takes place, changes the local impedance of the structure, affecting the overall frequency behavior of the device.

Despite we register a worsening of the scattering parameters with respect to the single cell configuration for the same high conductive medium, the reflection coefficient ($|S_{11}|$) never crosses -10 dB (Fig. 5.5 (a)), ensuring a good matching up to 1 GHz. Whereas the transmission coefficient ($|S_{21}|$) exhibits a more abrupt decrease, (Fig. 5.5 (b)), with a minimum of -4.4 dB at 1 GHz, possibly causing distortions and attenuation to the extremely short pulses (1-ns-pulse). As expected, with the decreasing of the conductivity the S-parameters improve especially at low frequencies, but without drastically changing their trends.

To prove the ability to transmit in any case very short pulse of duration slightly longer,

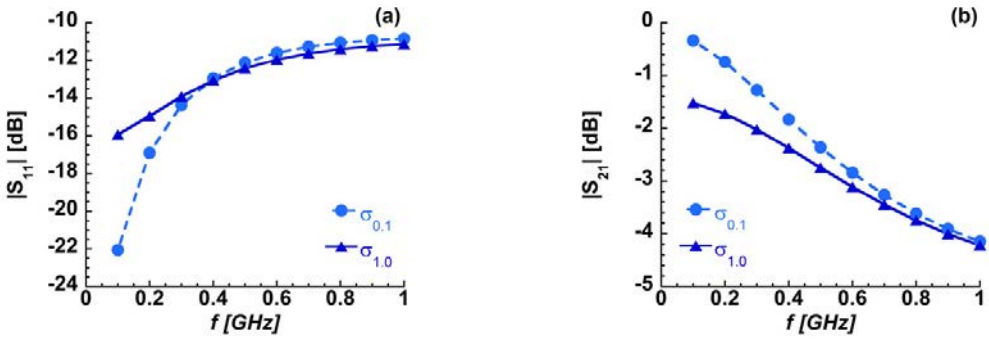

Figure 5.5: Scattering parameters, from 0.1 to 1 GHz, of the multi cell microchamber in the longitudinal channel configuration. The reflection (a) and transmission (b) coefficients of the low (0.1 S/m) and high (1.0 S/m) conductive media considered are reported in light blue dashed, and blue solid lines respectively

a trapezoidal signal, of 3 ns duration and 1.5 ns of rise/fall time, was applied to Port 1 and acquired at Port 2 (see Fig. 5.6 (a)) having the loaded channel a conductivity of 0.1 S/m. The voltage in time at the two ports (Fig. 5.6 (a)) shows that the signal was transmitted along the line with a negligible attenuation and distortion, assuring that the chamber for the multi cell use can be employed to deliver nsPEFs with duration down to 3 ns. The efficiency of the device in this configuration reaches 0.97.

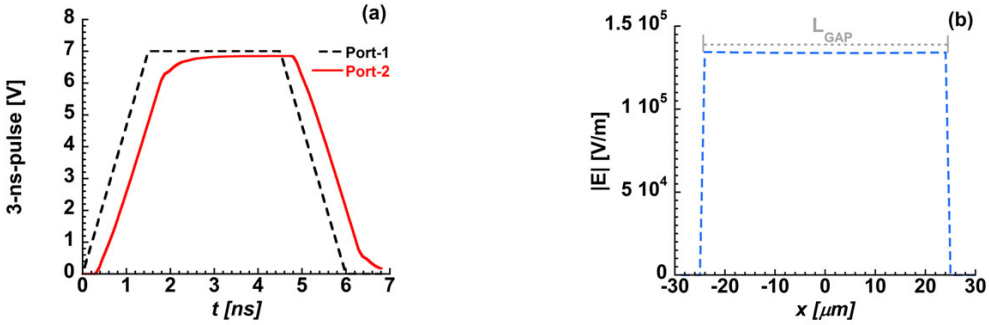

Figure 5.6: a) Electric signal 3-ns-pulse [V] over time, applied at Port 1 (black dashed line) and obtained at Port 2 (red solid line). b) E field intensity along the x axis in the center of the channel, between the strips (gap L_{GAP}), at y = 30 μm

Figure 5.6 (b) shows the electric field in the x direction perpendicular to the direction of propagation z, between the strips, where the cells are suspended. In this region the field is extremely homogeneous with a very low CV evaluated in the same ROI as the transversal configuration, which improves roughly of a factor 6 (CV = 0.006) reaching an intensity of 1.3 kV/cm, when 7 V are applied at Port 1. Consequently, also in this configuration it is possible to reduce the high power consumption, since to obtain tens of MV/m it is necessary to apply ~540 V.

5.1.4 Discussions and Conclusions

We suggest general guide lines to pursue in order to improve the performances of delivery systems for subnanosecond and nanosecond pulses and ensure experimental repeatability and reproducibility can be rationalized in the flow chart of Fig. 5.7. Considering that the general requisites to be fulfilled can be summarized in the following points:

- Preservation of the signal integrity through a broadband matching, allowing the propagation of both extremely short signals down to 1 ns as well as long pulses (μs)
- Versatile use for both single cell exposure and multi cell experiments, to answer the need for a flexible experimentation
- High efficiency to limit power consumption
- Real-time monitoring of the biological sample
- High cell viability maintenance, thanks to microfluidic channels
- Real-time measurements to monitor the voltage passing through the line
- Low radiated power to ensure the EM compatibility with the environment to satisfy safety standards

the first choice to take is which type of experimental protocol should be adopted: in the case of bulk EP, that allow the treatment of higher volumes of cells (see Table 2.2), the possible adjustments that can be made to improve the scattering parameters are narrowed, as previously explained in Section 2.3.2.2; the other protocol available is microscale EP.

The latter can count on more degrees of freedom to comply with the requirements indicated and to obtain the desired matching in the frequency range of interest dictated by the length of the voltage pulse. There are numerous MW structure one can consider composed by coplanar, not coplanar, cylindrical, flat, transparent, opaque strips and substrates that can be equipped with microfluidic channels loaded with various cell solutions and positioned in different configurations to allow for single or multi cell exposure. The throughput of the multi cell exposure can be eventually increased by the realization of an array of channels. If not already commercially available or published, this propagating transmission lines must be theoretically characterized before the realization. Only thanks the numerical design it is possible to adjust and optimize the scattering parameters and the intensity of the electric field in the ROI by easily changing different variables, e.g. the dimensions and materials of the structure, the position and the conductivity of the loaded channel, and the transition to the feeding. Finally, the experimental validation of the predicted performances, through the measurements of the transmitted, reflected and radiated power, of the generated and delivered signal, is necessary to provide evidences of the goodness of the microchamber. At this stage, if the measured performances of the system agree

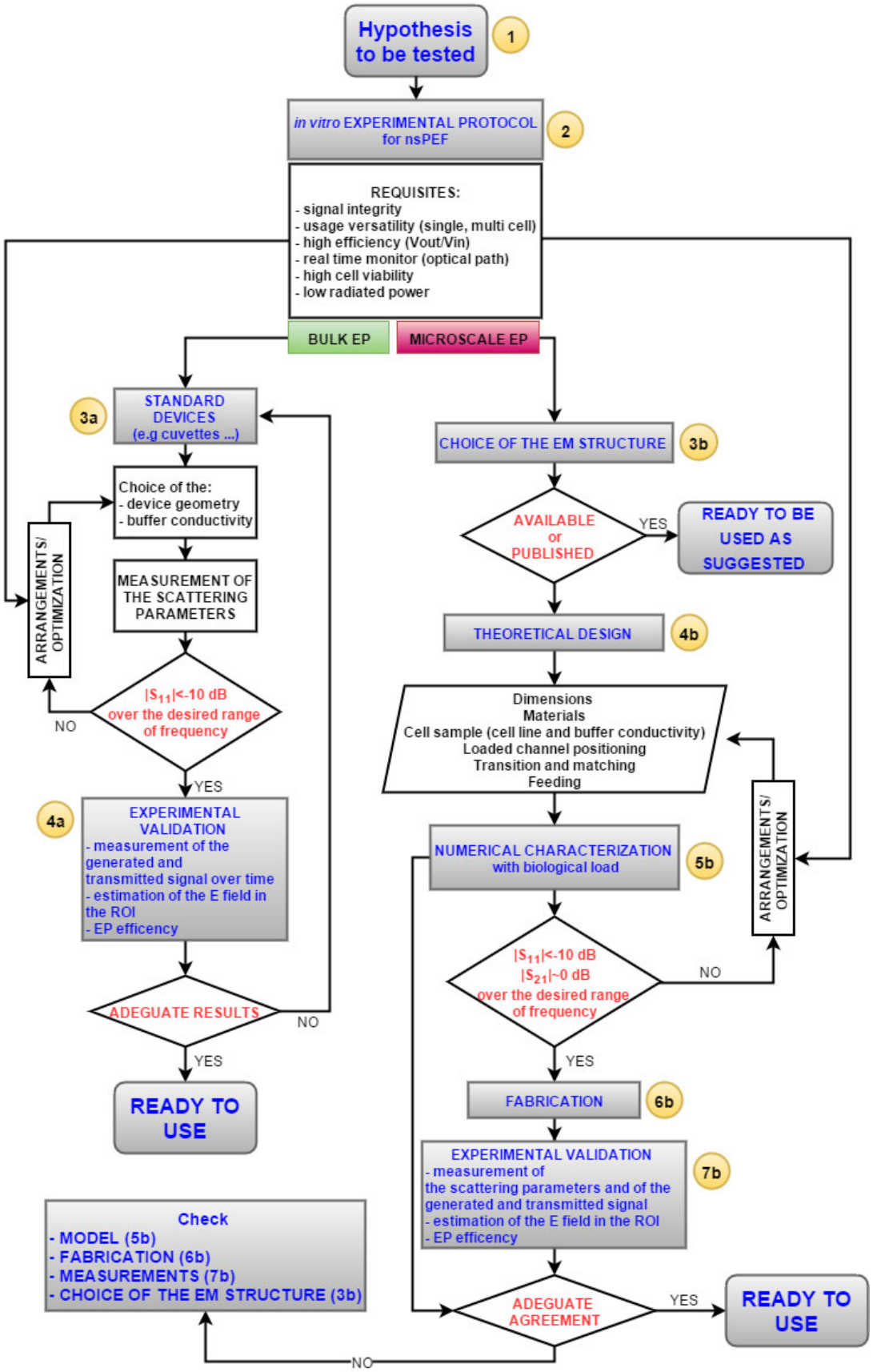

Figure 5.7: Standardized choice of the nsPEF device for optimal exposure conditions

with the theoretical ones, it is possible to perform EP experiments in safe and reliable conditions to produce an homogeneous and well controlled electrical field to the biological sample to ensure that cells are exposed to the same electric field intensity, independently from their position in the channel, and are therefore electropermeabilized in the same conditions.

Following this approach, we have designed a versatile microchamber for nsPEFs exposure useful to different experimental scopes. Indeed, by simply changing the PDMS cover it is possible to obtain a channel transversal or longitudinal with respect to the electric field propagation to hold the biological sample. The first configuration permits the trapping of a few number of cells in the gap between the strips allowing also a single cell exposure; whereas in the latter configuration multi cell experiments can be carried out since the volume of exposure will be the whole gap between the strips. Furthermore the PDMS cover coupled with the planar structure allows an easy handling of the cells and preserves their viability by allowing cell buffer flow.

The microchamber proposed is based on microstrip line technologies to overcome drawbacks of propagation phenomena related to the large spectral components of nsPEF signals (up to some GHz). Doing so, we ensured a broadband matching of the load with the generator, hence a constant value of the device impedance over the frequency band of interest (0.1-1 GHz) is obtained.

The reflection coefficient of the single cell microchamber is below -30 dB up to 1 GHz, while below -10 dB for the multi cell, indicative in both cases of a negligible mismatch between the generator and the applicator. However, the transmission coefficient in the two configurations shows a non-ideal behaviour, reaching -1.5 and -4 dB, respectively. As a consequence, the shorter pulse deliverable with negligible distortion and attenuation is a trapezoidal pulse of 1 ns for the single cell microchamber configuration, and 3 ns for the multi cell one.

The frequency performances of this device are an improvement compared to similar structures available in literature where the maximum frequency at -10 dB of the reflection coefficient is about 300 MHz [19-24] with consequent impact on the length of the pulse delivered without distortion (>3 ns). Additionally the efficiency, for the two configurations is above 0.95, coherently with the negligible attenuation observed.

For what concern the electric field intensity in the region of interest (ROI), i.e. in the gap between the strips where the loaded channel is set, it is homogenously distributed and reaches 130 and 140 kV/m, for the multi cell and the single cell respectively, when 7 V are applied at the input. This means that only 500 V are needed to deliver the tens of MV/m typical of nanosecond electroporation applications, reducing the power consumption of two folds with respect to previous reports [28].

This three conductors structure also ensures a low radiated power $4.46{\cdot}10^{-5}$ W (at 1 GHz)

for 1 W applied, usually halved compared to other planar structures (e.g. coplanar wave guides, microstip lines, slot lines).

Finally, the real-time monitoring of the cells is possible by inverted microscopy thanks to the use of a transparent ground (ITO) positioned below the quartz substrate. The three conductors set up allow also the real-time measurement of the pulse propagating through the structure, by direct connection with an oscilloscope via Ports 3 and 4, without the use of voltage probes that could introduce distortions depending on their bandwidth.

The evident advantages of the overall designing technique are related to ensuring experimental repeatability and reproducibility improving the know-how regarding the nsPEFs effects on living cells and their potentiality for therapeutic applications.

5.1.5 References

[1] H. Li, R. Bashir, Dielectrophoretic separation and manipulation of live and heat-treated cells of Listeria on microfabricated devices with interdigitated electrodes, Sens. Actuators B Chem. 86 (2002) 215-221.

[2] G. Mernier, N. Piacentini, T. Braschler, N. Demierre, P. Renaud, Continuous-flow electrical lysis device with integrated control by dielectrophoretic cell sorting, Lab. Chip. 10 (2010) 2077-2082.

[3] H.-L. Gou, X.-B. Zhang, N. Bao, J.-J. Xu, X.-H. Xia, H.-Y. Chen, Label-free electrical discrimination of cells at normal, apoptotic and necrotic status with a microfluidic device, J. Chromatogr. A. 1218 (2011) 5725-5729.

[4] R. Nuccitelli, K. Tran, S. Sheikh, B. Athos, M. Kreis, P. Nuccitelli, Optimized nanosecond pulsed electric field therapy can cause murine malignant melanomas to self-destruct with a single treatment, Int. J. Cancer J. Int. Cancer. 127 (2010) 1727-1736.

[5] L.M. Mir, H. Banoun, C. Paoletti, Introduction of definite amounts of nonpermeant molecules into living cells after electropermeabilization: direct access to the cytosol, Exp. Cell Res. 175 (1988) 15-25.

[6] M. Casciola, D. Bonhenry, M. Liberti, F. Apollonio, M. Tarek, A molecular dynamic study of cholesterol rich lipid membranes: comparison of electroporation protocols, Bioelectrochemistry. 100 (2014) 11-17.

[7] M. Szabo, M.I. Wallace, Imaging potassium-flux through individual electropores in droplet interface bilayers, Biochim. Biophys. Acta. (2015)

[8] SK.H. Schoenbach, S. Xiao, R.P. Joshi, J.T. Camp, T. Heeren, J.F. Kolb, et al., The Effect of Intense Subnanosecond Electrical Pulses on Biological Cells, IEEE Trans. Plasma Sci. 36 (2008) 414-422.

[9] R.P. Joshi, K.H. Schoenbach, Bioelectric Effects of Intense Ultrashort Pulses, Crit. Rev. Biomed. Eng. 38 (2010) 255-304.

[10] I. Semenov, S. Xiao, D. Kang, K.H. Schoenbach, A.G. Pakhomov, Cell stimulation and calcium mobilization by picosecond electric pulses, Bioelectrochemistry. 105 (2015) 65-71.

[11] L. Chopinet, M.-P. Rols, Nanosecond electric pulses: a mini-review of the present state of the art, Bioelectrochemistry Amst. Neth. 103 (2015) 2-6.

[12] C. Merla, S. El Amari, M. Kenaan, M. Liberti, F. Apollonio, D. Arnaud-Cormos, et al., A 10- High-Voltage Nanosecond Pulse Generator, IEEE Trans. Microw. Theory Tech. 58 (2010) 4079-4085.

[13] A. Silve, J. Villemejane, V. Joubert, A. Ivorra, L.M. Mir, Nanosecond pulsed electric

field delivery to biological samples: Difficulties and potential solutions, Adv. Electroporation Tech. Biol. Med. Boca Raton FL CRC Press Taylor Francis Group. (2011)

[14] C. Merla, A. Paffi, F. Apollonio, P. Leveque, G. D'Inzeo, M. Liberti, Microdosimetry for Nanosecond Pulsed Electric Field Applications: A Parametric Study for a Single Cell, IEEE Trans. Biomed. Eng. 58 (2011) 1294-1302.

[15] C. Merla, A. Denzi, A. Paffi, M. Casciola, G. D'Inzeo, F. Apollonio, et al., Novel Passive Element Circuits for Microdosimetry of Nanosecond Pulsed Electric Fields, IEEE Trans. Biomed. Eng. 59 (2012) 2302-2311.

[16] M. Liberti, F. Apollonio, A. Paffi, M. Pellegrino, G. d'Inzeo, A coplanar-waveguide system for cells exposure during electrophysiological recordings, IEEE Trans. Microw. Theory Tech. 52 (2004) 2521-2528.

[17] A. Paffi, M. Pellegrino, R. Beccherelli, F. Apollonio, M. Liberti, D. Platano, et al., A Real-Time Exposure System for Electrophysiological Recording in Brain Slices, IEEE Trans. Microw. Theory Tech. 55 (2007) 2463-2471.

[18] A. Paffi, F. Apollonio, G.A. Lovisolo, C. Marino, R. Pinto, M. Repacholi, et al., Considerations for Developing an RF Exposure System: A Review for in vitro Biological Experiments, IEEE Trans. Microw. Theory Tech. 58 (2010) 2702-2714.

[19] Y. Sun, P.T. Vernier, M. Behrend, L. Marcu, M.A. Gundersen, Electrode microchamber for noninvasive perturbation of mammalian cells with nanosecond pulsed electric fields, IEEE Trans. NanoBioscience. 4 (2005) 277-283.

[20] P. Krishnaswamy, A. Kuthi, Meng-Tse Chen, Shih-Jui Chen, P.T. Vernier, M.A. Gundersen, Compact high voltage subnanosecond pulsed power delivery system for biological applications, in: Pulsed Power Conf. 2007 16th IEEE Int., 2007 pp 476-480

[21] C. Dalmay, J. Villemejane, V. Joubert, O. Français, L.M. Mir, B. Le Pioufle, Design and realization of a microfluidic device devoted to the application of ultra-short pulses of electrical field to living cells, Sens. Actuators B Chem. 160 (2011) 1573-1580.

[22] C. Dalmay, J. Villemejane, V. Joubert, A. Silve, D. Arnaud-Cormos, O. Français, et al., A microfluidic biochip for the nanoporation of living cells, Biosens. Bioelectron. 26 (2011) 4649-4655.

[23] D. Arnaud-Cormos, P. Leveque, Y.-H. Wu, J.M. Sanders, M.A. Gundersen, P.T. Vernier, Microchamber Setup Characterization for Nanosecond Pulsed Electric Field Exposure, IEEE Trans. Biomed. Eng. 58 (2011) 1656-1662.

[24] Y.-H. Wu, D. Arnaud-Cormos, M. Casciola, J.M. Sanders, P. Leveque, P.T. Vernier, Moveable Wire Electrode Microchamber for Nanosecond Pulsed Electric-Field Delivery, IEEE Trans. Biomed. Eng. 60 (2013) 489-496.

[25] Leo G. Maloratsky, Reviewing the basics of microstrip, Microw. RF. 39 (2000) 79-88.

[26] R. Garg, I. Bahl, M. Bozzi, Microstrip Lines and Slotlines, Third Edition, Artech House, 2013.

[27] C. Merla, M. Liberti, F. Apollonio, G. d'Inzeo, Quantitative assessment of dielectric parameters for membrane lipid bi-layers from RF permittivity measurements, Bioelectromagnetics. 30 (2009) 286-298.

[28] E. Piuzzi, C. Merla, G. Cannazza, A. Zambotti, F. Apollonio, A. Cataldo, et al., A Comparative Analysis Between Customized and Commercial Systems for Complex Permittivity Measurements on Liquid Samples at Microwave Frequencies, IEEE Trans. Instrum. Meas. 62 (2013) 1034-1046.

Chapter 6

Perspectives / Perspectives

Ce chapitre décrit brièvement comment inspiré par nos résultats de simulations, nous travaillons actuellement d'une part pour étudier certaines propriétés des bicouches lipidiques (par exemple, la permittivité de l'interface eau / lipides) et le transport de molécules bioactives (par exemple colorants, médicaments, ...) afin de mieux caractériser les effets des champs pulsés électriques sur des cellules vivantes et de contribuer à l'élaboration de nouveaux protocoles qui permettent de mieux exploiter le potentiel de l'EP pour des applications thérapeutiques.

D'autre part un effort accru est en cours pour réaliser une micro chambre selon les modèles préétablis afin de vérifier ses performances et, à terme, de valider les résultats obtenus à partir de la partie de modélisation.

Perspectives / Perspectives

In the present work, we attempted to characterize some of electric properties (e.g. electric dipole moment, electric field distribution) of membrane models, namely lipid POPC bilayers with different concentration of cholesterol (0, 20, 30, 50 mol %); we found that with the increasing of cholesterol concentrations higher transmembrane voltages are needed to porate the membrane bilayer (Section 4.2). We computed the electric field distributions (see 4.1) and found that the cholesterol contribution has a negligible influence in the membrane electric field profiles. Also the electric dipole moment at the water/lipid interfacial region does not change dramatically, albeit a rise in the water orientation below the glycerol backbones (Section 4.1). However the water density profiles showed in the pure POPC bilayer the water penetrates more in the hydrophobic core both whit and without an external field applied (Section 4.1), meaning a favorable condition for pore formation. These results suggest that to give indications on the pore formation process other properties should be computed, e.g. the permittivity and diffusivity.

We also tried to rationalize experimental evidences of membrane permeablization to ions (Section 4.3) and small molecules (i.e. the peptide Tat_{11} and a siRNA molecule, see Section 4.4) through electropores to provide a model of the corresponding unknown molecular mechanism. When subject to microsecond pulses, i.e. the transmembrane voltage is above a critical value, we report for the peptide Tat_{11} a complete translocation in ∼10 ns without any interaction with the surrounding pore walls, and for the siRNA molecule a complete crossing in ∼30 ns despite its strong anchoring with the zwitterionic phospholipids headgroups, integrating experimental results. With our model we are able to shed light on the atomic mechanism of transport and on its time scale, which can be corroborated by other relevant observables, e.g. electric field distributions, pore hindrance, ...and that can be applied to other relevant molecules.

Finally, we designed an exposure device (Section 5.1) with a broadband frequency behavior, able to deliver ultra short electric pulses, down to 1 ns duration with rise and fall time of fractions of ns (i.e. with energy content up to some GHz), with high efficiency (above 0.90) to reduce the power consumption and to rich the desired intensity of electric field (MV/m), necessary to trigger the response of the plasma cell membrane and/or of the internal organelles. This should advance in the knowledge of nsPEFs effects on living cells and their potentiality for therapeutic applications. We are in the process of the realization

of our microchamber to verify its performances, and to carry out *in vitro* experiments with inverted microscopy coupled with fluorescent detection to study the permeabilization of cells and of their interior to extremely short nsPEFs.

Motivated by our molecular dynamic (MD) findings, we began to develop our work in two directions, both to improve the atomistic electroporation model. Below, we introduce the main purposes of these projects and to present some of the preliminary results.

6.1 Permittivity of water/lipid interfaces

Water near hydrated lipid bilayers plays an important role in understanding the mechanism of ultrashort pulses electric field (usPEFs) applications, both due to the assumption that water is the initiator of the pore creation process [1-4] and because water molecules in hydrophilic pores permit the transport of ions and molecules across the bilayer [5-7]. Moreover the dielectric properties of such hydration layers become fundamental for microdosimetry, if one wants a quantitative description of the electric distribution at nanometer resolution beyond the usual effective medium approach [8].

Several experiments have been carried out to study the phospholipids/water interface using various experimental methods: NMR [9], X-ray [10], IR/Raman [11], Terahertz Spectroscopy [12]. However to date, in the case of intense electric fields as the usPEF, the only way to have an insight on such molecular endpoints is by means of molecular dynamics (MD). In particular, several works have shed light on the structure and dynamics of phospholipid bilayers in aqueous solution at the atomic level of detail [13-15], addressing the questionable definition of the dielectric and low-dielectric regions of the lipid bilayers and observing that hydration water properties are highly dependent on the composition of the bilayer; nevertheless a detailed and accurate frequency description of the permittivity of these interfaces in presence of intense electric fields has not been carried out yet.

Our final aim is to estimate hydration layers dielectric permittivity frequency profiles in nanometer regions, when exposed to electric fields of high intensity as those of usPEF, for two different lipid bilayer compositions (with and without cholesterol), thus providing a way to link the molecular level to the continuum approach of the microdosimetry and dosimetry [16].

Stern et al. [13] derived an expression relating the static dielectric permittivity profile for a system nonuniform in one dimension to correlates between the net system dipole moment and the local polarization density. Lately, Gekle et al. [15] extended this methodology to frequency dependent profiles to obtain a spatially resolved dielectric tensor on the linear response level which follows from thermal fluctuations of the local polarization vector **P**(z).

Following these [13,15] approaches we implemented first the polarization correlation function:

$$c_\alpha(z,t) = \langle \mathbf{P}_\alpha(z,0) \cdot \mathbf{M}_\alpha(t) \rangle - \langle \mathbf{P}_\alpha(z) \cdot \mathbf{M}_\alpha \rangle, \tag{6.1}$$

where α is the normal or tangential component, $\mathbf{M}(\mathrm{t}) = \int_V \mathbf{P}(t) dV$ and stands for the overall system dipole moment, the angle brackets are time averages. The parallel component of the dielectric tensor in terms of the frequency f is:

$$\epsilon_{\|}(z,f) = 1 + \frac{\beta}{2\epsilon_0}\mathscr{L}[-\dot{c}_{\|}(z,t)], \tag{6.2}$$

with $\beta = \frac{1}{k_B T}$ the inverse of the thermal energy, and $\mathscr{L}$ the Laplace transformation of a function *g(t)*:

$$\mathscr{L}[g] = \int_0^\infty d\,t\, e^{-i2\pi f t}\, g(t). \tag{6.3}$$

For the perpendicular component we implemented:

$$\epsilon_{\perp}(z,f) = 1 + \frac{\frac{\beta}{\epsilon_0}\mathscr{L}[-\dot{c}_{\perp}(z,t)]}{1 + \frac{\beta}{V\epsilon_0}\mathscr{L}_{i2\pi f}[-\dot{C}\perp(t)] - \frac{\beta}{\epsilon_0}\mathscr{L}_{i2\pi f}[-\dot{c}_{\perp}(z,t)]}, \tag{6.4}$$

where V is the system volume and $C_{\perp} = \langle \mathbf{M}_{\perp}(0)\cdot\mathbf{M}_{\perp}(t)\rangle - \langle \mathbf{M}_{\perp}\cdot\mathbf{M}_{\perp}\rangle$ is the system correlation function.

For a full derivation of the above equations see [13,15].

The dielectric spectra can, then, be obtained as averages over discrete regions in space or over atomic populations, and one can use partial integrals or sums over the polarization correlation functions $c_{\alpha}(z,t)$.

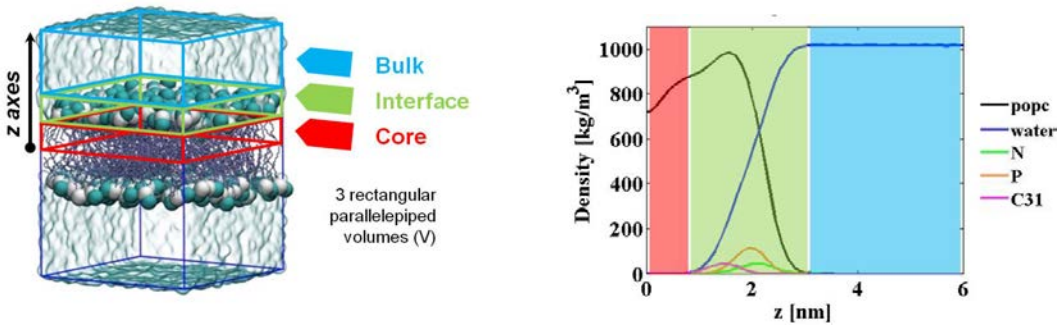

(a) *POPC bilayer scheme.* **(b)** *Density profiles.*

Figure 6.1: Definition of the regions of interest (ROI): the three ROI are hilaghted in red (hyohobic core), green (interface), and blu (bulk water). (a) pure POPC system, water is illustrate as cyan transparent, the lipid head groups in blue and white spheres and the tails in ice blue sticks; (b) density profiles (kg/m^3) along the axes perpendicular to the bilayer z for the different components of the simulation box: the water in blue, POPC lipids in black, the nitrogen atoms of the head groups in green, the phosphorus atoms of the head groups in orange and the carbon atom of the glycerol backbone in pink line.The center of the bilayer is in z = 0

In this work we defined the regions of interest as shown in Fig. 6.1.

We tested this approach first on a box of pure water (data not shown). The permittivity profile is in line with data previously reported on the same water model (TIP3P) [13], with a static value of the polarizability, ϵ_s, of 91±1 and a frequency of relaxation f_c of ~19.9 GHz. Notice that for homogeneous systems there is no need to differentiate between the normal and tangential components.

Here we show preliminary results on a 256 POPC bileyer fully hydrated at no salt concentration (Fig. 6.1) in rest condition (0 V/m applied) averaged over three independent simulations. In Fig. 6.2 we analyzed the permittivity of water at the interface region, as defined above, for the two components (tangential in panel a, and normal in panel b).

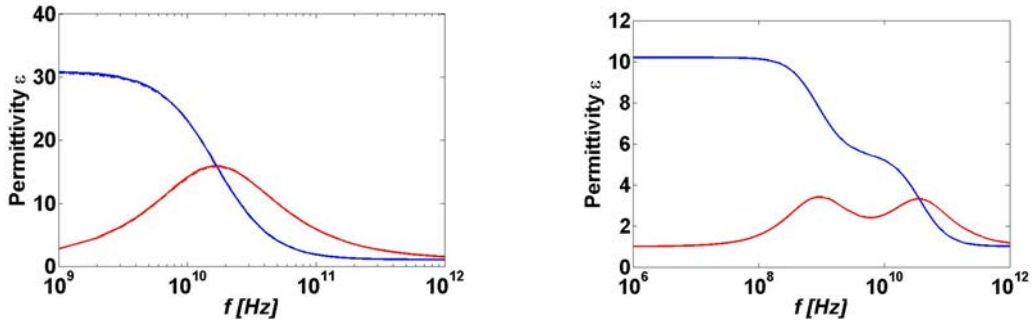

(a) *Tangential components.* **(b)** *Normal component.*

Figure 6.2: Permittivity profiles of the water at the interface: (a) Tangential component and (b) Normal component, of the polarizability ϵ' (blue line) and of the dispersion ϵ" (red line)

The real part of the permittivity, ϵ', is meaningful of the electric polarization, while the imaginary one, ϵ", of the dispersion of the system. Our analysis reveled that while the tangential components are representative of one population, with only one relaxation at 17 GHz, the normal of two different populations of water, having two relaxations at 0.92 and 36.91 GHz. This can be interpreted as follows: the local field produced by the lipid head groups influence the hydration water in such a way that, in the plane parallel to the bilayer, behaves all in the same fashion, attenuating an exogenous field of a factor of ~30.6 (ϵ_s) until one decade before the frequency of relaxation (17 GHz); while in the plane perpendicular to the bilayer, one faster population relaxes at 36.91 GHz with ϵ_s of 5.4, and a slower population with f_c 0.92 GHz and ϵ_s of 10.2.

The water at the interface therefore has a different behavior with respect to the bulk phase, and a specific fingerprint (given by the ϵ_s, and f_c) dependent on the lipids considered.

The next step of this project will be to consider the lipids contribution, the modulation of the cholesterol to the permittivity profile and to compute eqq. 6.2 and 6.4 for the systems when subject to exogenous electric fields.

6.2 Transport of fluorescent dyes

The dimensions, morphology and conductive properties of electropores, produced by electroporation (EP), are relevant to establish the permeability and selectivity of the plasma cell membrane to different molecules and consequently the eventual efficiency of biological and medical applications. The nanometer-range size of the pores unfortunately limits the possibility of their direct observation by conventional techniques. Experimentally there are three indirect common approaches to estimate indirectly the pores size: electrophysiological (voltage/current relationship), fluorescent (dyes) and/or imaging (cell swelling/shrinking). All these methods, however, suffer from specific limitations.

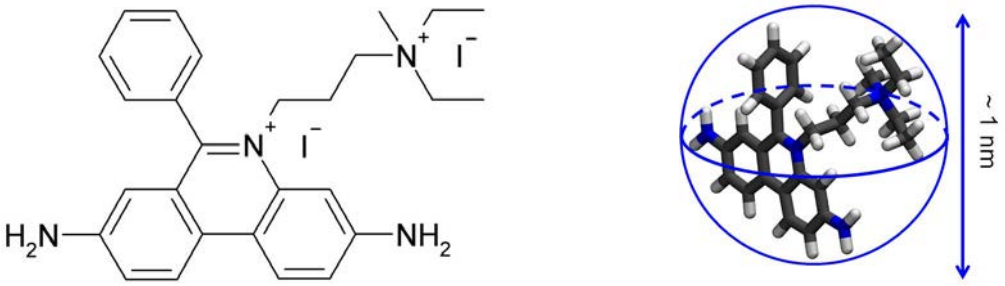

(a) *Structural formula of PI.* **(b)** *Diagram of PI.*

Figure 6.3: Propidium iodide fluorescent dye: (a) structural formula; (b) schematic of the molecule with the approximate diameter

In particular, the quantification of pore size based on the monitoring of the plasma membrane transport of small molecules (e.g. sugars, polyethylene glycols [17], bleomycin [18]) and fluorescent dyes (e.g. thallium ions [19], YO-PRO, propidium iodide [20]) together with the cell swelling or the shrinking detected by imaging have been obtained in the majority of cases from *in vitro* experiments on cells after exposing them to nanosecond long (≤600 ns) electric pulses. The findings emerging from these studies indicate that nanosecond pulses induce a high number of long-lived yet small pores, with radii of about 0.5-0.7 nm, that permit the passage of molecules such as propidium iodide (PI), yet avoid the massive flux known to follow the application of longer (millisecond) less intense (kV/cm) pulses [20-23].

Nevertheless the straight correlation between the dimension of a molecule and that of a electropore might be questionable for molecules that might interact strongly with the pore walls. Interacting molecules can associate with the membrane generating metastabe state and thus require a certain time to diffuse into the cytosolic milieu, especially if the pore is small (i.e. with comparable size), where they can be detected or where they can give rise to osmotic swelling/shrinking. Moreover, charged molecules can significantly perturb the local electrostatic environment in the pore proximity, inducing changes in pore size and morphology [24]. Thus, such class of measurements may not properly report the pore properties as directly generated by electric pulses.

Interesting enough, from our molecular dynamic (MD) results (Section 4.3) these pores have a diameter at least two folds what has been defined considering the PI dimension [17,20]. It could be extremely interesting to model such solutes (e.g YO-PRO, PI, bleomycin, sugars, ...) to shed light on the interactions taking place at the molecular level and to directly detect eventual effects on the pore induce by the presence of the molecule.

We are currently developing a force field for PI (Fig. 6.3), coherent with the CHARMM procedure proposed by Vanommeslaeghe et al. [25], to investigate the mechanism of transport of this dye through electroporated bilayers with atomic detail.

References

[1] D.P. Tieleman, The molecular basis of electroporation, BMC Biochem. 5 (2004) 10.

[2] M. Tarek, Membrane Electroporation: A Molecular Dynamics Simulation, Biophys. J. 88 (2005) 4045-4053.

[3] M.J. Ziegler, P.T. Vernier, Interface Water Dynamics and Porating Electric Fields for Phospholipid Bilayers, J. Phys. Chem. B. 112 (2008) 13588-13596.

[4] M. Tokman, J.H. Lee, Z.A. Levine, M.-C. Ho, M.E. Colvin, P.T. Vernier, Electric Field-Driven Water Dipoles: Nanoscale Architecture of Electroporation, PLoS ONE. 8 (2013) 1-9.

[5] M. Breton, L. Delemotte, A. Silve et al., Transport of siRNA through lipid membranes driven by nanosecond electric pulses: An experimental and computational study, J. Am. Chem. Soc. 134 (2012) 13938-13941.

[6] M.-C. Ho, M. Casciola, Z. A. Levine, and P. T. Vernier, Molecular dynamics simulations of ion conductance in field-stabilized nanoscale lipid electropores, J. Phys .Chem. B 117 (2013) 11633-11640.

[7] L. Chopinet, M.P. Rols, Nanosecond electric pulses: a mini-review of the present state of the art, Bioelectrochemistry Amst. Neth. 103 (2015) 2-6.

[8] M. Simeonova and J. Gimsa, The influence of the molecular structure of lipid membranes on the electric field distribution and energy absorption, Bioelectromagnetics, 27 (2006) 652-666.

[9] S. R. Wassall, Pulsed field-gradient-spin echo NMR studies of water diffusion in a phospholipid model membrane. Biophys. J., 71 (1996) 2724-2732.

[10] R.P. Rand, V.A. Parsegian, Hydration forces between phospholipids bilayers, Biochim. Biophys. Acta, 988 (1989) 351-376.

[11] W. Hübner, A. Blume, Interactions at the lipid-water interface, Chem. Phys. Lipids, 96 (1998) 99-123.

[12] K.J. Tielrooij, D. Paparo, L. Piatkowski, H.J. Bakker, M. Bonn, Dielectric Relaxation Dynamics of Water in Model Membranes Probed by Terahertz Spectroscopy, Biophys. J. 97 (2009) 2484-2492.

[13] H.A. Stern, S.E. Feller, Calculation of the dielectric permittivity profile for a nonuniform system: Application to a lipid bilayer simulation, J. Chem. Phys. 118 (2003) 3401-3412.

[14] R.P. Joshi, V. Sridhara, K.H. Schoenbach, Microscopic calculations of local lipid membrane permittivities and diffusion coefficients for application to electroporation analyses, Biochem. Biophys. Res. Commun. 348 (2006) 643-648.

[15] S. Gekle, R.R. Netz, Nanometer-Resolved Radio-Frequency Absorption and Heating in Biomembrane Hydration Layers, J. Phys. Chem. B. 118 (2014) 4963-4969.

[16] F. Apollonio, M. Liberti, A. Paffi, C. Merla, P. Marracino, A. Denzi, et al., Feasibility for Microwaves Energy to Affect Biological Systems Via Nonthermal Mechanisms: A Systematic Approach, IEEE Trans. Microw. Theory Tech. 61 (2013) 2031-2045.

[17] O.M. Nesin, O.N. Pakhomova, S. Xiao, A.G. Pakhomov, Manipulation of cell volume and membrane pore comparison following single cell permeabilization with 60- and 600-ns electric pulses, Biochim. Biophys. Acta. 1808 (2011) 792-801.

[18] A. Silve, I. Leray, L.M. Mir, Demonstration of cell membrane permeabilization to medium-sized molecules caused by a single 10 ns electric pulse, Bioelectrochemistry. 87 (2012) 260-264.

[19] A.M. Bowman, O.M. Nesin, O.N. Pakhomova, A.G. Pakhomov, Analysis of plasma membrane integrity by fluorescent detection of Tl(+) uptake, J. Membr. Biol. 236 (2010) 15-26.

[20] A.G. Pakhomov, E. Gianulis, P.T. Vernier, I. Semenov, S. Xiao, O.N. Pakhomova, Multiple nanosecond electric pulses increase the number but not the size of long-lived nanopores in the cell membrane, Biochim. Biophys. Acta. 1848 (2015) 958-966.

[21] J. Deng, K.H. Schoenbach, E. Stephen Buescher, P.S. Hair, P.M. Fox, S.J. Beebe, The Effects of Intense Submicrosecond Electrical Pulses on Cells, Biophys. J. 84 (2003) 2709-2714.

[22] P.T. Vernier, Y. Sun, L. Marcu, S. Salemi, C.M. Craft, M.A. Gundersen, Calcium bursts induced by nanosecond electric pulses, Biochem. Biophys. Res. Commun. 310 (2003) 286-295.

[23] P.T. Vernier, Y. Sun, M.A. Gundersen, Nanoelectropulse-driven membrane perturbation and small molecule permeabilization, BMC Cell Biol. 7 (2006) 37.

[24] F. Salomone, M. Breton, I. Leray, F. Cardarelli, C. Boccardi, D. Bonhenry, et al., High-Yield Nontoxic Gene Transfer through Conjugation of the CM18-Tat11 Chimeric Peptide with Nanosecond Electric Pulses, Mol. Pharm. 11 (2014) 2466-2474.

[25] K. Vanommeslaeghe, E. Hatcher, C. Acharya, S. Kundu, S. Zhong, J. Shim, et al., CHARMM general force field: A force field for drug-like molecules compatible with the CHARMM all-atom additive biological force fields, J. Comput. Chem. 31 (2010) 671-690.

Chapter 7

Summary and Conclusions / Résumé et Conclusions

Électroporation (EP) est une technique utilisée pour affecter l'intégrité des membranes cellulaires de plasma et / ou organites internes, conséquence de l'application d'un champ électrique externe d'énergie suffisante, dépendant de son intensité et sa durée. Il a été montré indirectement par de nombreuses études expérimentales et in-silico que ce phénomène résulte de la perméabilisation de la membrane par la formation pores aqueux. L'EP permet ainsi la vectorisation de molécules normalement non perméantes comme des ions, des solutés divers ou encore du matériel génétique. Les applications de la technique vont de l'électrochimiothérapie, à la vaccination à ADN.

Les simulations de dynamique moléculaire (DM) qui permettent la description microscopique, avec une résolution atomique, de la structure de la membrane et de son interaction avec la solution environnante, constituent un apport précieux aux résultats expérimentaux. Plusieurs études utilisant cette technique de modélisation ont été consacrées à décrire certains des aspects de l'EP (par exemple la formation de pores, leur évolution, le rôle de l'eau et des groupes de tête lipidiques, ...). Dans le cadre de ce travail, en utilisant des simulations de DM nous avons abordé plusieurs questions encore en suspens.

Nous avons ainsi quantifié le seuil d'EP de bicouches lipidiques contenant des concentrations croissantes de cholestérol (0, 20, 30, 50% en moles) utilisant des protocoles qui miment les deux modes types de pulses nsPEFs et μs-msPEFs. Les résultats obtenus en appliquant les deux méthodes indiquent que dans les deux cas les modèles de membranes à concentration en cholestérol croissante, nécessitent un voltage transmembranaire plus élevé pour perméabiliser (electroporer) la bicouche lipidique. Nous avons développé une procédure, mimant l'effet des μs-msPEFs en adéquation avec les expériences, qui permet de stabiliser les voltages appliqués à la membrane suffisamment longtemps pour déterminer la dimension des pores, leur conductance et sélectivité ionique.

Nous avons utilisé le même protocole pour étudier le transport de petites molécules

chargées, utilisés dans l'administration de médicaments, et comparé nos résultats avec des études similaires menées dans des conditions nsPEFs. Nous avons montré ainsi que le processus de transport assisté par EP a lieu dans la même échelle de temps (nanoseconde) que sous impulsions nsPEFs.

Une attention particulière a été accordée à la conception de micro-chambres afin de réaliser un dispositifs à large bande passante afin de transmettre sans atténuation et sans distorsion les pulses ns, qui sont caractérisés par une grandes composante spectrale. Une partie importante des travaux entrepris dans cette thèse mené en cotutelle, a été consacrée à la conception théorique (utilisant la Méthode des éléments Finis) d'un dispositif d'exposition, basé sur des systèmes de propagations de micro-ondes (MW), capable de délivrer des impulsions aussi courtes que la ns avec des temps de monté et de chute de 0,5 ns et une efficacité au dessus de 0.9. Ce dispositif tend à améliorer notre savoir-faire concernant les effets de nsPEFs sur les cellules vivantes et de leur potentialité pour des applications thérapeutiques.

Dans l'ensemble, le présent travail va dans le sens de l'élucidation des mécanismes de formation de pores utiles pour diverses applications biomédicales et technologiques. Il combine des méthodes théoriques et numériques: les résultats obtenus par le biais de simulations MD seront vérifiées expérimentalement grâce à une configuration d'exposition développée dans cette thèse.

Summary and Conclusions / Résumé et Conclusions

Electroporation enhances cell permeability to poorly permeant compounds [1,2], hence is widely used for a targeted and safe delivery of molecules to cells and tissues resulting in pre-clinical and clinical applications [3-10]. Nevertheless our restricted comprehension of this phenomenon, related to the nanometer size of the electropores and to the fast temporal scales of the EP dynamic not easily measurable experimentally, limits the development of new technologies and causes difficulties in controlling the process in clinical applications.

The characterization of membrane electropores, following the application of electric pulses on living cells and tissues, is of crucial in determining the permeability and selectivity of the membranes to different ionic and molecular species and consequently the potential efficacy of EP applications.

Therefore, in this Joint PhD thesis, we have attempted to shed light on different mechanisms of EP using molecular dynamics simulations to provide a description pore dynamic, ionic transport, and electrophoretic drift of small charged molecules under different EP protocols. When possible, each of these aspects has been verified against theoretical and experimental results in literature. Our MD approach has the advantage to allow for a characterization *in silico* of dynamics and quantities that are hardly accessible experimentally, and to support continuum models that are often based on assumptions and simplifications. Our atomic investigations suggest that the main features of pore formation and of ionic and molecular transport, following the application of electric pulses, have similar characteristics and dynamics independently if we model nsPEFs or μs-msPEFs. In particular we showed that the time scale of the most relevant aspects of this phenomenon take place in nanoseconds.

Hence, we also have faced the technological issue of realizing devices capable to transmit undistorted extremely short pulses (down to 1 ns duration with rise and fall time of fractions of ns). Using Finite Element Method we designed a microchamber to perform EP *in vitro* experiments in safe and reproducible conditions. Our project is implemented following designing rules typical of microwave propagating structures that ensure a broadband impedance matching between the source of the pulse (i.e. the generator) and the

load (i.e. the microchamber containing the cells). Our microchamber also presents other advantages, such as to reach high electric field intensities for "low" voltage applied, the real-time visualization of the effects on cells, and the possibility to expose either single- or multi-cells though the use of different microfluidic channels. This should advance in the technology of nsPEFs [11-16], and subsequently their potentiality for therapeutic applications.

The main results of our work can be summarized as follows:

- We presented our results regarding the modulation of lipid bilayer characteristics when 30 mol % of cholesterol is added. We found that at rest condition (0 V/nm applied) the cholesterol contribution in the electric field distribution has a mild influence in the membrane electric field profiles. However, the electric field applied to the sterol rich bilayer has to be two folds higher than in the pure POPC one to orientate the interfacial dipole moments in a similar manner. The water density profiles showed that under the same pre-pore condition in the pure POPC bilayer the water penetrates almost 1.5 times more than in the cholesterol rich system, a favorable condition for pore formation, suggesting that the interfacial water orientation should be considered together with other water properties, e.g. the diffusivity, to give indications on how easily pore forms in different bilayer.

- We quantified the EP threshold of libid bilayes with increasing concentration of cholesterol (0, 20, 30, 50 mol %) when the two protocol to model nsPEFs and μs-msPEFs are exploited. The results obtained applying the two approaches indicate that in both cases an increase in cholesterol concentration requires a higher transmembrane voltage to porate the membrane bilayer. Using the first protocol the EP threshold increases steadily doubling the intensity from 0 to 50 mol % [17]. Under μs-msPEFs, the EP threshold, as well as all the other structural characteristics of the bilayer, level-off above 30 mol % cholesterol. Additionally in the latter protocol, we identify a hydrophobic putative nature of the pore formed above this cholesterol concentration. The nature of such pores should in principle lead to different ionic and molecular transport across electroporated membranes and have a direct effect on pore lifetime and resealing time.

- We developed a procedure, mimicking μs-msPEFs, to stabilize electropores under different transmembrane voltages in mechanical condition (constant surface tension of bilayers) similar to experiments for long enough to determine the pore dimension, its conductance and selectivity to ion species. We found that for TM voltages ranging from 420 mV to 630 mV, the pore radius increases from 1 to 2.5 nm and the conductance from 6.4 to 29.5 nS. A qualitative comparison with the nsPEFs approach [18], lead to the conclusion that, under roughly the same TM voltage, similar values of radius (some nm) and conductance (tens of nS) are obtained. Despite a more detailed and systematic study should be carried out to quantitatively confront the two schemes, one can say that from MD simulations, no matter the type of electric pulse

applied, the characteristic of the pore will be in the same order of magnitude when the membrane undergoes the same TM voltage.

- We employed the same method to investigate the transport of small charged molecules, used in drug delivery, comparing our findings with similar studies conducted under nsPEFs conditions [19,20] with the attempt to rationalize the molecular up take. Our results are direct observations at the atomic scale of the electrotransfer of small charged molecules, siRNA (-42 charge, 13.89 kDa) and Tat_{11} (+8 charge, 1.50 kDa), thorough a cell membrane model subject to μs-msPEFs. For transmembrane voltages lower than 0.5 V no crossing of siRNA and a lag in the transport of Tat_{11} were observed. When the transmembrane voltage is above this critical value we report for the siRNA a complete crossing in ∼30 ns albeit its strong anchoring with the zwitterionic phospholipids headgroups, and for the peptide in ∼10 ns without any interaction with the surrounding pore walls. Interestingly we found that that the dynamic of the transport process takes place in the same time scale (nanosecond) that for shorter pulses (nsPEFs) previously reported [19,20].

- We designed a microchamber for usPEF *in vitro* experiments.

  To dimension our guiding structure we used a synthesis procedure based on available analytical closed-form expressions [21] for coplanar microstrip lines (i.e. two parallel strips over a planar substrate and a ground plane under it). This procedure allows to define the size of the device (e.g. the width of the strips, the height of the substrate of a given material, ...) for a specific characteristic impedance (i.e. $Z_0 = 50\ \Omega$).

  Analytical formulas are often based on assumptions and simplifications, we hence optimized this starting geometry with numerical modeling based on the Finite Element Method to obtain the impedance matching between the source of the pulse (i.e. the generator) and the load (i.e. the microchamber). The latter method enables the analysis of a more complex geometry: we modeled the microchamber containing, in the gap between the strips, a channel loaded with a water solution to represent the cell buffer medium. Measurements of different cell buffers were carried out to solve a reliable and realistic model of the cell suspension. We characterized the efficiency and the frequency behavior of the microchamber in two different configurations: for single- and multi-cell experiments, having respectively the channel perpendicular or parallel to the direction of electric field propagation.

  To quantify the matching and the transmission of the signal we studied the Scattering parameters, i.e. the reflection and transmission coefficient, in the frequency range defined by the spectrum of the signal (i.e. up to 1 GHz for the 1-ns-pulse we tested). The reflection coefficient of the single cell microchamber is below -30 dB up to 1 GHz, while below -10 dB for the multi cell, indicative in both cases of a negligible mismatch between the generator and the applicator. The transmission coefficient in the two configurations shows a non-ideal behavior, reaching -1.5 and -4 dB, respec-

tively, instead of the desirable 0 dB. In this conditions, the shorter pulse deliverable with negligible distortion and attenuation is a trapezoidal pulse of 1 ns (0.5 ns rise/fall time) for the single cell microchamber configuration, and 3 ns (1.5 ns rise/fall time) for the multi cell one.

The efficiency, defined as the ratio of the output over the input voltage, for the two configurations is above 0.95. When 7 V of input are applied at one port, the electric field intensity in the region of interest, i.e. in the loaded channel set in the gap between the strips, is homogenously distributed and reaches 130 and 140 kV/m, for the multi- and the single-cell, respectively. This means that only 500 V are needed to deliver tens of MV/m typically used in nanosecond EP applications, drastically reducing the power consumption.

This structure, composed by three conductors, also ensures a low radiated power $4.46\text{x}10^5$ W (at 1 GHz) for 1 W applied, usually halved compared to other planar structures (e.g. coplanar wave guides, microstip lines, slot lines).

The overall performances of this device are an improvement compared to similar structures available in literature [11-16] where the maximum frequency at -10 dB of the reflection coefficient is about 300 MHz and the efficiency does not overcome 0.8, meaning that only pulses longer than 3 ns with rise and fall times longer than 1 ns can be transmitted.

As a whole, the present work goes in the direction of elucidating some mechanisms of pore formation and transport of charged molecules useful for various biomedical and technological applications. It combines theoretical and numerical methodologies: the outcomes achieved by means of MD simulations will be verified experimentally through an exposure setup implemented following designing rules typical of MW propagating structures.

Inspired by our findings, we are currently working on one side to study the properties of lipid bilayers (e.g. the permittivity of the water/lipid interface) and the transport of molecules (e.g. dyes, drugs, ...) with atomic detail to advance in the knowledge of pulsed electric fields effects on living cells and to contribute to the development of new protocols that better regulate and exploit the EP potentiality for therapeutic applications. On the other side we aim at realizing our microchamber to verify its performances and to eventually validate the outcomes achieved from the modeling part.

References

[1] E. Neumann, A.E. Sowers, C.A. Jordan, Electroporation and Electrofusion in Cell Biology, Springer Science & Business Media, 1989.

[2] M. Tarek, Membrane Electroporation: A Molecular Dynamics Simulation, Biophys. J. 88 (2005) 4045-4053.

[3] M. Breton, L.M. Mir, Microsecond and nanosecond electric pulses in cancer treatments, Bioelectromagnetics. 33 (2012) 106-123.

[4] D. Miklavčič, B. Mali, B. Kos, R. Heller, G. Serša, Electrochemotherapy: from the drawing board into medical practice, Biomed. Eng. OnLine. 13 (2014) 29.

[5] M. Sällberg, L. Frelin, G. Ahlen, M. Sällberg-Chen, Electroporation for therapeutic DNA vaccination in patients, Med. Microbiol. Immunol. (Berl.). 204 (2014) 131-135.

[6] G. Serša, J. Teissie, M. Cemazar, E. Signori, U. Kamensek, G. Marshall, et al., Electrochemotherapy of tumors as in situ vaccination boosted by immunogene electrotransfer, Cancer Immunol. Immunother. CII. 64 (2015) 1315-1327.

[7] L.C. Heller, R. Heller, In Vivo Electroporation for Gene Therapy, Hum. Gene Ther. 17 (2006) 890-897.

[8] S. Chabot, J. Teissié, M. Golzio, Targeted electro-delivery of oligonucleotides for RNA interference: siRNA and antimiR, Adv. Drug Deliv. Rev. 81 (2015) 161-168.

[9] C. Jiang, R.V. Davalos, J.C. Bischof, A Review of Basic to Clinical Studies of Irreversible Electroporation Therapy, IEEE Trans. Biomed. Eng. 62 (2015) 4-20.

[10] L. Chopinet, M.P. Rols, Nanosecond electric pulses: a mini-review of the present state of the art, Bioelectrochemistry Amst. Neth. 103 (2015) 2-6.

[11] Y. Sun, P.T. Vernier, M. Behrend, L. Marcu, M.A. Gundersen, Electrode microchamber for noninvasive perturbation of mammalian cells with nanosecond pulsed electric fields, IEEE Trans. NanoBioscience. 4 (2005) 277-283.

[12] P. Krishnaswamy, A. Kuthi, Meng-Tse Chen, Shih-Jui Chen, P.T. Vernier, M.A. Gundersen, Compact high voltage subnanosecond pulsed power delivery system for biological applications, in: Pulsed Power Conf. 2007 16th IEEE Int., 2007 pp 476-480

[13] C. Dalmay, J. Villemejane, V. Joubert, O. Français, L.M. Mir, B. Le Pioufle, Design and realization of a microfluidic device devoted to the application of ultra-short pulses of electrical field to living cells, Sens. Actuators B Chem. 160 (2011) 1573-1580.

[14] C. Dalmay, J. Villemejane, V. Joubert, A. Silve, D. Arnaud-Cormos, O. Français, et al., A microfluidic biochip for the nanoporation of living cells, Biosens. Bioelectron. 26 (2011)

4649-4655.

[15] D. Arnaud-Cormos, P. Leveque, Y.-H. Wu, J.M. Sanders, M.A. Gundersen, P.T. Vernier, Microchamber Setup Characterization for Nanosecond Pulsed Electric Field Exposure, IEEE Trans. Biomed. Eng. 58 (2011) 1656-1662.

[16] Y.-H. Wu, D. Arnaud-Cormos, M. Casciola, J.M. Sanders, P. Leveque, P.T. Vernier, Moveable Wire Electrode Microchamber for Nanosecond Pulsed Electric-Field Delivery, IEEE Trans. Biomed. Eng. 60 (2013) 489-496.

[17] M.L. Fernández, G. Marshall, F. Sagués, R. Reigada, Structural and Kinetic Molecular Dynamics Study of Electroporation in Cholesterol-Containing Bilayers, J. Phys. Chem. B. 114 (2010) 6855-6865.

[18] M.-C. Ho, M. Casciola, Z.A. Levine, P.T. Vernier, Molecular Dynamics Simulations of Ion Conductance in Field-Stabilized Nanoscale Lipid Electropores, J. Phys. Chem. B. 117 (2013) 11633-11640.

[19] M. Breton, L. Delemotte, A. Silve et al., Transport of siRNA through lipid membranes driven by nanosecond electric pulses: An experimental and computational study, J. Am. Chem. Soc. 134 (2012) 13938-13941.

[20] F. Salomone, M. Breton, I. Leray, F. Cardarelli, C. Boccardi, D. Bonhenry, et al., High-Yield Nontoxic Gene Transfer through Conjugation of the CM_{18}-Tat_{11} Chimeric Peptide with Nanosecond Electric Pulses, Mol. Pharm. 11 (2014) 2466-2474.

[21] R. Garg, I. Bahl, M. Bozzi, Microstrip Lines and Slotlines, Third Edition, Artech House, 2013.

Électroporation (EP) est une technique utilisée pour affecter l'intégrité des membranes cellulaires de plasma et/ou organites internes, conséquence de l'application d'un champ électrique d'énergie suffisante, dépendant de son intensité et sa durée. Il a été montré indirectement par de nombreuses études expérimentales et *in-silico* que ce phénomène résulte de la perméabilisation de la membrane par la formation pores aqueux. L'EP permet ainsi la vectorisation de molécules normalement non perméantes. Les applications de l'EP vont de l'électrochimiothérapie, à la vaccination à ADN. Les impulsions électriques utilisés dans l'EP sont classées en deux familles: Les msPEF dont la longueur des impulsions est de l'ordre de la microseconde et l'amplitude de l'ordre de quelques kV/cm. Ils affectent principalement la membrane cellulaire plasmique. Les nsPEFs d'intensité de MV/m de durée de l'ordre de la nanoseconde, ceux eux sont capables de perméabiliser organites internes ainsi que la membrane plasmique et présentent l'avantage d'éviter les effets thermiques indésirables. Les simulations de dynamique moléculaire (DM) qui permettent la description atomique, de la structure de la membrane et de son interaction avec la solution environnante, constituent un appui précieux aux résultats expérimentaux. Plusieurs études utilisant la DM été consacrées à décrire certains des aspects de l'EP (par exemple la formation de pores, leur évolution, le rôle de l'eau et des groupes de tête lipidiques, ...) néanmoins des questions en suspens restent inexplorées:

- Comment la composition de la membrane affecte le seuil d' EP?
- Quelles sont la morphologie, la taille et la conductance des pores formés?
- Quels sont le mécanisme et l'échelle de temps de translocation de petites molécules à travers ces électropores?
- Y a t-il une différence notoire entre les effets des msPEFs et des nsPEFs?

Dans le cadre de ce travail, en utilisant des simulations de DM nous avons abordé ces questions pertinentes. Nous avons quantifié le seuil d'EP de bicouches lipidiques contenant des concentrations croissantes de cholestérol utilisant des protocoles qui miment les deux modes types de pulses nsPEFs et msPEFs. Les résultats obtenus indiquent que dans les deux cas les modèles de membranes à concentration en cholestérol croissante, nécessitent un voltage transmembranaire plus élevé pour perméabiliser la bicouche lipidique. Nous avons développé une procédure, mimant l'effet des msPEFs en adéquation avec les expériences, qui permet de stabiliser les voltages appliqués à la membrane suffisamment longtemps pour déterminer la dimension des pores, leur conductance et sélectivité ionique. Nous avons utilisé le même protocole pour étudier le transport de petites molécules chargées, utilisés dans l'administration de médicaments, et comparé nos résultats avec des études similaires menées dans des conditions nsPEFs. Nous avons montré que le transport assisté par EP a lieu dans la même échelle de temps (ns) que sous nsPEFs. Bien que les nsPEF ont l'avantage d'affecter les membranes cellulaires et celles des organites internes, la possibilité d'exploiter de telles impulsions pour la vectorisation de médicaments est encore en cours d'étude, car la capacité à fournir de manière fiable à des échantillons «biologiques» ces impulsions intenses ultra-courtes n'est pas trivial. Une attention particulière doit être accordée à la conception de micro-chambres afin de réaliser un dispositifs à large bande passante afin de transmettre sans atténuation et distorsion les pulses ns, qui sont caractérisés par une grandes composante spectrale, jusqu'à GHz. Une partie importante des cette thèse mené en cotutelle, a été consacrée à la conception théorique (utilisant la Méthode des éléments Finis) d'un dispositif d'exposition, basé sur des systèmes de propagations de micro-ondes, capable de délivrer des impulsions aussi courtes que la ns avec des temps de monté et de chute de 0,5 ns.

Electroporation (EP) is a technique used to affect the integrity of plasma cell membranes and/or internal organelles, consequence of the application of an external pulsed electric field of sufficient energy content, tuned by its strength and duration. It is proven by extensive indirect experimental and *in silico* evidences that this phenomenon results in the permeabilization of membrane structures by aqueous pores, allowing the transport of poorly- or non-permeant molecules, e.g. salts, ions, genetic material, and any other small solutes present. Applications of the techniques range from electrochemoterapy DNA vaccination and gene regulation. The electric pulses used in EP are categorized in two main families: msPEF, the length of the pulses is in the μs- ms scale and the amplitude in the order of kV/cm, their effect takes place mainly at the plasma cell membrane of cells; nsPEFs, higher magnitude (MV/m) over ns time scale, they act are able to permeabilize internal organelles as well as the plasma cell membrane, presenting the advantage of avoiding undesired thermal effects. Molecular dynamics simulations allow the microscopic description, with atomic resolution, of the membrane structure and its interaction with the surrounding solution, providing a substantial support to experimental findings. A considerable amount of work have been devoted to describe some of the aspects of EP using MD, (e.g. the pore formation, its evolution and reseal, the role of water and of lipid headgroups, ...) nevertheless outstanding questions remain unexplored:

- How does the composition of the bilayer affect the EP threshold?
- What are the morphology, size and conductance of pores formed?
- What are the mechanisms and time scales of translocation of small molecules through the electropores?
- Is there any difference when modeling nsPEFs and msPEFs?

As part of the present work, using MD simulations and comparing our results to other findings from our group, we addressed some relevant questions. We quantified the EP threshold of libid bilayes for the increasing concentration of cholesterol (0, 20, 30, 50 mol %) when the two protocol to model nsPEFs and msPEFs are exploited. The results obtained applying the two approaches indicate that in both cases an increase in cholesterol concentration requires a higher transmembrane voltage to porate the membrane bilayer. We developed a procedure, mimicking msPEFs, to stabilize electropores under different transmembrane voltages in mechanical condition similar to experiments for a time long enough to determine the pore dimension, its conductance and selectivity to ion species. We employed the same method to investigate the transport of small charged molecules, used in drug delivery, comparing our findings with similar studies conducted under nsPEFs conditions with the attempt to rationalize the molecular uptake. Interestingly we found that that the dynamic of the transport process takes place in the same time scale (nanosecond) that for nsPEFs. Despite the fact that nsPEFs have the advantage to affect both cell membranes and internal organelles and to further reduce thermal effects, the possibility to exploit nsPEFs for drug delivery is an ongoing research since the ability to reliably deliver to biological loads these ultra-short intense pulses is not trivial. Particular attention must be paid in the design of microchambers to realize a broadband devices to transmit without attenuation and distortion nsPEF, which exhibit large spectral components, i.e. spanning from MHz up to GHz. An important part of the current work has been devoted to the design (with Finite Element Method) of an exposure device, based on microwave propagating systems, able to deliver pulses down to 1 ns with rise and fall time of 0.5 ns.